Polyacrylonitrile Hollow Fibre Membranes For Gas Separation

Jian Zhou

A thesis submitted in accordance with

the requirements for the degree of Doctor of Philosophy

under the supervision of Dr. G. C. East and Prof. J. E. McIntyre

The candidate confirms that the work submitted is his own and that appropriate credit has been given where reference has been made to the work of others.

Department of Textile Industries

The University of Leeds

LEEDS LS2 9JT

England

January 1996

ABSTRACT

Polyacrylonitrile (PAN) hollow fibres have been spun by a dry-jet wet spinning technique, using a commercial PAN polymer (Courtelle) redissolved in dimethylformamide (DMF). After failure to produce satisfactory porous hollow fibres from PAN/DMF solutions, a series of studies on the porous substructure of PAN cast films prepared with a variety of additives in the casting solution and at varying temperatures of the coagulation bath were carried out. A porous and flexible PAN cast film was produced when it was precipitated in water at 55 °C with $CuSO_4$ present in the casting solution. Hollow fibres produced from a spinning solution composed of 25wt% PAN, 70wt% DMF and 5wt% $CuSO_4$ were more porous and flexible than those produced from 25wt% PAN and 75wt% DMF spinning solution, and appeared to be more suitable for gas separation studies.

The permeability of the PAN hollow fibre membranes to single gases was studied. The experimental results showed that the calculated pore radius on the surface of the fibre was in the range of 4 ~ 32 nm. After coating with silicone rubber, the membranes showed very poor gas permeability and selectivity. Since PAN has a low intrinsic gas permeability, the low permeability observed is ascribed to a thick skin layer. The low selectivity of the membranes is related to their high surface porosity ($> 10^{-4}$), or to the large pores present which are imperfectly blocked. With such fibres, little or no gas will pass through the membranes by solution-diffusion in the PAN.

In order to reduce the surface porosity on the skin layer of the hollow fibres, a dual-bath coagulation spinning system was used. The gas permeability of H_2 in these membranes is lower than that obtained by the single bath coagulation system, while the gas permeability of the other gases, such as CO_2 and CH_4, were too low to measure. These results indicate that a high selectivity can be obtained by the dual-

bath coagulation spinning system although the selectivity is accompanied by too low a permeability, which is itself caused by too thick a skin layer.

Surface modifications of PAN hollow fibre were carried out in order to modify the surface porosity of the fibres. After the treatments, the hollow fibre membranes did not give significant improvement in gas permeability and selectivity. But, when PAN hollow fibres were treated with cuprammonium hydroxide solution at room temperature, the fibres became coloured and no longer soluble in the usual solvents. The insolubility of the fibres is presumed to be due to a newly-formed crosslinked structure. The crosslinking of the fibres is reversed when the fibres are treated with EDTA solution. It has been observed that the presence of the copper in the fibres increases the tensile strength and decreases the elongation of the hollow fibres. The interaction of the PAN fibre with the cuprammonium hydroxide gave no improvement in gas separation performance but might be the basis for general acrylic fibre modification.

❀ TO MY DEAR DAUGHTER AND ❀

❀ THE PEOPLE I LOVE ❀

ACKNOWLEDGEMENT

The author wishes to express his gratitude to Dr. G. C. East and Prof. J. E. McIntyre for their constant help and valuable guidance and encouragement throughout the present work.

The author also wishes to thank Dr. V. Rogers for his various and interesting discussions, and kind help.

The author would like to acknowledge the contribution of all who helped him during the time of undertaking the research in Leeds, namely:-

CVCP committee for the ORS award, the University of Leeds for a Tetley and Lupton scholarship and the Department of Textile Industries for a maintenance grant.

Mrs. S. Hassell (Technical assistance), Mr. L. Johnson (Technical and IR analysis), Dr. M. G. Dobb and Miss H. M. Dyson (SEM micrographs), Mr. H. White (Fibre spinning), Mr. H. Rait (Equipment design).

Mrs. V. Whitehead (Clothworkers' library), Mr. R. N. Parmar, Mrs. W. H. Xia and all colleagues in laboratory 203A, and friends in 6 Blenheim Crescent and elsewhere.

Finally to my lovely daughter for her good health during the time of the research.

CONTENTS

List of figures

List of tables

List of schemes

List of symbols

C	Concentration of gas in the polymer,
C_D	Concentration of the dissolved permeant in Henry's law sorption
C_H	Concentration of the dissolved permeant in Langmuir sorption
C'_H	The hole saturation constant
b	The hole affinity constant
C_T	Total sorbed concentration;
S	Henry's law solubility constant
Q	The steady-state flux (gas flow reading)
l	Membrane thickness
D_H	Diffusion coefficient in Henry's law sorption
D_D	Diffusion coefficient in Langmuir sorption
$D_{eff}(C)$	Effective diffusion coefficient
$D(C)$	Concentration dependent diffusion coefficient
Tg	Glass transition temperature
V_f	Excess free volume (V_g-V_l)
V_g	Actual glassy specific volume,
V_l	Equilibrium volume of the densified glass
P	Permeability coefficient
P'	Gas permeation rate
P_i	Intrinsic permeability of the membrane to gas i
A_3/A_2	Surface porosity
l_1	coating layer thickness
l_2	Separating layer thickness
A	Surface area of the hollow fibre module, $A = \pi \times n \times L \times d_f$;

n	Number of fibres in the module
L	Length of fibre
$O.D$ (d_f)	Outer diameter of hollow fibre
$I.D$	Inner(lumen) diameter of hollow fibre
$\alpha_{i/j}$	Separation factor
K	Permeability coefficient (in porous media)
J	Volume flow
F	Molecular flux
Ko	Knudsen permeability coefficient
Bo	Geometric factor
η	Viscosity
$\overline{p}$	Mean pressure $(p_1+p_2)/2$
Δp	Differential pressure
p'	Atmospheric pressure
p_1	Pressure at high pressure membrane interface
p_2	Pressure at low pressure membrane interface
q	Tortuosity factor
v	Average molecular velocity
ε	Volume porosity
r	Pore radius
M	Molecular weight
R	Universal gas constant; Resistance (to permeate flow or electrical)
T	Temperature
ε/q^2	Effective porosity
ρ_c	Capillary pressure
γ	Surface tension of liquid
W_L	Weight-loss (%)
W_A	Weight increase (%)

List of abbreviation

RO	Reverse osmosis
PAN	Polyacrylonitrile
PET	Poly(ethylene terephthalate)
PSF	Polysulphone
PC	Polycarbonate
CA	Cellulose acetate
PES	Polyethersulphone
PDMS	Polydimethylsiloxane
1,5-ND	1, 5-naphthalene diamine
6F	Hexafluoroisopropylidene group
6FDA	2, 2-bis(3, 4-dicarboxy phenyl) hexafluoropropane dianhydride
PMDA	Pyrromellitic dianhydride
pp'-ODA	4, 4'-oxydianiline
mp'-ODA	3, 4'-oxydianiline
MDA	Methylene dianiline
IPDA	Isopropylidene dianiline
2, 4'-DATr	2, 4-diaminotoluene
3, 5'-DBTF	3, 5-diaminobenzotrifluoride
BTDA	3, 3', 4, 4'-benzophenone tetracarboxylic dianhydrie
BPDA	3, 3', 4, 4'-biphenyltetracarboxylic dianhydride
m-PDA	1, 3-Phenylenediamine
APAP	2-(3-aminophenyl)-2-(4-aminophenyl) propane
BAHF	2, 2'-bis(4-aminophenyl) hexafluoropropane
BAPHF	2, 2'-bis((4-aminophenoxy) phenyl) hexafluoropropane
BATPHF	2, 2'-bis(4-(4-amino-2-trifluoromethylphenoxy)phenyl) -hexafluoropropane

4,-4' APPP	2,2'-bis((4, 4'-aminophenoxy)phenyl) propane
DMF	N, N-dimethylformamide
NMP	N-methyl-2-pyrrolidinone
1-Fp	1-Formyl-piperidine
DMAC	N, N-Dimethylacetaminde
DMSO	Dimethylsulphoxide
DSC	Differential scanning calorimetry
TGA	Thermogravimetric analysis
SEM	Scanning electron microscopy
RM	Resistance model
EDTA	Ethylene diamine tetra-acetic acid
PSA	Pressure swing adsorption and absorption
FTIR	Infra-red
AS	As-spun hollow fibre membrane
CAS	Coated as-spun hollow fibre membrane
HF	Hollow fibre
GPU	Gas permeation units
S. E	Solvent exchange drying method
FFV	Fraction of free volume

CHAPTER 1

INTRODUCTION

1. 1 General introduction

During the 1980's, membrane-based gas separation science and technology emerged as a commercial process on a grand scale. Large-scale commercial uses of membrane-based gas separation have gradually displaced traditional gas separation processes such as cryogenics, pressure swing adsorption and absorption. This has led to intensified academic interest, with the result that published research in this field has increased substantially. In 1982, Lonsdale[1] cited over 400 references in the earlier 1980's in his review, even though the author still claimed that it only covered the most important references. One recent review[2] seeks to define the current scientific, technological and commercial boundaries of membrane-based gas separation processes and to project the position of these boundaries for the immediate future. The relationship among these three areas depends on advances in material science and engineering, and the limitations that dominate the application of membrane-based gas separation technology at the present time. Achievements over the past ten to fifteen years have promoted the current strong interest in membrane-based gas separations. The trend of steady progress in material and membrane formation may lead to such progress that there will be a long term growth in this membrane-based gas separation technology.

Over the past ten to fifteen years, the Department of Textile Industries at the University of Leeds has also been involved in this activity of hollow fibre membranes for gas separation. The work was initially conducted with British Gas Plc, as a part of their interest in the development of efficient hollow fibre membrane systems, especially for carbon dioxide and methane gases separations. The main research activities in this department have been based on fabrication of hollow fibres, characterisation of hollow fibre membranes and improving gas separation properties by post-treatment of polysulphone hollow fibre membranes.

1. 2 The basic membrane-based gas separation processes

The concept of gas separation with polymeric membranes is over 100 years old, but the widespread use of membrane-based gas separation has occurred only within the last 15 to 20 years. The development of gas separation membranes with sufficient permeability and selectivity makes commercialisation economically attractive in industrial applications of gas separation and purification.

A membrane will separate gases only if some components pass through the membrane more rapidly than others. The trade-off between gas permeation rate and separation properties is inherent in the most membrane materials, i.e. the permeation rate increases only with a decrease in separation factor.

Fig. 1.1 shows a typical membrane process, which can be performed using membrane based on one of three general transport mechanisms: Knudsen flow, molecular sieving, and solution-diffusion.

For porous membranes, as shown in Fig. 1.1(A), if they contain pores large enough to allow convective flow, then gas separation in the membranes will not occur. If the size of the pores is smaller than the mean free path of the gas molecules, Knudsen flow then replaces the convective flow. In this case, gas molecules interact with the pore walls much more frequently than with one another. Low molecular weight gases are able to diffuse more rapidly than heavier ones, and a separation occurs. In the limit of zero permeate pressure, the difference in transport rates of two components is inversely proportional to the square root of the ratio of their molecular weights[3]. If the pores are small enough, large molecules are unable to pass through them and are excluded by the membrane. Then, molecular sieving will dominate the membrane process. This molecular sieving is potentially useful in separating molecules of different sizes.

A. POROUS MEMBRANES

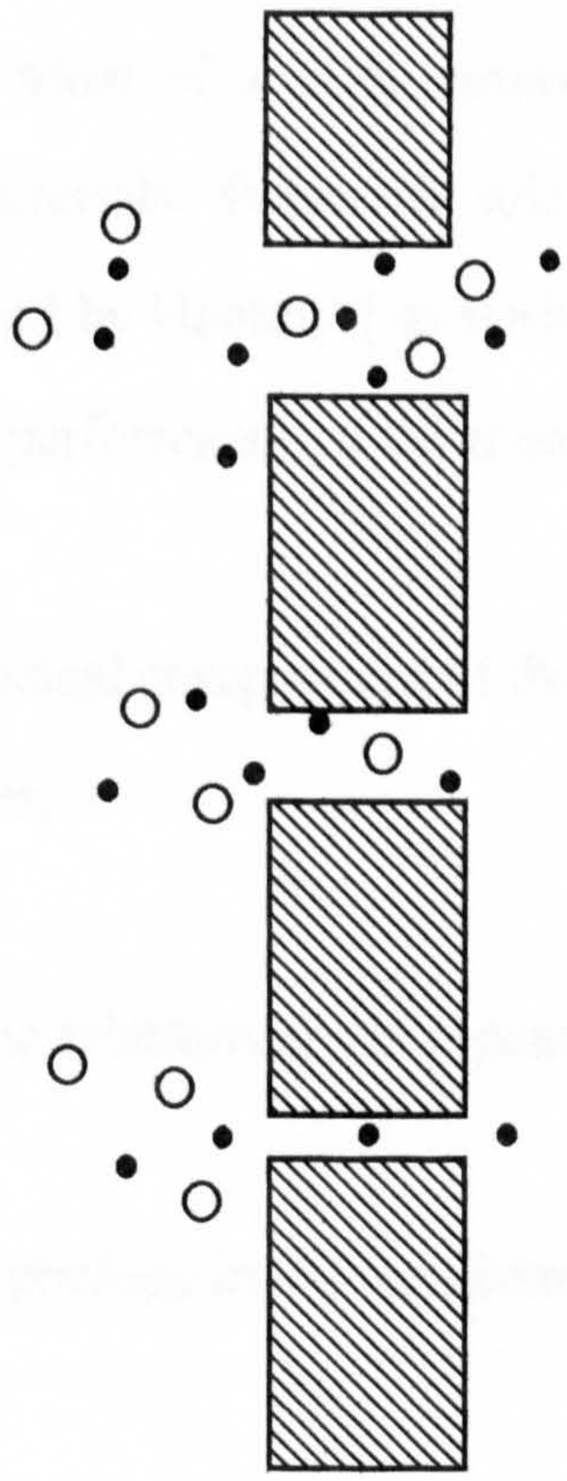

Convective flow through large pores. No separation occurs.

Knudsen diffusion through pores. Pores with diameter less than the mean free path of the gas molecules allow lighter molecules to preferentially diffuse through pore.

Molecular sieving. Large molecules are excluded from the pores by virtue of their size.

B. SOLUTION-DIFFUSION MEMBRANES

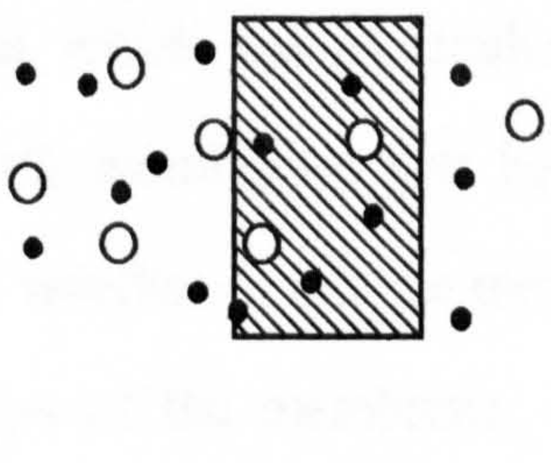

Gas dissolves into the membrane material and diffuses across it.

Fig. 1.1 Mechanisms for membrane-based gas separation processes[3]

For solution-diffusion membranes, as shown as in Fig. 1.1(B), the gas molecules pass through a nonporous membrane. The transport occurs when gas molecules dissolve into the membrane and then diffuse across it. The permeation rate of a permeant depends on the gas molecules' diffusion coefficient and solubility coefficient in the membrane. Most of today's commercial solution-diffusion membranes are made of polymeric materials. Polymeric solution-diffusion membranes for gas separation have been described by Hoehn[4] as having four structural levels, each of which influences the ultimate performance of the membrane. These structural levels are as follows:

Level 1 Chemical composition of the polymer that forms the selective membrane layer;

Level 2 Steric relationships in repeat units of the selective polymer;

Level 3 Morphology in the membrane's separating layer;

Level 4 The overall membrane structure, including structural relationships between the separating layer and the rest of the membrane.

The first two structural levels involve the chemistry of the polymer and its influence on the rate at which gas molecules diffuse through the membrane. At the third structural level, membranes can be classified as being symmetric or asymmetric, depending on whether or not the morphology of the membrane is the same across the entire thickness of the membrane. Symmetric (homogeneous) membranes have a uniform density across their thickness, while asymmetric membranes do not. In the fourth structural level, the separating layer which may be on the one side of the porous supporting layer governs the molecular transport rate and achieves the separation. The rate of gas transport across the membrane is inversely proportional to the thickness of the separating layer.

If the separating and porous supporting layers are formed in a single operation from a single material, the membrane is said to have an integrally skinned structure. On the other hand, if the separating layer is a coating on the porous supporting layer, or if a coating is applied over the separating layer, the membrane is said to be a composite membrane[3].

1. 3 Historical background

Prior to the 1960's, interest in membrane-based gas separation was primarily concentrated in academic circles. The first observation that different gases permeate through membranes at different rates is generally attributed to Mitchell[5], who reported this phenomenon in 1831. Cellulose nitrate, the first man-made polymer was studied by Schoenbein[6] in 1846 and produced commercially in 1869. In 1855, Fick[7] employed cellulose nitrate membranes in his classic study *Ueber Diffusion.* In the same year, Lhermite[8] contributed the concept of *solution*, that is, membrane-permeant interaction, to membrane permeation theory. Graham[9] appeared to be the first man to demonstrate experiments on the transport of gases and vapours in polymeric membranes in 1866. In fact, Graham became the father of membrane science and technology not only by devising and testing a permeability rate-measuring device using a flat membrane with a vacuum on one side, but also by postulating a mechanism for the permeation process. As noted by Stannett, ' this is the basis for the so-called solution diffusion model which is used in various forms and modifications in the handling of most membrane problems today.'[10]. In 1860, Schumacher[11] prepared the first tubular cellulose nitrate membrane, while the first flat membrane was discovered by Baranetzky[12] in 1872. The first series of microfiltration membranes with a graded pore size was prepared by Bechhold[13] in 1907. Bechhold was also the first to define the relationships between bubble point, surface tension and pore radius. The concept of pore-size distribution was developed by Karplus[14], who combined bubble point and permeability measurements.

The golden age of membranology (1960-1980) began in 1962 with the discoveries by Loeb and Sourirajan[15] of the first asymmetric integrally skinned cellulose acetate membrane for reverse osmosis (RO). The means to produce the cellulose acetate membrane for RO were applied to gas separation later. The key to this achievement was the development of a surfactant-aided method to allow the drying of asymmetric

cellulose acetate membranes without collapse of the porous substructure and destruction of the selective skin[16]. This development stimulated both commercial and academic interest, first in desalination by reverse osmosis (RO), and then in other membrane applications and processes.

In 1977, DuPont produced melt spun polyester hollow fine fibres with internal diameters of 36 μm for high pressure hydrogen separations[17]. A patent and an article by DuPont in the 1970's[18, 19] identified many glassy polymer materials with high intrinsic permeability. These materials had much better potential than the polyester hollow fibres which showed a low productivity for gas separation. Additionally, they could be used to form related materials for RO systems[20]. Indeed, coupled with solvent exchange drying developed for cellulose acetate and other polymers at that time[21], the potential existed to produce systems with properties competitive even by today's standards for hydrogen separation. A decision to focus on reverse osmosis applications in 1979 led to mothballing of the gas separation technology until the early 1980's. After DuPont's withdrawal from the gas separation field, Monsanto announced a revolutionary concept of the ' resistance model '[22]. This development resulted from research originally aimed at producing a composite selective silicone rubber membrane supported on the microporous polysulphone hollow fibres. Although in 1985, the membrane field was thought to have matured, there exists at present the real possibility of an imminent renascence-at least in gas separation[23].

1. 4 Theory of gas separation in membranes

The permeation of gases through polymeric membranes depends upon whether the membrane is porous or nonporous. For the porous membrane, the permeation of gas through it consists of Knudsen diffusion and Poiseuille flow. The mechanism of flow through the porous membrane will be discussed in section 4. 3. 2. This type of membrane exhibits low gas selectivity and, for more efficient separations, nonporous polymeric membranes are used.

In the nonporous membranes, the gas flow across the membrane is via a solution diffusion mechanism. This mechanism involves the following sequence of steps[24]; a), adsorption of the gas at one interface of the membrane, b) solution of the gas into the membrane at that interface, c) activated diffusion of the gas in and through the membrane, d) release of the gas from solution at the opposite interface, and e) desorption from the latter interface. During the gas transport in the membrane, the term permeation is used to describe the overall mass transport of the gas across the membrane, whereas the term diffusion refers only to the movement of the gas inside the matrix. The gas transport in nonporous membranes depends on whether the membrane is above or below its glass transition temperature, i.e. whether it is in the rubbery or glassy states.

Gaseous diffusion through rubbery polymer is generally well described by Fick's first law[25], which takes the following form for one-dimensional transport in a direction normal to the membrane interfaces

$$Q = -D(\frac{dC}{dx}) \qquad (1\text{-}1)$$

where Q is the flux, D is diffusion coefficient and C is the concentration of the penetrant in the membrane at a position co-ordinate x.

When the concentration of the penetrant in rubbery polymer is very low, Henry's law is then generally assumed to apply to describe the solubility of the gas in the polymer and

$$C = Sp \tag{1-2}$$

where C is the concentration of gas in the polymer, S is the Henry's law solubility constant for the particular polymer-gas pair, and p is the gas penetrant pressure[26]. The concentration of gas in the polymeric membrane is related linearly to the external partial pressure.

The permeability is defined in terms of the steady-state flux Q and the pressure or fugacity driving force, normalised by the membrane thickness l

$$P = \frac{Q}{\Delta p / l} \tag{1-3}$$

where Δp refers to the difference in pressure of the upstream and downstream sides of the membrane. For a concentration-dependent diffusion coefficient, Fick's first law equation (1-1) can be rewritten as

$$Q = -D(C)(\frac{dC}{dx}) \tag{1-4}$$

Substitution of the expression for steady-state flux, equation (1-3), into equation (1-4) yields

$$P = -D(C)\frac{dC}{dx}\cdot\frac{l}{\Delta p} \tag{1-5}$$

Although *D(C)* and *dC/dx* vary across the thickness of the membrane, the product of the two must be constant at each point in a flat membrane, since the steady-state permeability is constant for fixed upstream and downstream conditions[27], defined by equation (1-3). Therefore, the permeability can be described as the normalised integration of the product between an average diffusion coefficient *D* and an effective solubility coefficient *S*, as shown as follows:

$$P = DS \tag{1-6}$$

The overall selectivity of a polymeric membrane toward two different penetrant gases A and B can be expressed in terms of an ideal separation factor[27] by a ratio of pure gas permeabilities for the individual penetrants

$$\alpha_{A/B} = \frac{P_A}{P_B} \tag{1-7}$$

Gas sorption in glassy polymers is more complex than that in rubbery polymers. A simple Henry's law solubility model for rubbery polymers at low pressures fails to hold for glassy polymers. It is now recognised that gas sorption in glassy polymers obeys a more complex sorption isotherm, which is well described by a combination of Henry's law and Langmuir sorption terms[28]. A brief introduction to typical gas sorption isotherm forms for polymeric materials and gas diffusion in glassy polymers is in the following sections.

1. 4. 1 Sorption

Sorption describes penetration of permeant molecules into the polymer matrix. The permeant molecules may undergo various modes of sorption at the same time within the membrane. The mode of sorption may change with temperature, concentration, time and the polymer matrix. At equilibrium, it is the activity of the permeants which

defines the mode of sorption. Thus sorption characteristics are defined by the strengths of the interactions between gas and polymer. Some of the most common types of sorption behaviour are shown in Figure 1.2 (a) ~ (d)[29].

(1) Henry's law sorption

This type of sorption can be described by a linear Henry's law relation as expressed by equation (1-2) and illustrated in Figure 1.2 (a)[29]. Thus the sorption isotherm shows a linear dependence with pressure. It is generally observed in rubbery polymers at low pressure with gases of low solubility in the polymer.

(2) Langmuir sorption

This kind of sorption occurs at relatively low pressure and on specific sites within the polymer. These sorption sites are associated with microvoids or excess free volume formed from intersegmental packing defects which are fixed in the glassy state during the glass transition. It has been explained that the penetrant molecules sorbed in the Langmuir sites are much less mobile than those in the Henry's law sorption sites[30]. When a small amount of permeant is dissolved in the polymer, the concentration of the dissolved permeant C_H can be given by the Langmuir equation (1-7) and shown in Figure 1.2 (b).

$$C_H = \frac{C'_H bp}{1+bp} \qquad (1\text{-}7)$$

where C'_H is the hole saturation constant, which is a measure of the sorption capacity of the unrelaxed volume, p is the penetrant pressure, b is the hole affinity constant which represents the ratio of the rate constants of sorption and desorption of penetrant in the holes. This type of sorption is typically observed in the case of dye sorption by ionic polymers.

(a) Henry's Law

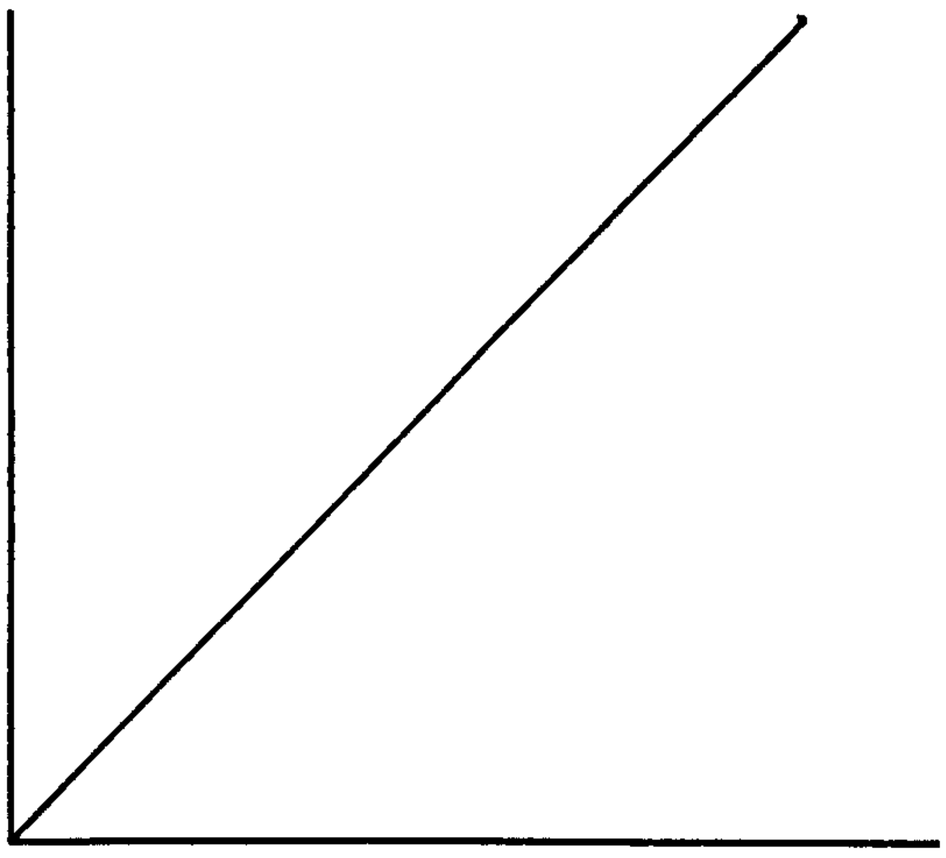

(b) Langmuir's Isotherm

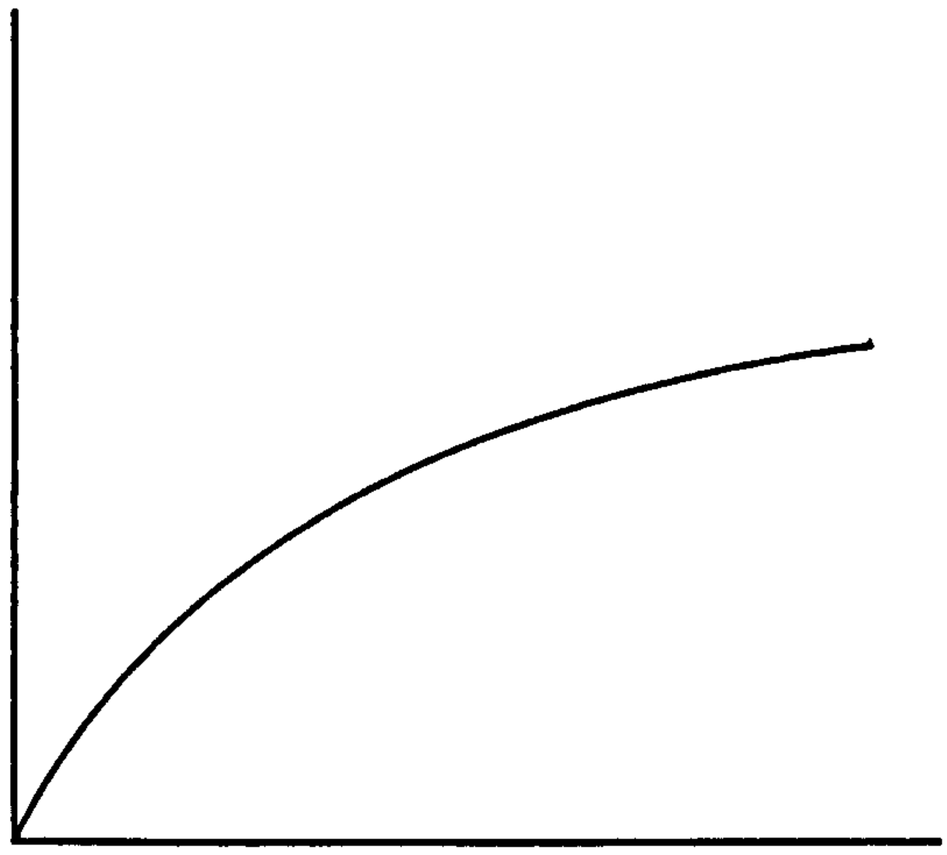

(c) Flory-Huggins

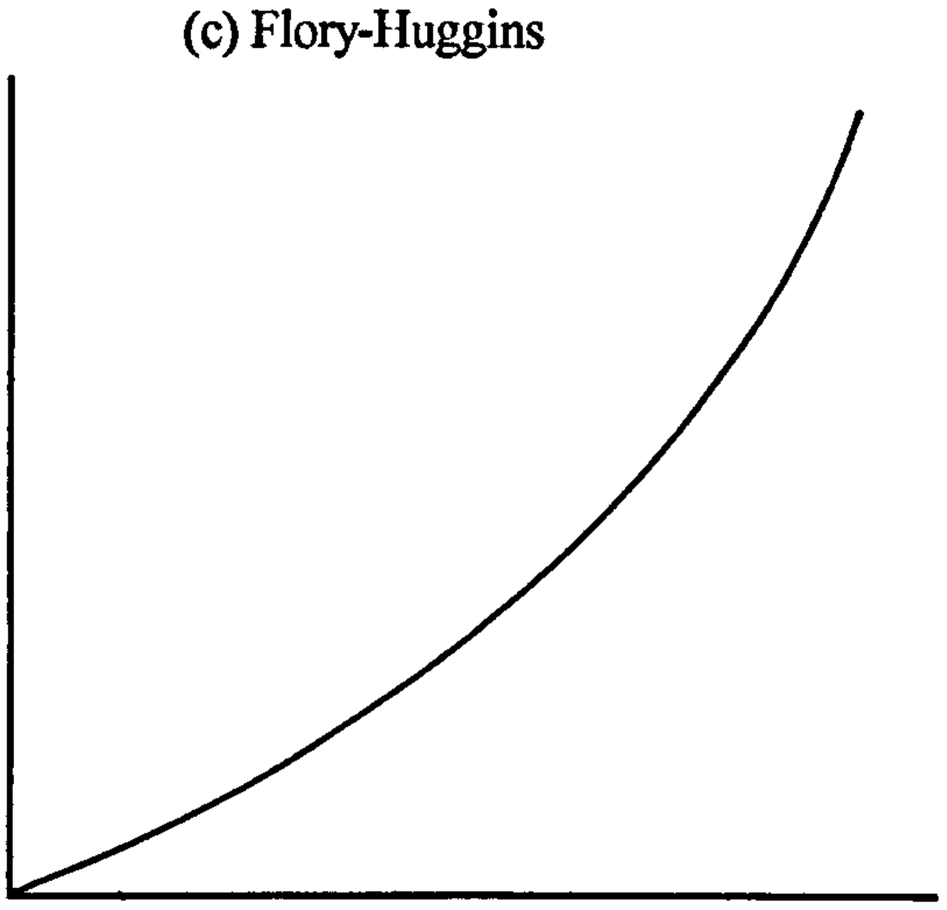

(d) Dual Mode Sorption

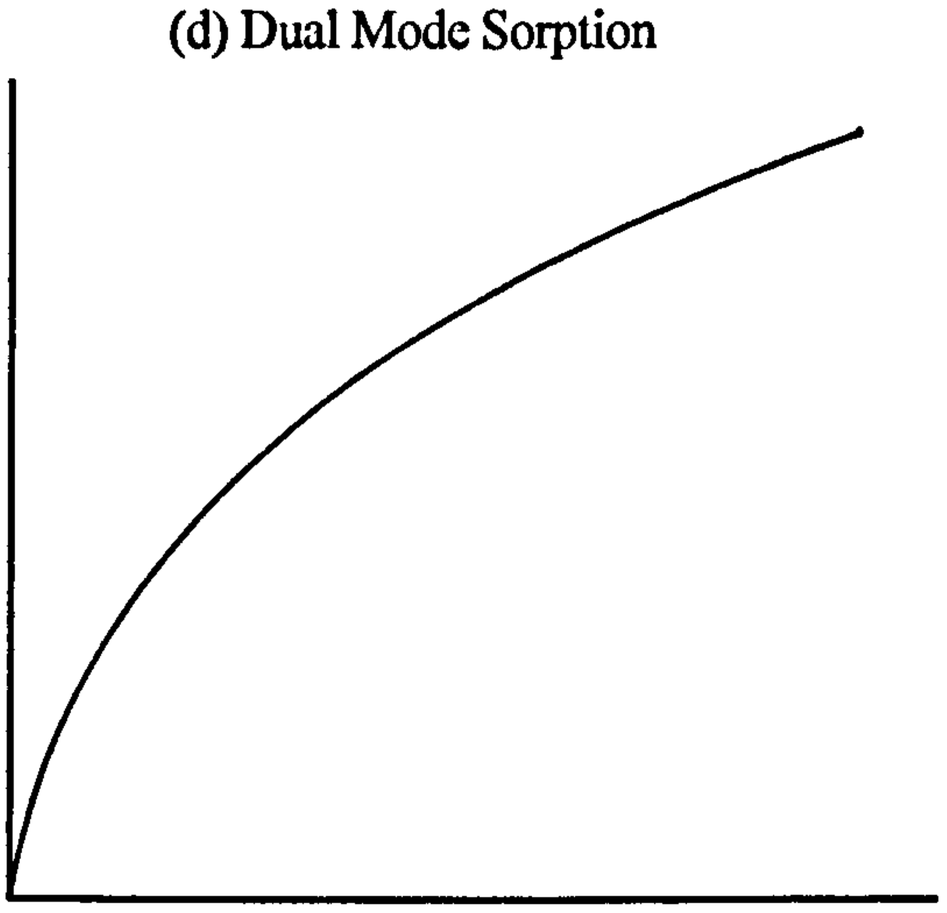

X axis: p, partial pressure of penetrant;

Y axis: C, concentration in polymer.

Fig. 1.2 Typical sorption isotherm behaviour[29]

(3) Dual-mode sorption

Dual-mode sorption theory postulates the existence of two types of sorption sites in a glassy polymer. One type is viewed as gaseous sorption into densified regions of the polymer, following Henry's law sorption at low concentration as in a rubbery polymer. Another is unique to glassy polymers, and is viewed as being due to uptake into the microvoids or excess free volume locked into the polymer when it is quenched below the glass transition. As illustrated in Fig. 1.3, there is a break in the volume versus temperature plot below the glass transition Tg. Below the glass transition, the excess free volume V_f is V_g-V_l, where V_g is the actual glassy specific volume, V_l is the equilibrium volume of the densified glass. This excess free volume is thought to be the result of trapped nonequilibrium chain conformations in the quenched glass, which result from the extraordinarily long relaxation times for segmental motions in the glassy state. This excess free volume present in the glassy polymer accounts for the sorption sites of additional penetrant above that observed in rubbery polymers. These sites are described as Langmuir sorption sites[31]. The total gaseous sorption in glassy polymers is described by the following equation (1-8) and illustrated in Fig. 1.2(d)

$$C_T = C_D + C_H = Sp + \frac{C'_H bp}{1+bp} \qquad (1\text{-}8)$$

where C_T is the total sorbed concentration; C_D is the concentration of the dissolved permeant in Henry's law sorption; C_H is the concentration of the dissolved permeant in Langmuir sorption.

For the special case in which the downstream pressure is effectively zero, the appropriate expression derived from the dual-mode sorption for steady-state permeability of a pure component in a glassy polymer is given by

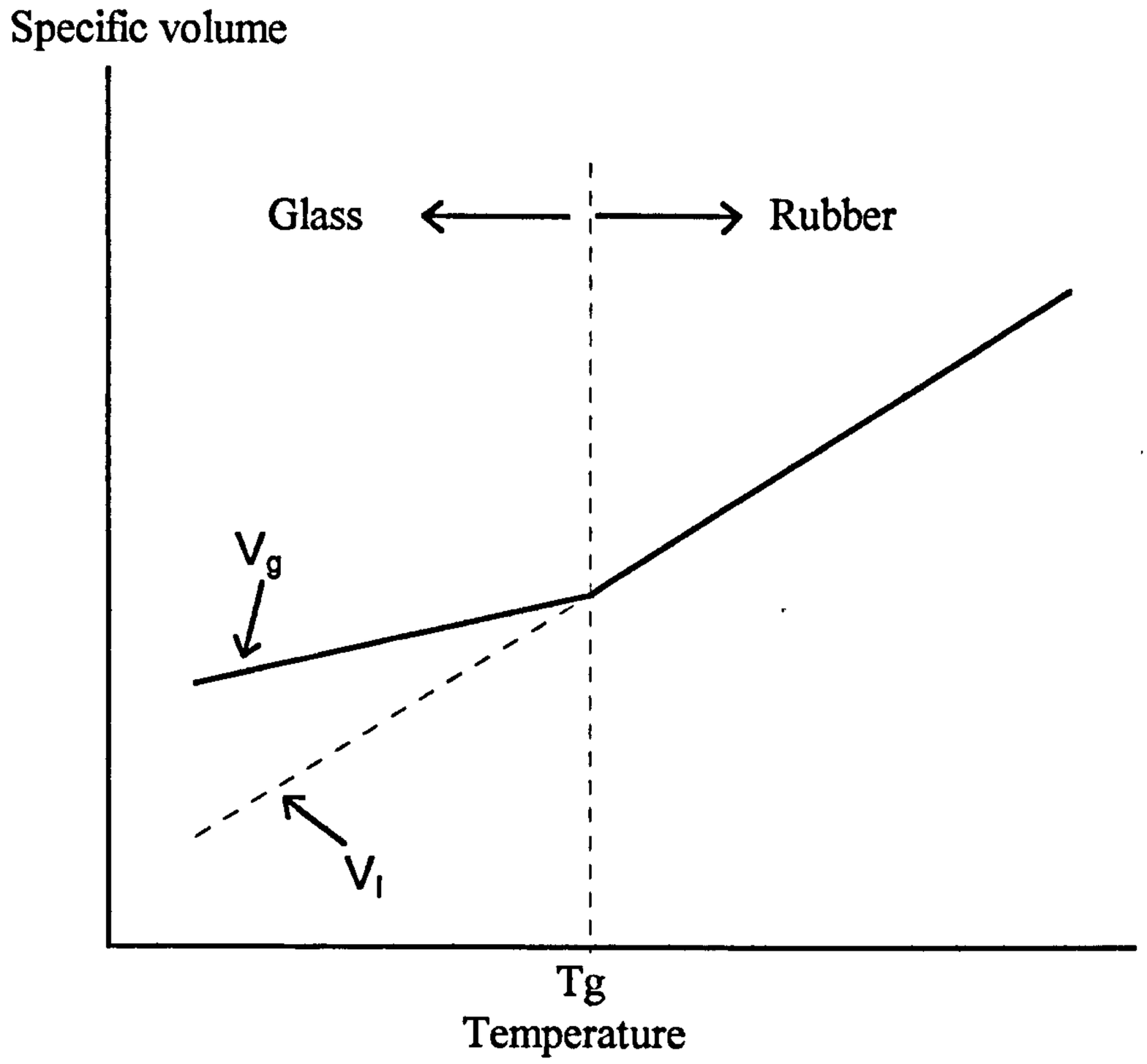

Fig. 1.3 Polymer specific volume as a function of temperature[31]

$$P = SD_D\left[1+\frac{FK}{1+bp}\right] \qquad (1\text{-}9)$$

where F refers to D_H/D_D, the ratio of the diffusion coefficients D_H in Henry's law sorption and D_D in Langmuir sorption, and K is C'_Hb/S.

The first term in equation (1-9) describes the transport of permeant governed by Henry's law, while the second term is related to the Langmuir sorption. This theory provides the most useful phenomenological description of gas transport in glassy polymers, especially by its 'partial immobilisation' version developed by Paul and Koros[32, 33], and by Petropoulos[34]. The dual-mode sorption model is strictly applicable in cases where the polymer is not significantly plasticized (swelled) by penetrant gas. Stern et al[35 ~ 37] have extended this model to the transport of plasticizing penetrants by taking into account the concentration dependence of the mutual diffusion coefficients. The model has also been widely applied to the study of

structure/permeability relationships of polymers. But the main limitation of this phenomenological model is that it is not predictive because the model parameters are not directly related to the chemical structure of the polymers.

(4) Flory-Huggins sorption

Another isotherm, Flory-Huggins sorption shown in Fig. 1.2(c), can be applied when the interactions between permeant molecules are stronger relative to permeant polymer interactions, and the solubility coefficient increases with increase in pressure. This sorption isotherm can be used for high penetrant uptake in rubbery polymers.

1.4.2 Diffusion

Diffusion describes the movement of the gas inside the polymer matrix. A model for the diffusion of gases in glassy polymers as the kinetic part of the dual-mode sorption theory has been developed by Vieth and Sladek[38]. There are seven postulates in the formulation of this model. More details are discussed elsewhere[39]. Here, a brief description of diffusion in polymers is introduced.

(1) Effect of concentration and pressure on diffusion

For transport in glassy polymers, the diffusion coefficient is usually found to be concentration dependent even in the absence of a strong affinity of the penetrant for the material. Koros[40] found that the diffusion coefficient for a gas in a glassy polymer is usually convex to concentration at low sorption levels, and is concave to concentration at higher sorption levels. The effective diffusion coefficient $D_{eff}(C)$ that is dependent on the local concentration of dissolved penetrant C_D, as well as other dual-mode terms defined in section 1.4.1, can be expressed as

$$D_{eff}(C) = D_D\{\frac{1+[FK/(1+\alpha C_D)^2]}{1+[K/(1+\alpha C_D)^2]}\} \qquad (1\text{-}20)$$

where α is *b/S*.

The concentration dependence of the diffusion coefficient has been shown to be predicted very well by equation (1-20) for CO_2 transport in poly(ethylene terephthalate)(PET)[40]. In some membrane applications, the effect of CO_2 on glassy polymer plasticization has received much attention. The CO_2 pressure necessary to induce plasticization is widely different and dependent on material properties. The effect of CO_2 concentration and pressure on the diffusion coefficient and permeability has been discussed in detail[41].

(2) Free-volume diffusion model

The free volume theory of diffusion in polymers was developed mainly by Fujita et al[42] in the 1960's. Since that time, several other versions have been developed by other research workers[43, 44]. The free-volume theory of transport postulated that movement of molecules depends on the free volume available and the availability of energy sufficient to overcome polymer-polymer attractive forces[45]. Vrentas and Duda[45] proposed that the specific volume of the polymer and polymer-penetrant mixture is composed of three components: a) the occupied volume, b) the interstitial free volume and c) the hole free volume. Redistribution of the interstitial free volume requires a large energy input, while on the other hand, redistribution of the hole free volume requires no additional energy; so this volume randomly migrates throughout the polymer matrix. Random mobility of the hole free volume may facilitate both a slow interdiffusion of polymer chains as well as penetrant transport. The free-volume of glassy polymers and the diffusion coefficients for polymer-penetrant mixtures are

history dependent because the free volume and diffusivity for a particular system depend on the thermal and concentration history of the system[46, 47]. Consequently, the diffusion coefficient for a system composed of a small amount of penetrant in a glassy polymer depends both on the rate at which the polymer sample is cooled through the transition temperature range, which sets its free volume, and on the extent of isothermal ageing at some temperature[48]. More detailed discussion has been given by others[49, 50].

Above all, the sorption and diffusion processes of gases in a polymer depend on many factors, such as the nature of the gases, temperature, polymer material and the free volume. Once the polymeric membrane material has been chosen, control of the kinetics of the sol-to-gel transformation is one of the means of achieving new molecular scale environments in the effective separating layer of the membrane. It is an approach that seeks to achieve physical alteration of the effective separating layer by control of the processing protocols such as applied stresses, cooling rates, and phase transformation kinetics during the phase inversion process. Other approaches as a means of achieving new molecular scale environments, which are being extensively investigated, are chemical modification of the backbone of the constituent polymer by polymerisation or copolymerization of new monomers[4] and physical modification by the blending of macromolecule or micromolecular species with a given polymer[51 ~ 52]. The approaches which involve chemical modification of the backbone of the polymer will be briefly treated in a subsequent section.

1. 5 Relationships between structure and permeability of polymer

In the previous sections, the gas transport mechanism has been introduced. Actually, the polymeric membrane material plays a very important role in gas separation membranes. Recently, the rapidly growing interest in gas separation membranes has led to the development of new materials specifically designed to enhance gas permeability and selectivity. Considerable data and correlations relating structure and permeability exist[53], but there are still no actual quantitative relations to guide detailed structure-permeability optimisation. Currently, the most reliable guide for understanding structure-mobility studies is based on a given family of polymers, such as polycarbonates, polysulphones and polyimides.

Polysulphone (PSF) and polycarbonate (PC) based on bisphenol A have been produced commercially since the 1960's for use in a wide range of applications. These two kinds of polymers have rather similar gas transport properties. The polysulphone has achieved considerable importance as a membrane material whereas the polycarbonate has not. The reasons for this includes a number of considerations but mostly involve the greater stability of the polysulphone to solvents, chemical attack, and heat.

A series of PC and PSF with the various structures are shown in Table 1.1[54]. The four symmetrically placed R groups on the phenyl rings of the bisphenol monomer are either H, CH_3, Cl or Br, whereas the connector group X between the two phenyl rings is either the common isopropylidene unit or the others, as shown in Table 1.1. Symmetrical replacement of hydrogen on the phenyl rings of the bisphenol by four methyl groups (TM = tetramethyl) for PC or PSF material with any connector group X has the effect of increasing the gas permeability coefficients three- to four- fold whereas the ideal gas separation factors remain essentially unchanged for each gas pair. In terms of membrane performance, this effect contrasts with the

Table 1. 1 Effect of symmetrical phenyl ring substitution and connector group structure on properties of polycarbonates[a] and polysulphones[b][54]

Acronym	X	R	Tg (°c)	FFV[c]	P_{CO_2} (barrers)[d]	α_{CO_2/CH_4}	P_{O_2} (barrers)	α_{O_2/N_2}
PC	$-C(CH_3)_2-$	H	150	0.164	6.8	19	1.6	4.8
PSF	$-C(CH_3)_2-$	H	186	0.156	5.6	22	1.4	5.6
TMPC	$-C(CH_3)_2-$	CH_3	193	0.180	17.6	22	5.6	5.1
TMPSF	$-C(CH_3)_2-$	CH_3	242	0.171	21	22	5.6	5.3
TCPC	$-C(CH_3)_2-$	Cl	230	0.179	6.7	30	2.3	6.4
TBPC	$-C(CH_3)_2-$	Br	263	0.133	4.2	34	1.36	7.4
HFPC	$-C(CF_3)_2-$	H	172	0.195	24	23	6.9	4.1
HFPSF	$-C(CF_3)_2-$	H	192	0.168	12	22	3.4	5.1
TMHFPC	$-C(CF_3)_2-$	CH_3	208	0.216	100	24	32	4.1
TMHFPSF	$-C(CF_3)_2-$	CH_3	248	0.196	72	24	18	4.5
TBHFPC	$-C(CF_3)_2-$	Br	255	0.200	32	36	9.7	5.4
PSF-O	-O-	H	181	0.150	4.3	24	1.1	5.6
PSF-F	$-CH_2-$	H	179	0.151	4.5	24	1.1	5.5
TMPSF-F	$-CH_2-$	CH_3	232	0.163	15	26	3.3	5.4

a PC

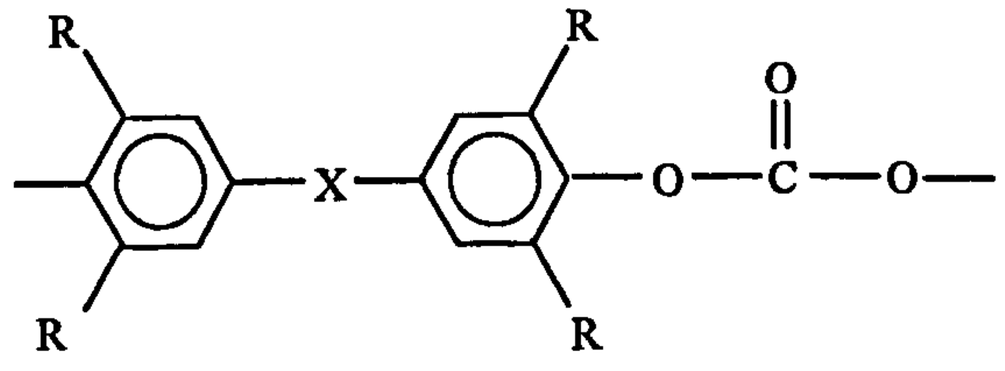

b PSF

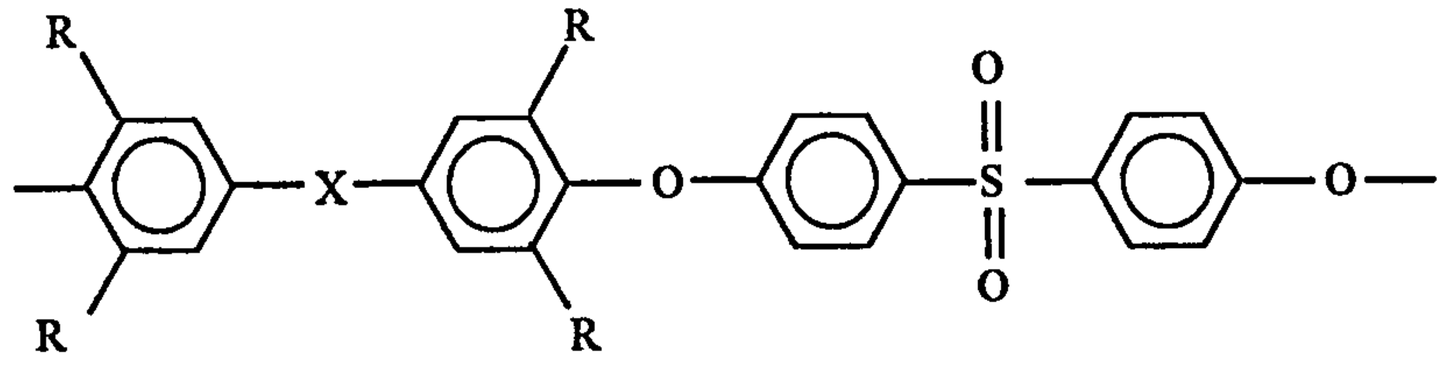

c FFV: the fractional free volume; d Barrers: $P\times10^{10}$ cm^3 (STP) cm/cm^2 s cmHg

usual trade-off between selectivity and permeability. It is very interesting that all the materials containing the hexafluoro isopropylidene (HF=hexafluoro) are substantially more permeable, i.e., by a factor of about 4, than the corresponding polymers with regular isopropylidene units. They have equal or higher selectivity for CO_2/CH_4[55] but lower selectivity for O_2/N_2 relative to the corresponding polymers with the hydrogen form of isopropylidene. The materials that combine the HF-isopropylidene with tetramethyl or tetrabromo ring substitutions are especially interesting. The combined effects greatly increase Tg, FFV (the fraction of free volume) and permeability with constant or improved CO_2/CH_4 selectivity, but O_2/N_2 selectivity is not improved by this fluorinated connector group.

Considerable information is available on the dependence of permeability, diffusion, and solubility coefficients for He, O_2, N_2, CO_2 and CH_4 on the structures of a variety of polycarbonates and polysulphones, mainly due to the extensive and well-planned studies of Paul, Koros, and their co-workers[56~60], and to other investigations[101]. For many years, PSF has been an important membrane material for gas separations. The first large scale membrane separation process, developed by Monsanto Co. in the late 1970's, utilised asymmetric hollow fibre membranes of PSF coated with a thin layer of silicone rubber[22].

Polyimides are another very important group of polymers for gas separation membranes. Recently, these polymers have been investigated extensively because some of them exhibit a remarkably higher gas selectivity as well as a higher permeability than many other glassy polymers. Since the pioneering work of Hoehn[4, 19], the variety of studies in this field has been summarised in the review by Stern[61]. A substantial insight has been gained in the past ten years into the effects of variations in the chemical structure of polyimides on gas solution and transport in these polymers. As a result, polyimides exhibiting increasingly higher gas selectivities and permeabilities are being developed in academic and industrial laboratories.

The studies involved in this field show that the following structural modifications are required, in order to enhance the selectivity and permeability of polyimides, toward light gases:

(1) The backbone chains must be stiffened by inhibiting their intrasegmental (rotational) mobility;

(2) Intersegmental packing of the polymer chains must be simultaneously prevented;

(3) Interchain interactions must be weakened and, if possible, eliminated.

Hoehn[4] has described some of the structures that could satisfy the above criteria. These structures are shown in Scheme 1.1.

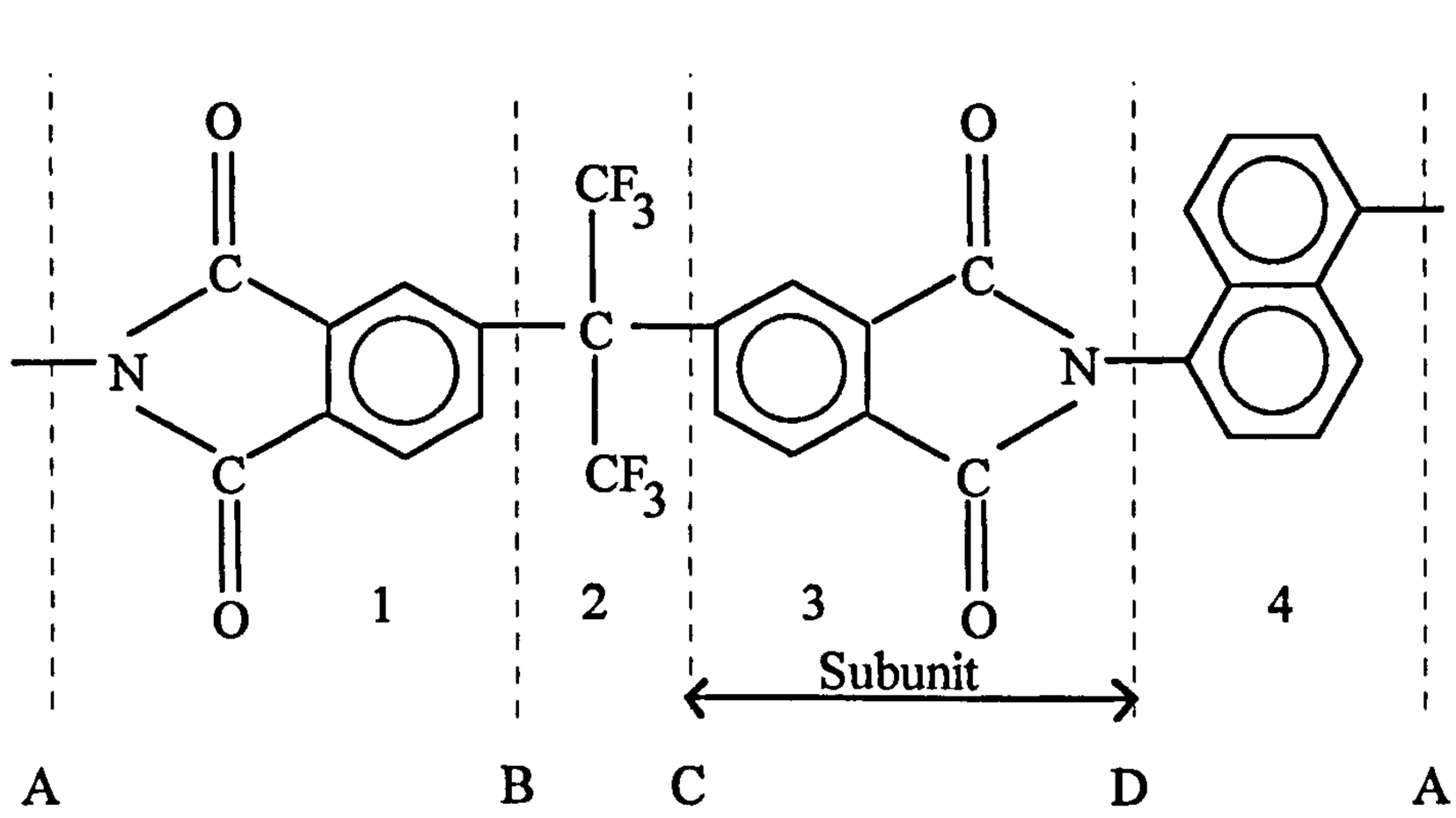

Scheme 1.1 1,5 ND-6F polyimide[4]

This polyimide structure used for gas separations contains: a) four rigid subunits(1, 2, 3, 4) connected by non-linear bonds, b) four bonds with restricted rotation(A; B; C; D;), and c) predominantly aromatic character.

Koros and his co-workers[62] were among the first to study systematically the effects of subtle modification of the structures of two similar types of aromatic polyimides on their gas permeability and selectivity. The structures of these polyimides are shown in Scheme 1. 2.

As seen in Scheme 1. 2, the diamines differ only in that their two phenyl rings are separated by -O-, $-CH_2-$ and $-C(CH_3)_2-$, species, respectively. The more interesting result is that almost all 6FDA polyimides exhibit both a higher gas permeability and a higher selectivity than the PMDA polyimides with same diamine moieties, the data being shown in Table 1. 2.

From the results in Table 1. 2, it can be seen that the selectivity of the 6FDA polyimides decreases to a much lesser extent with increasing permeability than the selectivity of the PMDA polyimides upon substitution of increasingly bulkier diamines. The higher permeability and selectivity of the 6FDA polyimides, when compared to the PMDA polyimides, is due to the presence of the bulky $-C(CF_3)_2-$ groups in their dianhydride moiety. Such groups hinder intersegmental mobility, and thereby stiffen the backbone chains, and also inhibit intersegmental chain packing.

The remarkable differences in the permeability coefficients, P_{CO_2}, of these polyimides presented in Table 1.2 are due primarily to the differences in the diffusion coefficients D_{CO_2}, whereas the solubility coefficients, S_{CO_2}, vary relatively little, as shown in Table 1.3. D_{CO_2} and hence also P_{CO_2} increase as the size of the dianhydride moiety is increased from PMDA to 6FDA or as the size of the diamine moiety is increased from ODA through MDA to IPDA.

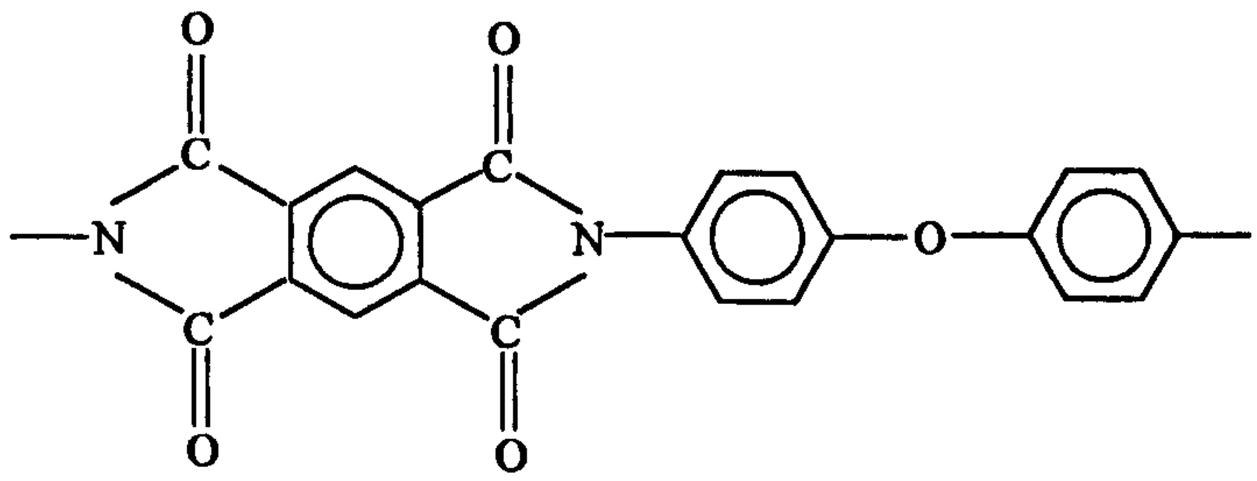

PMDA-ODA

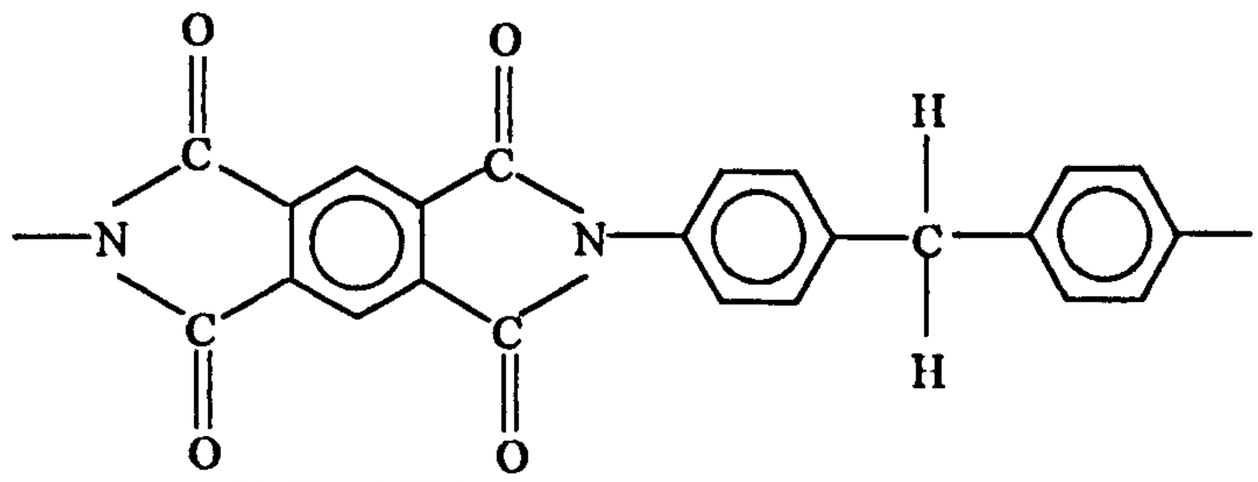

PMDA-MDA

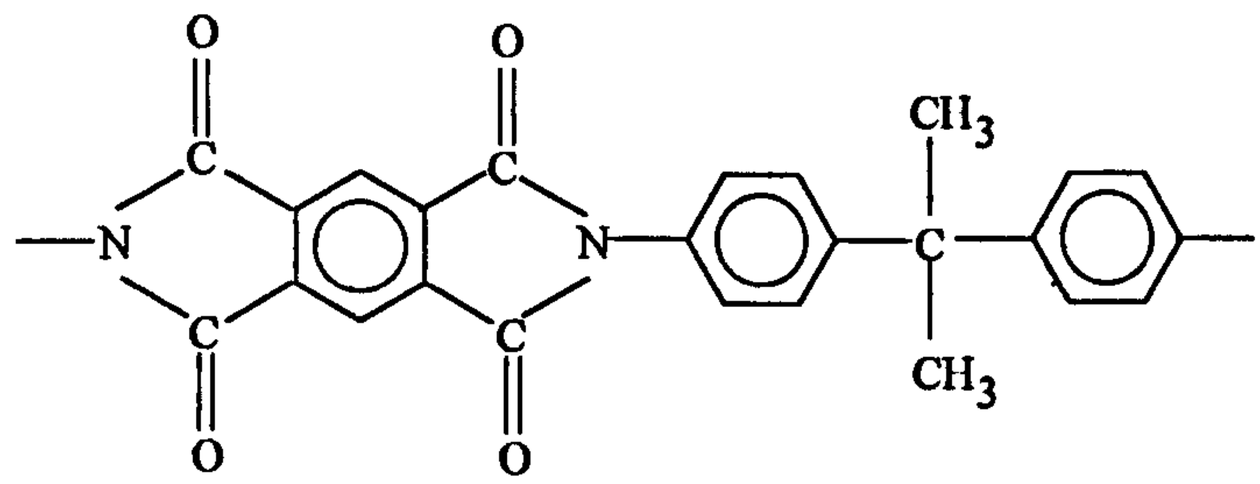

PMDA-IPDA

6FDA-ODA

6FDA-MDA

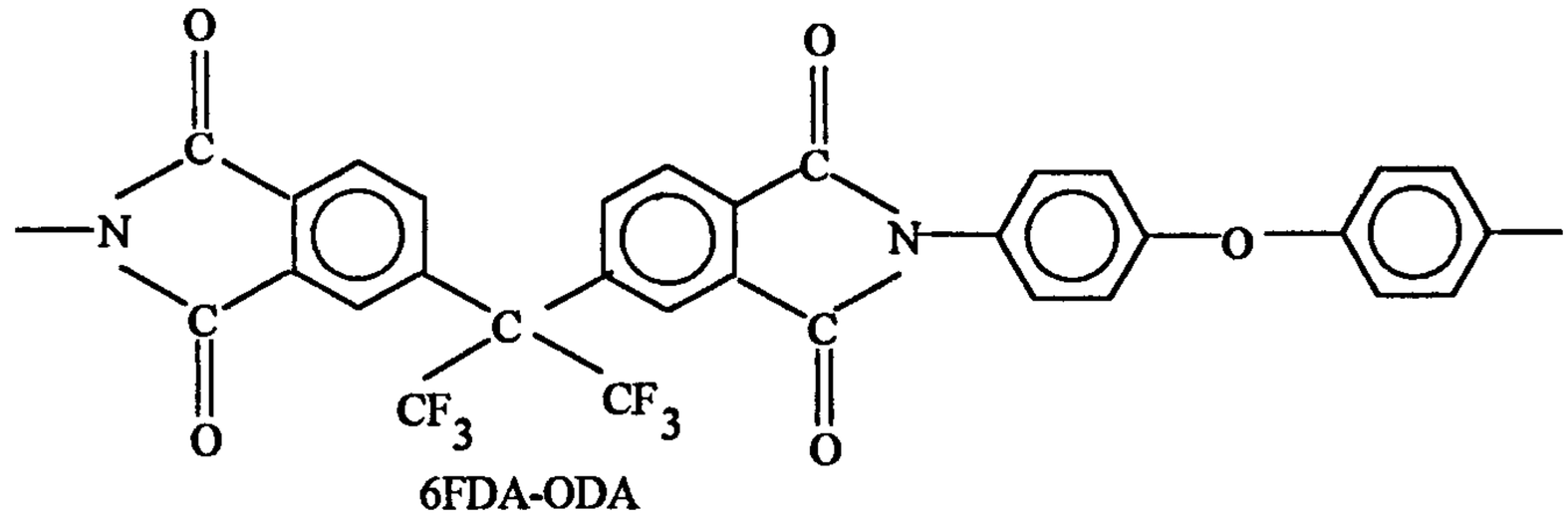

6FDA-IPDA

Scheme 1.2 Structure of PMDA- and 6FDA-based polyimides with analogous diamine moieties[62]

Table 1.2 Permeability coefficients and overall selectivity for several light gases in six aromatic polyimides[62, 63]

Polymer	P_{He}[a]	$\alpha_{He/CH4}$	P_{CO2}	$\alpha_{CO2/CH4}$	P_{O2}	$\alpha_{O2/N2}$	P_{CH4}	$\alpha_{N2/CH4}$
PMDA-ODA	8.0	135	2.71	45.9	0.61	6.1	0.59	1.8
PMDA-MDA	9.4	94	4.03	42.1	0.98	4.9	0.10	1.8
PMDA-IPDA	37.1	41	26.8	29.7	7.10	4.7	0.90	1.6
6FDA-ODA	51.5	135	23.0	60.5	4.34	5.2	0.38	2.2
6FDA-MDA	50.0	117	24.2	56.3	4.60	5.7	0.43	1.9
6FDA-IPDA	71.2	102	30.0	42.9	7.53	5.6	0.70	1.9

a: Units: $P \times 10^{10}$[cm^3 (STP) cm/s cm^2 cmHg];

Table 1.3 Permeability, solubility and diffusion coefficients for CO_2 in PMDA and 6FDA polyimides[62, 63]

Polymer	P_{CO2}[a]	D_{CO2}	S_{CO2}	$\alpha_{CO2/CH4}$	S_{CO2}/S_{CH4}	D_{CO2}/D_{CH4}
PMDA-ODA	2.71	56.5	4.80	45.9	3.84	11.9
PMDA-MDA	4.03	90.0	4.47	42.1	3.58	12.0
PMDA-IPDA	26.8	409.8	6.57	29.7	3.77	7.9
6FDA-ODA	23.0	358	6.43	60.5	3.70	16.3
6FDA-MDA	24.2	370	5.21	56.3	3.36	13.4
6FDA-IPDA	30.0	538	5.58	42.9	3.53	12.1

a: Units: $P \times 10^{10}$[cm^3 (STP) cm/s cm^2 cmHg]; $D \times 10^{10}$[s cm^2];

$S \times 10^{2}$[cm^3 (STP)/cm^3 (polymer) cmHg];

Tanaka et al[64] recently determined the permeability, diffusion and solubility coefficients for H_2, CO, O_2, N_2, CO_2 and CH_4 in a number of fluorinated and nonfluorinated polyimides. The chemical structure of the dianhydrides and diamines incorporated in these polyimides are represented in Scheme 1.3. The polyimide 6FDA-BAHF, which contains -$C(CF_3)_2$- groups in both moieties and no mobile -O- linkages, exhibits the highest gas permeability of all these fluorinated and nonfluorinated polyimides. The gas selectivity of this polyimide is also higher than expected for such a high permeability, by comparison with the permeability/selectivity relationships of the other polyimides.

Stern et al[61] synthesised a number of fluorine containing aromatic polymers. The structures are shown in Scheme 1.4. The polyimides contain -$C(CF_3)_2$- groups in either their dianhydride or diamine moieties, or in both moieties. As viewed from the bottom to the top of Scheme 1.4, the polyimides have increasingly larger fluorine content (as wt% of the repeat unit) and increasingly shorter aromatic diamine moieties. Moreover, the top two polyimides in Scheme 1.4, namely, 6FDA-2, 4'-DATr and 6FDA-3, 5'-DBTF, do not contain any mobile -O- linkages. Among these polymers, the 6FDA-3, 5'-DBTF exhibits excellent CO_2/CH_4 selectivity and permeability to CO_2. By contrast, the substitution in polyimides with branched or extended (long) diamine moieties in these 6FDA-based polyimides tends to lower both the permeability and selectivity[65, 66].

As early as 1986, Skyes and St. Clair[67] showed that the permeability of CO_2 in some BTDA-based polyimides could be enhanced by a factor of 40 without a significant loss in the CO_2/O_2 selectivity. In contrast to the results obtained in PMDA-based polyimides, the permeabilities of these BTDA-based polyimides gradually increase with decreasing Tg of the polymer and hence with increasing large scale chain motions, whereas the CO_2/O_2 selectivity is relatively constant.

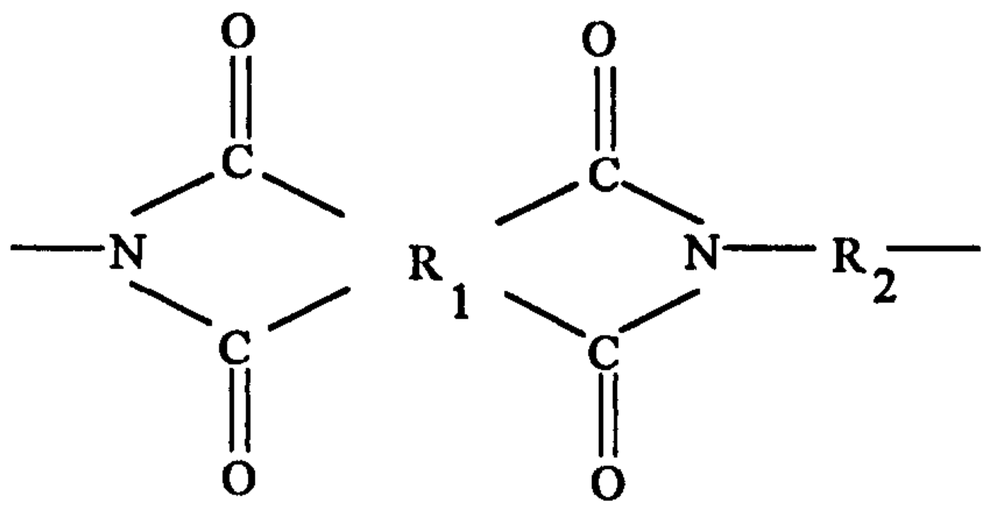

General Structure

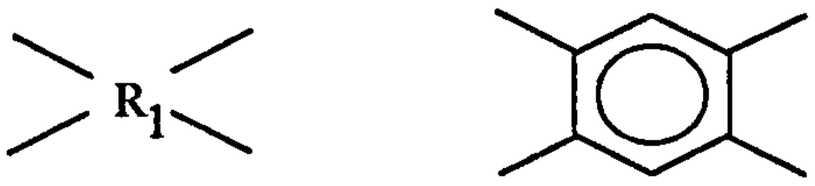

PMDA

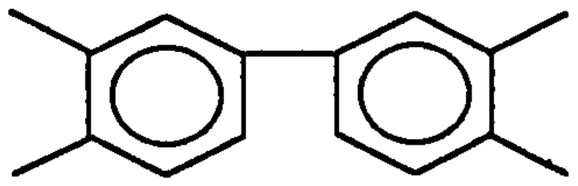

BPDA

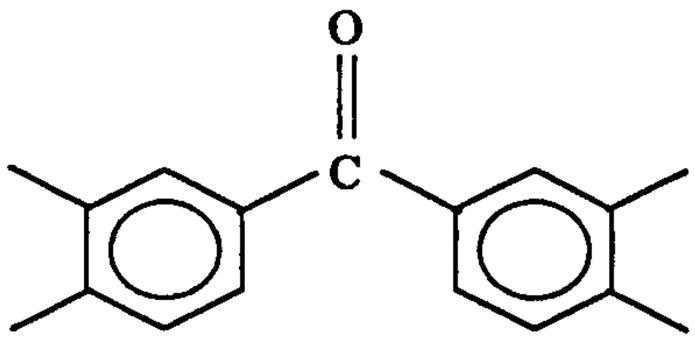

BTDA

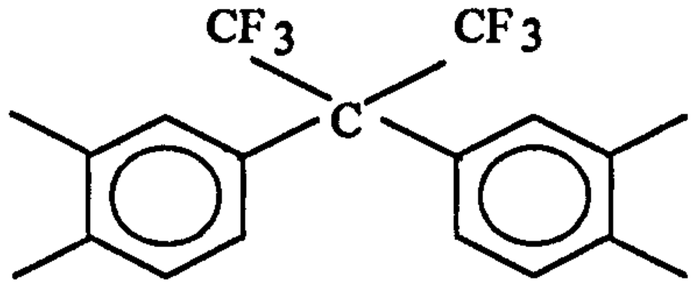

6FDA

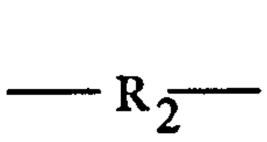

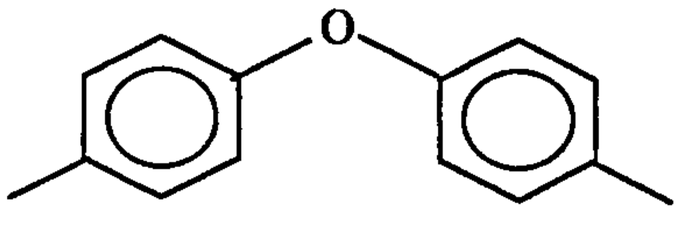

PP'-ODA

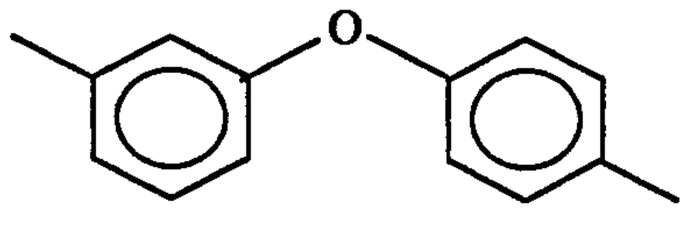

mP'-ODA

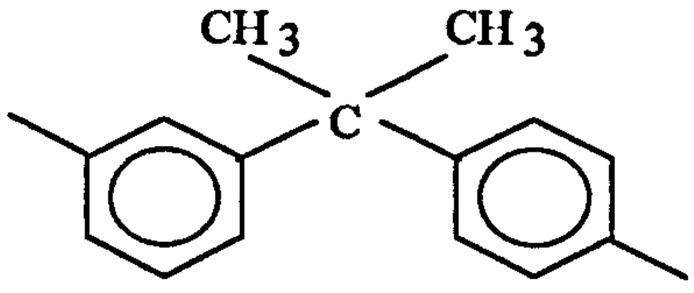

APAP

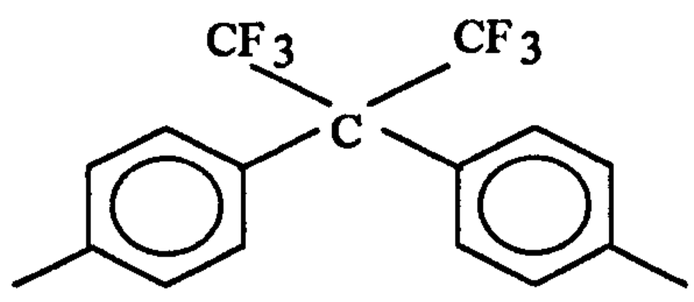

BAHF

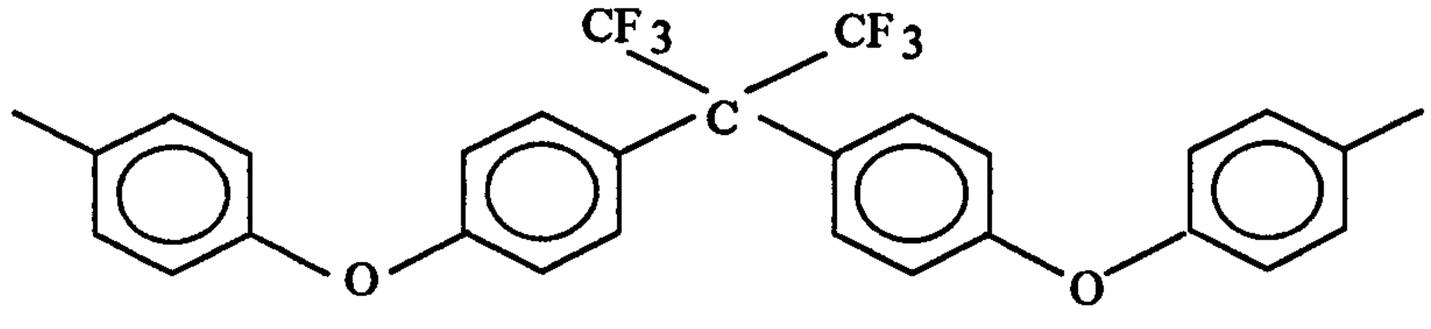

BAPHF

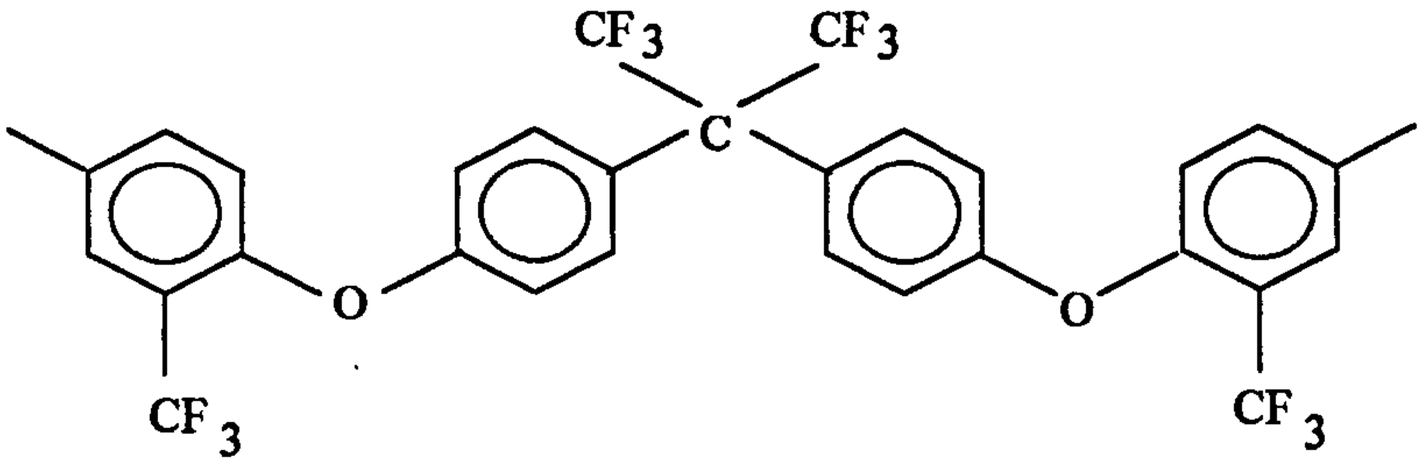

BATPHF

Scheme 1.3 Structures of dianhydride and diamine moieties in some fluorinated and nonfluorinated polyimides[64]

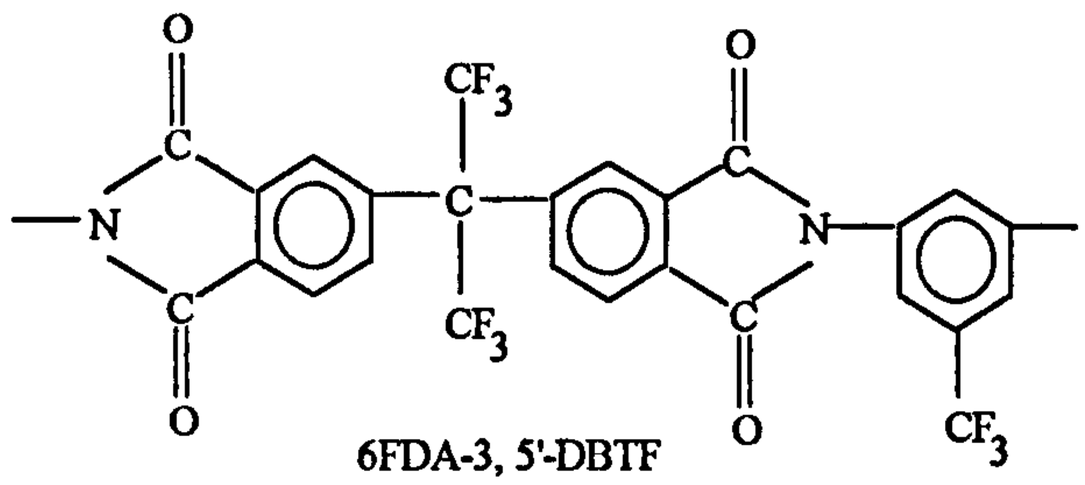

6FDA-3, 5'-DBTF

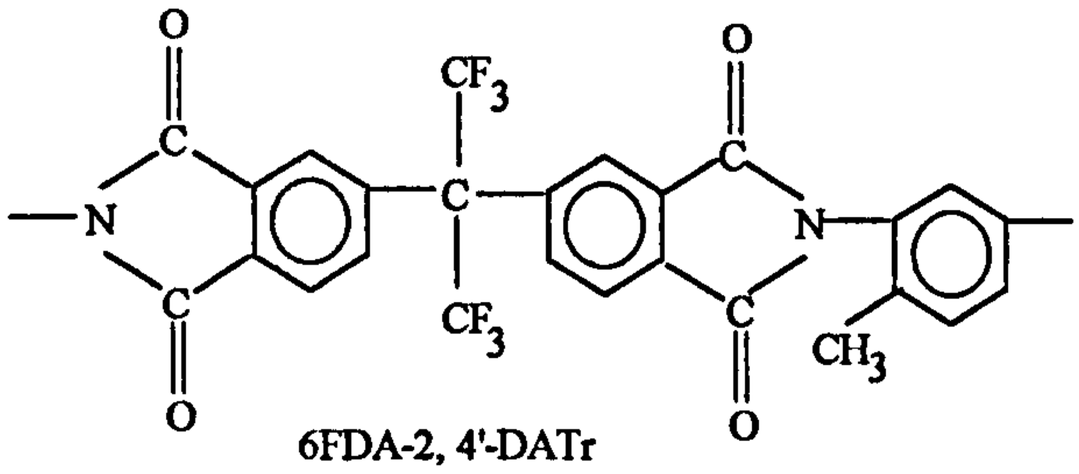

6FDA-2, 4'-DATr

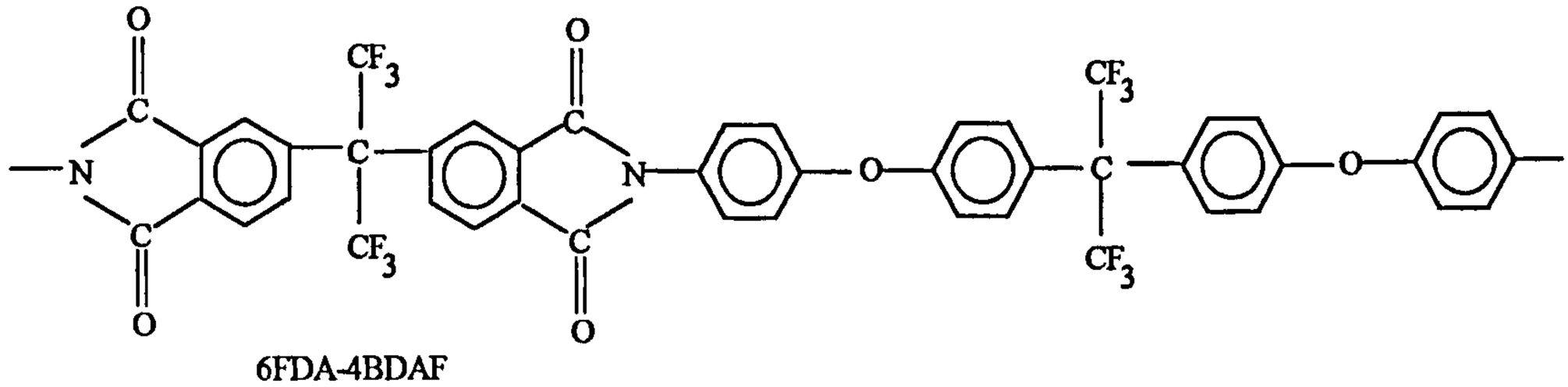

6FDA-4BDAF

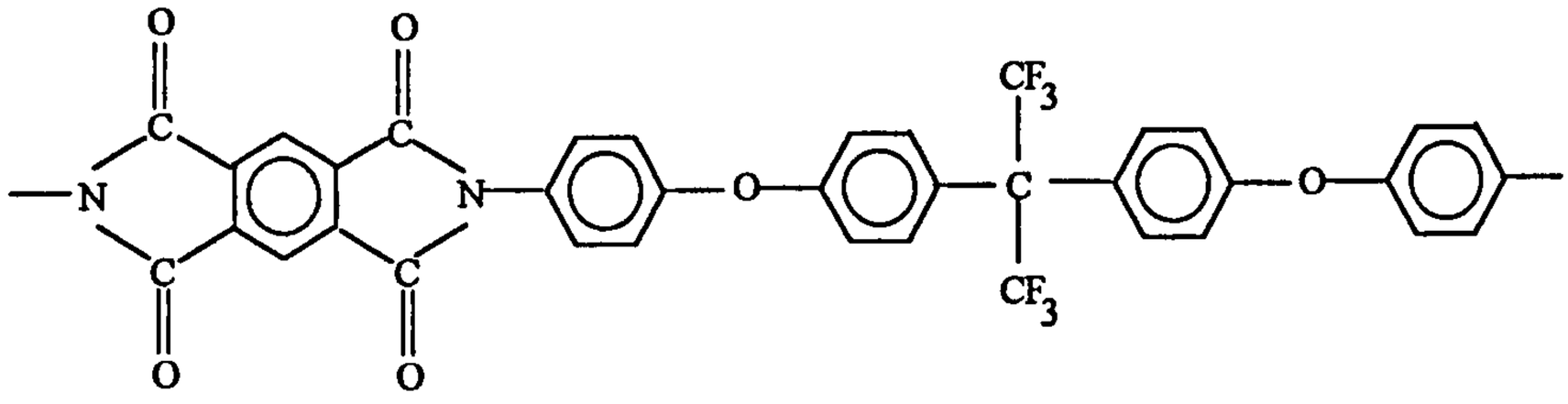

PMDA-4BDAF

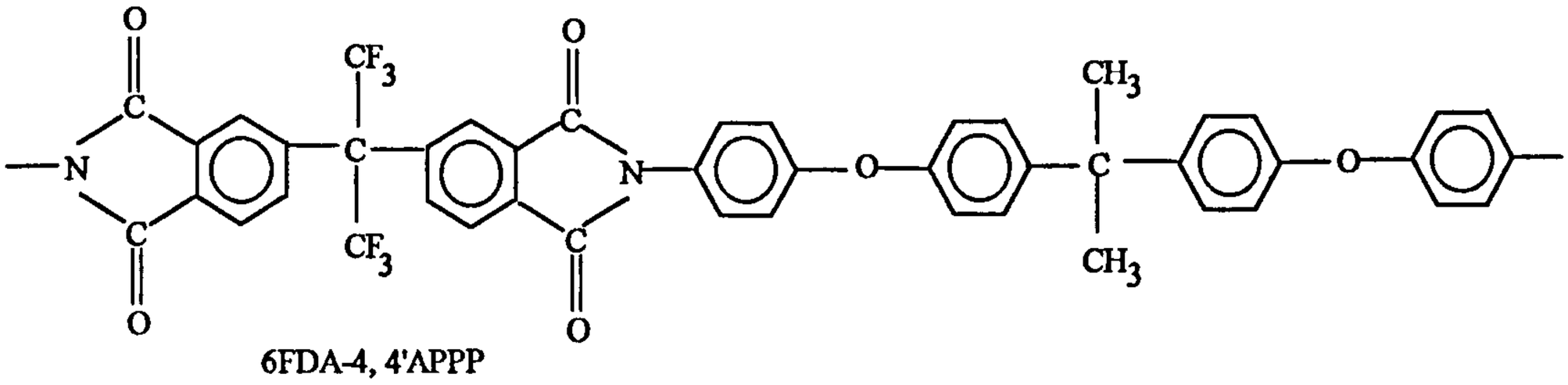

6FDA-4, 4'APPP

Scheme 1.4. Structure of polyimides with increasingly higher fluorine content and shorter and stiffer diamine moieties (shown from the bottom to the top of the figure)[61]

Although some polyimides offer excellent CO_2/CH_4 separation characteristics, they are generally less well suited for the O_2/N_2 separation due to either poor selectivity or low O_2 permeability. This raises the issue of engineering or "tailoring" a polymer to a specific separation or application because polymers that excel in one particular gas pair separation may not be optimum for other gas pairs.

Although many additional polymers could be cited for interesting structure-property relationships, a notable example of a polymer with outstanding permeability properties must be mentioned here. Polypyrrolone is a "step-ladder" polymer derived from aromatic dianhydrides and aromatic diamines. Permeability, diffusion and solubility coefficients for He, O_2, N_2, CO_2, and CH_4 in polypyrrolone have been determined by Walker and Koros[68]. The permeability (P_{CO_2}=27.6) of the polymer is higher than that of 6FDA-ODA polyimides (P_{CO_2}=23). The overall values of He/CH_4 (164.8) and O_2/N_2 (6.5) selectivities of polypyrrolone are slightly higher than those of 6FDA-ODA (He/CH_4 = 135.4, O_2/N_2 = 5.2), whereas its CO_2/CH_4 (51.1) selectivity is lower than that of 6FDA-ODA (CO_2/CH_2 = 60.5). The structure of this polymer is shown in Scheme 1. 5. Walker and Koros [68] have related qualitatively the differences in the permeability and selectivity of the two polymers to specific structural differences.

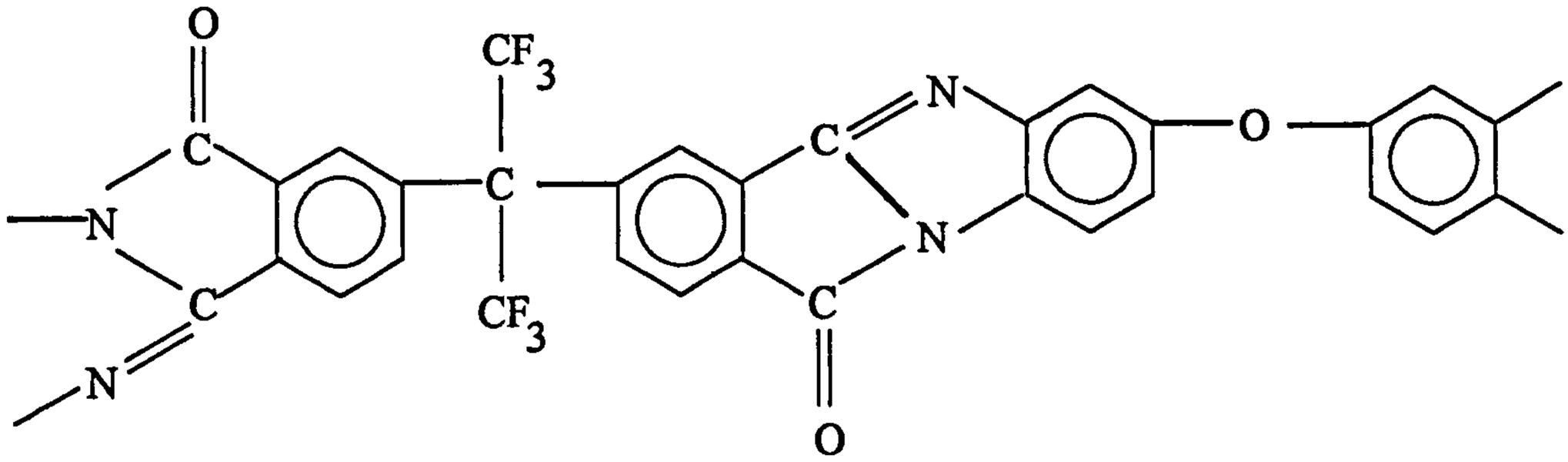

Scheme 1.5 Structure of polypyrrolone[68]

There is another polymer, polyaniline, also worthy of mention here. This polymer has been reported to have remarkable selectivity[69]. The selectivity values of 3590 for H_2/N_2, 30 for O_2/N_2, and 336 for CO_2/CH_4 surpass the highest previously reported values of 313, 16, and 60 for the nonconjugated polymers poly(trifluorochloroethylene), celluose nitrate, and a fluorinated polyimide, respectively. The process for tailoring gas selectivity of a polyaniline membrane involves first enhancing the permeabilities of gases with small diameter (< 3.5 Å) by doping and undoping the polymer film with counterions of an appropriate size. High selectivities are then achieved by decreasing the permeabilities of larger gases (> 3.5 Å diameter) through controlled redoping of the polymer. The permanent morphological changes induced in this conjugated polymer system and others indicate the potential for development of universal membranes for gas separations.

1. 6 Membrane formation

The major hollow fibre membrane formation techniques used in recent times can be grouped into two broad phase inversions: (a) wet phase inversion, (b) dry-jet wet phase inversion. Recently, the most common industrial approach to form membranes for gas separation has involved dry-jet wet phase inversion processes[70 ~ 73]. The wet process has also been recently the most interesting topic described in the literature on membrane structures used for solution diffusion separations.

1. 6. 1 Wet phase inversion process

In the wet phase inversion process, the polymer solution is extruded into a bath containing a liquid miscible with the solvent but not a solvent for the polymer. In this coagulation bath, the polymer is precipitated from the solution, and a solid gel fibre containing considerable amounts of solvent and precipitating agent is formed. This process can be rationalised by the phase diagram. The information from the phase diagram, and the rate of precipitation of the polymer solution have been combined to explain the membrane structure. The phase diagram gives the relationship between the compositions of the solid (polymer-rich) and the liquid (polymer-poor) phases during precipitation. However, the phase diagram is only a thermodynamic description of the overall phase distribution at equilibrium.

The Flory-Huggins theory can be used to explain the thermodynamic stability of a ternary membrane forming system[74]. A typical isothermal ternary phase diagram is shown in Fig. 1.4. The diagram shows (1) the stable region, (2) the metastable region, located between the binodal and the spinodal boundaries, and (3) the unstable region. The binodal and spinodal coincide at the critical point "CP". For most high

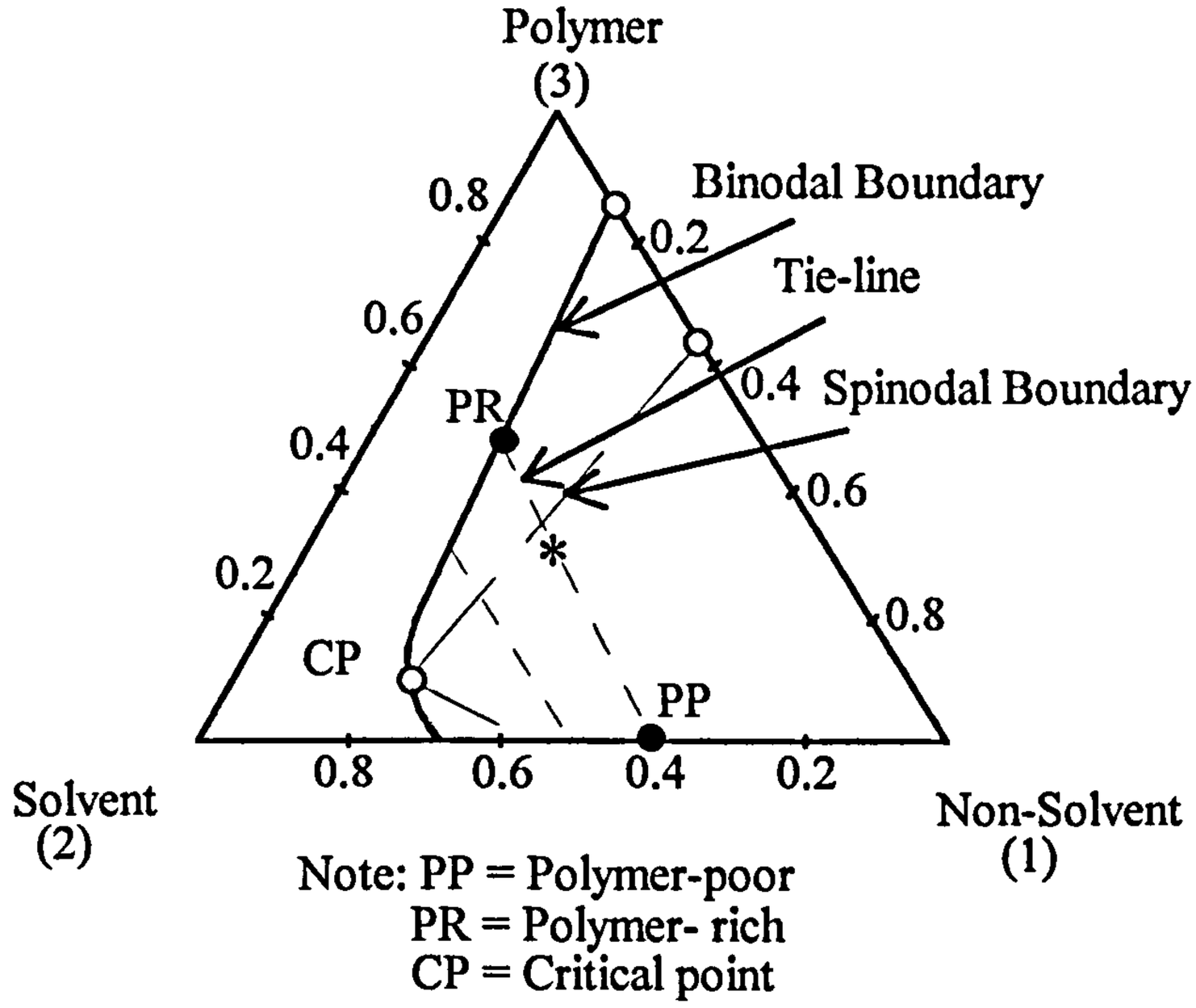

Fig 1. 4 Schematic representation of the ternary phase diagram for a membrane forming system[74]

molecular weight polymers ($\overline{M}$w >10^4 g/mol) the critical point is located at polymer concentration of 5 vol.% or less. The tie-lines are connecting equilibrium polymer-rich "PR" and polymer-poor "PP" points. A phase separation process is occurring at a point represented by * anywhere within the two-phase boundaries along the indicated tie lines. The composition of the two phases is defined by the tie lines and in relative proportions given by the position of the point * relative to the two phases boundaries at "PR" and "PP". As the composition of the mixture point at * approaches the "PR" point, the relative amount of the phase-separated polymer-rich fraction increases.

If the local mixture composition * lies in either of the regions between the outer binodal boundary and the spinodal boundary, a two-phase structure forms by the generation of a nucleus of the 'dispersed phase'. This nucleus grows to larger and larger size and eventually intersects other similarly growing structures to produce interconnectivity. This is said to be a nucleation and growth process, by its nature

producing either polymer-rich phase dispersed in a polymer-poor matrix (for low polymer concentrations relative to the critical point, CP) or polymer-poor phase dispersed in polymer-rich matrix (for higher polymer concentrations relative to the critical point, CP). Thus, at lower polymer concentrations, nucleation and growth of polymer-rich phase leads to polymer powder or low integrity polymer agglomerates. Nucleation and growth of the polymer-poor phase at rather higher polymer concentration in the upper metastable region results in a more or less closed cell morphology. It is generally believed that the microporous substructure of asymmetric membranes originates from nucleation and growth of the polymer-poor phase[75, 76].

Unlike the metastable region where nucleation and growth processes dominate, if the point * achieves a composition within the spinodal region, bounded by the dashed line in Fig. 1. 4, the corresponding phase separation process is determined by the spinodal mechanism. This phase separation proceeds instantaneously and results initially in a regular, highly interconnected structure that tends to coarsen during later stages of spinodal decomposition. The spinodal decomposition results in a regular, highly interconnected structure which has been proposed to form the skin layer[77], as well as the substructure[78] of asymmetric membranes. The phase diagram, as shown in Fig 1.4, is the thermodynamic description of the system in equilibrium determining the overall phase distribution. However, the actual membrane structure is determined by kinetic parameters[79].

Strathmann[79] used the schematic phase diagram in Fig. 1.5 to describe the precipitation pathway of the casting solution during membrane formation. During membrane formation, the system changes from a composition A, which represents the initial casting solution composition, to a composition C, which represents the final

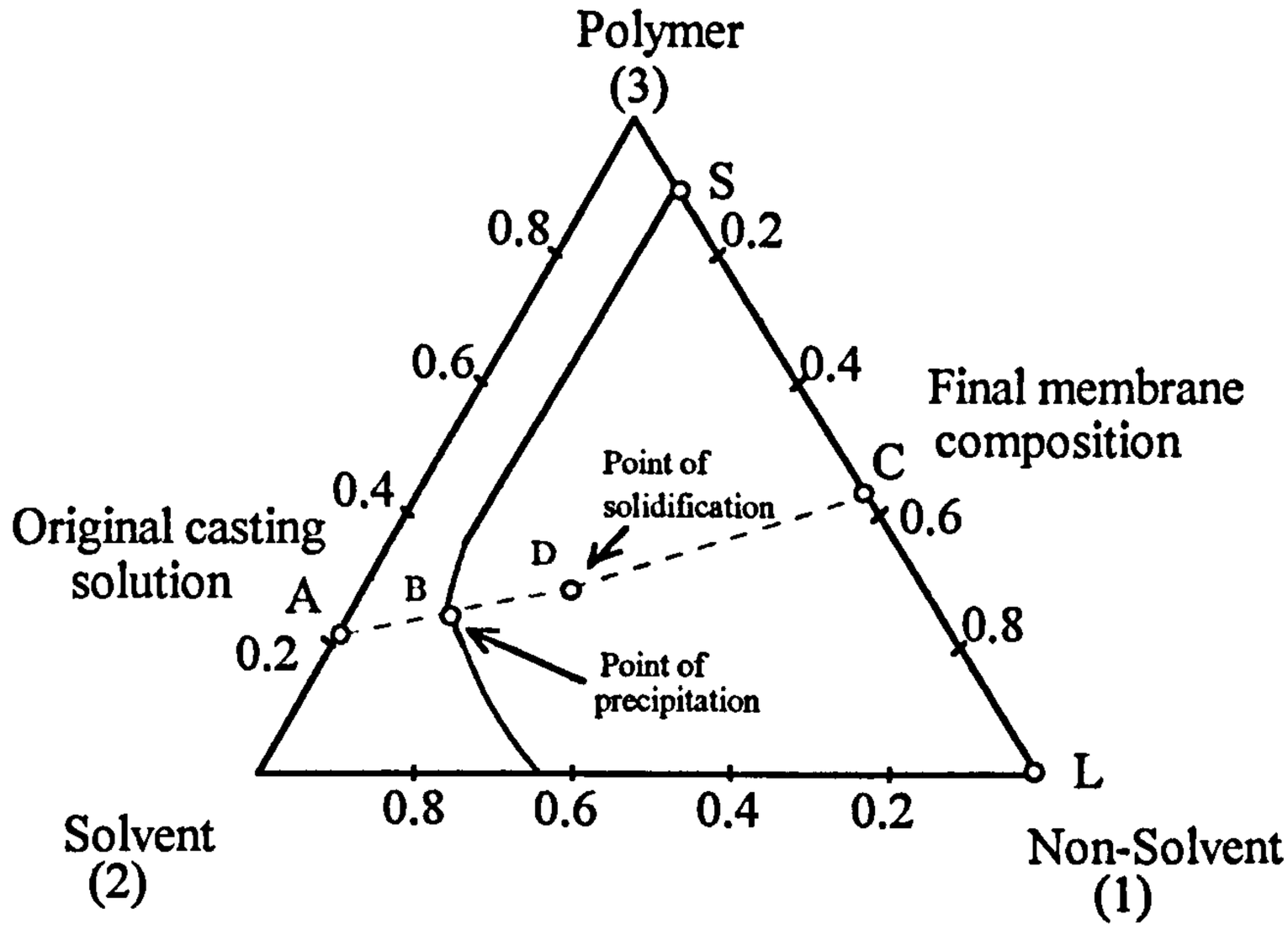

Fig. 1.5 Schematic ternary phase diagram of showing the precipitation pathway of the casting solution during membrane formation[79]

membrane composition. At the composition C, two phases are in equilibrium, a solid (polymer-rich) phase which forms the final membrane structure, represented by point S, and a liquid (polymer-poor) phase which constitutes the point L. The position C on the line S-L determines the overall porosity of the membrane. The entire precipitation process is thus represented by the path A to C, during which the solvent is exchanged by the precipitant. The point B along the path is the composition at which the first polymer precipitates. As precipitation proceeds, more solvent is lost and precipitant is imbibed by the polymer-rich phase, and the viscosity rises. At some point the viscosity is high enough for the precipitated polymer to be regarded as a solid. This composition is shown as D in Fig. 1.5. Once the precipitated polymer solidifies, further bulk movement of the polymer is hindered. Volume changes produced by further solvent-precipitant exchange, produce stress in the polymer. The overall polymer-precipitant system shrinks or expands depending upon whether precipitant uptake is less than or greater that solvent loss, i.e. on the position of line A-C. However, the polymer-rich phase always shrinks because the casting solution is

typically 15~23% solid (point A), whereas the final polymer-rich phase is typically 80~90% solid (point S).

1. 6. 2 Dry-jet wet phase inversion process

In some dry-jet wet phase inversion processes, liquid-liquid phase separation in the outer-most layer of the membrane structure is induced by solvent evaporation; the bulk of the membrane structure is subsequently formed by solvent-nonsolvent exchange during a quench step.

To obtain evaporation induced phase separation in the cast membrane (dry phase inversion), the casting formulations must be altered to include sufficient volatile solvent and non-volatile nonsolvent to cause the nascent membrane to be essentially at the point of incipient phase instability as shown in Fig. 1.6. During the evaporation-induced dry stage of the process, a gas stream passes over a properly formulated casting solution having a starting composition at A, almost at the binodal boundary. Sufficient volatile solvent is lost to convert the outside few micrometers of the nascent membrane into a spinodally decomposed structure with an average composition such as A" shown in Fig. 1.6. This process becomes apparent instantaneously by the formation of a fine haze on the surface of the nascent membrane[80]. Although the occurrence of the dry phase inversion step is extremely important for achieving pore-free skin layers, the exact thickness of the dry phase separated structure appears to be second-order importance in the generation of the effective dense skin-layer thickness. This observation provides insight into the process and its most important elements.

If the spinodal structure in the outermost membrane region vitrifies instantaneously during the following quench step (wet phase inversion), it appears logical that the skin layer of the quenched membranes will be microporous. These pores would

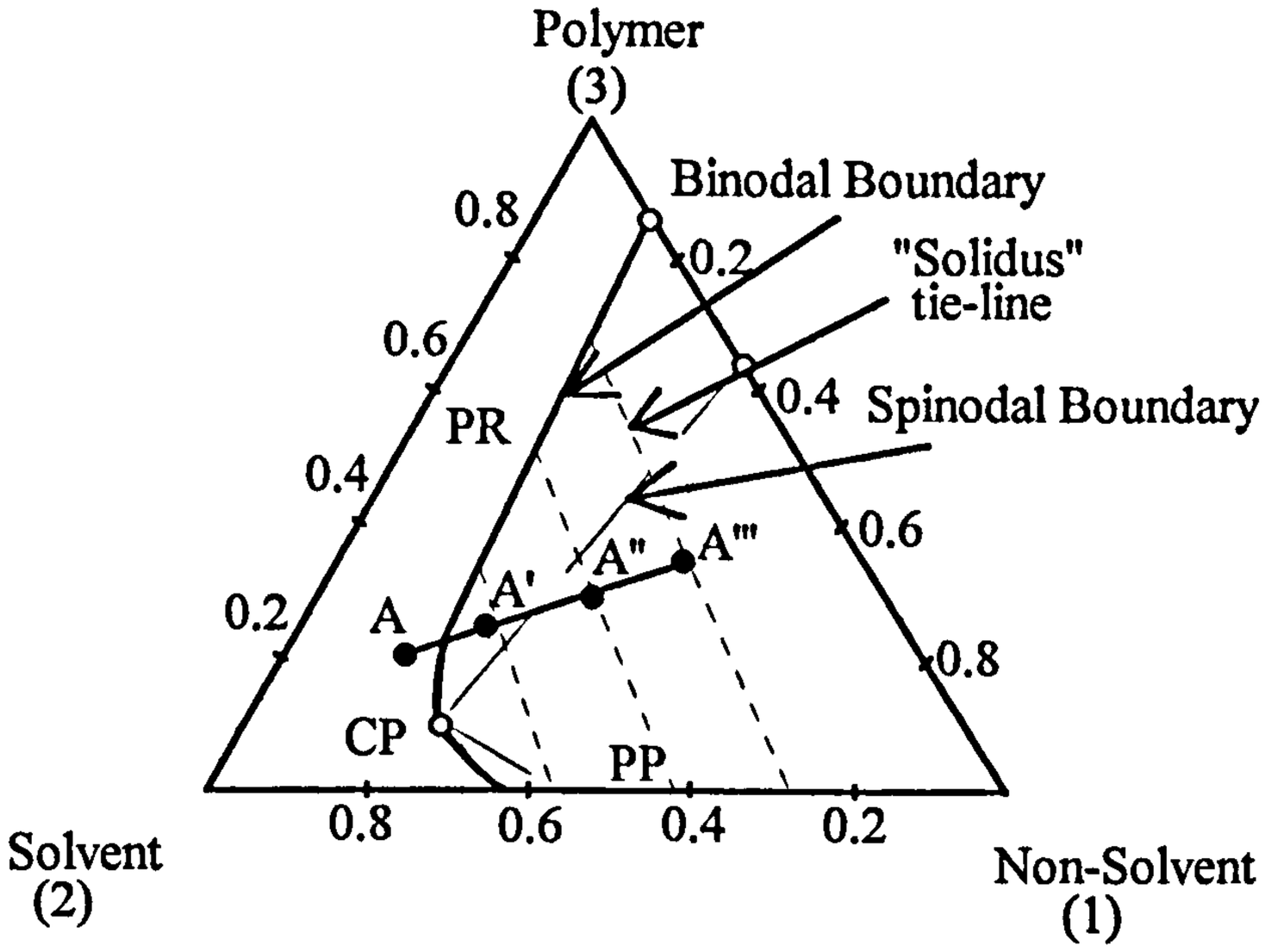

Fig. 1.6. Schematic representation of diffusion paths initiating near the binodal boundary and potentially penetrating to the metastable (nucleation and growth) region (A'), the unstable (spinodal decomposition) region (A") or the "Solidus tie-line" (A''') where phase separation yields a morphology that is vitrified immediately upon phase separation and which is unable to evolve[74].

result from the interstitial spaces of the polymer-poor phase present in the outermost region of the quenched membrane at the point of vitrification. On the other hand, gas permeation experiments have demonstrated that optimised membranes formed by dry-jet wet phase inversion can show ultrathin and defect-free skin layers[80]. Hence, it has been suggested that an additional physical process leads to the coalescence of the surface network into an essentially homogeneous skin layer during the evaporation step. More details about the coalescence process have been discussed[74].

1. 7 Recent developments for asymmetric hollow fibre membranes for gas separation

The development of the asymmetric skin type of hollow fibre membranes for gas separation has received considerable interest. The work is based on the advances in both polymeric membrane materials and the membrane fabrication processing. Recently, many new materials with better separation characteristics, i.e. permeability and selectivity, have been invented such as tetramethyl ring-substituted polycarbonates, polysulphone and hexafluoro modified polyimides[54, 62, 63]. Since most high selectivity polymers have low permeabilities, a useful hollow fibre membrane formed from such a kind of polymer requires an ultrathin dense skin layer on the top of a much more porous sublayer. If there had been no breakthrough in spinning asymmetric hollow fibres with a thin dense skin layer, and a porous substructure, the high separation performance of these polymers would have very limited applications. The credit must be given to Monsanto[70, 81] for this breakthrough in manufacturing asymmetric hollow fibre membranes for gas separation.

During the dry-jet wet spinning process, precipitation of polymer can be initiated from inside and outside of the hollow fibre. Although the mechanism of membrane structure formation via polymer precipitation has been investigated, it is still not easy to spin a hollow fibre with an ultrathin dense skin layer on the top of a porous sublayer, with the required pore size distribution, especially for a new polymer material. This is due to the fact that many factors are involved in the fibre spinning process. Table 1. 4 shows these factors and their effect on the fibre morphology[82].

The technologies for producing asymmetric membranes were extensions of the Loeb-Sourirajan technique[15] developed for reverse osmosis (RO) application. The

Table 1.4 Factors affecting fibre morphology[82]

Factors	Effects
Molecular sizes of solvents	Solvent exchange rate
Solubility differences	Coagulation rate
Gravitation force	Orientation and defects
Solid content	Fibre morphology and defects
Core solvent speed/viscosity	Finger void structure/layer
Temperature	Affects all the above parameters

principle of forming hollow fibres and flat sheets by a phase inversion process is similar, even though there are some differences between them in the fabrication process. The major difference between the fabrication of asymmetric hollow fibres and flat sheet membranes is that, in the former, two coagulation surfaces are forming in the spinning process (internal and external surfaces), while there is only one coagulation surface for an asymmetric flat sheet membrane. Usually, in the fabrication of hollow fibre membranes, water or a solvent-nonsolvent mixture is used as an internal coagulant and the coagulation process begins first at the inner surface of the fibre immediately after passing through a small air-gap. The external coagulation takes place in the coagulation bath. As a matter of fact, it was claimed to be unreliable to produce hollow fibre spinning by using the same process conditions developed for the fabrication of an asymmetric flat sheet membrane[82], but it is still very useful to use the fabrication conditions of flat sheet membranes as a rough guide to predict the structure of as spun hollow fibres.

The formation mechanism of the asymmetric flat sheet membrane has been investigated by Strathmann[79] and Smolders[83]. Exchange of solvent and

nonsolvent across the interface during the phase separation can lead to a variety of characteristic asymmetric structures.

To explain membrane skin formation, it has been suggested that the skin layer is formed by an increase in the concentration of polymer in the surface layer of the solution caused by evaporation[84]. This explanation has been widely accepted in the dry-jet wet spinning process. However, it does not explain the existence of skinned membranes formed when no evaporation occurs. Strathmann[79] proposed that the polymer layer which precipitated during the first few microseconds at the upper-most surface of the membrane would not be able to coagulate and separate into two phases before a solid gel was formed. The layer of polymer thus formed had a homogenous structure which would then uniformly densify by simple syneresis.

Macrovoids often appear in the structure of flat sheet and hollow fibre membranes. Understanding the formation mechanism of macrovoids has meant that macrovoids are now under control in membrane production. Although there are several theories for the formation of macrovoids, the formation process can be divided into two steps[83]. One is the initiation of macrovoids; the second is their growth. Many research workers[79, 85 ~ 87] suggest that the initiation of the voids is caused by interfacial phenomena because the onset of the formation of macrovoids often occurs at the interfacial boundary between the immersed solution film and the coagulation bath. Surface tension gradients as the driving force which accounts for the initiation of convection cells at the interface of the film has been proposed by Matz[86], Frommer and Messalam[85]. Strathmann et al[79] and Graig et al[87] suggested that mechanical stresses cause rupture of the thin top layer, which is formed immediately after immersion of the solution film. These rupture points form the initiation points for the macrovoids. However, macrovoid formation sometimes starts at a large distance from the interface between the solution film and the coagulation bath, as observed by Smolders[83]. He agreed with Grobe et al[88], who proposed that the

nucleation and growth of polymer-poor phase was responsible for the initiation of macrovoids.

The growth of macrovoids is dependent on different driving forces which can be introduced by interfacial tension variation[85] and shrinkage[79] or collapse phenomena[76]. After observing that macrovoids can start at a distance from the interface between the solution film and the coagulation bath, Smolders[83] suggested that the driving force induced by interfacial tension variation is not the only process to form macrovoids. The propagation of macrovoids might occur independently from the interfacial tension variation.

The formation of macrovoids in the hollow fibre membranes prepared from a polymer-solvent-nonsolvent system can be suppressed or even eliminated by choosing an appropriate solvent-nonsolvent pair, increasing the polymer concentration and the viscosity in the spinning solution[89], and by addition of solvent to the coagulation bath[90].

Since most of the factors, such as solvent and nonsolvent exchange rate, solubility parameter and dope rheology, are a function of temperature, the temperature at the spinneret and the coagulation bath temperature significantly affect the fibre morphology and mechanical properties, and the gas separation properties which have been observed[82].

Generally speaking, an increase in temperature decreases the viscosity of the spinning solution, but increases the solvent and nonsolvent exchange rates and the solubility. Such combined effects tend to produce a more porous structured membrane with increased permeation rates. In the dry-jet wet spinning process, the temperature surrounding the air-gap or spinneret can result in the early evaporation of the solvent to form a dense skin layer. Similarly, the introduction of vapours of solvent and

moisture in the air-gap can initiate the phase inversion process earlier at the outer surface of the fibre, which again results in the formation of a dense skin layer. In the subsequent solvent exchange, and washing and drying processes, hollow fibres come under different elongation stresses due to removal of the solvents and these stresses thereby cause two effects: they may either initiate crack propagation in both the inner and outer surfaces or induce chain orientation[82]. During the drying process, the fibre will undergo densification which can be advantageous or disadvantageous depending on its extent. Excessive densification is commonly encountered with polar, and hence hydrophilic, polymers where polymer-water interaction is almost as strong as the surface tension of water[89].

However, drying can be effected with minimum loss of porosity by using two drying methods. One is the solvent exchange drying method: i.e., sequentially replacing water with liquids of lower surface tension, first with a mixture of water and an miscible organic nonsolvent, and second with a volatile nonpolar nonsolvent such as hexane, followed by drying. Another one is incorporating a nonsolvent with a high boiling point (bp>150°C) such as decane, or butyl ether into the spinning or casting solution so that water will leave the membrane prior to the departure of the hydrocarbon nonsolvent[91]. Using these drying methods with cellulose acetate membranes, gas separation factors and permeation rates have been significantly increased[92]. The solvent exchange drying method has been used for drying PAN hollow fibre; the changes in mean pore size diameter and gas permeation rate have been observed in this present study, and detailed results are described in section 4. 3. 2.

Another two important breakthroughs in the fabrication of hollow fibres should be mentioned here. One is the development of second generation PSF hollow fibre membranes for gas separation by Monsanto[93]. Another one is the development of

a dual bath coagulation method for the preparation of asymmetric PES hollow fibre membranes for gas separation by van't Hof and his co-workers[94].

The development of the second generation asymmetric hollow fibre membranes for gas separation described by Monsanto in 1990 is based on an increased free volume, and is explained by a "transient template" theory[95]. For polymeric membrane materials, linear macromolecules can be considered as long spaghetti-like cylinders whose diameters increase in the regions where axial side-chain groups are present. Such groups are, in effect, permanent templates which determine both packing density and the regularity of interchain displacement. Although the introduction of different side-chain groups to the bulk polymer is possible by synthesising new polymers, it is often accompanied by increased costs of materials, and possibly some problems of poorer processing and mechanical properties.

Considering these disadvantages, Kesting and his co-workers[95] have argued for the use of commercially available polymers together with a solvent layer that sheaths the macromolecules in the nascent membrane. This solvent layer acts as a "transient template" to control macromolecule packing density in the final membrane. The larger the solvent entity, the thicker will be the solvent layer that surrounds the macromolecules in a sol. Once gelation has occurred, rapid and complete removal of this solvent layer from the gel results in the incorporation of a higher level of free volume in the final membrane. After successful use of Lewis acid:base complexes (i.e., propionic acid:NMP) as transient templates, the second generation of polysulphone gas separation membranes showed a fourfold increase in oxygen permeability with no loss in oxygen/nitrogen selectivity[93]. The enhanced gas permeation performance in the second generation of PSF hollow fibre membranes is the result of the membranes' skin layer being not only very thin, but also of increased free volume and with a graded density.

A dual bath coagulation method is an additional interesting quenching method[94]. By this method, defect-free selective layers can be formed; however, the layers could be thicker than by a single bath coagulation system. This new dual bath coagulation system involves two quench processes. In the first process, the cast polymer solution or nascent fibre contacts a nonsolvent in the first bath for a very short time (e.g 0.7 sec.). The nonsolvent in the first coagulation bath has a low interaction with the solvent in the dope. During this time, a thin concentrated polymer layer is formed at the interface while the underlying region is effectively unchanged. In the second process, the fibre is immersed in the second coagulation bath, containing a strong nonsolvent. Upon immersion in the second bath, instantaneous demixing occurs in the underlying region to produce a highly open porous support for a defect free skin that develops if the thin concentrated surface layer reaches its gelled state prior to undergoing phase separation. According to the results obtained by van't Hof et al[94], the asymmetric polyethersulphone (PES) hollow fibre membranes prepared from the dope containing 35 wt% PES in NMP/glycerol (9:1) solvent mixture, coagulated in glycerol (or 1-pentanol) and water as the first and second coagulants, respectively, showed a much higher separation factor α_{CO_2/CH_4} of 50 ~ 55 without any additional coating.

As the results from the above two developments show, these improvements make it possible to increase the gas permeability and the selectivity of a polymer by changing the physical structure of the hollow fibre membrane.

1. 8 Gas separation processes in industrial applications

Gas separation processes are fundamental processes of separation and purification used in the chemical industry. Since Monsanto successfully moved into the hydrogen and petrochemical purge stream recovery application in the early 1980's, a blossoming of scientific membrane development programs has occurred in several companies in the US, Japan and Europe. About 50 years ago, Weller and Steiner[96] considered membrane processes for the separation of hydrogen from hydrogenation tail gas, enrichment of refinery gas, air separation, and helium recovery from natural gas.

Gas separation membranes have been used in a wide variety of application areas, as shown in Table 1.5[97]. However, commercial membranes capable of performing these separations economically have only become available within the last 15 years. The list of commercial scale membrane suppliers in Table 1.6 shows their scale of activity in membranes for gas separation. This list contains 20 suppliers, which is to be expected with any newly emergent, exciting technology. With the development of membrane science and technology, the final winners in this membrane competition will be those companies that have consistently supported research and development.

Gas separation membranes have to compete with the traditional gas separation technologies such as cryogenics, pressure swing adsorption and absorption (PSA), as illustrated by Maclean[98] who lists a separation technology comparison. Table 1.7 shows the advantage and disadvantages of each separation technology.

Table 1.5 Gas separation membrane usage[97]

Gas mixture	Application
H_2/N_2	Hydrogen recovery from purge streams in ammonia plant.
H_2/CO	Hydrogen ratio adjustment in synthesis gas.
H_2/Hydrocarbons	Hydrogen recovery from hydrogenation process.
CO_2/Hydrocarbons	Acid gas treatment and landfill gas upgrading.
H_2O/Hydrocarbons	Natural gas dehydration.
O_2/N_2	Oxygen enriched air and nitrogen blanketing.
He/N_2	Helium recovery.
He/hydrocarbons	Helium separation.
Hydrocarbons/Air	Hydrocarbon recovery and pollution control.
H_2O/Air	Air dehumidification.
H_2S/Hydrocarbons	Sour gas treatment.

For general economic considerations, the membrane systems also have many other advantages over the traditional technologies, especially in low capital investment, ease of operation, as well as being light weight and compact in nature. A comparison between the membrane and traditional processes in hydrogen recovery is illustrated in Table 1. 8. As the results show, the membrane system is competitive with PSA and cryogenic separation technologies over a wide range of operating conditions.

However, in a recent review Spillman[97] pointed out that a comparison of costs between membrane and traditional technologies seems to be quite difficult for the follow reasons: (a) the operation conditions are different from each other, and (b) the improvement in the performance of membrane-based systems and competition between the membrane suppliers changes the cost of production. In a single stage

Table 1.6 A list of companies supplying commercial membranes for industrial gas separations[97]

Company Name	CO_2	H_2	O_2	N_2	Others[a]
A/C Technology(AVIR)	X		X	X	
Asahi Glass(HISEP)			X	X	
Cynara(DOW)	X				
Dow(Generon)			X	X	
Du Pont/L, Air Liquid(MEDAL)		X		X	
Grace Membrane Systems	X	X			X
Hoechst-Celanese(Separex)	X	X			X
International Permeation	X				X
Membrane Technology & Research					X
Nippon Koan K.K.					X
Osaka Gas			X		
Oxygen Enrichment Co.			X		
Permea Pure					X
Permea(Air Product)	X	X	X	X	X
Techmashexport(USSR)			X		
Tejin Ltd.			X		
Toyobo			X		
Ube Industries		X	X	X	X
Union Carbide(Linde)	X	X	X		
UPO/Union Carbide	X				

a: Includes solvent recovery, dehumidification, and/or helium recovery membranes

Table 1.7. Separation technology comparison[98]

Technology	Advantage	Disadvantage
Cryogenics	high purity low energy high recovery	high capital complex integration
PSA[a]	medium high purity low capital low energy	lower recovery single product
Membrane	flexibility high working pressure simple high recoveries	medium purity possible recompression required of permeate
Absorption	removal of acid gas to ppm levels	high partial pressure required for physical solvent and chemical solvent

a: PSA is presure swing adsorption and absorption

Table 1.8 A comparison between the membrane and traditional process in H_2 recovery[99]

	Membrane	PSA	Cryogenics
Relative investment	1	1 to 3	2 to 3
Maximum operating pressure(psi)	2000	600	1000
Minimum hydrogen content in feed(%)	15 to 20	50	20
Maximum hydrogen purity(%)	99	99.999	98.5
Maximum hydrogen recovery(%)	95	85	95
Product pressure/feed pressure	Lower	Same	Same
Fractionation of heavies	No	No	Yes
Modularity	Yes	No	No
Ease of operation	Very easy	Average	Average

membrane based gas separation process, the product recovery can only be increased at the expense of product purity. However, higher product purity and recoveries can be both achieved by using multiple membrane stages, but this leads to increases in the capital investment of gas separation membrane systems. For both single- and multiple-stage membrane processes, customers are always looking for the most cost-effective solution for their problem, while the membrane suppliers has to provide cost estimates based on the membrane cost and performance properties. In order to provide the customer with the lowest cost process to achieve the desired separation,

some membrane suppliers also make non-membrane technologies. Nevertheless, the present rising trend of membrane-based gas separations is expected gradually to replace most of these traditional gas separation processes.

1. 9 Scope of present investigation

Polysulphone hollow fibre membranes for gas separation have been systematically investigated by Rogers, Senn[100], Brown[101] and Deshmukh[102] in the Department of Textile Industries. After this work on the fabrication of asymmetric polysulphone hollow fibres and the improvement of gas separation performance of the membranes, it was proposed to investigate the possibility of using commercially available polyacrylonitrile (PAN) for gas separation hollow fibre membranes. The main task of this work was to search for conditions to fabricate asymmetric PAN hollow fibres and to evaluate the gas separation performance of such PAN hollow fibre membranes. Apart from these objectives, problems encountered during this study were also investigated.

CHAPTER 2

EXPERIMENTAL

2. 1 Materials

2. 1. 1 Membrane forming polymer

The polyacrylonitrile co-polymer used in this study was obtained from Courtaulds in the form of "Courtelle" (15.0 dtex/filament in tow form) and was redissolved in DMF. The components of the polymer were assumed to be as shown in Scheme 2. 1.

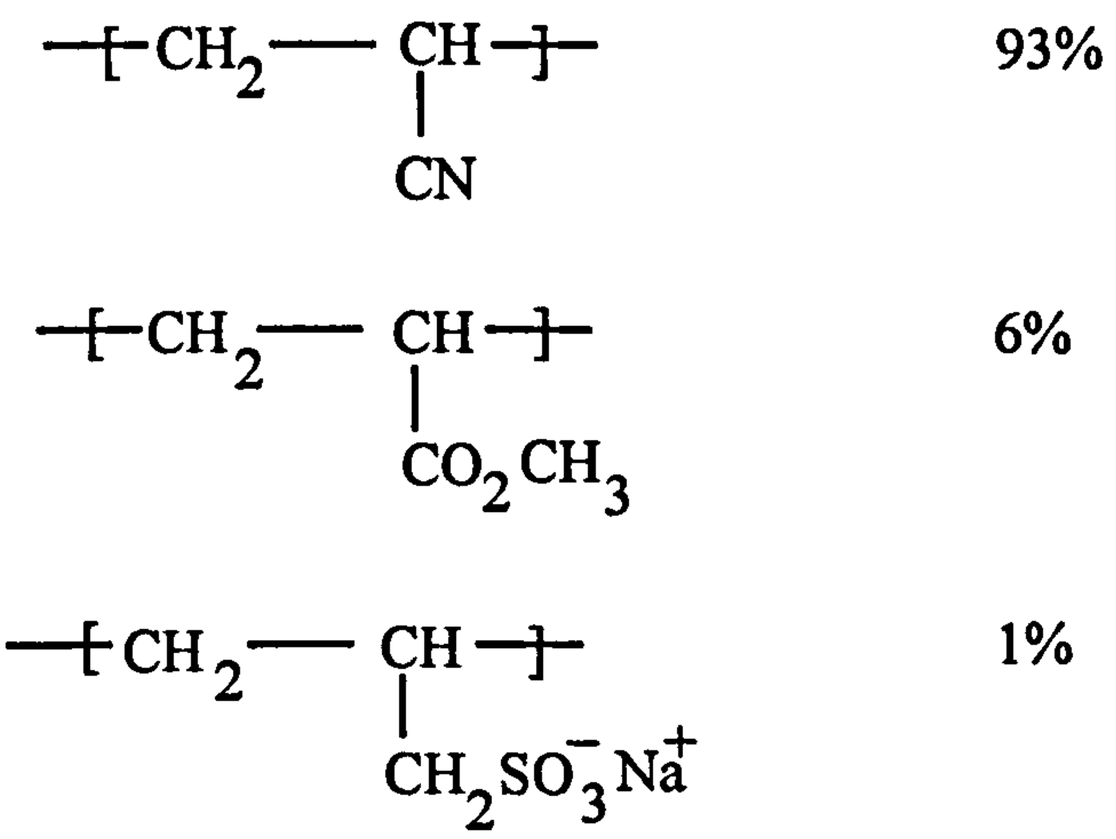

Scheme: 2.1 The chemical components of "Courtelle" polyacrylonitrile

Some polyacrylonitrile homopolymer was used to compare with the co-polymer, which was obtained from Bayer in the form of "Dralon T 100 glzd" (2.4 dtex/60 mm staple fibre).

2. 1. 2 Solvents, nonsolvents and additives for film and hollow fibre fabrication

N,N-dimethylformamide (DMF), N-methyl-2-pyrrolidinone (NMP), 1-Formyl-piperidine obtained from (BDH), were used as solvents in the film casting and hollow fibre spinning solutions. Formamide (BDH), glycerol (Hopkin and Williams Ltd.) and some inorganic salts were used as nonsolvents and additives to the casting and

the spinning solutions. The solvents, nonsolvents and additives were used without further purification.

2. 1. 3 Fibre mounting adhesive

The adhesive used for mounting the hollow fibres in module form was Quick Set Epoxy Adhesive (contained epoxy resin and epoxy hardener) which was obtained from RS components; epoxy putty was also supplied by RS components.

2. 1. 4 Dip coating materials

The coating material was used for sealing the defects on the surface of the hollow fibres. Sylgard 184 (Dow Corning) and the supplied curing agent were used as the coating materials, which were dissolved in 2-methylbutane (BDH).

2. 1. 5 Permeant test gases

The test gases such as H_2, CH_4 and CO_2 were supplied by BOC industrial gases. These gases were used for gas transport measurements on the permeation test rig without further purification. Table 2. 1 shows the purity of these gases.

2. 1. 6 Other chemicals used

Table 2.2 shows the other chemicals used in fabrication and post-treatment of hollow fibres.

Table 2.1 Purity of the test gases[102]

Gases	Purity	Impurities
H_2	99.99%	O_2 10 ppm
		N_2 100 ppm
		H_2O 100 ppm
		CO, CO_2 + hydrocarbons<6 ppm
CH_4	C.P.>99%	N_2 + Ar 0.8%
		O_2 1 ppm
		CO_2 1 ppm
		H_2 2 ppm
		H_2O 2 ppm
CO_2	>99.995%	KOH in Sol^n < 100 ppm
		hydrocarbons < 10 ppm
		Oil < 2 ppm
		halogens < 5 ppm
		Sulphur < 5 ppm
		CO < 1 ppm
		H_2O < 25 ppm
N_2	OFN	H_2O < 10 ppm
		O_2 < 10 ppm

Table 2.2 Chemicals used in fabrication and post-treatment of hollow fibres

Chemicals	Source
Hydroxylamine hydrochloride:	May & Baker Ltd
Sodium Carbonate:	BDH
Cuprammonium hydroxide:	Vickers Laboratories
Dichloromethane:	BDH
$CuSO_4$ $5H_2O$:	Vickers Laboratories
Ethylene diaminetetra-acetic acid (EDTA)	BDH
$NaCO_3$	BDH
CuCl:	Aldrich
LiCl:	Aldrich
$ZnCl_2$:	Aldrich
Hexane	Aldrich
Isopropanol	Aldrich
Propionic acid	Aldrich
Fluorotrichloromethane	Lancaster

2. 2 Fabrication processes

2. 2. 1 Solution-cast films

2. 2. 1. 1 Preparation of the casting solution

The selected polymer, "Courtelle" polyacrylonitrile (PAN) (in fibre form) was first washed with dichloromethane in a Soxhlet extractor for six hours in order to remove

the finishing oil on the surface of the fibres, which were then dried in air. The washed PAN fibre was vacuum oven dried at 45°C overnight to remove any water present in the fibre and stored in a desiccator before use.

During the process of preparation of the casting solution, part of the required solvent (i.e. DMF) was first added to a reaction flask containing the PAN fibres in order to swell and dissolve them, the rest of the solvent (mixed with non-solvent, or additive when required) was then poured into the reaction flask. The temperature in the flask was slowly raised to 80°C. The stirrer (Heidolph RZR2 Stirrer) was set to stir the polymer solution. As the dissolution proceeded, the polymer dope viscosity increased and hence the stirrer was set at its higher torque level to maintain the stirring speed. After about six hours of stirring, a homogeneous polymer solution was obtained. Then the solution was subjected to degassing by storing the flask in a hot water or an oil bath overnight to remove the micro bubbles left in the solution; this procedure can avoid any loss of solvent and prevent the formation of a skin layer on the top surface of the solution. Typically, a solution was made using 25g "Courtelle", 70g DMF and 5g $CuSO_4$ $5H_2O$; a homogeneous green coloured solution was obtained.

2. 2. 1. 2 Viscosity measurement

The zero shear rate viscosity of the polymer solutions was measured by a Haake rotary viscometer with sensor system SV I.

2. 2. 1. 3 Film casting

The film casting procedure was developed essentially to allow a quick assessment of particular combinations of polymer, solvent and coagulant. The equipment consisted of a piece of glass plate (70 mm × 110 mm ×4 mm) and a metal rail, as shown in

Fig. 2.1. As cast, the film had a fixed wet thickness (250 μm) and width (60 mm). The film was prepared by the phase inversion process. The polymer solution was cast at room temperature on to the glass plate using a draw down technique. After exposure to air at room temperature for 15 seconds, the plate was immersed in the coagulation bath with various precipitants. When required, the temperature of the coagulation bath was varied between 20°C and 75°C. After the films were coagulated, and separated from the glass plate, they were removed from the bath for washing in water for one week with regularly changed water. They were then allowed to dry in air, a weight being placed on the top of the film to avoid curling during the drying process.

2. 2. 2 Hollow fibre production

2. 2. 2. 1 Preparation of the spinning solution

The spinning solution was prepared in the same way as described in section 2. 2. 1. 1. A typical spinning solution was made using 25g "Courtelle", 70g DMF, and 5g $CuSO_4\,5H_2O$.

2. 2. 2. 2 Dry-jet wet spinning PAN hollow fibres

A dry-jet wet spinning technique was utilised to spin the PAN asymmetric hollow fibres using a specially designed tube-in-orifice spinneret, as shown in Fig. 2.2. The spinning equipment and process were previously used by Rogers, Senn[100], Brown[101] and Deshmukh[102] to produce hollow fibre membranes from polysulphone (PSF). After some modifications, it was possible to spin PAN hollow fibres on this equipment and also to make a smaller quantity of hollow fibres than the earlier workers, as shown in Fig. 2.3 and Fig. 2.4 ~ 2.6. The degassed spinning dope obtained from the above procedure (see section 2.2.1.1) was poured into the spinning

pot. The degassing of the polymer solution was repeated in the pot prior to spinning by heating the pot up to 60°C ~ 65°C using a heating jacket for two hours. Any trapped micro-bubbles in the dope, produced by the dope transfer into the pot rose to the surface, and were hence easily removed before spinning. The degassed dope was fed from the pot under 25 psi N_2 pressure into a Slack and Parr gear wheel metering pump (0.3 ml/min. metering capacity). The temperature of the pot was monitored with a thermocouple. The dope passed through a filter pack into a heating tube with circulating hot water which was kept at the same temperature as the pot. The dope then passed through a tube-in-orifice type spinneret, and then a liquid thread-line was formed from the spinneret. After the dope emerged, the pump extrusion rate was set to the required throughput. The internal coagulant was injected via a peristaltic pump through the spinneret capillary at the desired rate and thus the fibre expanded into its characteristic hollow fibre form and the precipitation process began. The fibre was passed through an air gap of 20 ~ 100 mm and into a 1m long coagulation bath of water at a temperature of 60°C ± 5°C. PTFE guide rollers were used to deliver the fibre through the bath and out onto a series of washing rollers and a collecting drum (From time to time, other temperatures and spinning conditions were used; these will be stated in the results section.).

Generally, underneath the collecting drum was a trough of water. This ensured that the fibres were always wet and the water continued to extract the residual solvent from the fibres, because a large amount of residual solvent was still left in the fibres at this point. If there were not a trough of water, the fibres would redissolve on the surface layer and clump together. The fibres were then cut on the collecting drum using a scalpel. This produced a bunch of fibres 0.6 m long which were then tagged with a coloured rubber band for identification and placed in a wash bucket. The wash water was changed daily over two to three weeks. The fibres were dried at room temperature, by hanging them vertically so as to avoid curling. After drying, the hollow fibres were stored in a safe place.

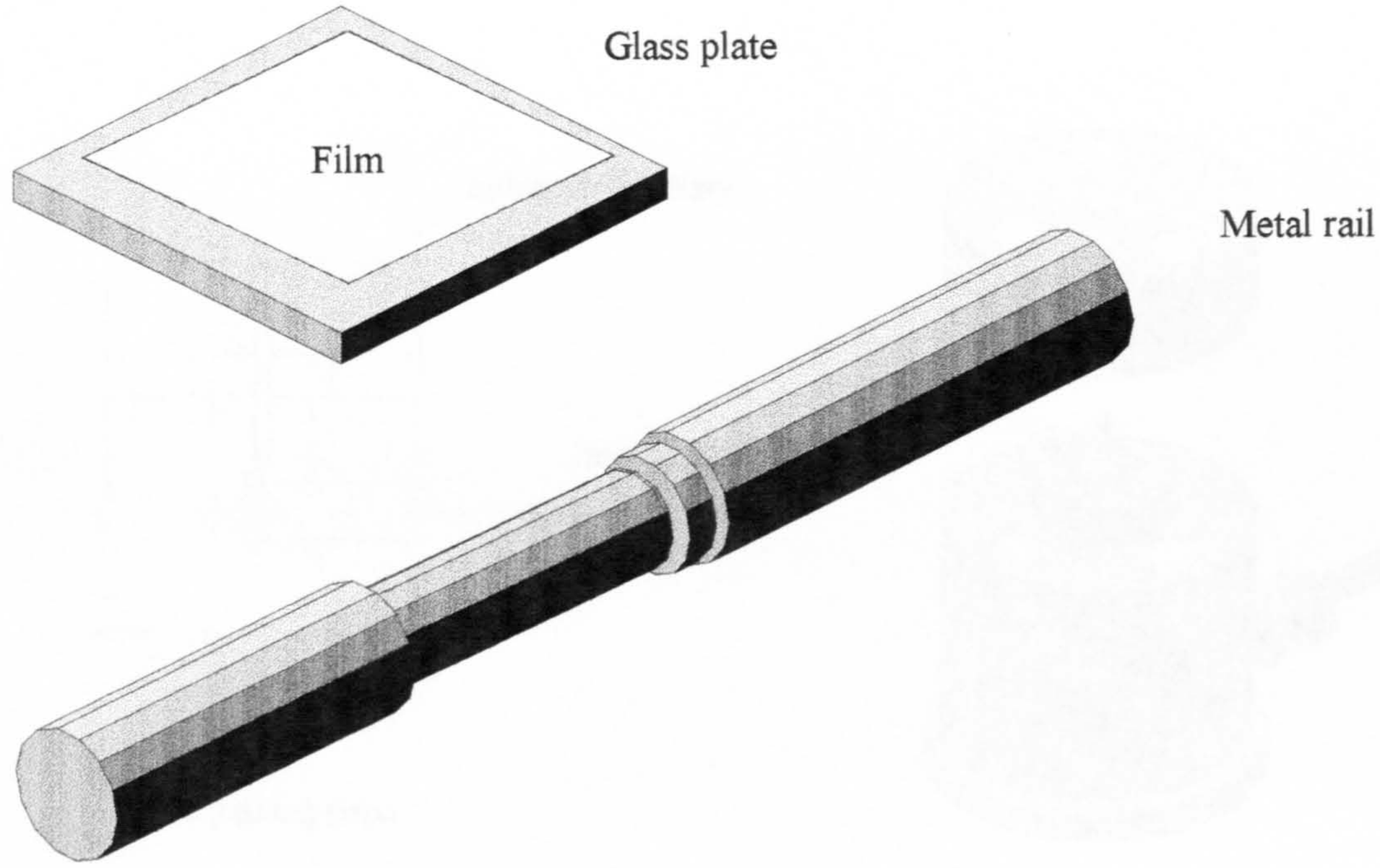

Fig. 2.1 Schematic equipment for film casting

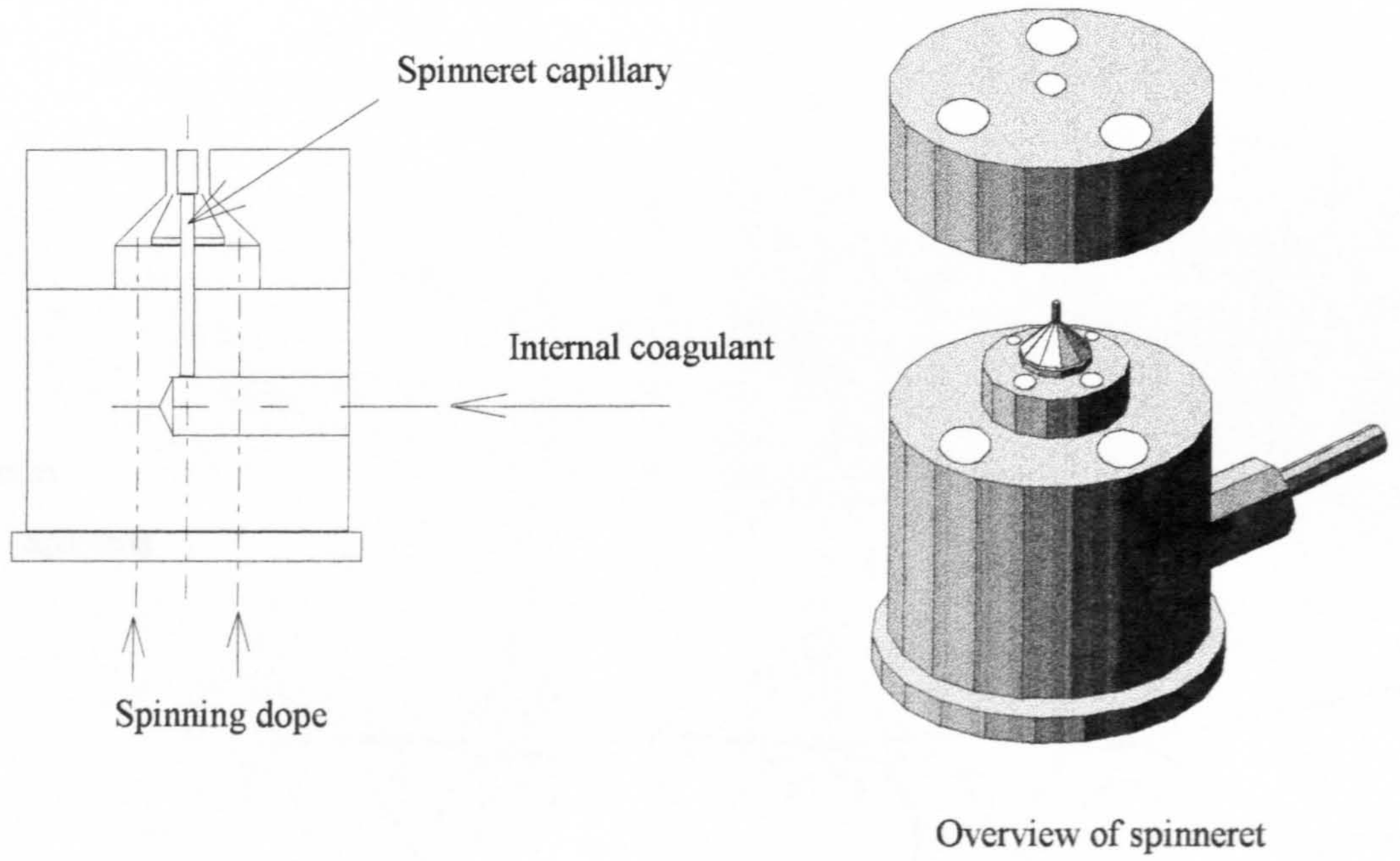

Fig. 2.2 Tube-in-orifice spinneret used in the production of hollow fibre

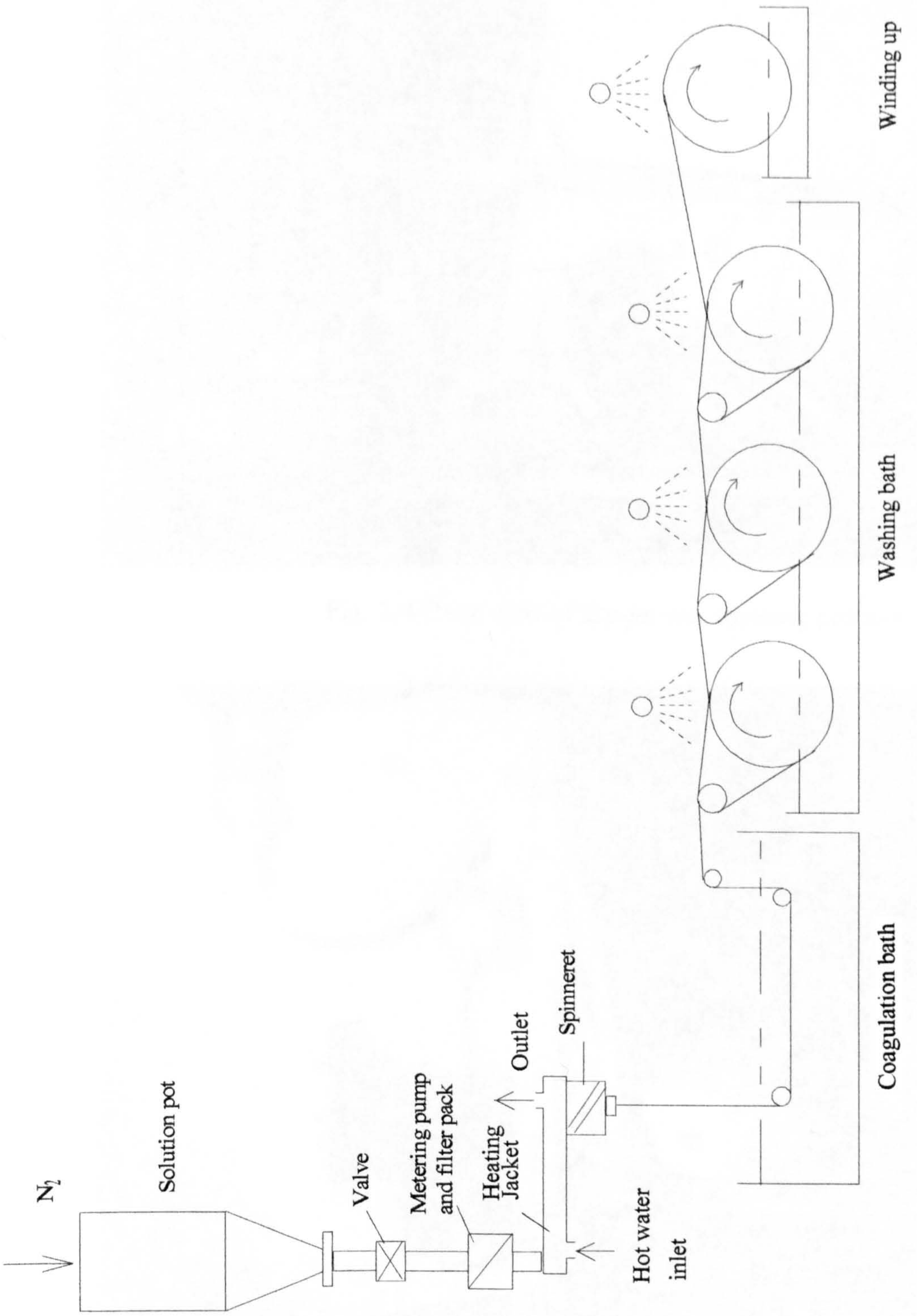

Fig. 2.3 Schematic diagram of dry-jet wet spinning process

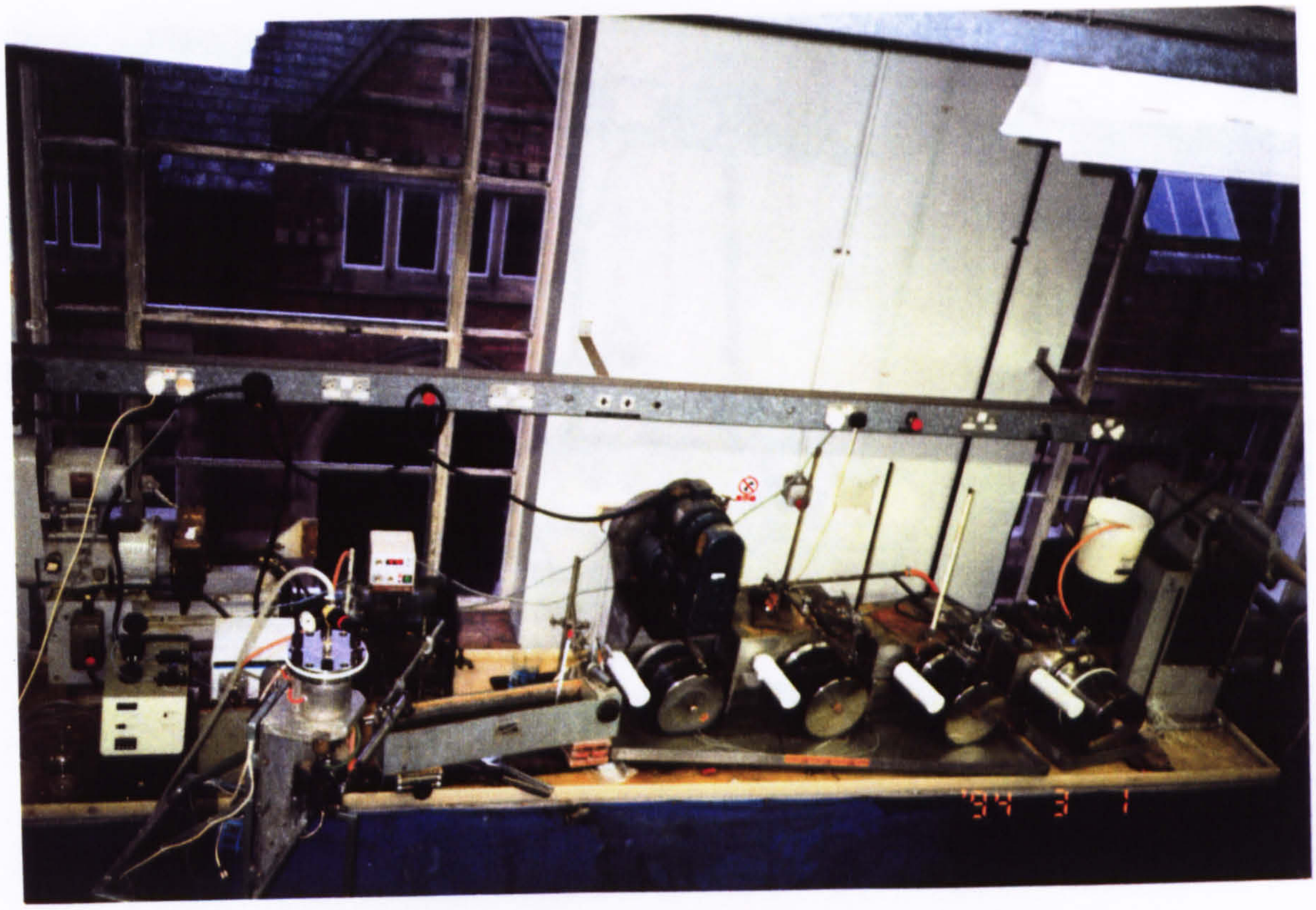

Fig. 2.4 Over view of dry-jet wet spinning process

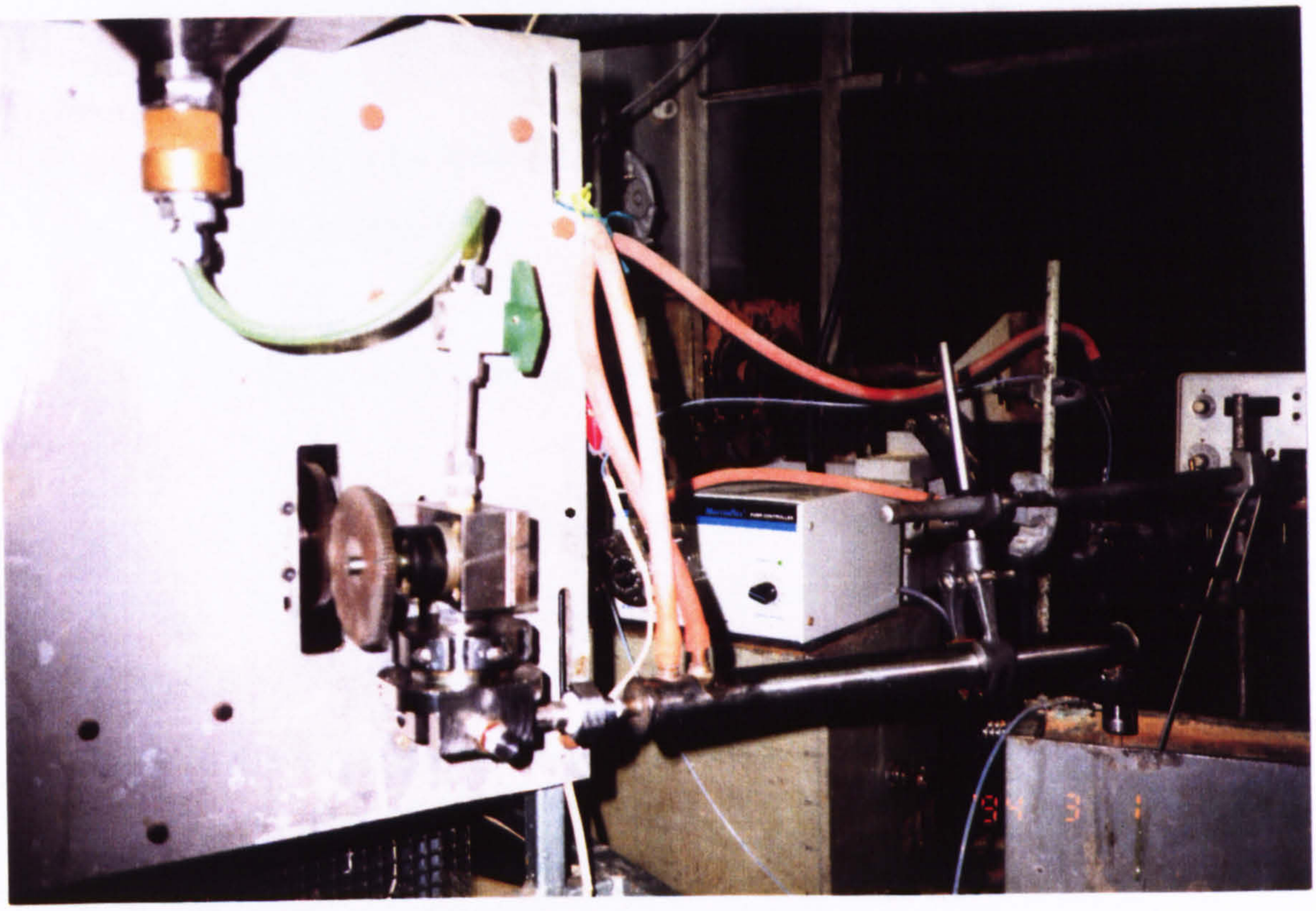

Fig. 2.5 Polymer extrusion process

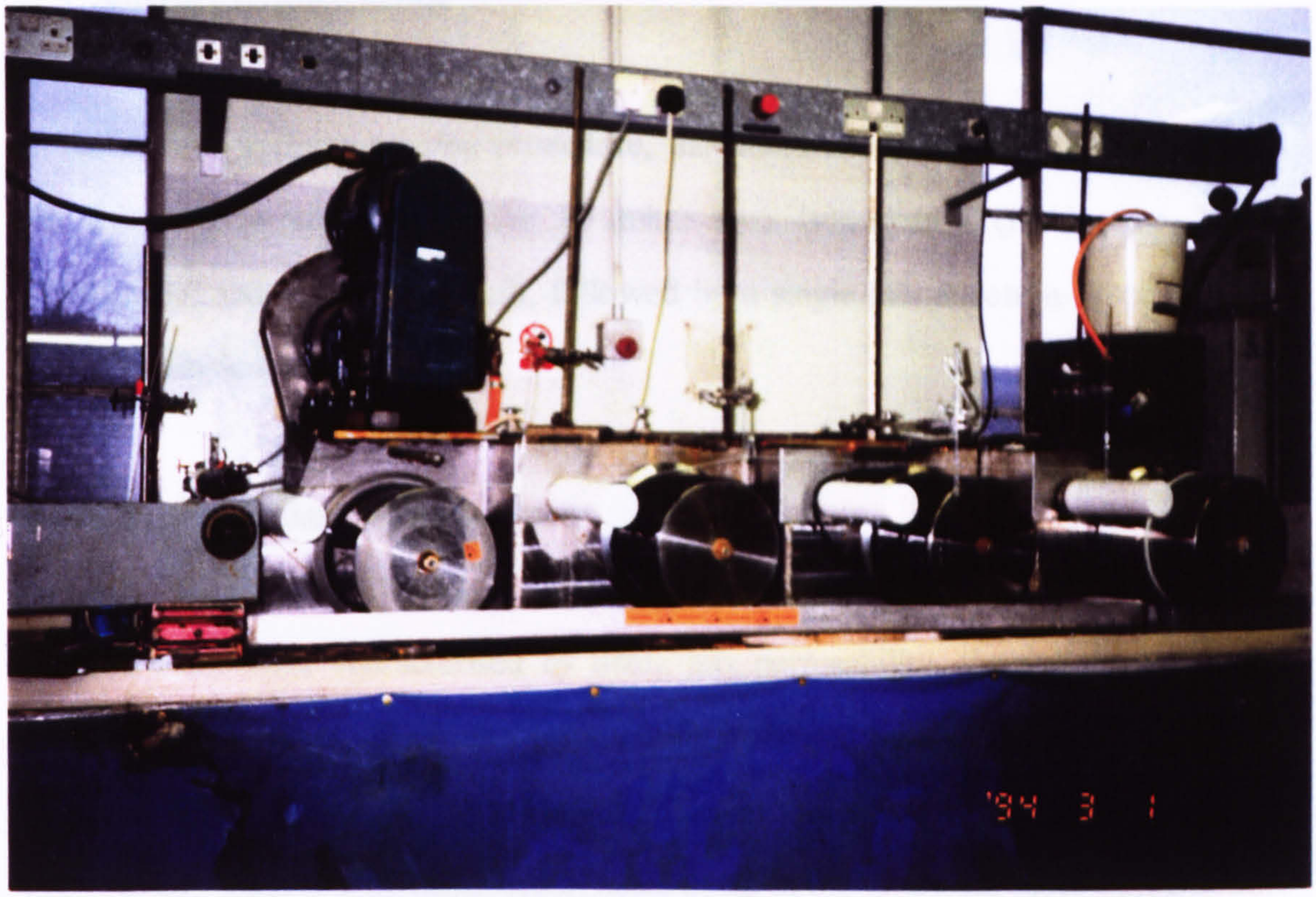

Fig. 2.6 Washing and collecting drum

2. 3 Solvent exchange drying

In the solvent exchange drying procedure, the fibres were sequentially immersed in the following solvents, each for 10 min.: two isopropanol (IPA), two 20/80 IPA/hexane, and two hexane bath, followed by a single immersion in Freon and air drying at ambient temperature.

2. 4 Characterisation of hollow fibres

Hollow fibres were characterised by using gas permeability, thermal analysis, and infrared spectroscopy. Their dimensions were measured by various techniques, such as scanning electron microscopy (SEM), micrometer screw gauge and optical microscopy. They will be described in more detail in the following sections.

2. 4. 1 Measurement of fibre dimensions

The fibre dimensions, i.e. outer diameter (O.D) and inner diameter (I.D) were measured by various methods.

2. 4. 1. 1 Scanning electron microscopy (SEM)

The diameter of the fibre can be very accurately measured by SEM. Before examination on the SEM, the fibres were fractured in liquid nitrogen to avoid smearing the cross-section of the fibres, then coated with gold. This enabled accurate cross-sectional measurements to be made from the SEM micrographs. The information obtained by SEM not only gives dimensional information but also gives morphological information pertaining to the coagulation conditions.

2. 4. 1. 2 Micrometer screw gauge

This is the quickest method for measuring the outer diameter of a fibre. Providing the jaws are not closed too tightly, measurements are quite accurate and a mean value of the fibre diameter can be obtained from repeated measurements.

2. 4. 1. 3 Optical microscopy

This method can also be used to check fibre dimensions. The method is very useful when a large number of measurements are required, even though it is less accurate than SEM, and less convenient than the micrometer.

It was also used to measure the diameter of the crosslinked PAN hollow fibres in DMF using a glass cell containing DMF and the fibres.

2. 4. 2 Thermal analysis

Thermal analysis methods such as differential scanning calorimetry (DSC) and thermogravimetric analysis (TGA) were used to characterise the original PAN as-spun hollow fibre and the hollow fibre treated with cuprammonium hydroxide solution.

2. 4. 2. 1 Differential scanning calorimetry (DSC)

Fibre samples were examined using a DuPont 2000 thermal analyser and 910 DSC cell, samples being run under nitrogen (50 ml/min.) with a 20°C/min. heating rate. In the case of hollow fibre samples, the fibres were laid parallel in the aluminium DSC pan so as to give as good a thermal contact as possible.

2. 4. 2. 2 Thermogravimetric analysis (TGA)

The weight-loss (%) versus temperature behaviour (including residual solvent content) of the fibres was determined using a TGA 951 module with the DuPont thermal analysis system. Samples were run in an atmosphere of nitrogen (50 ml/min.) with a 15°C/min. heating rate.

2. 4. 3 Pore radius determination by gas permeability

The procedure of using simple gas flux experiments to determine the pore radius is now well established. This procedure involves measuring permeation flow rates over a range of pressure drops and by using a combination of viscous and Knudsen flow equations, a mean pore radius for a particular model can be calculated.

2. 4. 4 Fourier transform infra red spectroscopy (FTIR)

The original PAN as-spun hollow fibre and the hollow fibre after treatment with cuprammonium hydroxide were examined and characterised using a Perkin Elmer FTIR 1724X spectrometer. The sample was ground to powder and then mixed with KBr and a compressed disc made again for transmission analysis.

2. 4. 5 UV-visible spectrophotometry

The UV-visible absorption of the solutions of $CuSO_4$ in water, $CuSO_4$ in DMF and PAN in $CuSO_4$/DMF solution were examined on a Philips PU 8720 Scanning UV/VIS Spectrophotometer in the Department of Colour Chemistry. Water was used as reference.

2. 4. 6 Elemental analysis

The PAN as-spun hollow fibres after treatment with cuprammonium hydroxide were analysed for copper content. The elemental analyses were carried out in the analytical division of the chemistry department. The carbon, hydrogen and nitrogen were measured on the Carlo Erba Model 1106 Elemental Analyser. Copper was determined by atomic absorption.

2. 4. 7 Mechanical properties

The tensile properties of the original hollow fibres and the crosslinked fibres were tested on an Instron tensile tester, model 1026. The gauge length was 20 mm, cross-head speed was 50 mm/min. The strength was measured at 20°C, 65% RH.

2. 5 Post spinning operations

2. 5. 1 Mounting hollow fibres for permeation experiments

Hollow fibres were mounted into a "module" form, as illustrated in Fig. 2.7, which was then fixed into the permeation chamber of the testing rig assembly. In general, one module contained ten hollow fibres, in which the fibres 0.3m long were threaded through the copper tube until 3 cm protruded from the top. The fibres were then glued in the tube by injecting the epoxy resin from the top until the inside of the tube was completely filled with the resin. The epoxy resin hardened after 30 min.. Fig. 2.8 shows the mounting of the hollow fibres in the copper tube. The protruding fibres were then cut using a scalpel blade so that the bore of the hollow fibres became exposed for gas transport. The most successful and easy way found to ensure open bores, without distorting the fibre shape was to chop the protruding epoxy

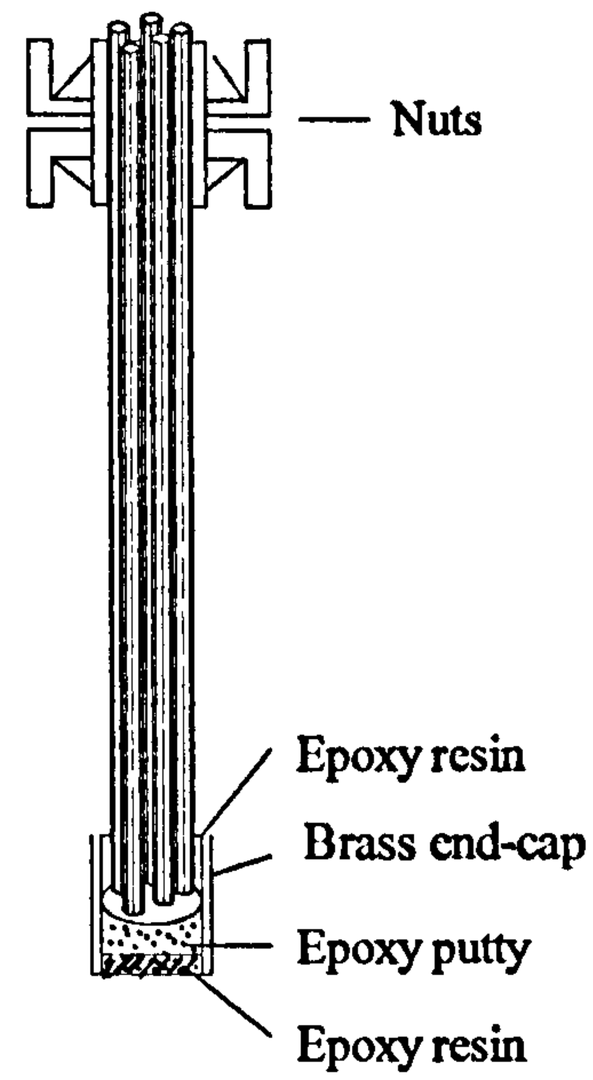

Fig. 2.7 Schematic diagram of the hollow fibre module

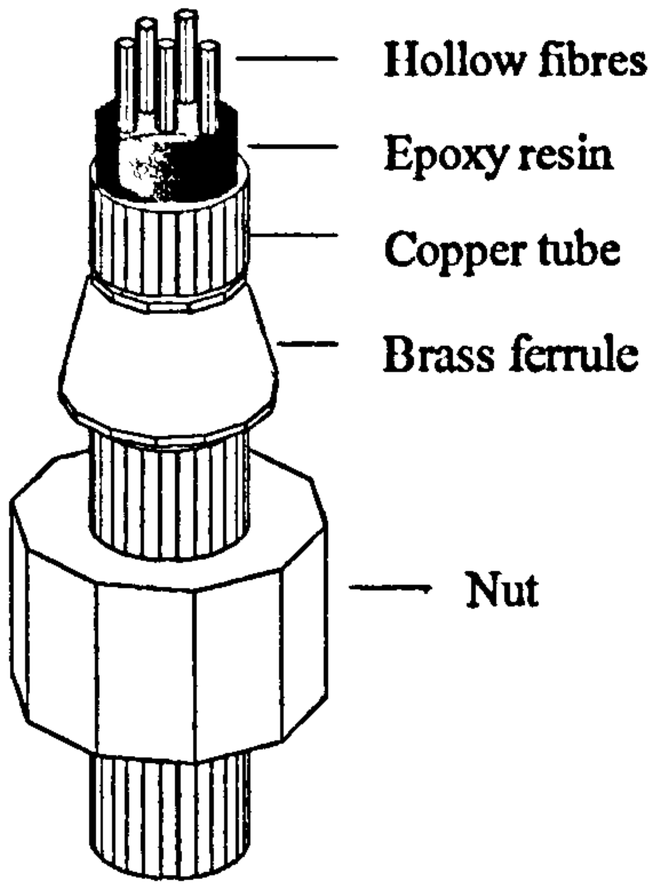

Fig. 2.8 Schematic diagram of the hollow fibre mounted in copper tube

coated fibres with the scalpel. Thirty minutes after the epoxy resin had been injected into the inside of the tube, the hollow fibres were cut to a length of 21 cm from the bottom edge of the copper tube. At this end of the fibres, the bores were then sealed into a 1 cm brass end-cap so that only the bores at the other end were available for gas transport.

2. 5. 2 Post-treatment of the hollow fibres

2. 5. 2. 1 Dip coating

In general, fibres were coated in module form with a coating solution of 5 wt% Sylgard 184 (Dow Corning) in 2-methylbutane with the curing agent (0.05 wt%) provided by the supplier. The module was first put under vacuum and then immersed in a measuring cylinder contained the coating solution for ten minutes. After 10 minutes, the module was removed from the coating solution and was kept under vacuum for another ten minutes. Subsequently, the vacuum was released and the module was stored for two weeks to cure the coating film at room temperature before permeation experiments were carried out.

2. 5. 2. 2 Hydroxylamine treated hollow fibre

The original PAN as-spun hollow fibres were immersed in a solution of hydroxylamine hydrochloride ($HONH_3^+Cl^-$) and sodium carbonate. The solution was made up with hydroxylamine hydrochloride (18.75g), sodium carbonate (14.06g) to a total volume of 250 ml, in a measuring cylinder, in which the original PAN as-spun hollow fibre was placed. After being treated at a temperature of 50°C for 10 minutes, the fibres were taken out of the cylinder and cooled down in the air. Then the treated fibre was washed with distilled water and later dried at room temperature.

2. 5. 2. 3 Cuprammonium hydroxide solution treated hollow fibre

The original PAN as-spun hollow fibres were immersed in cuprammonium hydroxide solution (containing 15g copper, 200g ammonia in 1 litre of the solution) at room temperature. After a series of times, the fibres were washed with distilled water for one week and then dried in air.

The crosslinked PAN hollow fibre obtained after treatment with cuprammonium hydroxide solution, were placed in test tubes containing sufficient DMF to cover them at room temperature for one week. After one week in DMF, the swollen hollow fibres were removed from the solvent and placed in further DMF solvent for one extra day in order to further wash out any dissolved PAN within the insoluble crosslinked hollow fibres. Finally, samples were washed in distilled water for 24 hours to remove any DMF in the fibres. After 24 hours washing, the fibres were dried. Each sample was weighed after drying at 30 °C for 24 hours under vacuum. The weight-loss percentage was calculated from the weights of the samples before and after treatment in DMF, as shown in the following equation (2-1).

$$W_L\% = \frac{W_C - W_R}{W_C} \times 100\% \qquad (2\text{-}1)$$

where: W_L is the weight-loss (%) of the crosslinked fibres;

W_C is the weight of the crosslinked fibres;

W_R is the residual weight of the crosslinked fibres after one week's treatment in DMF.

The weight increase % after the cuprammonium treatment was calculated from the following equation (2-2):

$$W_A\% = \frac{W_C - W_U}{W_U} \times 100\% \qquad (2\text{-}2)$$

where: W_A is the weight increase (%) of the fibres after treatment with the reagent;

W_C is the weight of the fibres after treatment with the reagent;

W_U is the weight of the fibres before treatment.

2. 5. 2. 4 EDTA solution treated hollow fibre

The crosslinked PAN hollow fibres were treated with ethylene diaminetetra-acetic acid (EDTA) solution, using 200 ml of 0.1M EDTA solution containing 0.4M $NaCO_3$. After being treated at room temperature for a series of times, the fibres were washed with distilled water and later dried in air.

2. 5. 2. 5 Annealing hollow fibre membranes

a) Hot water treatments

The fibres, while in module form, were subjected to a variety of hot water treatments. The temperature used was 90°C and immersion was of the order of minutes.

b) Vacuum oven treatment

Fibre samples were held in vacuum at temperature between 40°C ~ 190°C for

periods of 30 minutes each time. The temperature was chosen to be below and above the Tg of the as-spun hollow fibres.

2. 6 Determining the gas separation performance of hollow fibre membranes

The gas separation performance of the hollow fibre membranes is characterised by two parameters, namely the gas permeability and the selectivity. The quickest and simplest way to assess the performance of a gas separation membrane is to use single gas transport using the permeation test rig, which was originally designed and built with the aid of British Gas Plc by Senn[2]. This rig was subsequently reconstructed by Brown[3] and placed in a small room (1.7m × 1.7m × 2m high) with 9 cm thick wall containing 8 cm of polystyrene as insulating material and a well sealed door. This kept the day to day temperature variations inside the room to a minimum.

The rig, as shown in Fig. 2.9, consisted essentially of a permeating chamber into which the fibre module was fastened. Gas was applied to the permeation chamber. The pressure was set to the desired level and measured using a temperature compensated Heise pressure gauge which had previously been adjusted to zero to compensate for daily changes in atmospheric pressure. The pressure at the permeation side was always kept at atmospheric pressure by opening the permeation valve to the full extent in the permeation chamber. The gas which permeated through the wall of the hollow fibre passed through the bore and was fed to a soap film flow meter, as shown in Fig. 2.10, and thus the volume flow per unit time of this permeated gas was measured. Using this soap film flow meter, a number of measurements were made for the volume flow rate and the mean and standard deviation were taken on all measurements.

This is a very accurate way to measure gas flow on a laboratory scale. When using a soap film meter, it is necessary to ensure that the soap film meter is thoroughly

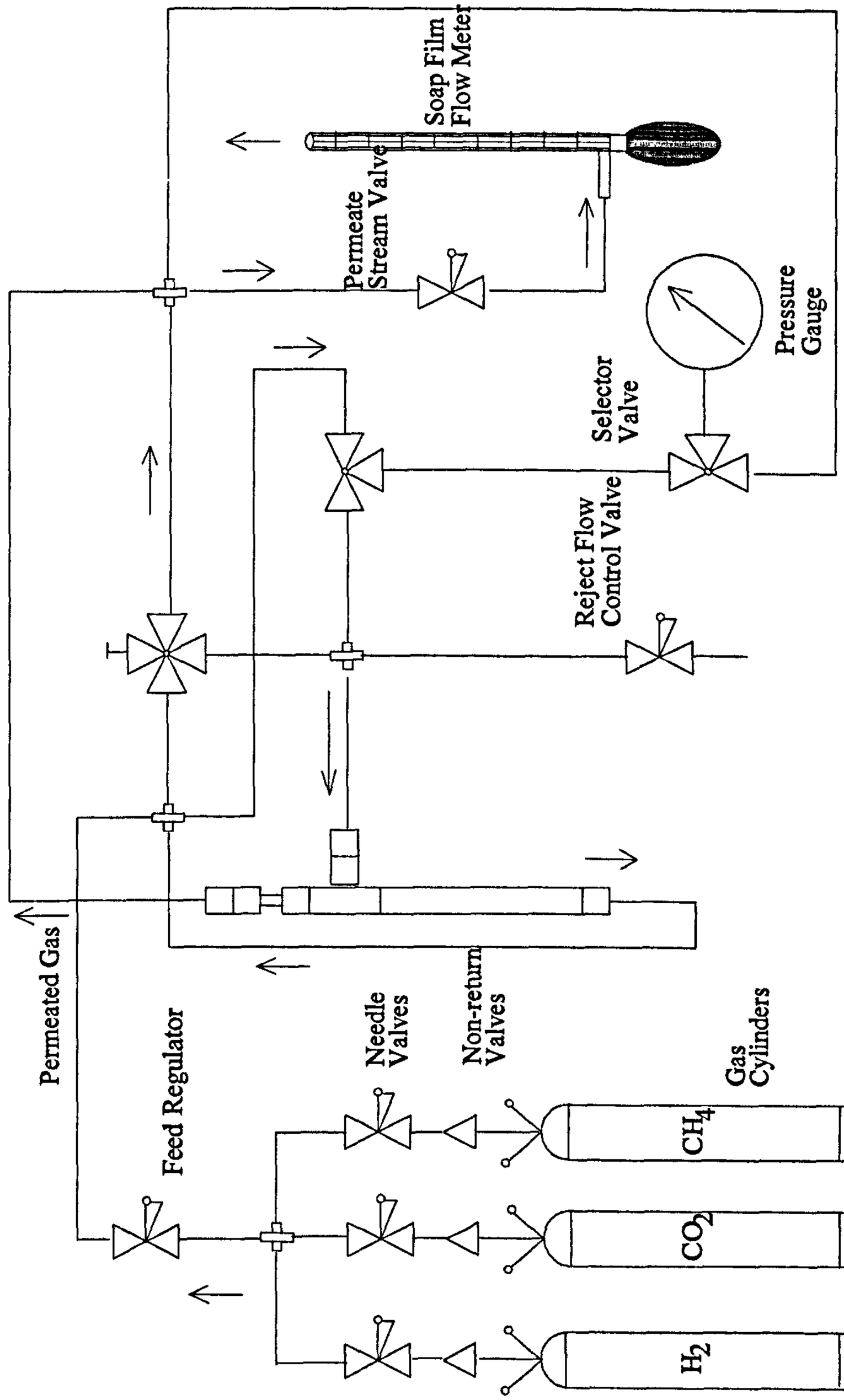

Fig. 2.9 Schematic diagram of the gas permeation rig

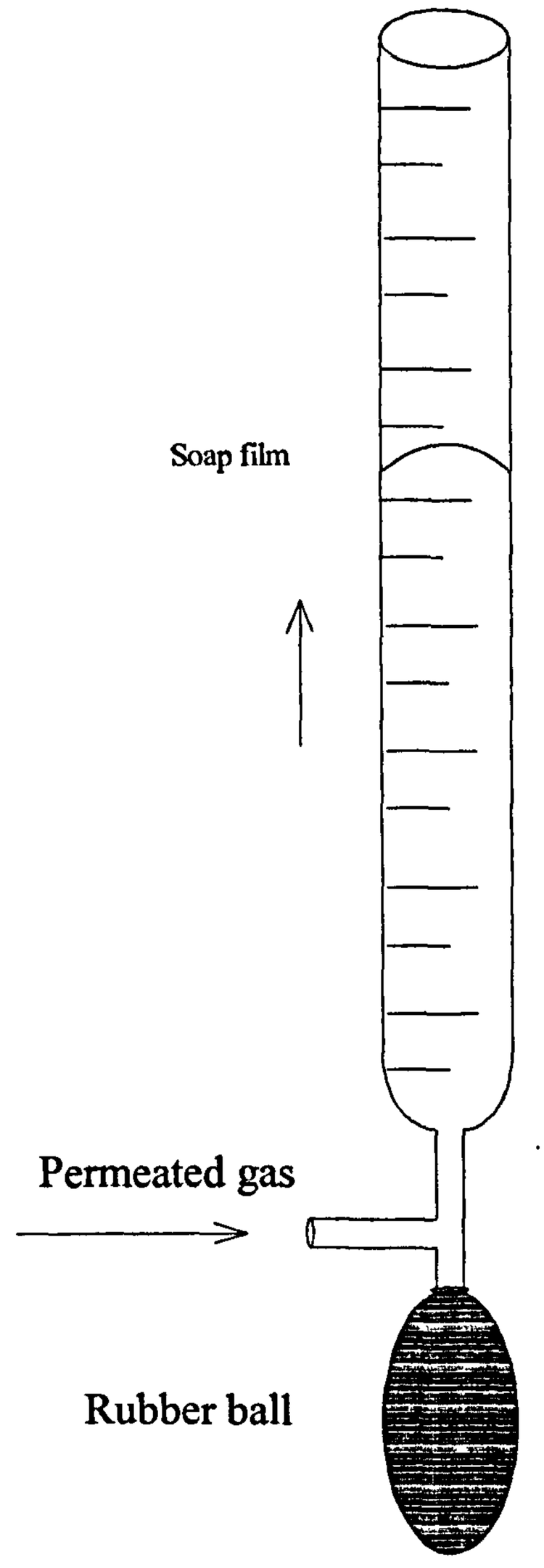

Fig. 2.10 Schematic diagram of flow rate measuring soap film meter

wetted with the soap solution. This is to prevent contact hysteresis between film and dry glass since this could lead to erratic flow measurements being made. Thus the gas flow of permeating gas could be accurately measured for all the gases required and the ideal performance assessed. Typically flows of gases were measured accurately between 100 cm^3/s and 5×10^{-3} cm^3/s. In this flow range the flow of gas in the tube is a laminar flow since the Reynolds number was calculated to be lower than the critical Reynolds number (Re_{cr}=2300).

The performance of the hollow fibre modules was assessed using the equation:

$$\frac{P}{l} = P' = \frac{Q}{\Delta p \cdot A} \qquad (2\text{-}3)$$

where:

P is the permeability coefficient, {cm^3 (STP) cm/cm^2 s cmHg};

Q is the apparent gas flow reading, (cm^3/s);

l is the effective skin thickness of the hollow fibre, (cm);

P' is the gas permeation rate, (cm^3 (STP) /cm^2 s cmHg);

Δp is the differential pressure applied in the module, (cmHg);

A is the surface area of the module,(cm^2), $A = \pi \times n \times L \times d_f$;

n is the number of fibres in the module;

L is the length of fibre, (cm);

d_f is the outer diameter of the fibre, (cm).

In general, absolute permeability, i.e., where the thickness of the membrane is known, is expressed in Barrer units:

$$1\ Barrer = \frac{cm^3(STP)\cdot cm}{cm^2\cdot s\cdot cmHg}\times 10^{-10}$$

However, for convenience when dealing with the permeation rate constants for hollow fibres, the units used are gas permeation units (GPU).

$$1\ GPU = \frac{cm^3(STP)}{cm^2\cdot s\cdot cmHg}\times 10^{-6}$$

The units of GPU are commonly used for describing gas permeability, and are also used in this work.

Once measurements had been carried out on the permeation rates of the single gases H_2, CH_4 and CO_2, the ideal separation factors were calculated using the ratios of the permeation rates of the single gases, as shown in the following equations:

$$a_{H_2/CH_4} = \frac{P_{H_2}}{P_{CH_4}}$$

$$a_{CO_2/CH_4} = \frac{P_{CO_2}}{P_{CH_4}} \qquad (2\text{-}4)$$

CHAPTER 3

SOLUTION-CAST FILMS

3. 1 Introduction

The preparation of asymmetric membranes by a phase inversion process is a standard technique nowadays. In the solution-cast film technique, a very thin layer of a homogeneous polymer solution is firstly cast and then contacted with a nonsolvent for the polymer which is miscible in all proportions with the polymer solvent. Exchange of solvent and nonsolvent across the interface introduces phase inversion in the polymer film, which can lead to a variety of characteristic asymmetric or symmetric structures.

Solution-cast films from polyacrylonitrile (PAN) polymer solution were prepared by dissolution of the polymer in a solvent to form a solution, followed by the application of a thin film of the solution on to a clean glass plate and completed by the phase inversion in the precipitant.

There are only a few references[70, 103, 104] to the study of PAN asymmetric hollow fibre membranes and to utilising them directly for gas separations, even though polyacrylonitrile membranes are frequently used in many ultrafiltration and pervaporation separations[105 ~ 111]. Having failed to produce PAN hollow fibres with a "sponge-like" porous substructure (as seen in SEM micrograph, Fig. 4. 1) by dry-jet wet spinning in the initial stages of this study, it was recognised that it would be necessary to use a solution-cast film technique to find out whether PAN cast films could be made with a dense, thin skin layer on the top of a porous substructure by the phase inversion process. If a cast film with a porous substructure could be produced by this process, hopefully, it would be a guide to the conditions needed to produce hollow fibres with a similar porous substructure. Once the fibre was produced, the next question would be to find out if it could be used for gas separations.

In this chapter, the work is described which concentrated on solution-cast film experiments in the search for suitable solvent and nonsolvent systems, and precipitating conditions, which would be suitable for making PAN cast film with a dense, thin skin layer on top of a porous substructure.

3. 2 Experimental

PAN casting solutions were prepared as described in section 2. 2. 1. 1 and the solution-cast films were made as described in section 2. 2. 1. 3.

In the solution-cast film technique, the polymer solution was cast on to a glass plate using a draw down technique; the glass plate was then immersed in the precipitant. During the phase inversion process, the term "precipitation time" was defined to describe the rate of the film precipitation. The precipitation time is recorded from the time the cast film was immersed in the precipitation bath till the film separates completely from the glass plate. The shorter the precipitation time, the more rapidly the polymer precipitates in the precipitant.

It had been observed earlier that different solvents and precipitants affect the structure of PSF cast film produced by phase inversion[100]. In the present study, four different precipitants were chosen initially to examine the porous structure of cast films so as to obtain some basic knowledge of the relationship between the film structure and the coagulating conditions. The structure of the film was examined by scanning electron microscopy (SEM).

3. 3 Results and discussion

3. 3 1 Effect of precipitant

Fig. 3.1 (a) ~ (d) show the transverse sections of the films prepared from a 25 wt% PAN and 75 wt% DMF solution coagulated in four different precipitants. As the results show, the films have very dense structures. It was noticeable that the precipitation time of the PAN films in these precipitants was much longer than that of polysulphone (PSF) polymer (the precipitation time is about 7 seconds for PSF in water) under the same conditions. The precipitation time of the PAN film in water was about 44 seconds, while the PAN films in formamide, ethanol, and acetone do not separate completely from the glass plate even after a couple of hours. Table 3. 1 summarises the results. In general, as the precipitation time of the PAN film increases, the more dense is the structure of the cast film.

The experiments clearly showed that the dense structure of the PAN films was related to the very long precipitation times (slow precipitation rate). Generally, during the phase inversion process, a high ratio of fluxes Js/Jn (i.e. the flux of solvent Js outwards from the polymer to the flux of non-solvent Jn inwards the polymer) yields dense and homogeneous polymer structures. It has been observed that the ratio of the diffusion coefficients Ds/Dn (i.e. the diffusion coefficient of solvent Ds outwards from the polymer to the diffusion coefficient of nonsolvent inwards to the polymer) in the PAN/DMF/ethanol system is greater than that in the PAN/DMF/water systems and so is the ratio of fluxes Js/Jn[112]. This leads to even denser structures when using ethanol as precipitant than that obtained from using

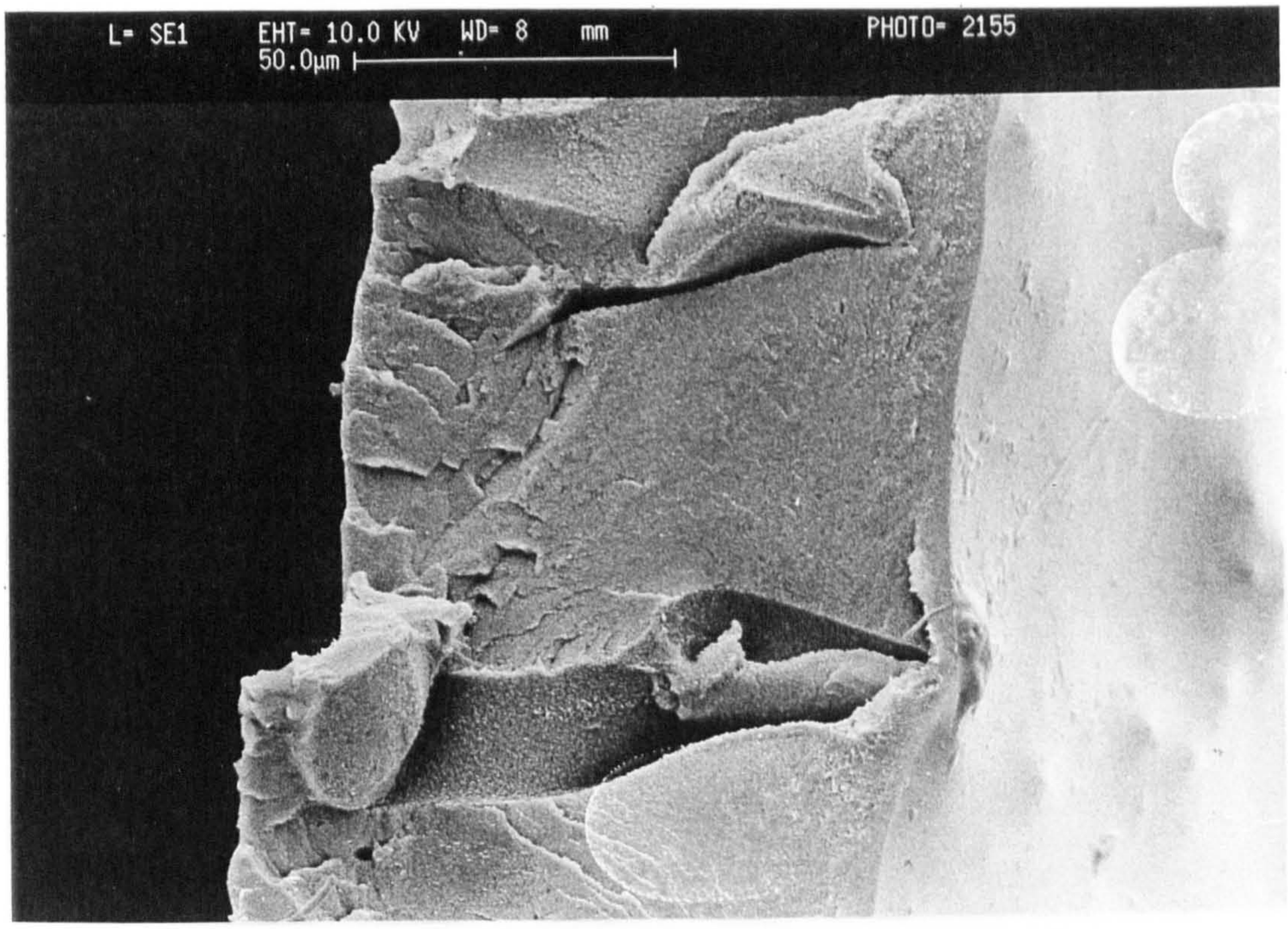

Fig. 3.1 (a)

Fig. 3.1 (b)

Fig. 3.1 SEM micrographs of transverse sections of cast films prepared from 25 wt% PAN and 75 wt% DMF solution, coagulated in different coagulants at 25°C, (a): water, (b): acetone,

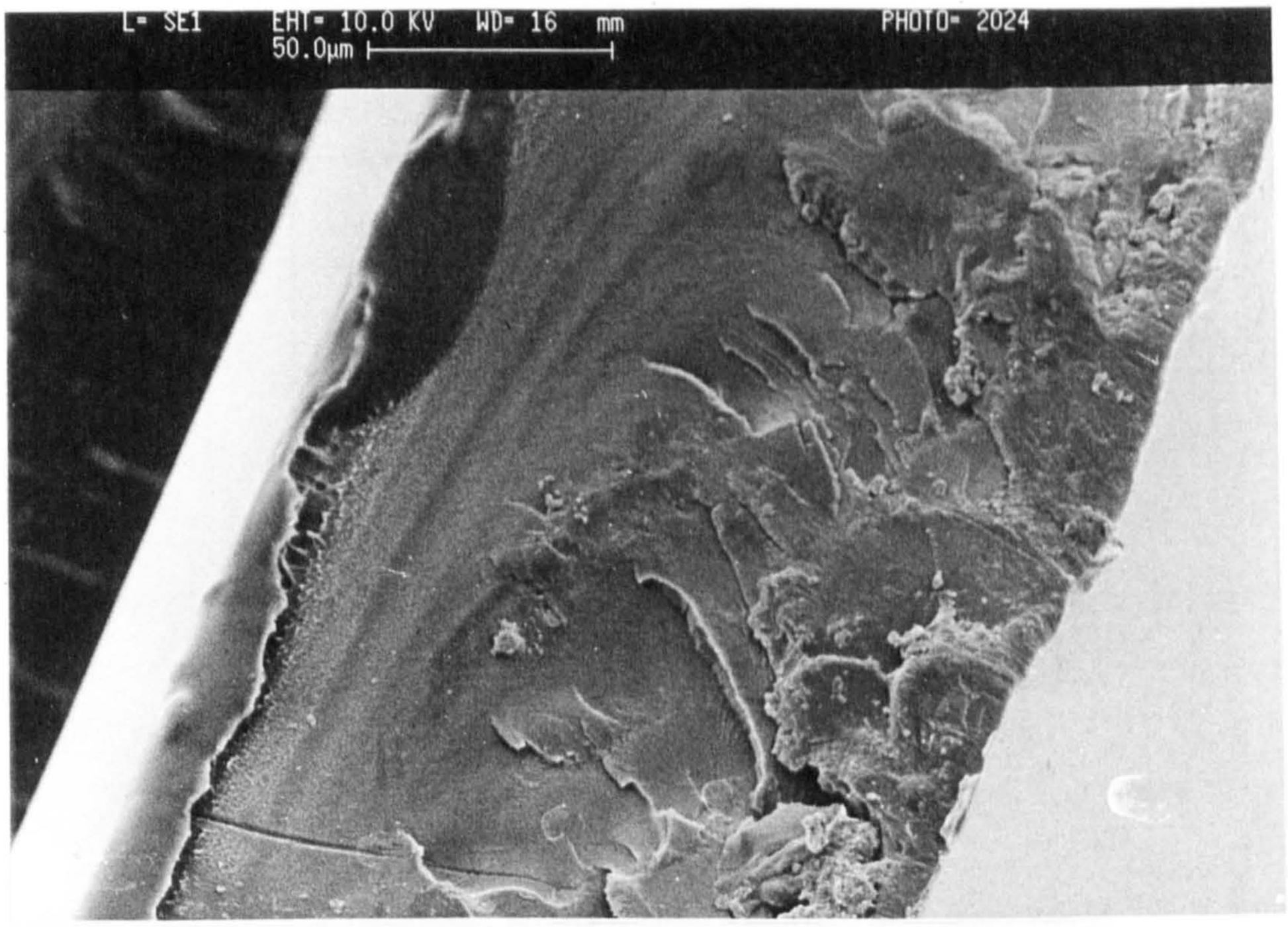

Fig. 3.1 (c)

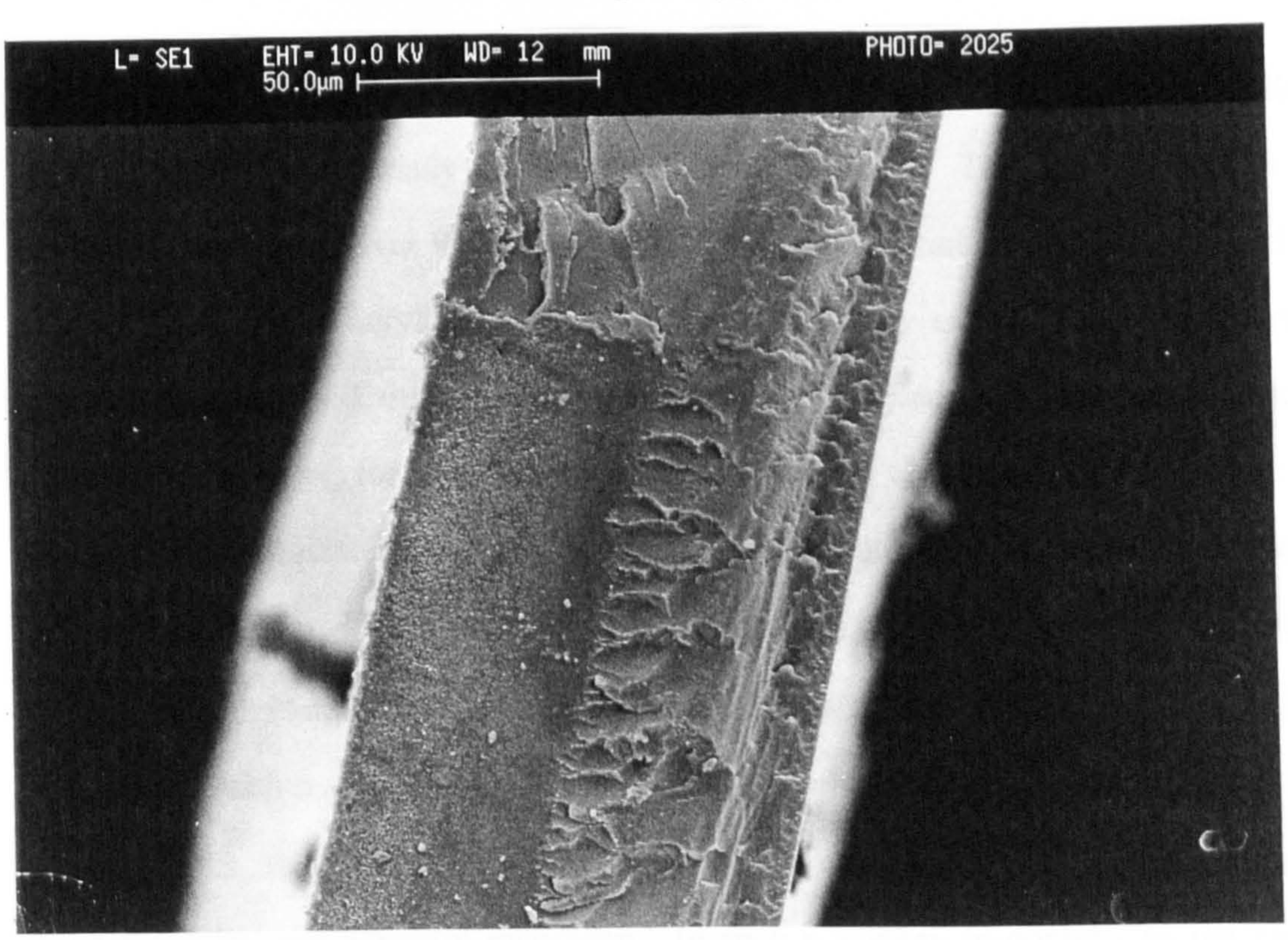

Fig. 3.1 (d)

Fig. 3.1 SEM micrographs of transverse sections of cast films prepared from 25 wt% PAN and 75 wt% DMF solution, coagulated in different coagulants at 25°C, (c): ethanol, (d): formamide

Table 3.1 Effect of precipitant on the precipitation time of PAN/DMF cast film at 25 °C

Precipitant	Precipitation time
Water	44 sec
Acetone	>2 h
Ethanol	>2 h
Formamide	>2 h

water. This result is confirmed by the results observed in present study.

Another serious problem observed in these PAN/DMF cast films was that the films were quite brittle, especially the film precipitated in water. The film was broken or cracked when folded over 90 degrees. This phenomenon had also been mentioned in studies of wet-spun acrylic fibres[113]. Such fibre may exhibit a porous, coarse-grained structure and may show brittleness if the polymer precipitation is almost instantaneous during the wet spinning process. In this circumstance, an increase of temperature (associated with an accelerated precipitation rate) yields even more brittle fibre. If this precipitation rate can be retarded through an increase of solvent content in the coagulation bath, it produces more flexible fibres. If some other nonsolvent, such as glycerol or hexanetriol, is present in the coagulation bath, more homogeneous, fine-grained structure fibre will be obtained. The fibre will have a good flexibility and abrasion resistance. In such a system, in contrast to the rapid coagulation systems, an increase in the coagulation bath temperature often leads to improved mechanical properties of the fibre.

The results obtained in this study indicated that the cast films showed a nonporous structure, but were still brittle. It was considered that the thickness of the films might be the main reason for the brittleness. Another reason might be related to the shrinkage of the solid polymer accompanying the composition change during the phase inversion that causes stresses in the cast film. If these stresses cannot be easily relieved by the movement of polymer chains, they would build up and make the final film brittle.

The problem is that the thickness of the cast film must be kept at a certain level, say about 120 μm, to correspond to the wall thickness of the hollow fibre. It cannot be reduced to the same order as the diameter of an acrylic fibre, which is normally around 20 μm. Presumably, if a cast film with a fine, "sponge-like" porous substructure can be produced, it would have to be no more brittle than the previously cast films. Obviously, in order to obtain such a kind of porous substructure with preferably flexible character, first of all, it is necessary to find conditions which produce a "sponge-like" porous substructure film during the phase inversion process. The following sections describe the experiments carried out to investigate the effect of coagulation bath temperature and nonsolvent or additives present in the casting solution on the morphology of the cast film.

3. 3. 2 Effect of coagulation bath temperature

The effect of coagulation bath temperature on the properties of acrylic fibres has been already reported[114]. This initial work was, of course, on the structural characteristics related to textile fibre use, where it is important to avoid any pore formation in the fibres. By contrast, the present study is primarily interested in producing fibres, which are required to have a "sponge-like" porous substructure. The effect of higher coagulation bath temperatures on the PAN cast film was studied using water as coagulant. Water was chosen because it would be advantageous to

use it as the coagulant since it is the cheapest both in terms of its own cost and in term of waste disposal and/or recovery. In addition other nonsolvents may not be suitable for high temperature study due to possible flammability hazards.

It was found that the precipitation time was reduced as the coagulation bath temperature was increased. This was because both the diffusion rates of solvent and nonsolvent increased with the increase of temperature. Fig. 3.2 shows a transverse section of the film prepared from 25 wt% PAN and 75 wt% DMF in a water bath at 75°C. The structure of the film precipitated at the higher temperature showed numerous macrovoids together with a porous polymeric matrix, while the equivalent film produced at room temperature showed a dense, nonporous structure, as shown in Fig. 3.1 (a). In general, macrovoid formation occurs under rapid precipitation conditions for many polymeric membrane materials, as has been reported by many workers[79, 85, 86, 90, 115]. The PAN cast film with such macrovoids and porosity is also believed to form because of a rapid precipitating process. Hence, the morphology of PAN/DMF cast films can be changed by increasing the coagulation bath temperature, though the film structure were still not suitable for use in an asymmetric hollow fibre membrane, and the film was still brittle.

Table 3. 2 summarises the results of the effect of coagulation bath temperature on the PAN cast film. At higher temperatures, the precipitation time was shorter, and a porous film was obtained.

3. 3. 3 Effect of additives in the casting solution

It has been claimed in the literature that additives such as nonsolvents, and inorganic salts, etc. can strongly affect the porosity of membranes produced by phase inversion processes[100, 116]. In the present study, it was found that polyacrylonitrile polymer had a strong tendency to form a dense structure due to a very slow precipitation

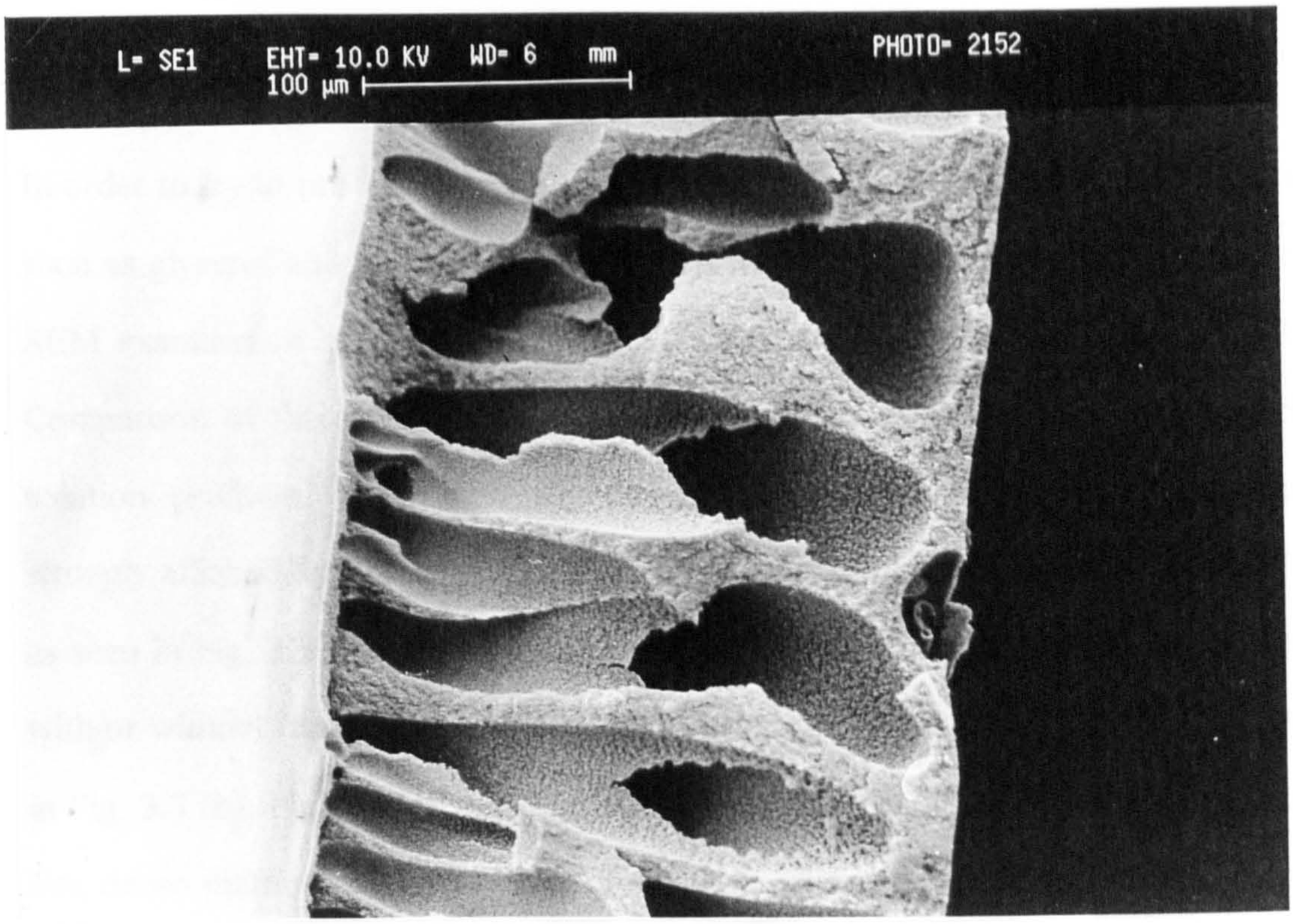

Fig. 3.2 SEM micrograph of transverse sections of cast film prepared from 25 wt% PAN and 75 wt% DMF solution and coagulated in water bath at 75 ° C

Table 3.2. Effect of coagulation bath temperature on the porosity and the precipitation time of PAN /DMF cast film

Temperature (° C)	Film porosity	Precipitation time (sec.)
25	dense film	44
75	porous film	22

process, while other polymers studied in this Department such as polysulphone tended to form a microporous substructure associated with very fast precipitation process in the same solvent-precipitant environment.

In order to try to produce PAN cast film with a porous substructure, some additives such as glycerol and formamide were added to the casting solution. The results of SEM examination of these different PAN films are shown in Fig. 3.3 ~ Fig. 3.5. Comparison of these SEM micrographs showed that these additives in the casting solution produced films with slightly different morphological structures, again strongly affected by the temperature. If the coagulation bath temperature is at 30°C, as seen in Fig. 3.3 (a), Fig. 3.4 (a); and Fig. 3.5 (a), the films have a dense matrix with or without macrovoids. If the coagulation bath temperature is at 55°C, as seen in Fig. 3.3 (b), Fig. 3.4 (b) and Fig. 3.5 (b), the films exhibit larger macrovoids and less dense matrices as well. The number of macrovoids and the porosity of the polymeric matrix increase with an increase in coagulation bath temperature. All the films obtained by adding glycerol, formamide and mixtures of them also exhibited a brittleness, which was independent of the temperature, and not significantly less than the PAN films first made.

While both of the organic additives used here affected the morphology of the cast film, the substructure of these films was still not satisfactory for use in gas separation membranes. It is believed that the structure of these cast films presented here reflects the strong interaction between DMF and PAN polymer. It has been reported that the interaction between DMF and the -CN groups in polyacrylonitrile retards the removal of the solvent from a cast film. It was rather difficult to remove completely the solvent from the film[117]. This result is related to the long precipitation times of the cast film in this study during the phase inversion. The slower the DMF flows outwards, the longer the precipitation time and the denser the final film.

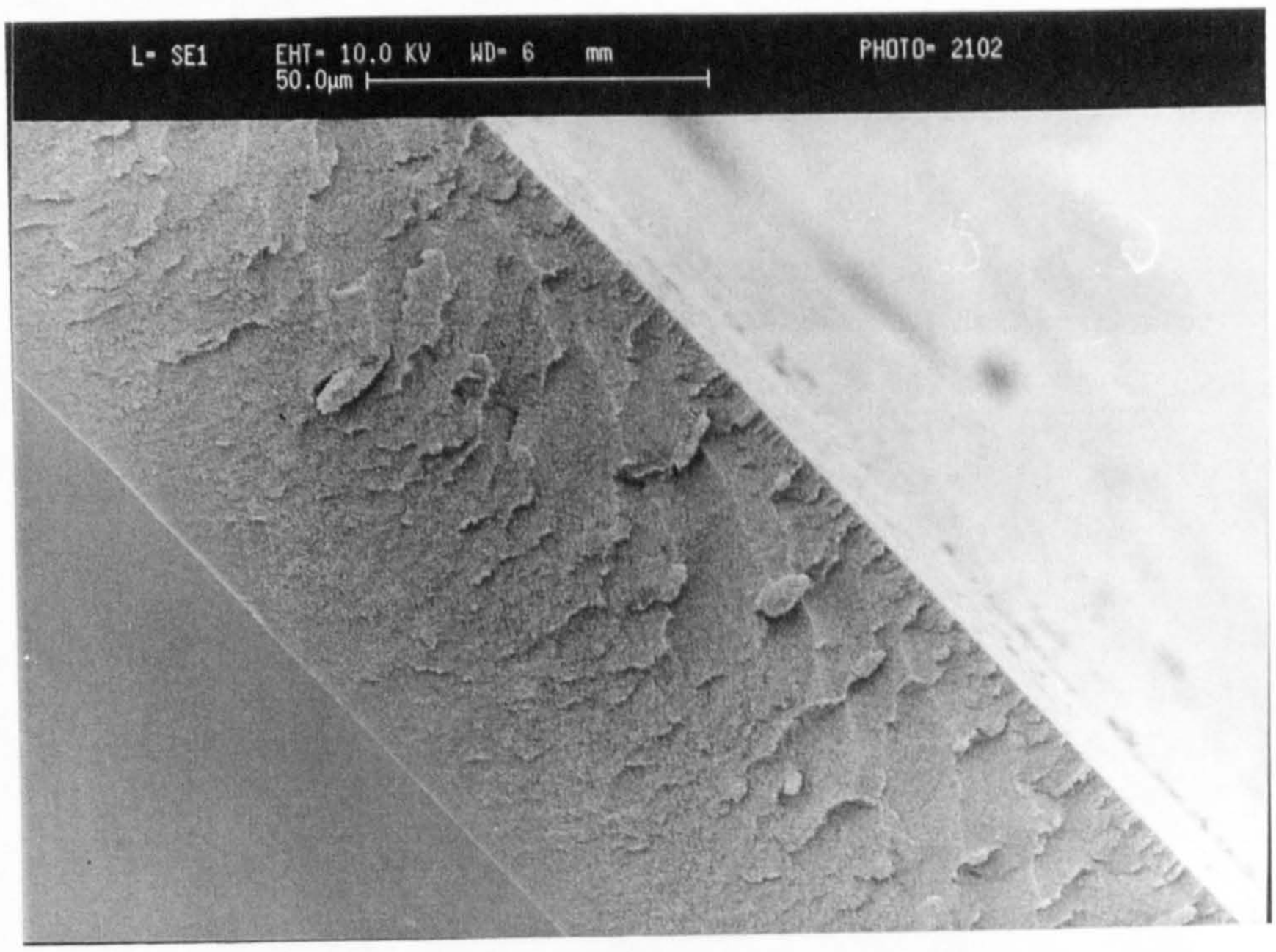

Fig. 3.3 (a) Precipitated in water at 30 ° C

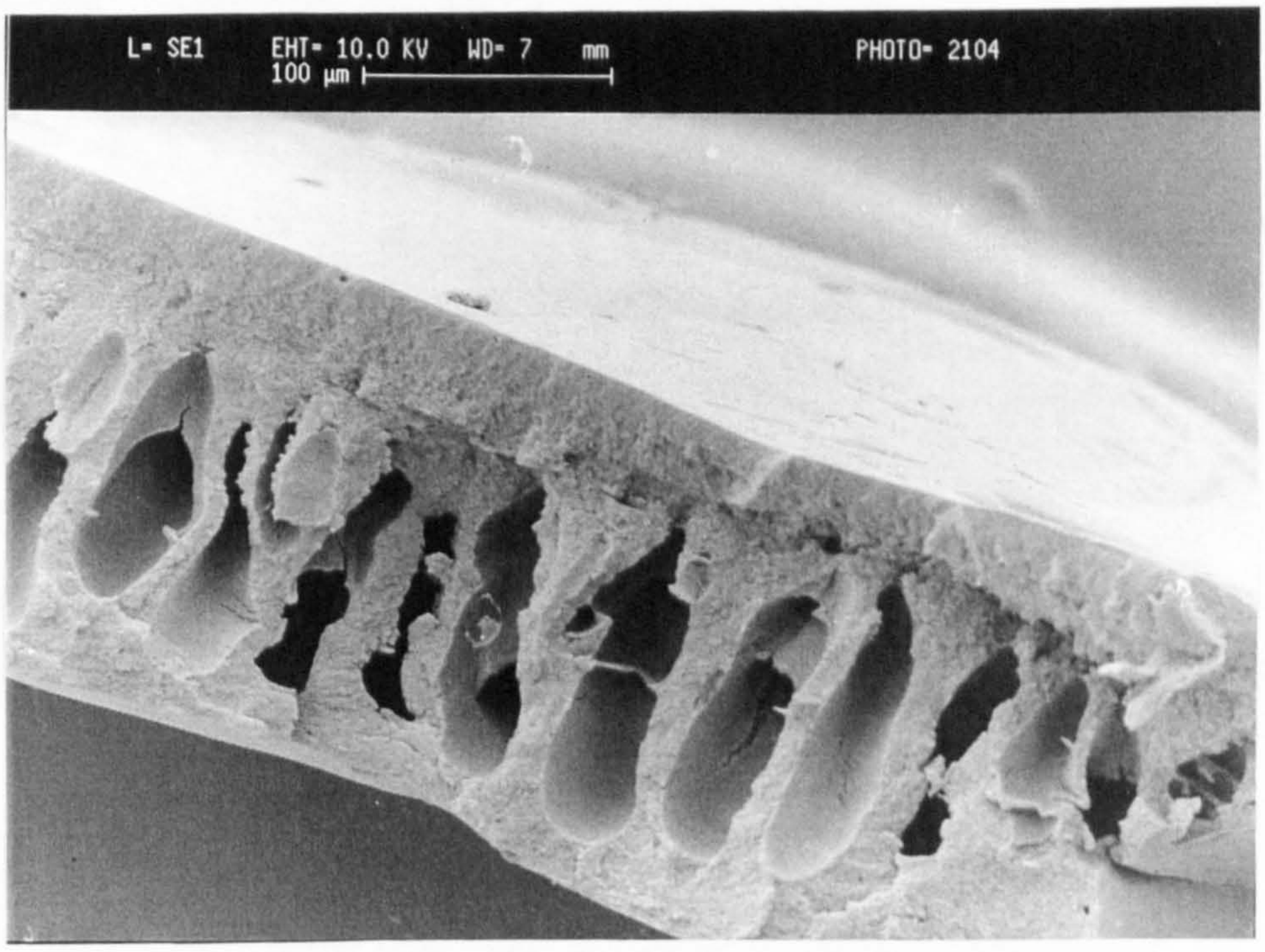

Fig. 3.3 (b) Precipitated in water at 55 ° C

Fig. 3.3 Effect of temperature on the structure of cast films made from PAN/DMF/Glycerol: 21.5/70/8.5 (wt% ratios)

Fig. 3.4 (a) Precipitated in water at 30 ° C

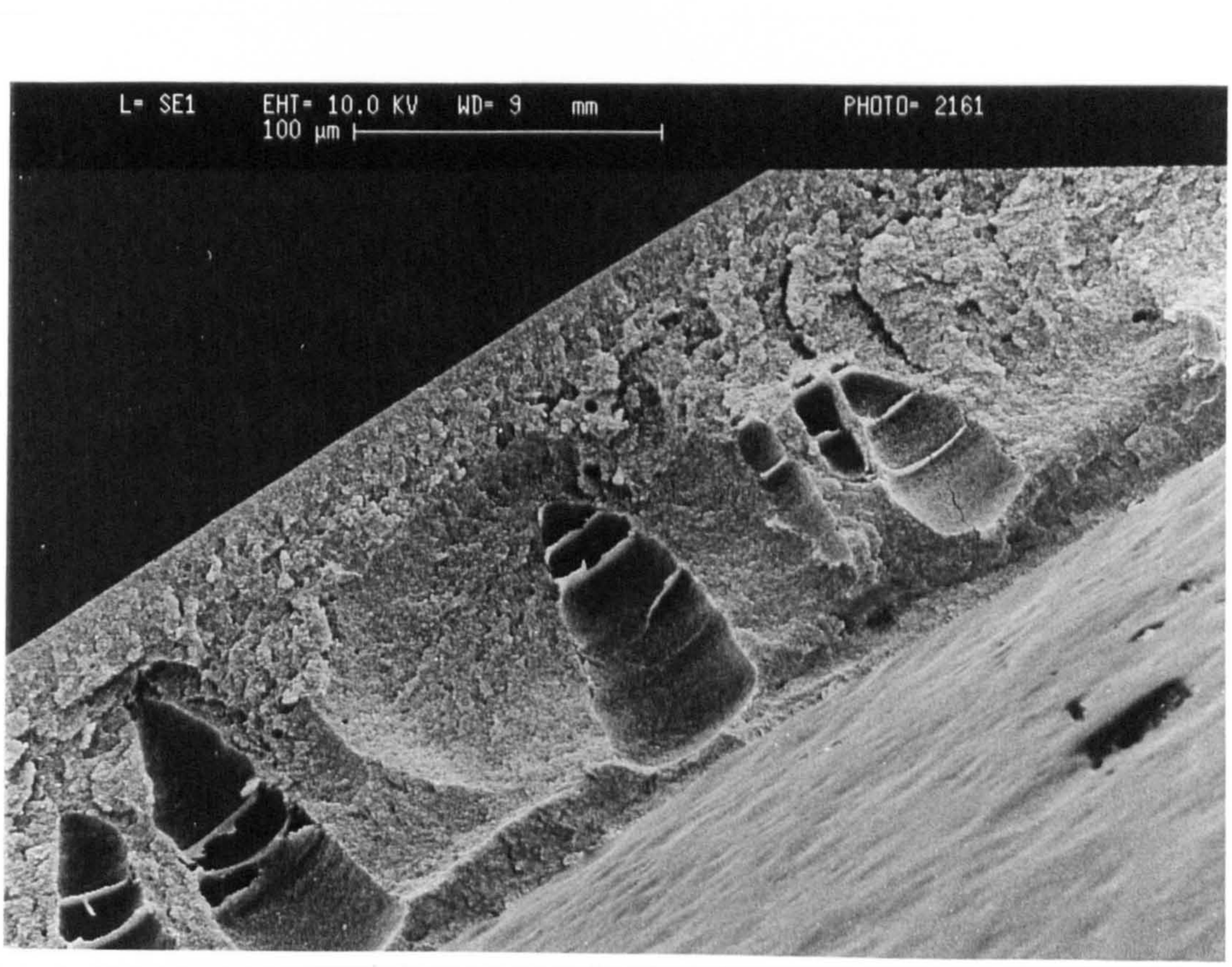

Fig. 3.4 (b) Precipitated in water at 55 ° C

Fig. 3.4 Effect of temperature on the structure of cast films made from PAN/DMF/Formamide: 25/67.5/7.5(wt% ratios)

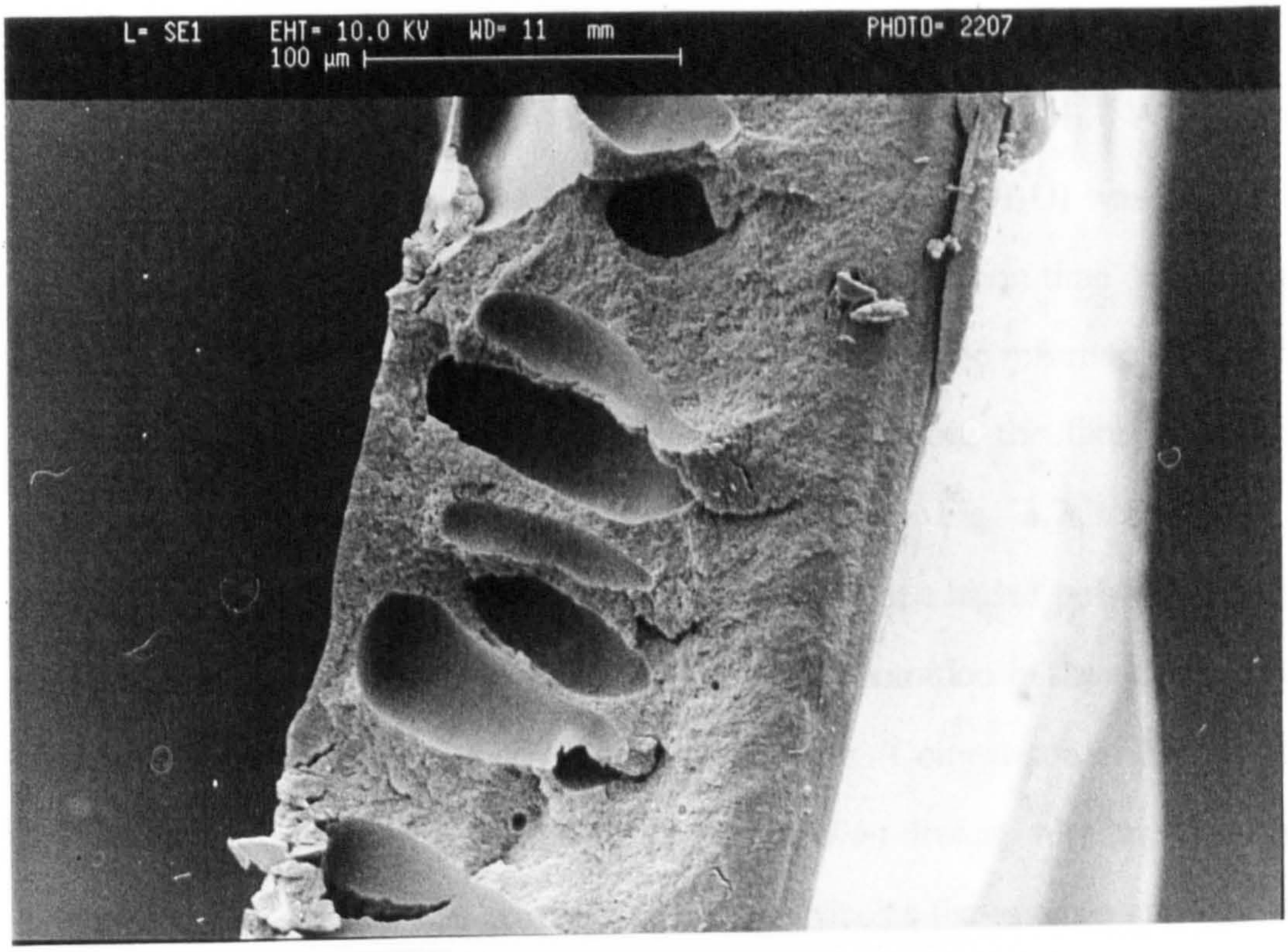

Fig. 3.5 (a) Precipitated in water at 30 ° C

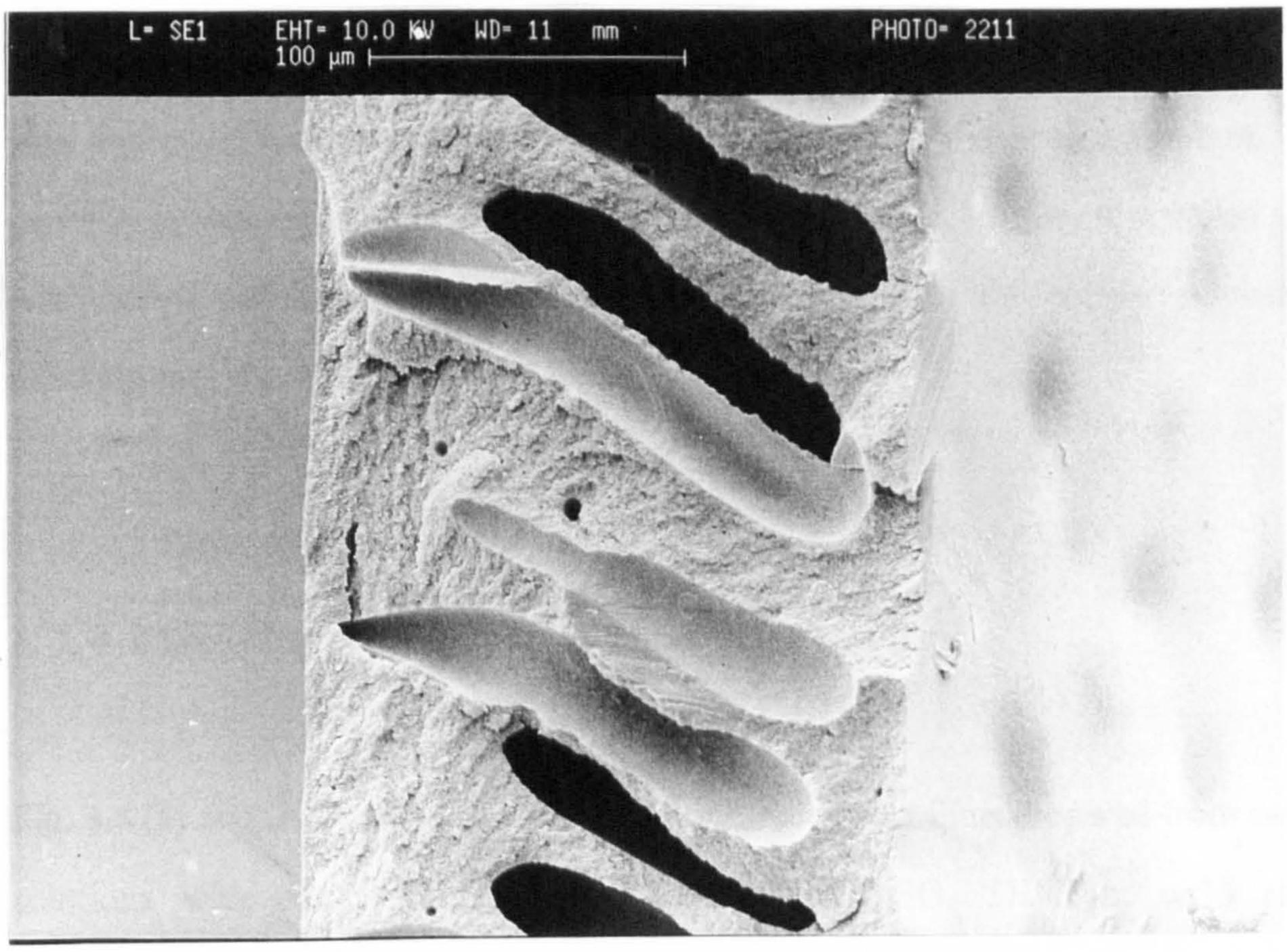

Fig. 3.5 (b) Precipitated in water at 55 ° C

Fig. 3.5 Effect of temperature on the structure of cast films made from PAN/DMF/Glycerol/Formamide: 21.5/68.5/3.6/6.4(wt% ratios)

Because copper salts were known to have an effect on the dyeing of acrylic fibres, experiments were carried out in which copper salts were added to the PAN/DMF/GLY solution (GLY is the abbreviation for glycerol). A significantly improved result was found when copper sulphate ($CuSO_4$ $5H_2O$) was added to the casting solution containing PAN/DMF/GLY. The precipitation time of the film was decreased. The film also had a finer porous matrix and large macrovoids even when coagulated at 30°C, as shown in Fig. 3.6. In addition, the film showed more flexibility and was no longer too brittle to handle. Fig. 3.7 shows the SEM micrograph of the PAN cast film, which was prepared at a higher polymer and copper sulphate concentrations with a decreased GLY concentration in the casting solution. The film was coagulated at 55°C of coagulation bath. Comparison of Fig. 3.6 & Fig. 3.7, shows that the morphological structure had been dramatically improved by the changes in composition and temperature. In particular the number and size of the macrovoids was significantly reduced.

This result was very surprising in the first instance, because the properties of the film were improved on the addition of the copper sulphate to the casting solution. The experiment was repeated and the results were reproducible. So, more detailed work was carried out in order to find out the precise role of the copper sulphate in affecting the morphology of PAN films.

3. 3. 4 Effect of metal salts on the structure of the cast films

Fig. 3.8 (a) and (b) show the porous substructures of cast films prepared from casting solutions with compositions of PAN/DMF/GLY/$CuSO_4$ $5H_2O$ in wt% ratios: 25/71/2/2 and 25/69.5/2/3.5. The porosity of the cast films increased with the increase of additive concentration in the casting solution, as seen from the data in Table 3. 3, where the measured porosity is reflected in the dry film thickness.

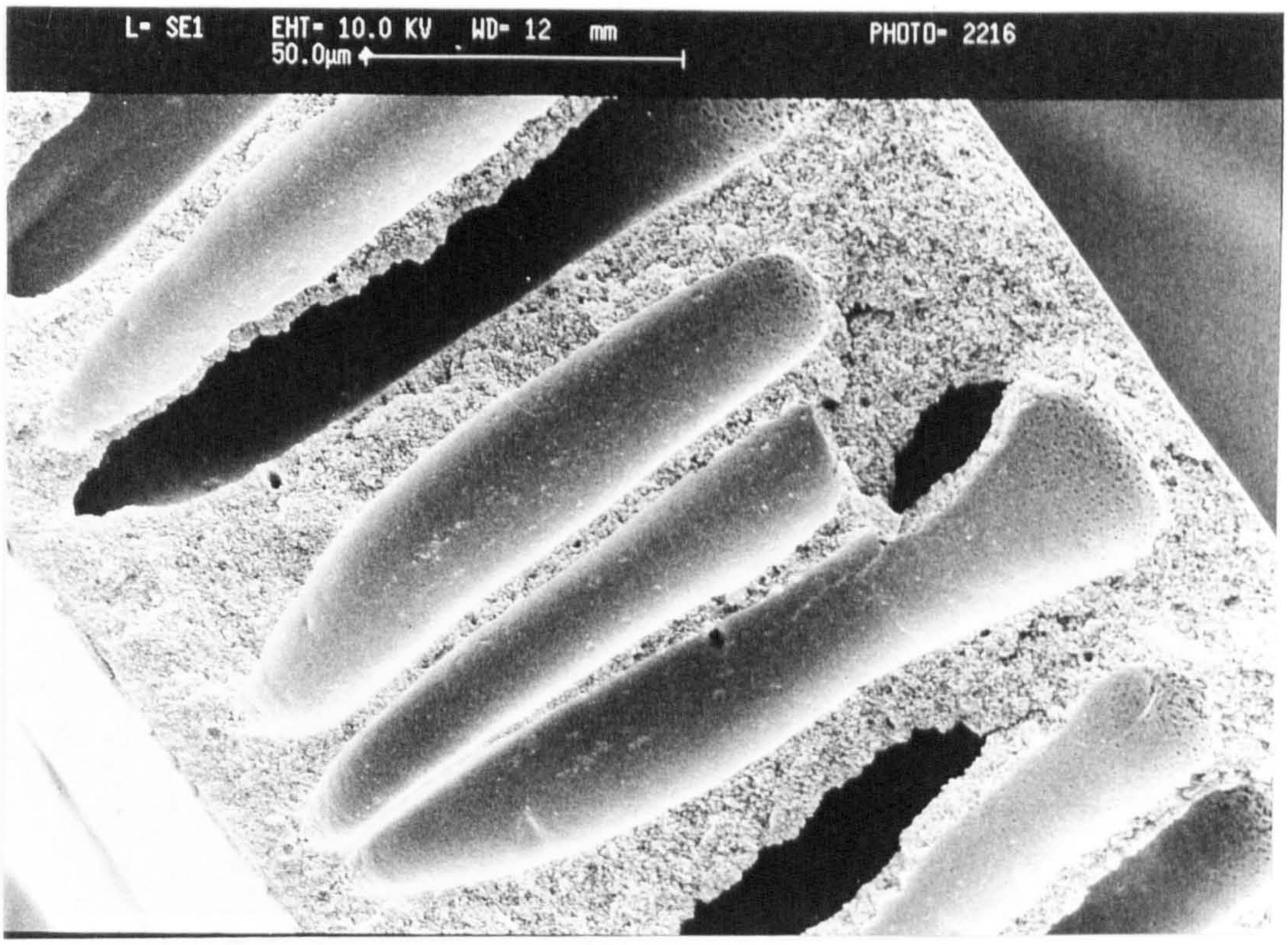

Fig. 3.6 SEM micrograph of transverse section of cast film prepared from PAN/DMF/GLY/$CuSO_4$ in wt% ratios: 17/74/8/1, coagulated in water bath at 30°C

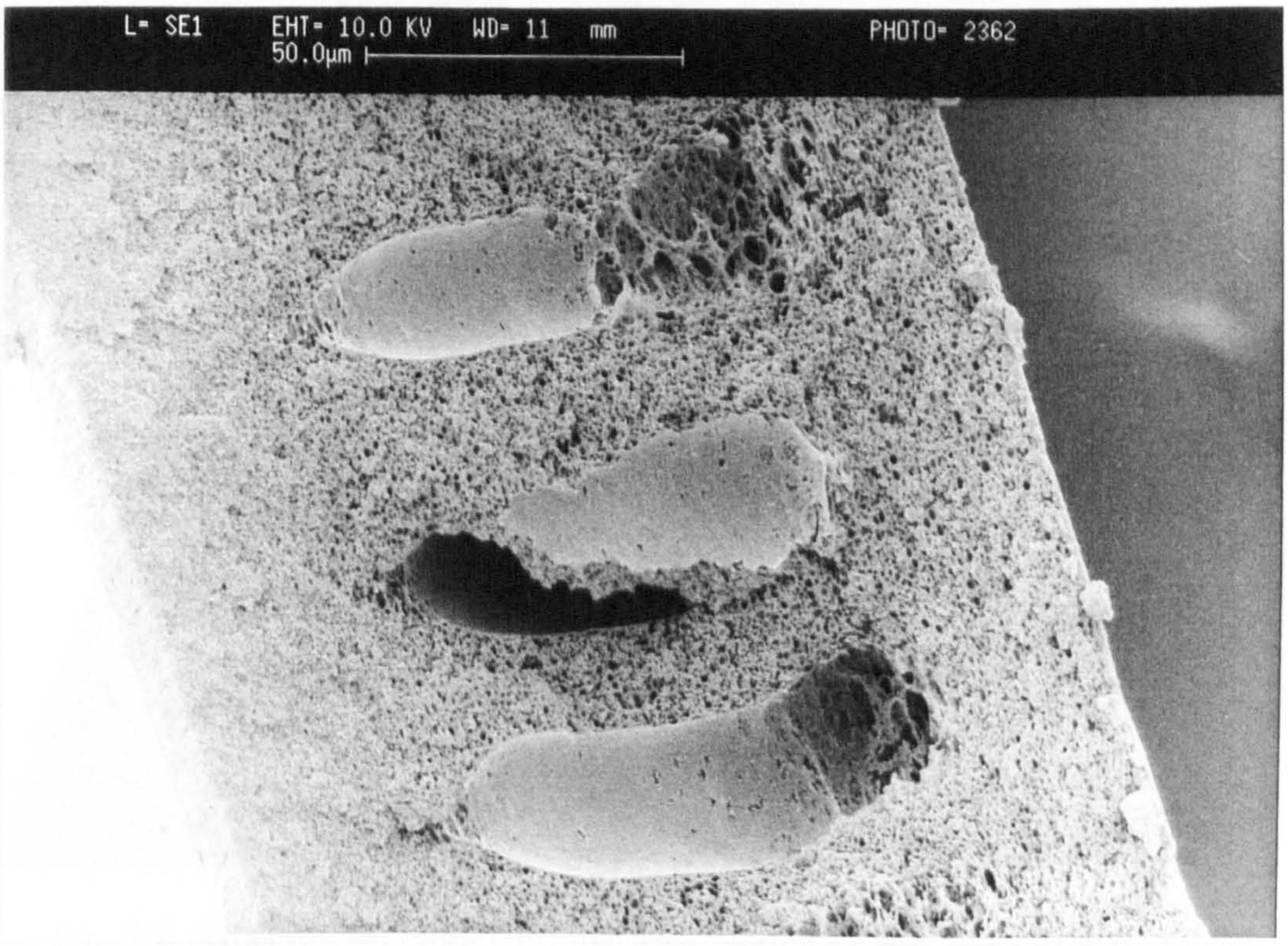

Fig. 3.7 SEM micrograph of transverse section of cast film prepared from PAN/DMF/GLY/$CuSO_4$ in wt% ratios: 23.5/70.5/3.5/2.5, coagulated in water bath at 55°C

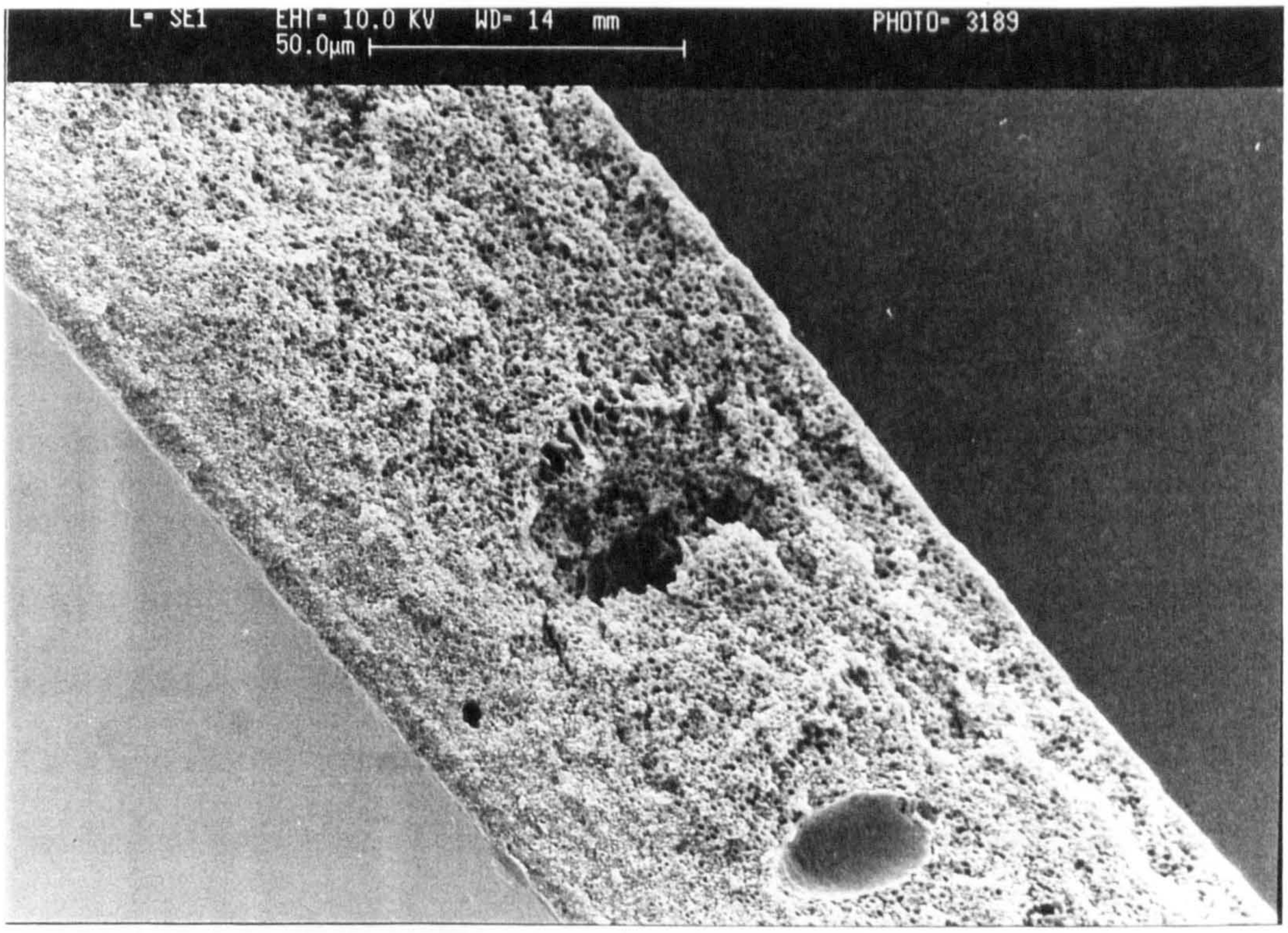

(a)

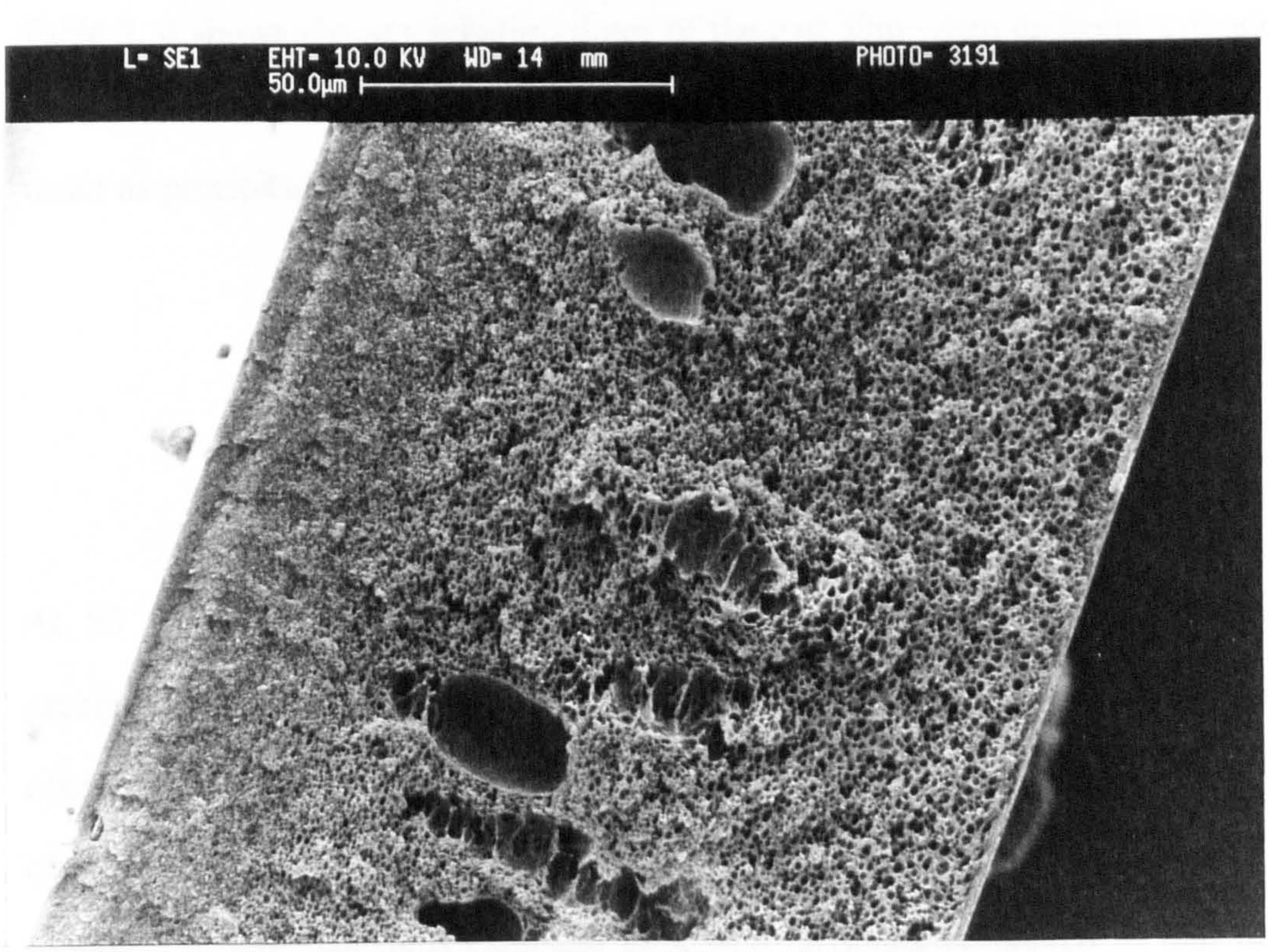

(b)

Fig. 3.8 SEM micrographs of transverse section of cast films prepared from PAN/DMF/GLY/$CuSO_4$ in wt% ratios, coagulated in water bath at 55°C
(a) PAN/DMF/GLY/$CuSO_4$: 25/71/2/2
(b) PAN/DMF/GLY/$CuSO_4$: 25/69.5/3.5/2

Fig. 3.9 (a) ~ (c) show the porous substructure of cast films made from casting solutions with various compositions of PAN/DMF/$CuSO_4$ $5H_2O$, with no GLY added. In all cases, it was found that the film still had the porous structure. If only GLY is used as the additive, the cast film does not show a "sponge-like" porous structure apart from macrovoids, as seen previously in Fig. 3.3. This means that it is the presence of the $CuSO_4$ that mainly affects the structure of the film. With increasing concentration of $CuSO_4$ in the casting solution, the structure of the film shows more porosity with macrovoids still present. Table 3.3 shows that the thickness of the cast film increased with increasing $CuSO_4$ concentration, which means that there was increasing porosity in the film. It is therefore clear that the $CuSO_4$ in the PAN casting solution changes the morphology of the cast film and its mechanical properties. These results promoted a study on the effect of other metal salts on the film morphology.

Table 3. 4 shows the precipitation times of the cast film when different salt additives were present in the dope. The data show that the precipitation time of the cast film in water as precipitant at 25°C increases in the following sequence:

$$CuSO_4 < ZnCl_2 < CuCl < LiCl$$

At 55°C, the precipitation times are all decreased, which means that the film precipitates more rapidly at higher temperatures as expected. Most of the films obtained showed an opaque appearance, which was due to the microporous structure of the films. The film showed a pale green colour when CuCl was present in the casting solution. All films exhibited improved flexibility compared to that obtained from the PAN/DMF casting solution with or without organic additives. The flexibility of the film seemed to be related to the porosity of the cast film. The more porous the structure, the more flexible the film.

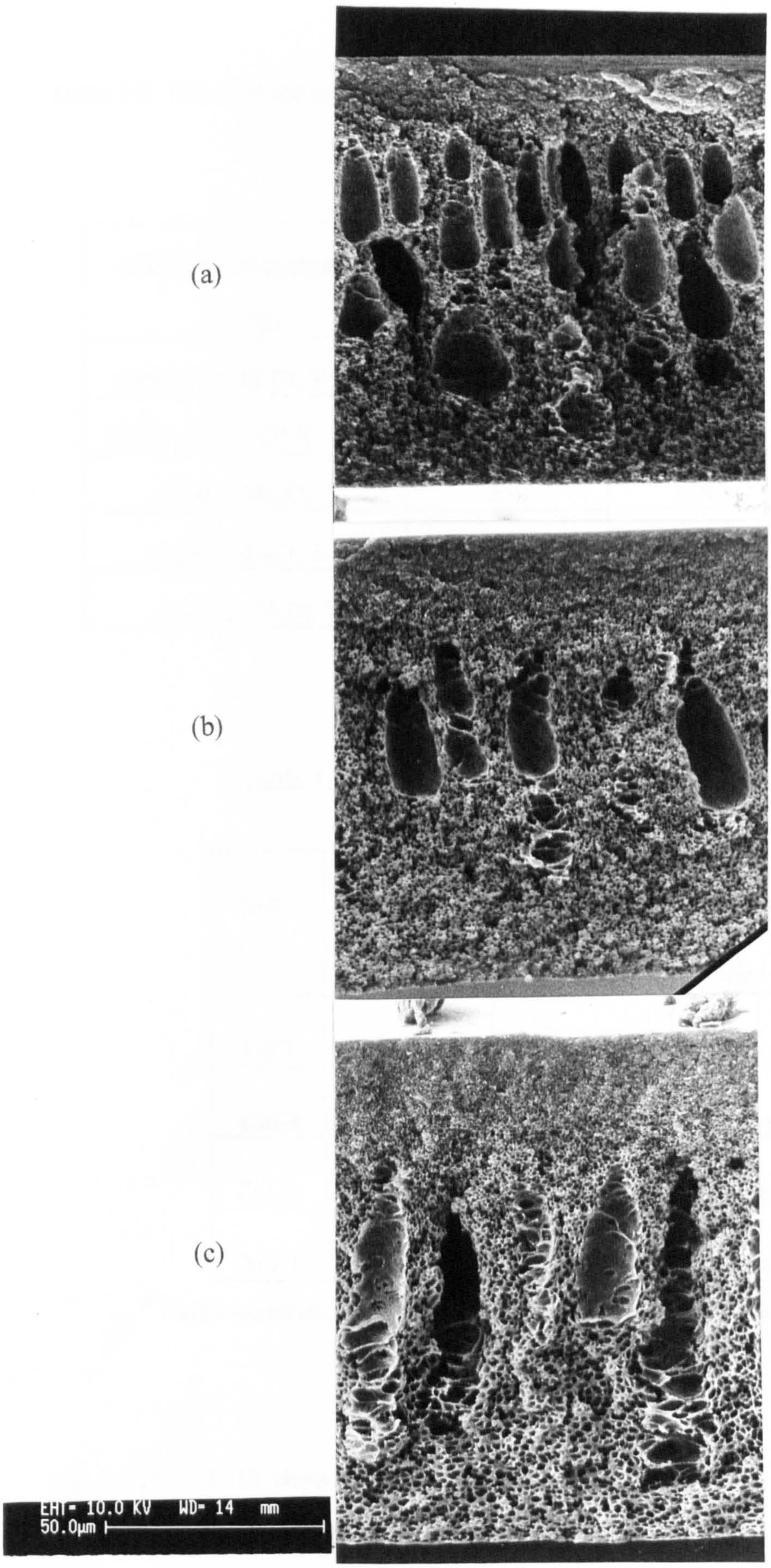

Fig. 3.9 SEM micrographs of transverse section of cast films prepared from PAN/DMF/$CuSO_4$, in wt% ratios, coagulated in water bath at 55°C

(a): PAN/DMF/$CuSO_4$: 25/73/2

(b): PAN/DMF/$CuSO_4$: 25/71.5/3.5

(c): PAN/DMF/$CuSO_4$: 25/70/5

Table 3.3 Effect of the additives concentration on the thickness of the cast film from 25% PAN in DMF casting solution

Additive concentration (wt%)	Wet thickness (μm)	Dry thickness (μm)	Shrinkage (%)
$CuSO_4$ $5H_2O$/GLY: 2/2	250	89	64
$CuSO_4$ $5H_2O$/GLY: 2/3.5	250	98	60
$CuSO_4$ $5H_2O$: 2	250	102	59
$CuSO_4$ $5H_2O$: 3.5	250	114	54
$CuSO_4$ $5H_2O$: 5	250	142	43

Table 3.4 Effect of salts on the precipitation time[a]

Salts	Precipitation Time in H_2O at		Appearance of Dried Films
	25°C	55°C	
LiCl	33 sec.	17 sec.	opaque
CuCl	27 sec.	15 sec.	pale green
$ZnCl_2$	25 sec.	19 sec.	opaque
$CuSO_4$	24 sec.	13 sec.	opaque

[a] : Salt concentration 5 wt% in 25 wt% PAN and 70 wt% DMF casting solution.

Fig. 3. 10 ~ 3. 12 show the SEM micrographs of these films, as can be seen, the porosity of the film depends on the salt additive used in the casting solution. However, there is no clear relationship between the precipitation time and the porosity of the film. When $ZnCl_2$ or CuCl is added to the casting solution, the cast

Table 3.5 Effect of salts on the thickness of the cast film and its top skin layer prepared from PAN/DMF/salts: 25/70/5(wt%)

Salts	Thickness of Wet Film (μm)	Thickness of Dried Film (μm)	Shrinkage of Dried Film (%)	Thickness of Top Skin Layer** (μm)
LiCl	250	102	59	5
CuCl	250	93	63	-
$ZnCl_2$	250	88	64	3
$CuSO_4$	250	86(142*)	65.6(43*)	0.2

*: data taken from Table 3.3;
**: estimated from SEM

film shows a porous substructure, as shown in Figs. 3.10 and 3.11. When LiCl or $CuSO_4$ is present in the casting solution, a more porous substructure results, as shown in Figs. 3.12 and 3.13. Comparing the four salts, the film not only has a more porous substructure, but also has a very thin skin layer on the top of the porous substructure when $CuSO_4$ was used, as the data in Table 3.5 indicate. Such a thin skin is likely to give faster permeation rates.

In general, the dried film thickness is related to the porosity of the dried film, that is the thicker the film, the more porous the substructure. As the results obtained from the SEM study show, the thickness of the dried film is smallest when $CuSO_4$ was in the casting solution, as shown in Table 3.5. This result contradicts the results given in Table 3.3 and is thought to be misleading, though no reason could be given. Nevertheless, as shown in Figs. 3.10 to 3.13, there is a gradual increase in the size of the pores in the substructure progressing from the top to the bottom surface of the film. These porous films show a dense skin layer on the top surface of the porous film, while the skin on the bottom surface show some pin holes when LiCl and $CuSO_4$ were in the casting solution, as seen as in Figs. 3.14 and 3.15.

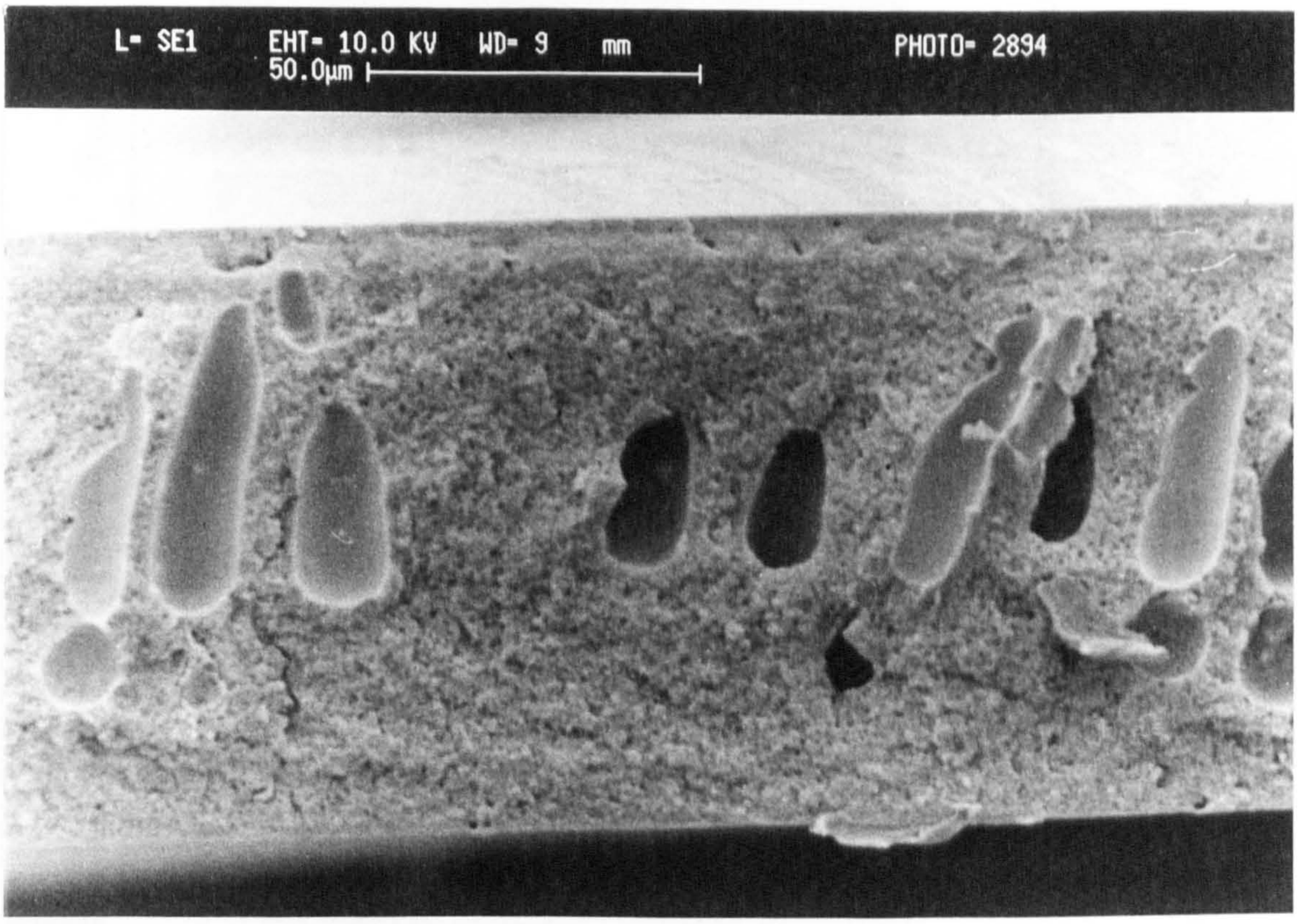

(a) Transverse section

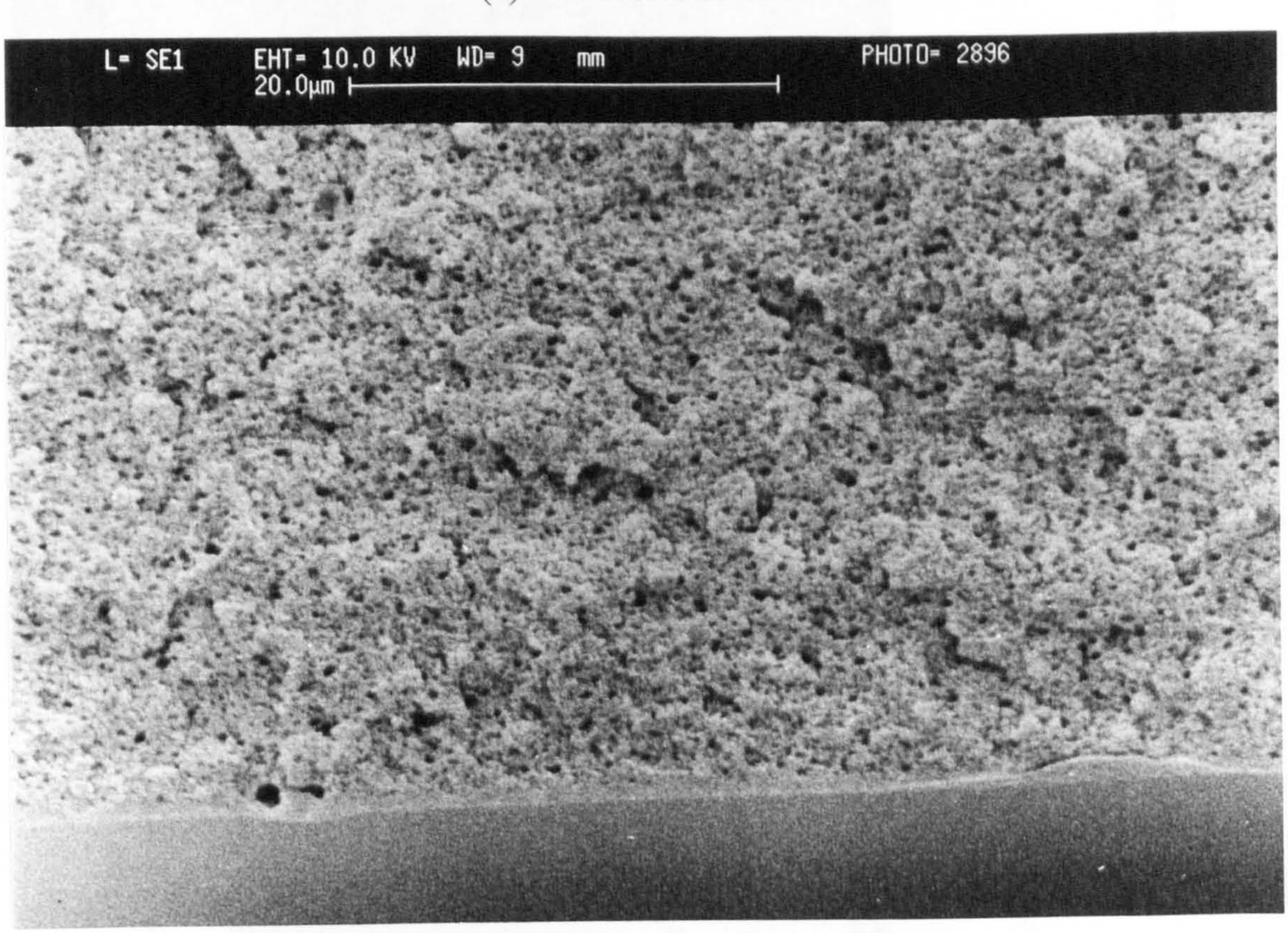

(b) Bottom skin cross-section

Fig. 3.10 SEM micrographs of transverse section of cast film prepared from PAN/DMF/CuCl: 25/70/5(wt%); coagulated in water at 55 °C

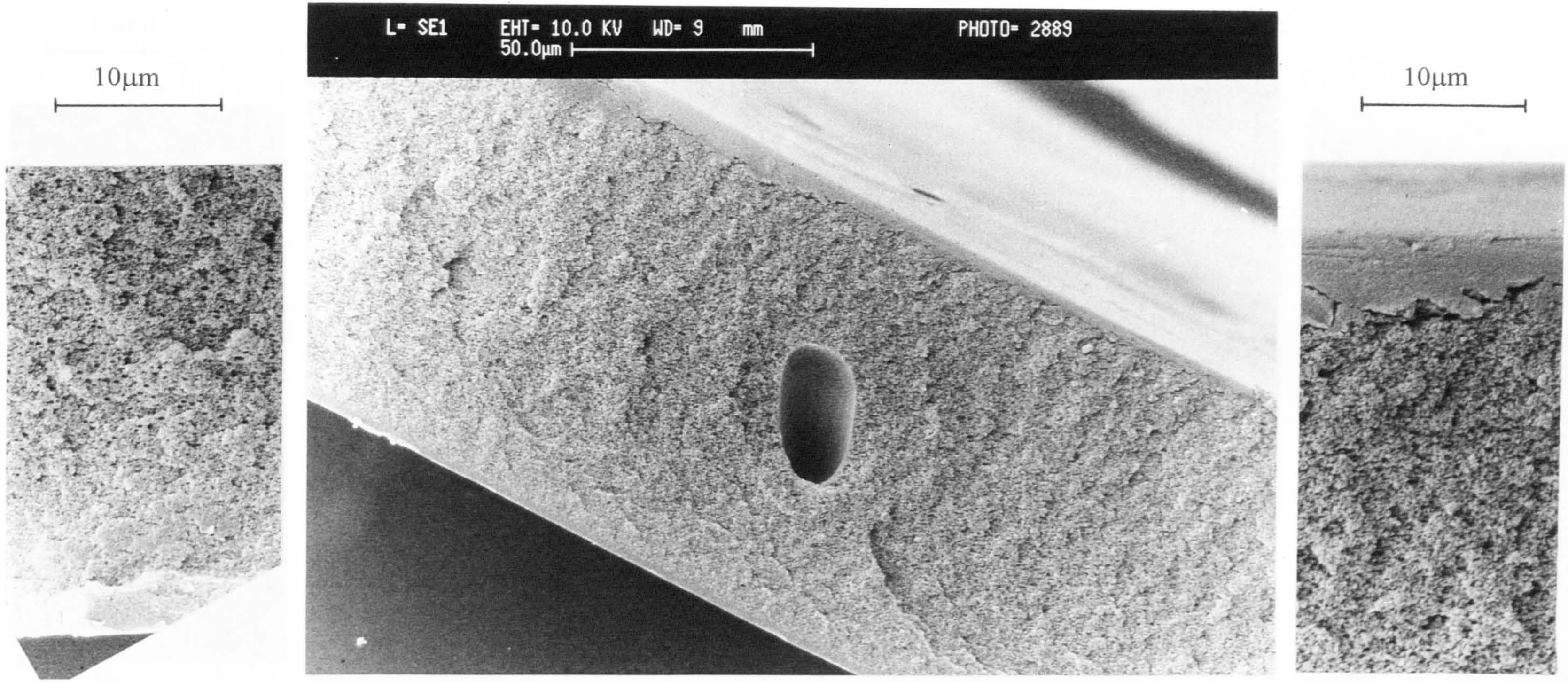

Fig. 3.11 SEM micrographs of transverse section of cast film prepared from PAN/DMF/$ZnCl_2$: 25/70/5(wt%), coagulated in water bath at 55°C

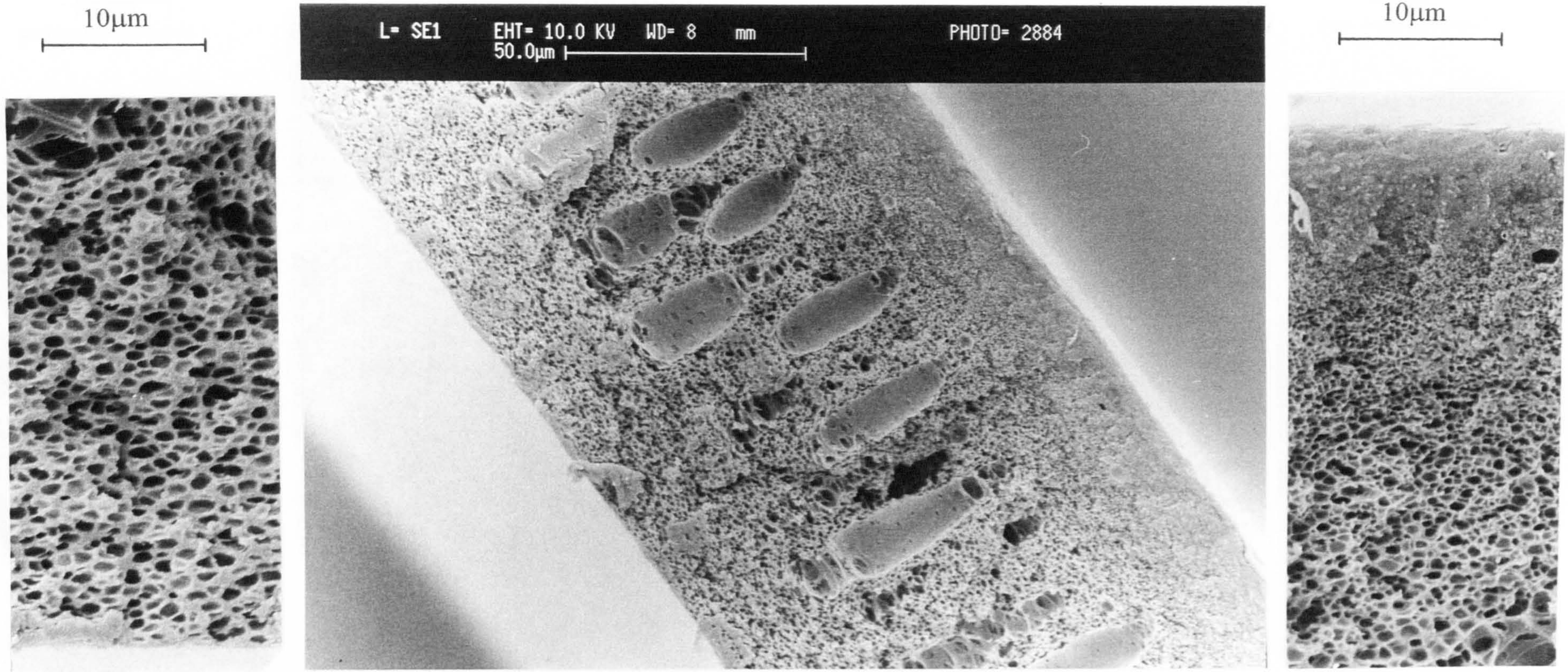

Fig. 3.12 SEM micrographs of transverse section of cast film prepared from PAN/DMF/LiCl: 25/70/5(wt%); coagulated in water bath at 55°C

Fig. 3.13 SEM micrographs of transverse section of cast film prepared from PAN/DMF/$CuSO_4$: 25/70/5(wt%); coagulated in water bath at 55°C

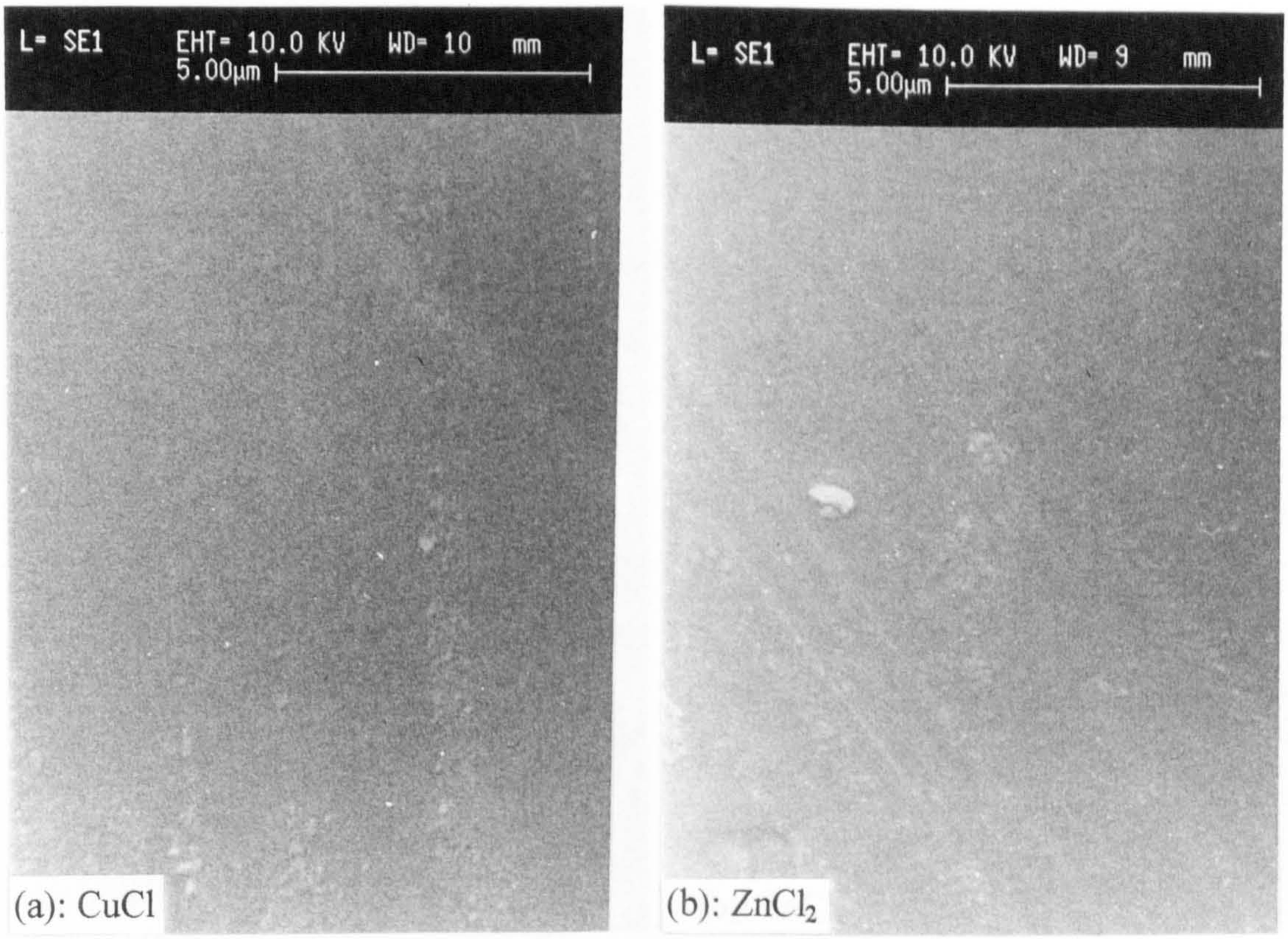

Fig. 3.14 SEM micrographs of top surface structure of cast films prepared from PAN/DMF/salt: 25/70/5, in wt% ratios, coagulated in water at 55 °C.
(a): PAN/DMF/CuCl; (b):PAN/DMF/$ZnCl_2$;
(c) PAN/DMF/LiCl; (d): PAN/DMF/$CuSO_4$ $5H_2O$

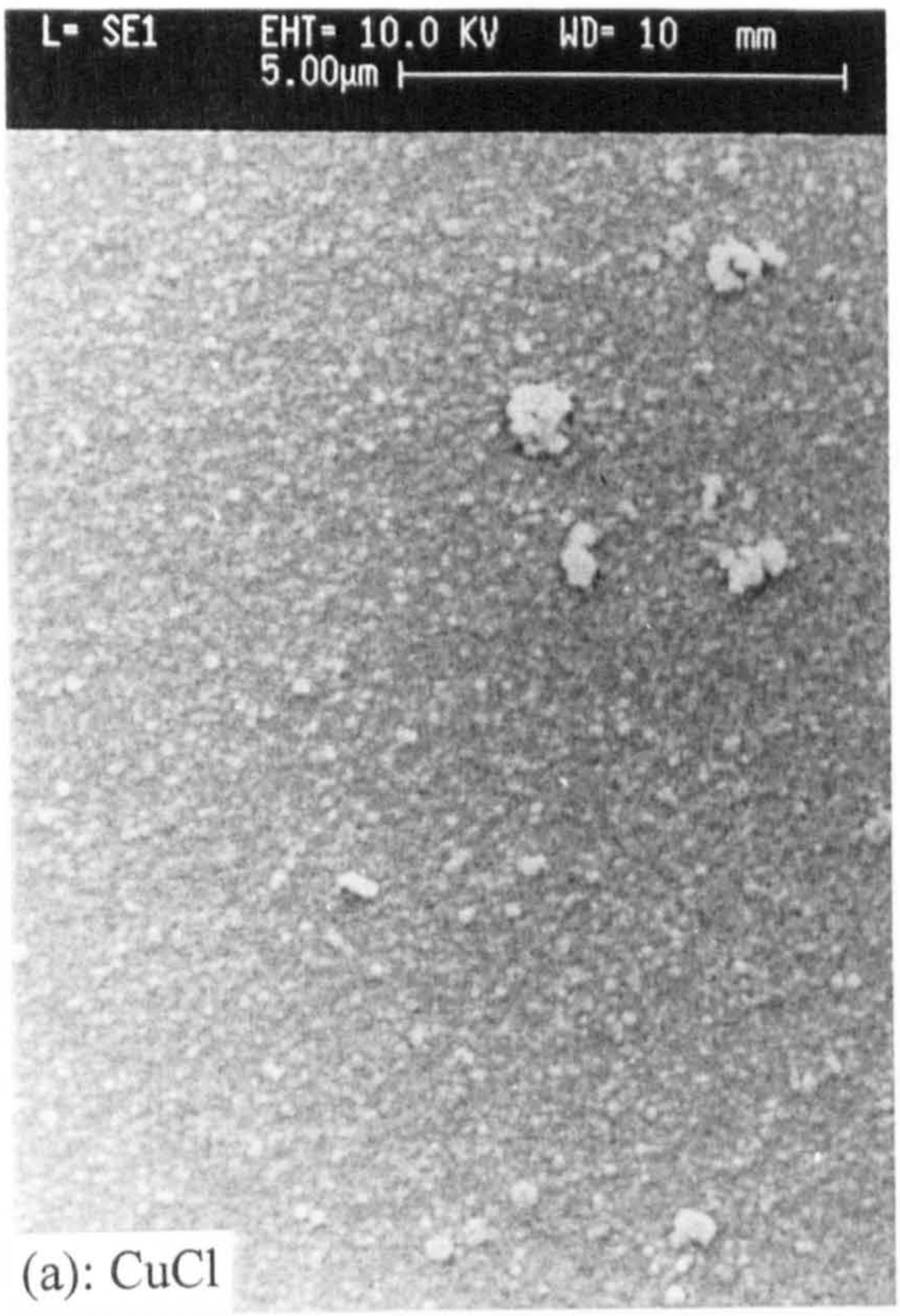

(a): CuCl

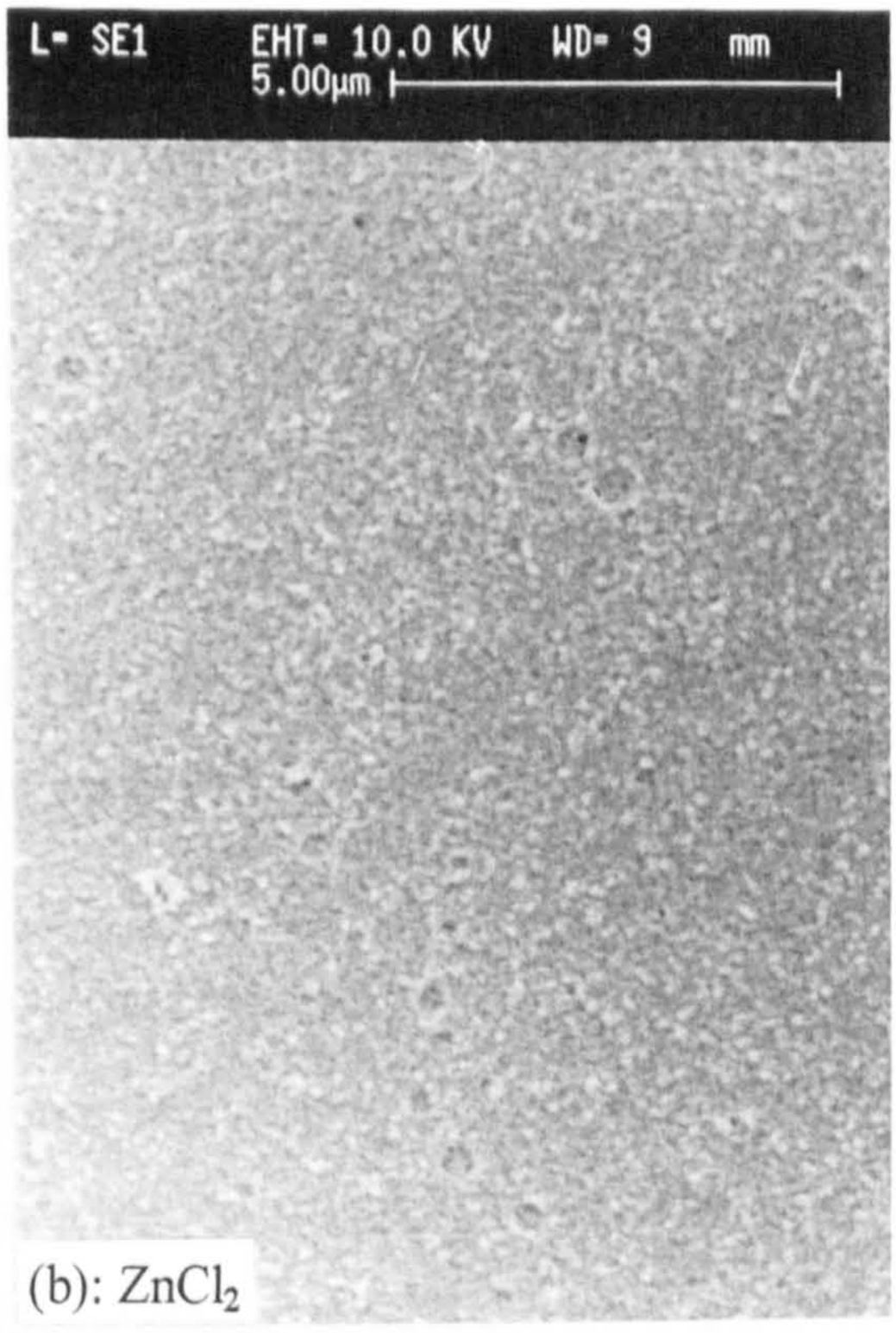

(b): $ZnCl_2$

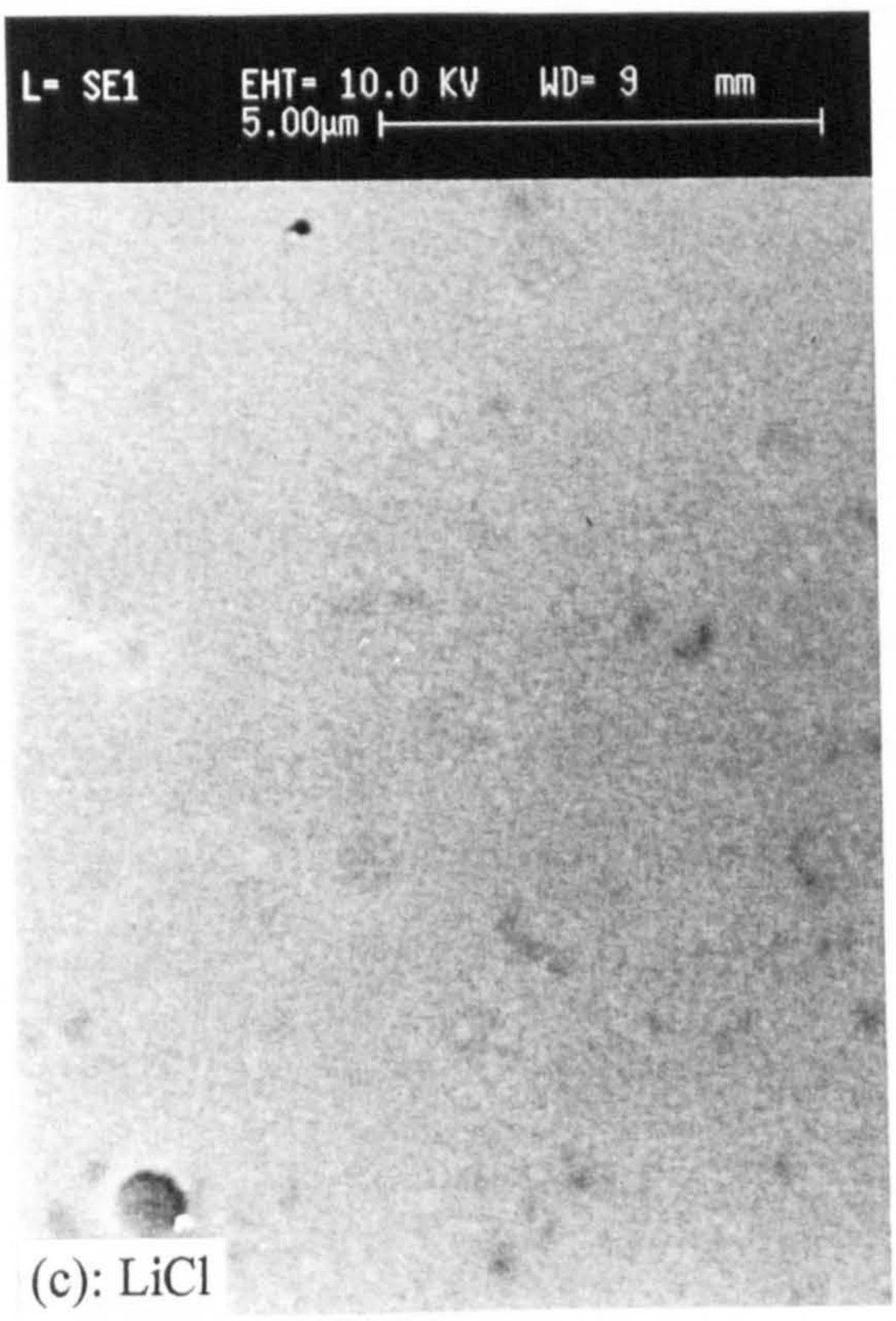

(c): LiCl

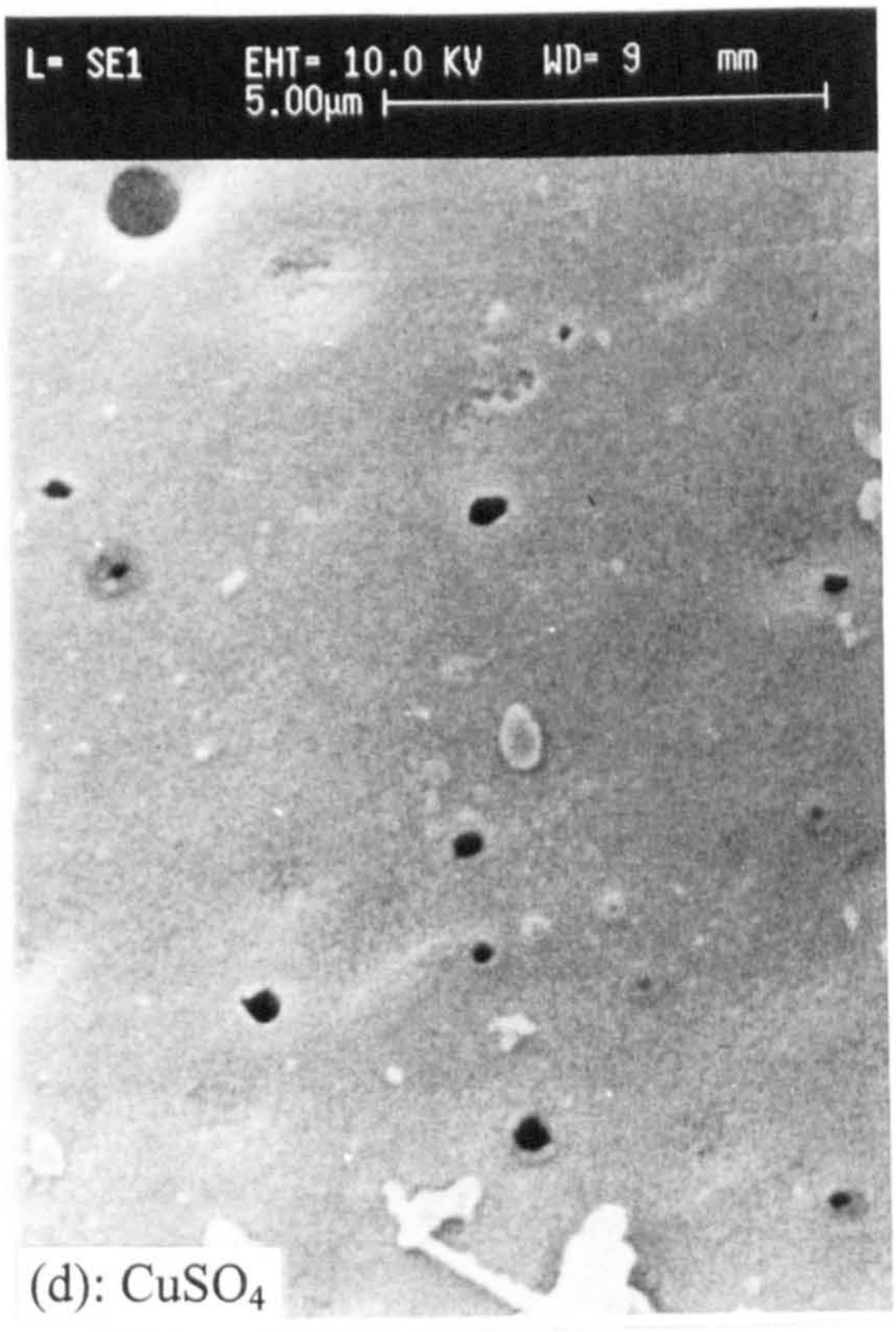

(d): $CuSO_4$

Fig. 3.15 SEM micrographs of bottom surface structure of cast films prepared from PAN/DMF/salt: 25/70/5, in wt% ratios, coagulated in water at 55 °C.
(a): PAN/DMF/CuCl; (b):PAN/DMF/$ZnCl_2$;
(c) PAN/DMF/LiCl; (d): PAN/DMF/$CuSO_4$ $5H_2O$

Above all, it is clear that these metal salt additives are more powerful than formamide or glycerol additives in altering the porous substructure of the PAN cast film. The porosity and thickness of these PAN films are dependent on the nature of the additive. In this work, a solvent system for PAN, DMF plus salt, has been found from which a flexible and porous substructure film can be produced. The effect of the $CuSO_4$ present in the casting solution suggested that there must be some interaction between the salt and the DMF, and also between the mixed solvent and the PAN, as a result of which the $CuSO_4$ enhances the polymer precipitation rate and promotes pore formation during the phase inversion process.

The interaction between $CuSO_4$ and DMF was inferred from the colour of the dope. Normally, the colour of $CuSO_4$ in water is blue. When $CuSO_4$ is dissolved in DMF the solution is green. When PAN polymer was dissolved in DMF containing $CuSO_4$, the polymer solution was also green. The colour change on mixing $CuSO_4$ and DMF may be taken as evidence to show that the DMF may form a series of complexes with $CuSO_4$ $5H_2O$ by successive displacement of water. For example, the species $[Cu(DMF)(H_2O)_4]^{2+}$, $[Cu(DMF)_2(H_2O)_3]^{2+}$, ..., $[Cu(DMF)_4(H_2O)]^{2+}$ might be formed.

The results from UV-visible spectrophotometry showed that the solution of $CuSO_4$ $5H_2O$ in DMF had an absorption maximum at 810 nm, while in water the absorption maximum is at 800 nm. DMF itself shows a maximum 270 nm, as shown in Table 3.6. The UV-visible spectral band is shifted to a slightly longer wavelength after the interaction of $CuSO_4$ $5H_2O$ and DMF which corresponds to the colour change. When a very low concentration of PAN was presented in the $CuSO_4$-DMF solution, the spectral band of the solution has a peak at 808 nm, just below the $CuSO_4$-DMF solution.

Table 3.6 The results of UV-visible spectra of $CuSO_4 5H_2O$ in water and DMF

Sample	Solution	Maximum absorption band (nm)
1	DMF	273
2	0.016M $CuSO_4 5H_2O$ in water	800
3	0.011M $CuSO_4 5H_2O$ in DMF	810
4	0.18‰ PAN in sample 3	808

Table 3. 7 The viscosity of PAN/DMF and PAN/DMF/$CuSO_4 5H_2O$ solutions

Polymer Solution	Viscosity (Pa.s)	
	25°C	60°C
PAN/DMF:25/75	195	50
PAN/DMF/$CuSO_4$: 25/72/3	234	115

If it is presumed that complex formation does occur between $CuSO_4$ and DMF, then this complex formation is believed to cause a reduction in the DMF solvent power so that it leads to increased polymer-polymer interaction. Table 3.7 shows the results of measuring the zero-shear rate viscosity of the polymer solutions. It can be seen that the viscosity of the solution is increased when $CuSO_4$ $5H_2O$ is present in the solution. It is not clear that this increase would be expected from the formation of DMF-$CuSO_4$ complex. Complex formation would make a 'poorer' solvent for the PAN which then might coil up and give a lower viscosity. Perhaps the viscosity might increase due to increased polymer-polymer interaction, giving some form of polymer association in the poorer solvent medium. Whatever happens, it is necessary to argue

that complex formation favours a reduced interaction between the polymer and the DMF, and hence facilitates the removal of the solvent during the phase inversion.

It has been observed that the precipitation time is decreased when $CuSO_4$ $5H_2O$ was present in the solution. Additionally there is already evidence that the addition of lithium salts to DMF solutions of PAN leads to films from which the DMF is more easily removed[117]. This also supports the effect of LiCl on the porous substructure of cast film produced by phase inversion in this study. It seems to be that complex formation between $CuSO_4$ and DMF acts as a "transient template" to promote pore formation in the final cast film. These results are strongly parallel to the role of propionic acid in the phase separation of polysulphone from NMP solutions[95].

Further investigation of the complexing between the cupric ion (Cu^{2+}) and DMF was carried out by IR spectroscopy. Unfortunately, the IR spectra showed only a very slight C=O band shift in the solution of Cu^{2+} in DMF (from 1661 to 1657), as shown in Fig. 3.16. It is difficult to take this as evidence to confirm the existence of complexing between the Cu^{2+} and DMF. But, it has been reported[118 ~ 120] that the absorption band of the C=O would shift to lower frequencies when complexes form between metal ions and ligands containing the carbonyl group.

As was mentioned above, the addition of $CuSO_4$ to the casting solution changes the morphology of the film. Although this result was thought to be due to complexing of Cu^{2+} with DMF, it also draws attention to a possible complexing between Cu^{2+} and the -CN group in the PAN, which affects the porous substructure of the cast film during the phase inversion process. The complexing between copper and the nitrile group in polyacrylonitrile has been mentioned in other fields[121 ~ 124]. Feild et al[121] reported the "copper" technique for dyeing acrylic fibres, which used a small

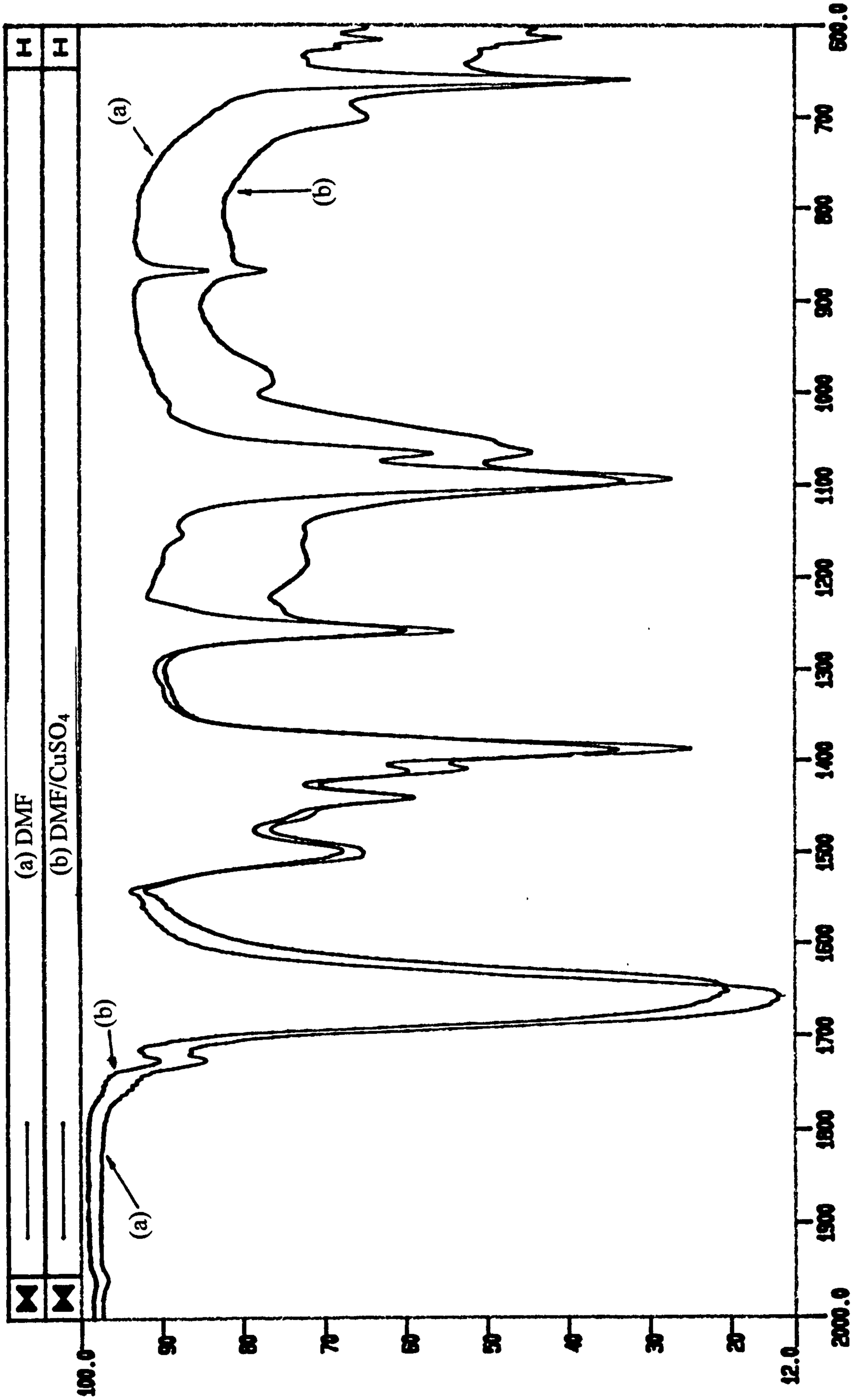

Fig. 3.16 FTIR spectra of DMF (a) and DMF/$CuSO_4$ (b)

amount of dissolved cuprous copper, obtained by reducing cupric acetate or sulphate in the dye bath to improve the dyeing of the fibres. The copper ions in this case were claimed to serves as a "bridge" between the fibre molecules and the dye molecules. In the production of electroconductive PAN fibre[122], the fibres were immersed in a cupric salt solution; the absorbed cupric ions were then reduced to cuprous by the sulphurous reducing agent. The electroconductivity is obtained through co-ordination bonds between cuprous sulphides and nitrile groups. If preoxidized PAN fibres were pretreated with cuprous chloride, the carbon fibres produced have mechanical properties much higher than those obtained from untreated precursor[123]. The effect of cuprous salt on PAN fibre during thermostabilization also shows that the glass transition temperature of PAN treated with cuprous salt is 45°C higher than that of the untreated samples[124].

As the results from these references shown, there seems no doubt that cuprous ions show a tendency to complex with the nitrile group of PAN. It also shows that PAN can absorb cupric ions.

In order to know whether the Cu^{+} in the PAN/DMF casting solution favours the production of a porous casting film, CuCl (5 wt%) salt was added to the casting solution. All the CuCl did not appear to dissolve. After the film precipitated in the precipitant (water), it changed colour from colourless to pale green after two/three days of washing. The colour was similar to the solution of $CuSO_4$ in DMF. This is almost certainly because the Cu^{+} oxidised in the air and Cu^{2+} complexed with the residual DMF which was still in the cast film. So the cast film colour changed to pale green slowly. Because CuCl is not very soluble in DMF, it is unlikely that there is a complex of Cu^{+} with DMF. The cast film showed a less porous substructure than when $CuSO_4$ was in the casting solution. Hence, there is no evidence for DMF-Cu^{+} complexing but it cannot rule out Cu^{+}-PAN complexing.

Let us suppose there is a complex of Cu^{2+} with -CN groups in PAN. If this formed, the precipitation rate would increase because the ability of the DMF to complex (or solvate) with the -CN group would be reduced by the presence of the Cu^{2+}-CN complex. This would allow an easier removal of the solvent from the cast film during the phase inversion process. The atomic absorption analysis results show only very small amounts of copper (less than 0.2%) in the dried film, which means that most of the copper was leached out of the film during the period of washing. Unfortunately, the IR spectrum of the dried film in this study does not show any significant difference between the films with and without $CuSO_4$ present, as seen in Fig. 3.17. The difference that do occur are due to H_2O (3490 cm^{-1}) and a band at (1450 ~ 1750 cm^{-1}) which was variable from sample to sample of Courtelle.

Nevertheless, there is no doubt in this study that the Cu^{2+} present in the casting solution had a profound effect on the morphology of the cast film, but there is no convincing evidence for complexing between Cu^{2+} and -CN. In later studies, a very interesting result was obtained after the PAN hollow fibres were treated with cuprammonium hydroxide solution, in that the PAN hollow fibre was no longer soluble in DMF. This result may be taken as evidence that there is a complex of copper with the polymer. This will be discussed in Chapter 5.

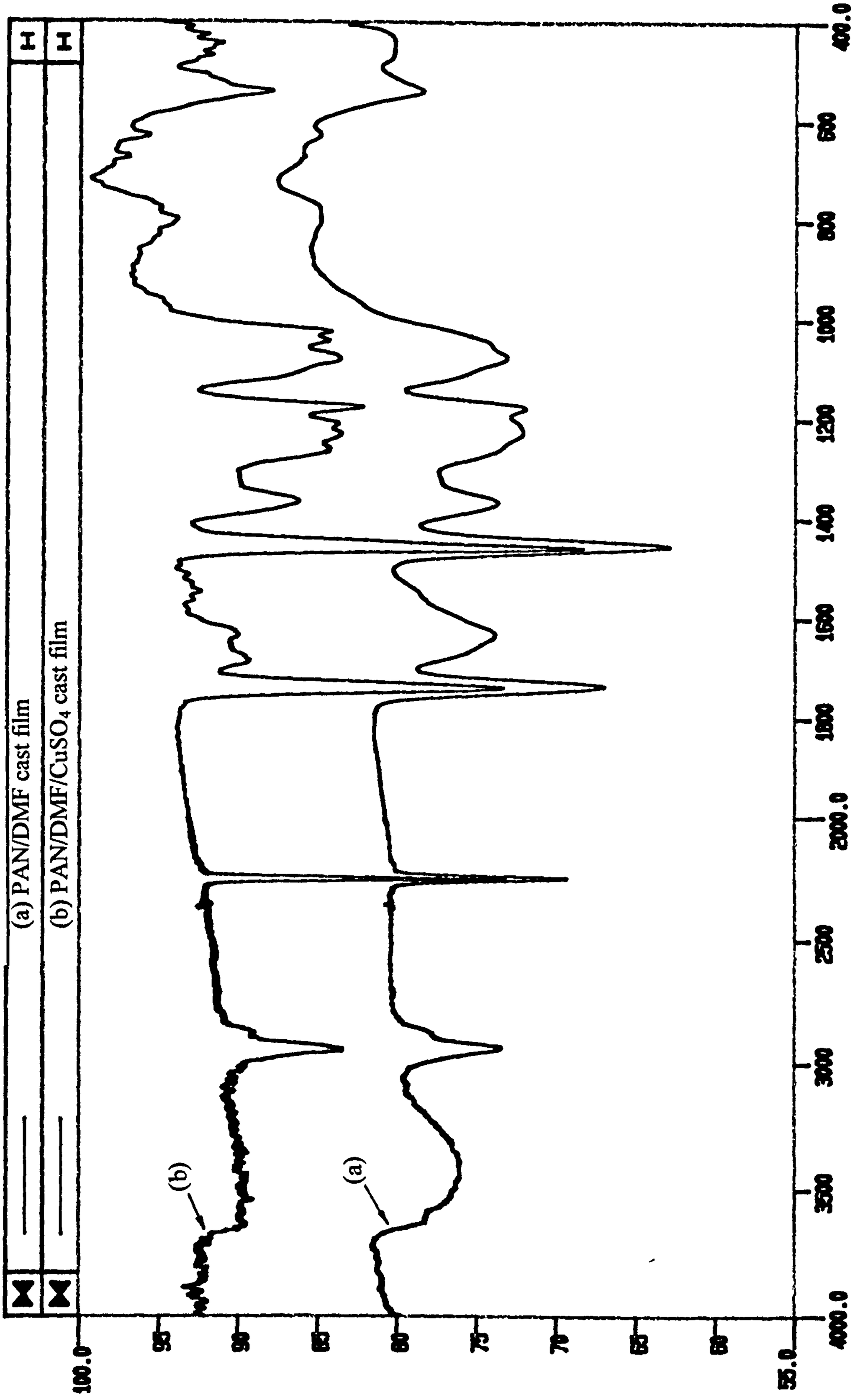

Fig. 3.17 FTIR spectra of dried films: (a) PAN/DMF cast film; (b) PAM/DMF/$CuSO_4$ cast film

CHAPTER 4

PAN HOLLOW FIBRE MEMBRANES

4. 1 Introduction

Hollow fibre membranes used for ultrafiltration and gas separations have been studied for more than 10 years in this Department. Rogers and Senn[100] studied the effect of various spinning conditions on the morphology and dimensions of hollow fibres based on polysulphone (PSF) and polyetherketone materials. They showed that the macrovoid structure and porous substructure can be modified by changing the spinning parameters and the composition of the polymer spinning solution. They also investigated different solvents and solvent/nonsolvent systems in order to reduce the macrovoid structure in hollow fibres. Among the systems studied for PSF, DMAC, DMF, 1-Fp, and 1-Fp/FA, the 1-Fp/FA(9:1) solvent/nonsolvent system resulted in a macrovoid-free structure, and the resulting fibres were found to possess a porous substructure with a thin top skin layer.

Brown[101] and Deshmukh[102] optimised the spinning conditions and found that the 1-Fp/FA(9:1) type PSF hollow fibres still had poor gas separation properties even after being Sylgard coated. A significant amount of residual solvent, about 3%, in PSF as-spun hollow fibres had been detected by thermogravimetric analysis (TGA). The residual solvent in the hollow fibres was responsible for the poor gas separation performance of PSF hollow fibres. In order to remove the residual solvent from the hollow fibre membrane, Brown used a vacuum oven treatment technique at 115 °C, which was below the Tg of the polymer. This treatment was found to be very effective in removing residual solvent from the hollow fibres. After this treatment, the gas permeation rates of the as-spun hollow fibre membranes for H_2, CO_2 and CH_4 were reduced by more than 50% because of the densification of the PSF hollow fibres during the treatment. However, the separation factors were still found to be in the Knudsen flow regime. After coating these hollow fibre membranes with Sylgard 184, the membranes showed very good separation factors which were about twice those of the Sylgard coated as-spun hollow fibre membranes without the vacuum oven

treatment. Deshmukh revealed a relationship between the washing procedures and the residual solvent content in the PSF as-spun hollow fibres. The washing procedure had a significant effect on the residual solvent content in the as-spun hollow fibre membranes. In order to reduce the residual solvent in the as-spun hollow fibres as much as possible, three weeks of thorough washing in water, changing the water daily, was recommended[102].

Membranes used in separation technologies can be either in film or in hollow fibre form. In this study, the fabrication of PAN asymmetric hollow fibre membranes was investigated. Membranes in hollow fibre form not only provide a greater amount of membrane separating surface area per unit volume of separation apparatus than that which is provided by film membranes, but also are generally self-supporting even under operating conditions. More recently, hollow fibre membranes have been widely used in membrane separation processes. The apparatus is also attractive in the aspects of convenience, in size and reduced complexity of design. Polyacrylontrile has very good gas separation factors, especially for the separation of gases such as hydrogen from nitrogen and methane (α_{H_2/N_2}=625, α_{H_2/CH_4}=10000, respectively), but it has very low gas permeabilities[125, 126]. In order to examine the possibility of using PAN hollow fibre membranes for gas separation technology, basically, it was necessary to spin hollow fibres with an asymmetric structure which was composed of a thin, dense skin layer on the top of a porous substructure to obtain as high gas permeability as possible.

4. 2 Experimental

Polyacrylonitrile spinning solutions were prepared as described in section 2.2.2.1 and the spinning processes for the hollow fibre membranes were outlined in section 2.2.2.2. After studying the experience of spinning hollow fibres described by

previous research workers[100 ~ 102], the first two spinning runs were carried out in order to get some spinning experience and know-how of spinning PAN hollow fibres. Afterwards, more serious spinnings were carried out to obtain the best possible asymmetric structures of PAN hollow fibres.

4. 3 Results and discussion

4. 3. 1 Morphology and fibre dimension measured by SEM

Figs. 4.1 and 4.2 show the cross sections of the hollow fibres from the first two spinning runs. Fig. 4.1 reveals that the hollow fibre made from 25 wt% PAN in 75 wt% DMF spinning solution had a dense polymeric matrix with collapsed macrovoids, and a deformed cross sectional structure. These micrographs also show that a serious shrinkage of fibre was occurring during the precipitation and drying processes, which caused the macrovoids to collapse. When an addition of $CuSO_4$ was made to the PAN/DMF spinning solution, the hollow fibre not only had a porous polymeric matrix with some macrovoids, but also showed fewer collapsed macrovoids in the cross sectional view, as seen in the SEM micrographs in Fig. 4.2, in agreement with the results obtained by film casting when $CuSO_4$ was present in the casting solution (Chapter 3). The position of the lumen of the hollow fibre was not in the centre of the fibre, which was believed to be caused by a combination of factors related to the failure to centre the tube in the orifice and also to the ease of distorting the filament cross section on collection.

There are many factors which affect the morphology of asymmetric hollow fibres, for example, polymer concentration, solvent/nonsolvent system, temperature of coagulation bath, additives in the spinning solution, and coagulation bath

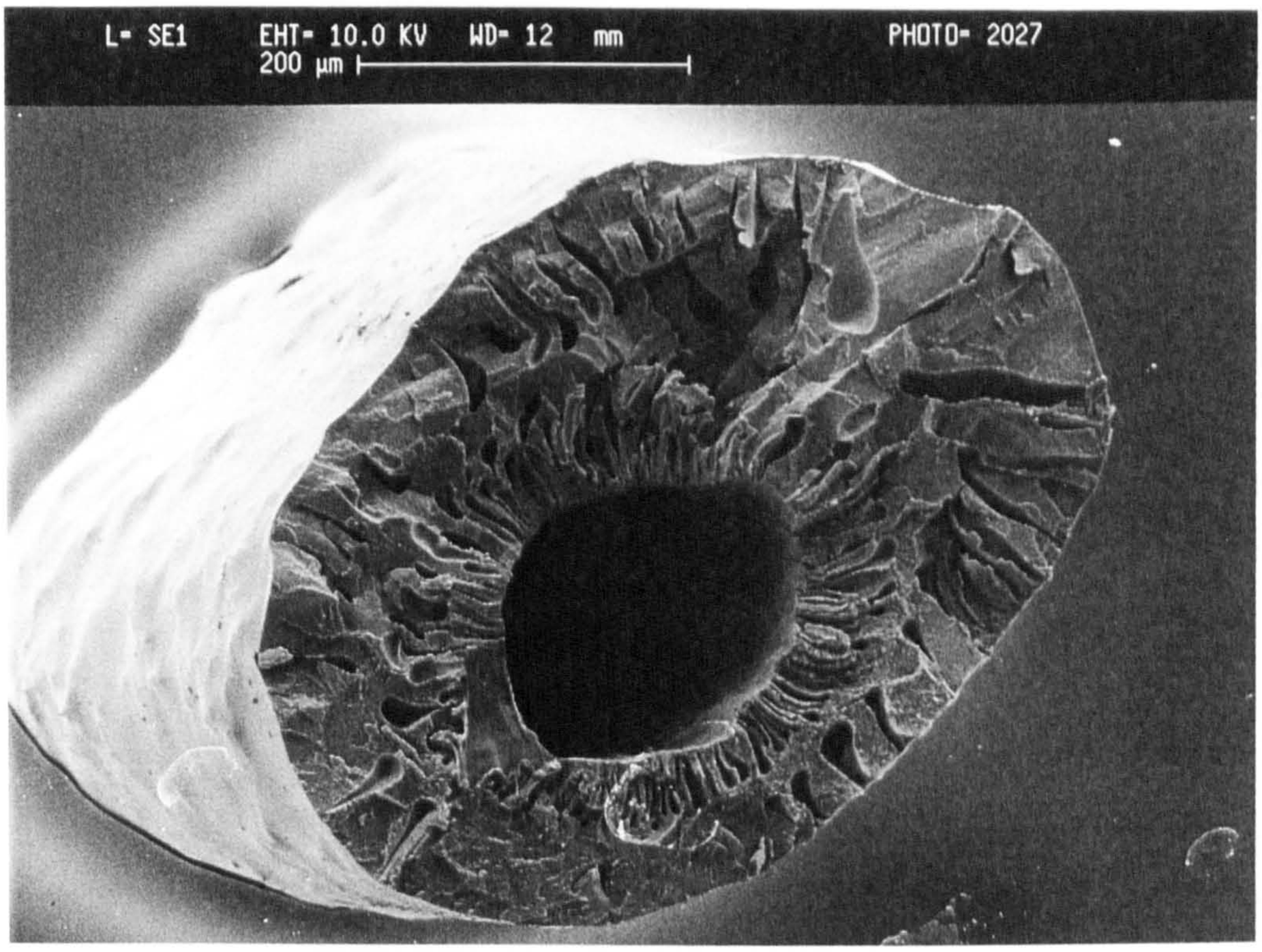

Fig. 4.1 (a).The cross section of hollow fibre

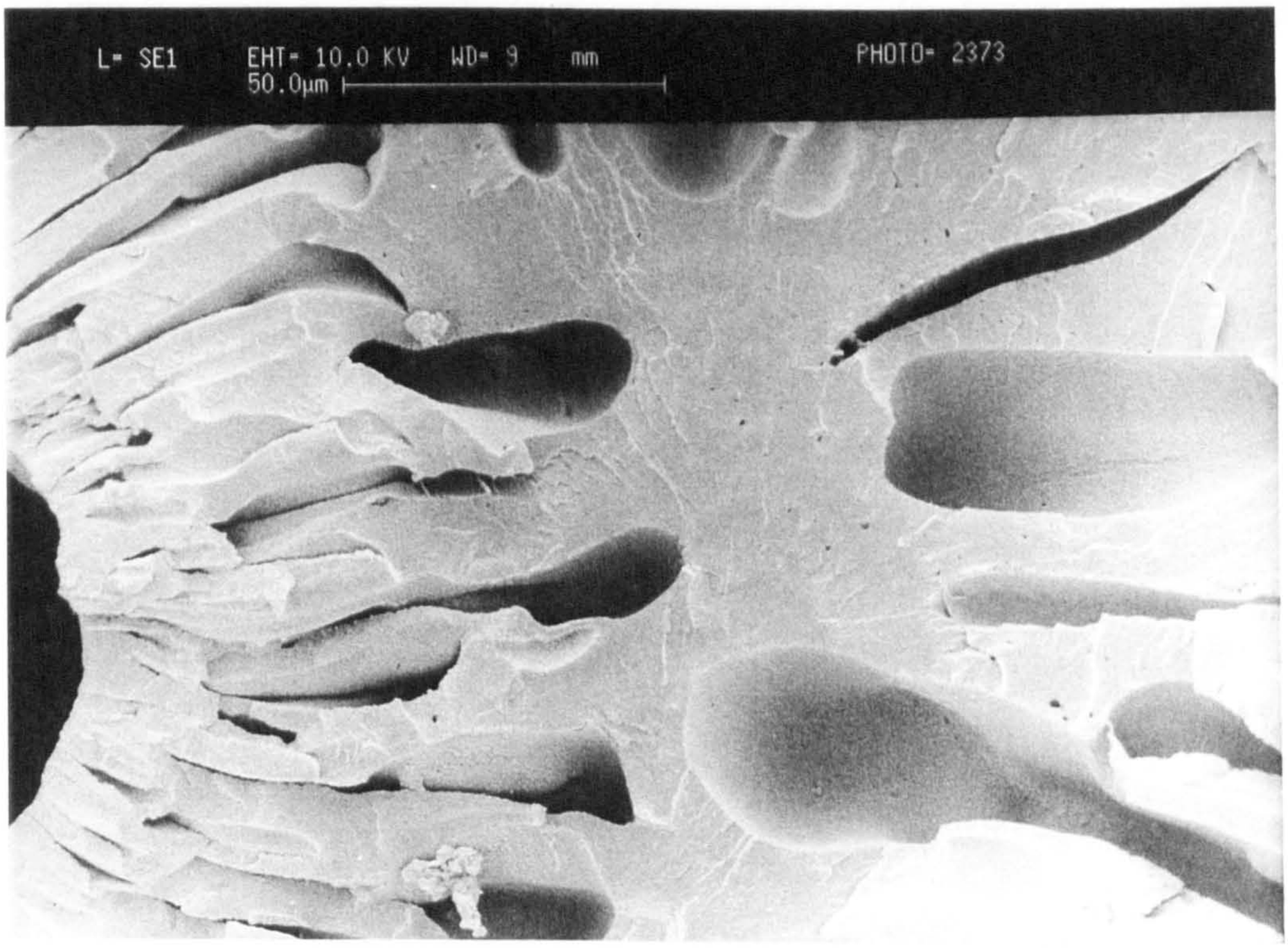

Fig. 4.1 (b). Enlarged cross section of the hollow fibre

Fig. 4.1. SEM micrographs of the cross section of PAN hollow fibre spun from 25 wt% polyacrylonitrile in 75 wt% DMF, precipitated in water bath at 5 °C

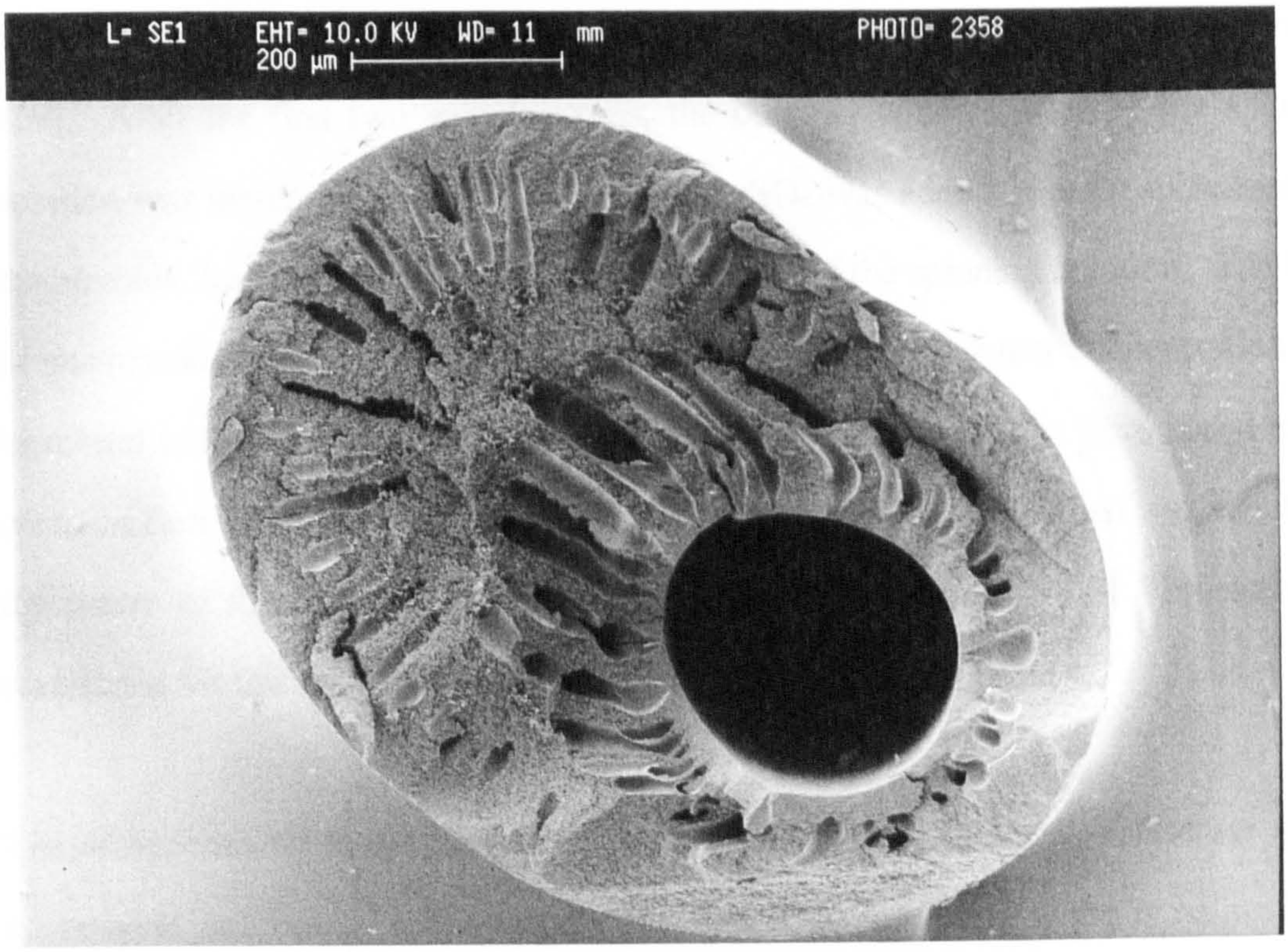

Fig. 4. 2 (a).The cross section of hollow fibre

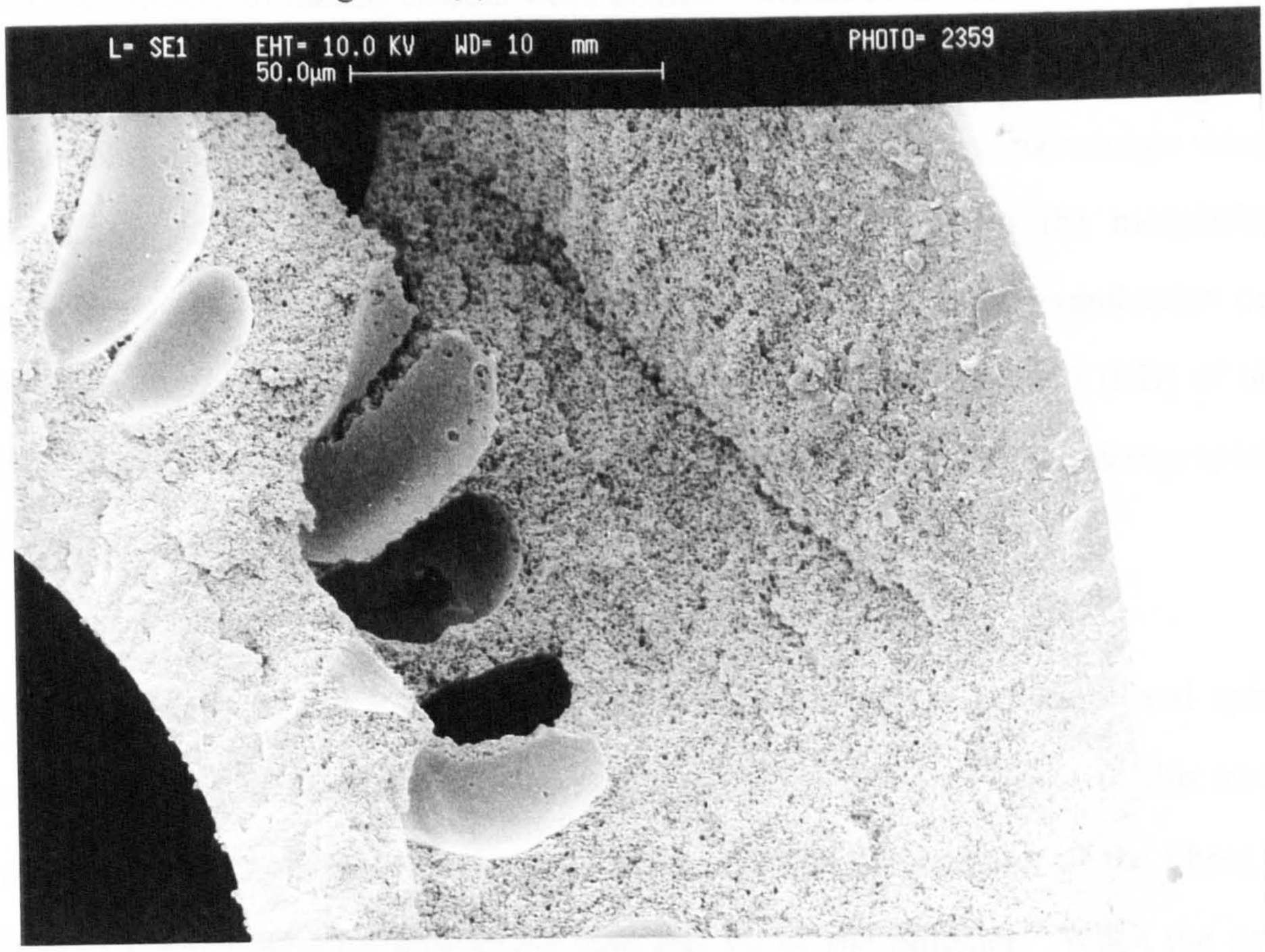

Fig. 4.2 (b). Enlarged cross section of the hollow fibre

Fig. 4.2. SEM micrographs of the cross section of PAN hollow fibre spun from 23.5 wt% polyacrylonitrile in 70.5 wt% DMF, 3.5 wt% $CuSO_4$ and 2.5 wt% GLY, precipitated in water bath at 50 °C ~ 55 °C

composition[100, 101, 127, 128]. The general mechanism for the formation of asymmetric hollow fibres using phase inversion has been described by Strathman[79, 129]. After the first two spinning runs, the polymer concentration of the spinning solution was increased to 25 wt% in DMF, $CuSO_4$ was added in order to reduce the macrovoids, leading to an increase in the viscosity of the spinning solution. The level of macrovoids in the hollow fibres was reduced when the polymer concentration was increased in the presence of $CuSO_4$ in the spinning solution. The fibre had a round cross-section and a porous substructure, and the position of the lumen was exactly in the centre of the fibre, as seen in the SEM micrographs in Fig. 4.3. The spinning conditions for this spinning Batch No: 25/05/00 are given in Table 4.1.

The dimensions of the hollow fibres were measured by SEM, digital screw gauge micrometer and optical microscope. The first measurement was the most accurate, but the number of measurements were limited because of the difficulties in preparing samples. The second measurement was also very accurate, but it can only be used to measure the outsider diameter of the hollow fibres. The optical microscope was used to collect initial information about the fibre dimensions and the morphological structure of the hollow fibre, and to select the best samples for examination on the SEM. Table 4. 2 shows the outer diameter (O.D) and inner diameter (I.D) of typical PAN hollow fibres (Batch No: 25/05/00) as measured from SEM micrographs, see Fig. 4.3.

The diameters of the PAN hollow fibres varied with the spinneret and spinning conditions, which is clear from the results obtained by Senn[100]. In this study, it was found that attempts to anneal the fibres reduced the diameter of the fibres, even though the temperature was lower than the Tg of the polymer. When the as-spun hollow fibres were annealed in hot water or in a vacuum oven at elevated temperatures, the diameter of the fibre decreased, as shown in Table 4.3. The

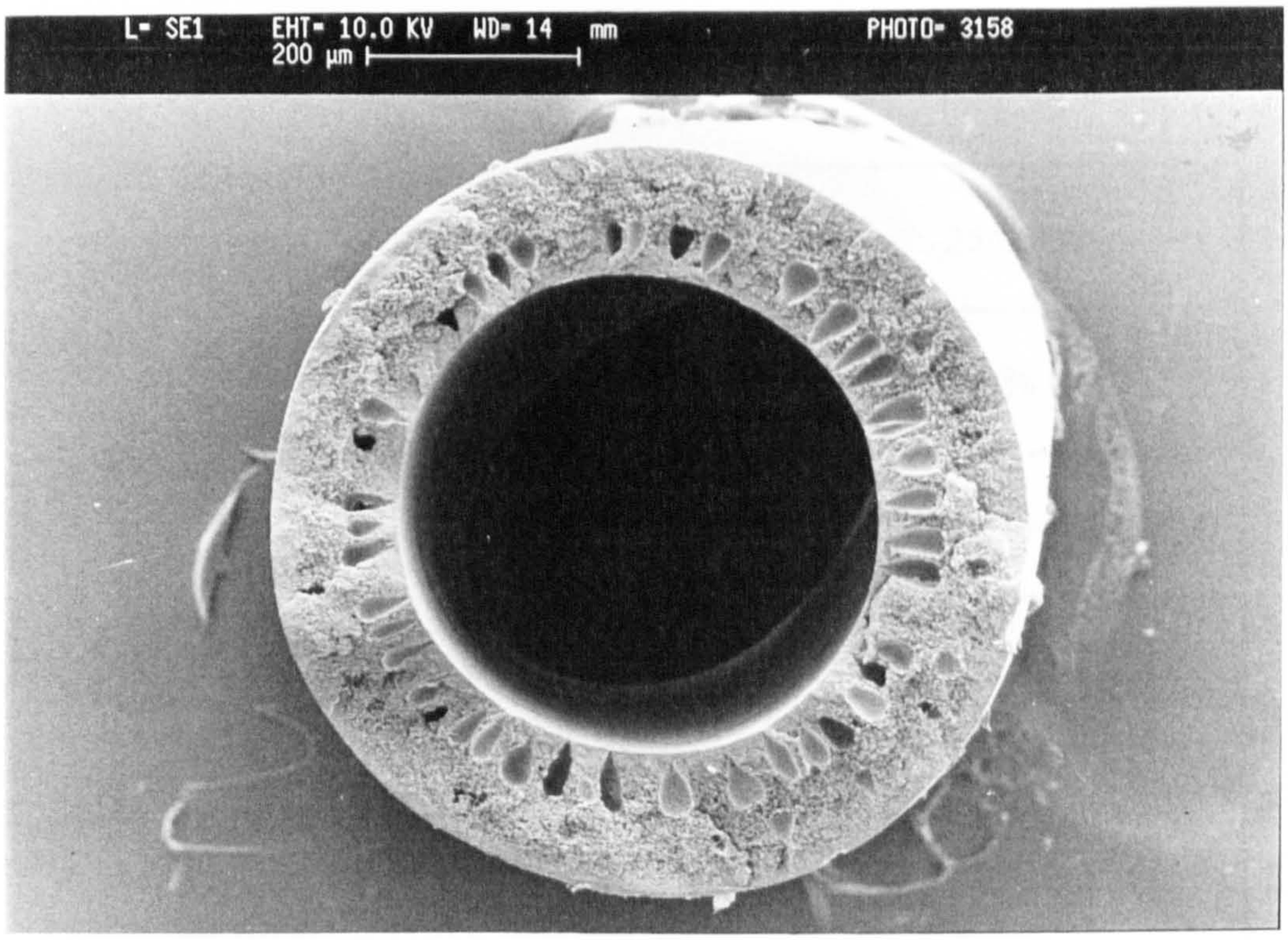

Fig. 4.3 (a).The cross section of hollow fibre

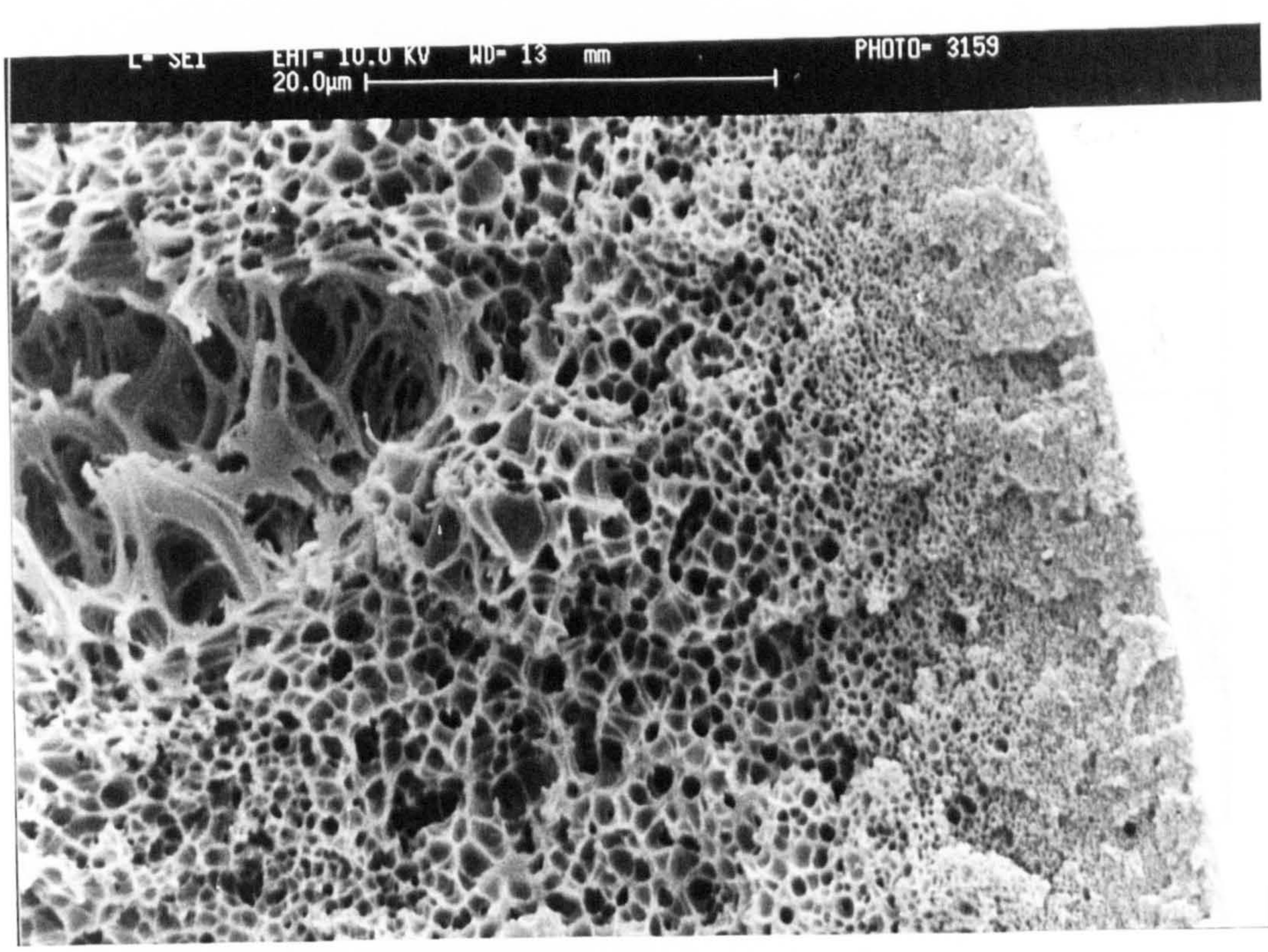

Fig. 4.3 (b). Enlarged cross section of hollow fibre

Fig. 4.3. SEM micrographs of the cross section of PAN hollow fibre spun from 25 wt% polyacrylonitrile in 70 wt% DMF and 5 wt% $CuSO_4$, precipitated in water bath at 50 °C ~ 55 °C

Table 4.1 Spinning conditions

Spinning batch No:	25/05/00
Polymer concentration	25 wt% PAN
Solvent/additive	DMF/$CuSO_4$=70/5(wt%)
Spinneret dimension	580/330/150 μm
Polymer extrusion temperature	60 °C
Coagulation bath temperature	50 °C~55 °C
N_2 pressure	30 psi
Jet gap	30 mm
Linear extrusion rate	16.03 m/min.
Stretch ratio	0.44 (0.67)
Water injection rate	1.06 ml/min.
Water injection temperature	40 °C

Table 4.2 PAN hollow fibre dimensions (Batch No:25/05/00)

Mean O.D (μm)	Mean I.D (μm)
770	450

reduction in the diameter was expected when the fibres were treated at elevated temperatures above the Tg of the polymer. At this higher temperature, annealing a porous fibre results in a diminution of the porosity of the fibre, which will lead to densification and shrinkage. The diameter of the fibres will then be decreased. The results in Table 4.3 also show that the diameter of the fibres is decreased even in water at a temperature (65 °C) that is lower than that of the Tg of the polymer (in the dry state). The reason for this is that the introduction of thermal energy causes transitional motion of various elements which form the borders of the pores in the fibre[130]. Another reason may be that the Tg of PAN polymer will be lower when it is in the wet environment[131].

Table 4. 4 shows the effect of coagulation bath temperature on the diameter of the as-spun fibre. In a single coagulation bath system, the diameter of the fibre was increased when the temperature of the coagulation bath increased. This result can be related to the increase in the precipitation rate and the increase in porosity of the fibres. In the earlier cast film study (Chapter 3), increasing the coagulation bath temperature increased the precipitation rate and the porosity of the cast film during the phase inversion process. As expected, therefore, a similar result was noted in the dry-jet wet spinning of the fibres. Under the same spinning conditions, increasing the porosity of the hollow fibre will lead to an increase in the outer diameter of the fibre.

Table 4. 3 Effect of temperature on the diameter of PAN hollow fibre membranes during annealing treatments

Sample	Treatment Conditions	Diameter(s.d*) (μm)	
		Before	After
Batch No: 25/35/21 as-spun hollow fibre	1 min. at 65 °C in H_2O	648 (3.9)	642 (3.8)
	2 min. at 65 °C in H_2O		635 (9.9)
	1 min. at 90 °C in H_2O		616 (2.2)
	2 min. at 90 °C in H_2O		619 (6.7)
	20 min in vacuum oven at 40 °C	672 (3.5)	672 (3.7)
	70 °C		670 (9.1)
	100 °C		658 (10.6)
	130 °C		637 (5.6)
	160 °C		627 (10.0)
	190 °C		617 (4.1)

*: Standard deviation

Table 4.4 Effect of coagulation bath temperature on the diameter of PAN hollow fibre membranes

Sample	Coagulation bath temperature.	Diameter(s.d) (μm)
Batch No: 25/35/00	30 °C	570 (10.2)
	40 °C	606 (9.5)
	50 °C	632 (9.0)
	60 °C	646 (8.9)

Table 4.5 Effect of drying procedures on the diameter of PAN hollow fibre membranes

Sample	Drying methods	Diameter(s.d) (μm)
Batch No: 25/35/21	Air dried	636 (3.7)
	S.E dried [a]	650 (4.3)
Batch No: 25/35/22	Air dried	591 (5.1)
	S.E dried	609 (7.0)
Batch No: 25/05/00	Air dried	702 (9.6)
	S.E dried	718 (1.8)

a: S.E is solvent exchange drying method.

PAN hollow fibres are produced by the dry-jet wet spinning process which involves phase inversion. Therefore the fibres are produced initially in the wet state and must be dried prior to use. The end products, after washing in water for a period of time, are invariably wet membranes. It is necessary to consider the effects of the drying process on the porosity of the end products. The PAN hollow fibres were subjected to two different drying processes: one was drying the fibres in air after the washing period; another was drying the fibres by a solvent exchange procedure, as described in section 2. 2. 3. From the results shown in Table 4.5, the diameters of the fibres are larger when the fibres are subjected to drying by the solvent exchange drying method than when dried in air. This result can be explained by the higher surface tension of water. As can be seen in Fig. 4.1, a significant fibre shrinkage and collapse of macrovoids can occur in PAN hollow fibre. This collapsing force was suggested to be the capillary pressure acting on the pore structure ($P_c=2\gamma/r$, where γ is the surface tension of the liquid, r is the radius of the capillary). When water is removed from the wet porous fibres during drying[91], a significant collapsing force will cause a loss of porosity in the porous layer of the fibres, so that drying may well result in

densification. When the porous PAN hollow fibres were dried by a solvent exchange method, the water was sequentially replaced by liquids of a lower surface tension than water producing a lower collapsing force. This can be effected with a minimum loss of porosity. During the drying process, the residual solvent in the fibres will also be extracted by the solvent exchange. This result was confirmed in a study on PSF hollow fibre membranes for British Gas Plc (see Appendix). After the fibre was dried by the solvent exchange drying method, the fibres not only have a larger diameter than those dried in air, but also have larger pores on the surface of the fibres. This will be shown in the next section.

4. 3. 2 Pore radius and effective porosity of PAN hollow fibre membranes

Separation properties of asymmetric hollow fibre membranes for gas separations are adversely affected by skin defects occurring during the skin formation. It has been clearly demonstrated by many workers[22, 101, 102] that it is very difficult to produce a thin skin with a defect-free structure. Attempts to spin hollow fibres which had an effectively nonporous skin layer generally resulted in fibres which gave relatively slow gas permeation, since the skin layer thickness was increased significantly. It is obvious that skin structural parameters of the hollow fibre such as skin thickness, surface porosity and mean pore radius, and morphology control the gas permeation performance. Recently, several mathematical models[132 ~ 134] have been developed for characterising the skin of asymmetric hollow fibre membranes.

According to the mathematical models, these methods can be classified into two main groups: one is based on porous membranes, another is based on the presence of a very small number of pores in the skin layer of the membranes. In the former, most of the gas flow would pass through the pores because the resistance to flow of the pores was so much less than the resistance to flow of the dense portion of the surface. The gas separation factors observed would be characteristic of Knudsen

flow. In the latter, a considerable amount of gas would flow through the dense portion of the surface. The gas separation factor obtained would result from a combination of Knudsen flow in the pores and solution-diffusion flow in the dense portion of the surface. Due to the different assumptions involved in these mathematical models, different results for the mean pore radius have been obtained by others[101, 102] when different gases and models were used for characterising the skin structure.

In a method introduced by Yasuda and Tasil[134], which was based on gas flow in porous media, the mean pore radius and effective porosity of microporous membranes can be determined by gas permeation rate measurements. The total gas flux through porous membranes is dependent on the molecular weight of the gas (M), the gas viscosity (η), temperature (T) and pressure (p), as well as the pore radius of the membrane. The following theoretical considerations applying to the calculation of the mean pore radius and effective porosity have been described by this method. The gas flux J through the hollow fibre can be generally expressed by the flux equation:

$$J = K\frac{\Delta p}{l} \tag{4-1}$$

where: K is the permeability coefficient ($m^2\ s^{-1}$); Δp is the pressure difference across the membrane of thickness (Pa); l is the thickness of the sample (m).

$$K = \frac{l\,p'}{A\,\Delta p}\cdot Q \tag{4-2}$$

where: A is the area of the fibres (which is calculated from $A = n\pi d_f L$, where n is the number of fibres and L is the fibre length, d_f is the average outer diameter of the fibre. Q is the volume flow rate at pressure p', measured in our apparatus with a bubble

flow meter. p' is the atmospheric pressure. The expression Qp'/A is equivalent to J and is expressed in units of volume flow ($N\,m^{-1}\,s^{-1}$).

The permeability coefficient K of a microporous hollow fibre membrane can be expressed by combining viscous and Knudsen flow terms:

$$K = Ko + \frac{Bo}{\eta}\bar{p} \tag{4-3}$$

$$\frac{Q}{\Delta p} = Ko \cdot \frac{A}{l\,p'} + \frac{Bo}{\eta} \cdot \frac{A}{l\,p'} \cdot \bar{p} \tag{4-4}$$

where: Ko is the Knudsen permeability coefficient ($m^2\,s^{-1}$); Bo is the geometric factor of a membrane (m^2); η is the viscosity of the permeate gas (Pa s); $\bar{p}$ is the mean pressure (Pa). The mean pressure is given by the mean pressures on both sides of a membrane, i.e.$(p_1+p_2)/2$, whereas the differential pressure Δp is given by (p_1-p_2).

It has been shown[134] that Ko and Bo can be generally expressed by the following two equations, for practically all kinds of porous membranes:

$$Ko = \frac{4\,\delta\,v\varepsilon\,r}{3\,k_1\,q^2} \tag{4-5}$$

$$Bo = \frac{r^2\varepsilon}{k_2\,q^2} \tag{4-6}$$

where: δ/k_1 and k_2 are constants (0.8 and 2.5 respectively) as estimated by Carman[135] for all porous membranes; q is a tortuosity factor; v is an average molecular velocity; ε is porosity; r is the mean pore radius.

The average molecular velocity v of a gas is given by:

$$v = \sqrt{\frac{8RT}{\pi M}} \tag{4-7}$$

where: M is molecular weight, R is the universal gas constant, T is temperature. The average molecular velocity can be considered as a constant for a gas at a given temperature.

The equivalent mean pore radius r can be calculated by combining equations (4-5), (4-6) and (4-7):

$$r = \frac{16}{3}\left(\frac{Bo}{Ko}\right)\sqrt{\frac{2RT}{\pi M}} \tag{4-8}$$

When nitrogen is used as the gas in the measurements, equation (4-8) is transformed (for use at 298 °K) to yield:

$$r = 73.33\left(\frac{Bo}{Ko}\right)\sqrt{T} = 1265.87\left(\frac{Bo}{Ko}\right) \tag{4-9}$$

The effective porosity is expressed by:

$$\varepsilon / q^2 = 2.5\frac{Bo}{r^2} \tag{4-10}$$

Equation (4-9) indicates that the mean pore radius r can be calculated from the pressure dependence of the gas permeability of a porous membrane without further estimates of porosity ε and tortuosity factor q. According to equation (4-4), the

value of KoA/lp' can be obtained from a plot of $Q/\Delta p$ versus $\overline{p}$ by extrapolation of permeability data to zero pressure, and $BoA/\eta lp'$ is obtained from the slope of the line, as shown as in Fig. 4.4. The term of ε/q^2 is used to describe effective porosity, which can be calculated from equation (4-10). Equations (4-5) and (4-6) do not provide means to calculate ε and q independently; thus, the ratio ε/q^2 is used to allow comparisons. Practically, as the value of ε/q^2 increases, the effective porosity increases. However, such an increase does not require a corresponding increase in permeability, since the permeability coefficient is also a function of the mean pore radius r, as shown by combining equation (4-3) and (4-10):

$$K = Ko + \frac{r^2 \overline{p}}{2.5\,\eta}(\varepsilon / q^2) \qquad (4\text{-}11)$$

In order to determine the mean pore radius of PAN hollow fibre membranes, the volume flow rate Q was measured using a soap film flow meter, as shown in Fig. 2.10. The flow rates of different gases, namely H_2, CO_2 and CH_4 were measured over a range of pressures for a typical module consisting of 10 hollow fibres, each 10 cm long. Because the PAN as-spun hollow fibres were so porous, very high flow rates were observed when using 10 fibres, 20 cm long. To reduce the flow rate, shorter fibres and a smaller number of fibres were used for the measurements carried out using H_2, CO_2 and CH_4. A module consisting of two hollow fibres, 5 cm long was also used for most of the measurements carried out using N_2. The gas permeation rates of these modules are shown in Table 4.6.

Fig. 4.4 shows that linear relationships between the permeability coefficient and the mean pressure are obtained. From these plots, the values of the Knudsen permeability coefficient and the geometric factor, the mean pore radius and effective

Table 4.6 Effect of differential pressure on permeation rate

Flow rate Q $(m^3\ s^{-1}) \times 10^6$	Δp $(Pa \times 10^5)$	$\overline{p}$ $(Pa \times 10^5)$	$Q/\Delta p$ $(m^3\ s^{-1}\ Pa^{-1}) \times 10^{11}$
For H_2*:			
3.958	1.38	1.69	2.868
8.237	2.76	2.38	2.984
13.437	4.14	3.07	3.246
18.403	5.52	3.76	3.334
For CH_4*:			
1.799	1.38	1.69	1.304
3.678	2.76	2.38	1.333
6.035	4.14	3.07	1.458
8.551	5.52	3.76	1.549
For CO_2*:			
0.777	1.38	1.69	0.563
1.750	2.76	2.38	0.634
2.871	4.14	3.07	0.694
4.018	5.52	3.76	0.728
For N_2**:			
0.279	2.00	2.00	0.140
0.358	2.50	2.25	0.143
0.442	3.00	2.50	0.147
0.524	3.50	2.75	0.150
0.619	4.00	3.00	0.155
0.699	4.50	3.25	0.155
0.800	5.00	3.50	0.160

*: Measured on a module consisting of 10 fibres, 10 cm long;
**: Measured on a module consisting of two fibres, 5 cm long.

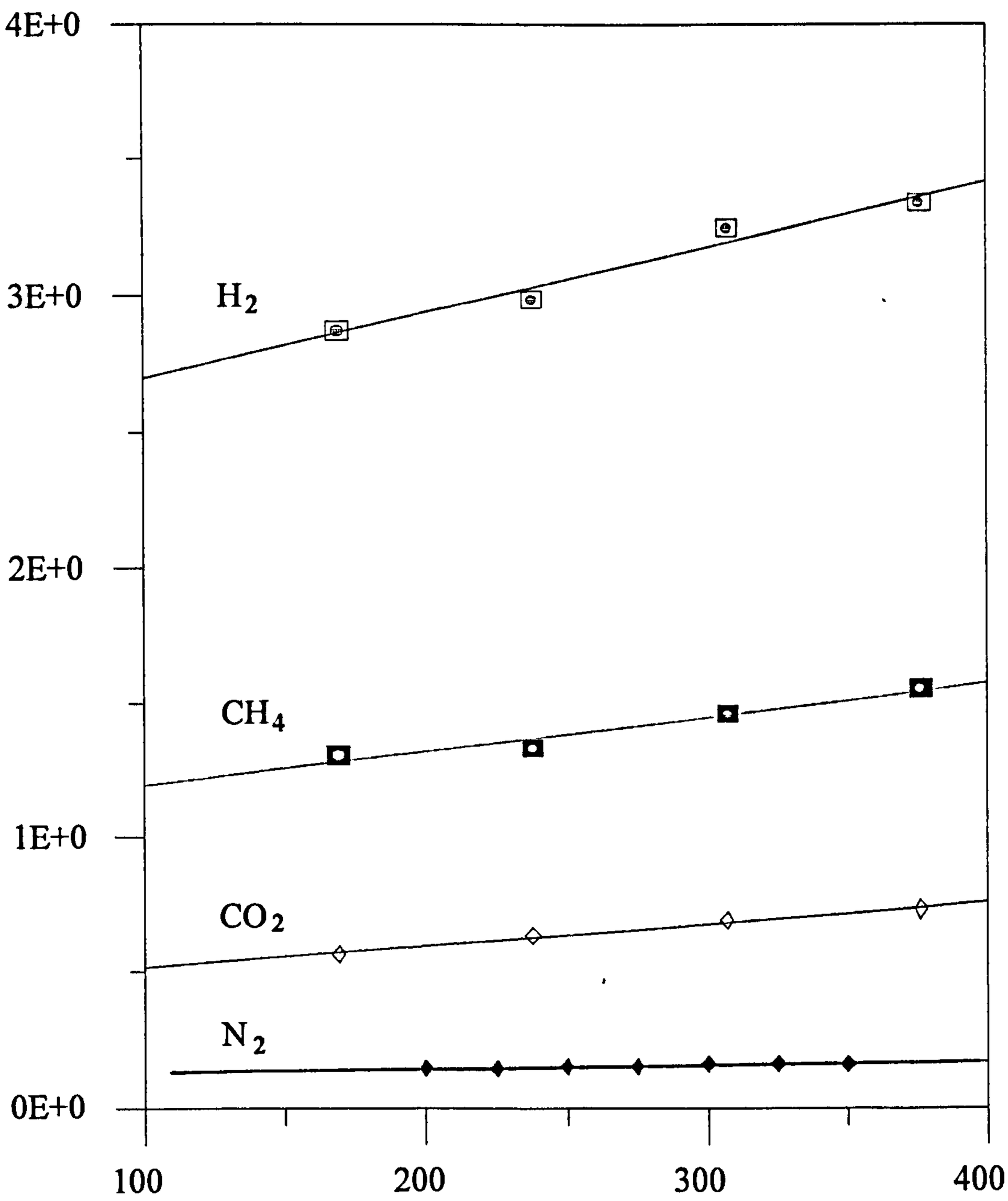

Fig. 4.4. Permeability coefficient versus mean pressure

Table 4.7 Gas viscosity[136]

Gas	Viscosity η (Pa s)
H_2	88.0×10^{-7}
CH_4	109.2×10^{-7}
CO_2	146.3×10^{-7}
N_2	175.0×10^{-7}

Table 4.8 Effect of testing gas on mean pore radius and effective porosity of PAN hollow fibre membranes

Hollow Fibre Designation	Gases Tested	*Ko*	*Bo*/η	*Bo*	Mean pore radius *r* (nm)	Effective porosity $(\varepsilon/q^2)\times10^2$
PAN/DMF/$CuSO_4$	H_2*	1.83×10^{-7}	1.79×10^{-13}	1.57×10^{-18}	40.85	0.24
/GLY	CH_4*	7.97×10^{-8}	9.29×10^{-14}	1.01×10^{-18}	21.33	0.56
=23.5/70.5/3.5/2.5	CO_2*	3.25×10^{-8}	5.97×10^{-14}	8.76×10^{-19}	27.25	0.30
	N_2**	8.47×10^{-8}	8.42×10^{-14}	1.71×10^{-18}	25.64	0.65

*: Measured on a module consisting of 10 fibres, 10 cm long
**: Measured on a module consisting of two fibres, 5 cm long.

porosity are obtained. Table 4.7 shows the gas viscosity data. The calculated mean pore radius and effective porosity are listed in Table 4.8.

For a given porous membrane, the value of the mean pore radius of the membranes should be the same regardless of the nature of the testing gas if the method is perfectly valid for porous membranes. From Table 4.8, quite different values for the

mean pore radius were obtained between H_2 and other gases. Similar results had been observed earlier by other workers[101, 102]. Yasuda and Tasil[134] had used this method to test Millipore filters of known pore radius using the gases He, N_2 and CO_2. All the gases gave answers close to the actual pore radius of the filters, so that Yasuda was able to claim that this method was a simple and reasonable means of estimating mean pore radius in microporous membranes. Cabasso et al[137] used the same method to calculate the mean pore radius only from nitrogen permeability data. The different results obtained in this study were possibly due to the different gases having different interactions with the membrane, which might be related to the intrinsic gas permeation properties of the polymer.

Once the value of r was determined, the effective porosity (ε/q^2) can be calculated from equation (4-10). Since ε and q cannot be calculated independently, therefore, the ratio of ε/q^2 was used to characterise porous membranes. Results obtained from PAN hollow fibres are shown in Table 4. 8. Different values for the effective porosity were also observed when different gases were used. These variations are also believed to be related to the different gas having different interactions with the membrane. These values are quite larger than the values obtained by Brown[101] on polysulphone hollow fibre where $\varepsilon/q^2 = 1.17 \times 10^{-6}$, while the values obtained by Yasuda[134] on polysulphone films where $\varepsilon/q^2 = 0.27$, but in the similar values obtained by Cabasso[137] on polysulphone hollow fibres where $\varepsilon/q^2 = 0.26 \sim 4.6 \times 10^{-2}$.

Other workers[138, 139] have used the Knudsen's capillary tube model to describe the gas flow through porous membranes. The nature of the gas flow through a porous membrane depends on the ratio between the mean free path λ and the pore diameter. The mean free path λ is:

$$\lambda = \frac{3\,\eta}{2p} \times \frac{(\pi RT)^{\frac{1}{2}}}{\sqrt{2\,M}} \qquad (4\text{-}12)$$

When the mean free path of the gas molecules is much larger than the pore radius, individual molecules will not collide with each other[138]. The molecular flux, which is in the Knudsen flow range, is given by:

$$F = \frac{8\,r}{3\,l} \times \frac{(p_1 - p_2)}{(2\,\pi MRT)^{1/2}} \qquad (4\text{-}13)$$

where: p_1 is high pressure side of membrane; p_2 is low pressure side of membrane; l is capillary length; M is molecular weight; r is pore radius.

When the mean free path is reduced to less than the pore radius under a high pressure, the gas flow will be viscous and follows the Poiseuille law. For circular capillaries, the laminar flow is given by:

$$F = \frac{r^2}{16} \times \frac{p_1^2 - p_2^2}{l\,\eta\,RT} \qquad (4\text{-}14)$$

(The equation is expressed as $F = \frac{r^2}{8} \times \frac{p_1^2 - p_2^2}{l\,\eta\,RT}$ by Kesting [139])

In the intermediate pressure range, the flow has been described by Present and Pollard[140] as the sum of the above two equations:

$$F = \frac{a(p_1 - p_2)}{M^{1/2}} + \frac{b(p_1^2 - p_2^2)}{\eta} \qquad (4\text{-}15)$$

where a and b are constants, which can be determined by experiment. This relationship shows that the permeation of gas through porous membranes consists of Knudsen flow and Poiseuille flow. It is clear that separation is possible only when the flow is in the Knudsen flow regime. Thus, when the proportion of Poiseuille flow increases, the efficiency of separation drops until complete Poiseuille flow results, in which there is no significant separation.

The constants a and b were calculated from equation (4-16), obtained by rearranging equation (4-15), and a plot of $F/\Delta p$ versus $\bar{p}$, which was of similar from to equation (4-4).

$$\frac{F}{\Delta p} = \frac{a}{\sqrt{M}} + \frac{2b}{\eta}\bar{p} \qquad (4\text{-}16)$$

The calculated results are show in Table 4. 9. After rearranging equations (4-13) and (4-14), the mean pore radius of the membrane can be calculated using the following equation:

$$r = \frac{b}{a} \times \frac{128 \times (RT)^{\frac{1}{2}}}{3 \times \sqrt{2\pi}} \qquad (4\text{-}17)$$

Table 4.9 The calculated constants of a and b, and mean pore radius

Gas	*a*	*b*	Mean pore radius *r* (nm)
H_2*	3.29×10^{-12}	3.18×10^{-22}	81.70
CH_4*	4.07×10^{-12}	2.05×10^{-23}	42.66
CO_2*	2.75×10^{-12}	1.77×10^{-22}	54.50
N_2**	5.72×10^{-12}	3.46×10^{-22}	51.27

*: measured on a module consisted 10 fibres, 10 cm long;
** : measured on a module consisted two fibres with 5 cm long.

It is believed that this model (Hwang's model) is built upon Knudsen's capillary tube model. In practice, diffusive transport in a porous membrane differs from that in Knudsen's capillary tube model because pores have a finite length and are random in direction[141]. Consequently, an effective diffusion coefficient is always used, which corrects the Knudsen diffusion coefficient to account for the effects of porosity (ε) and tortuosity (q) of the porous membrane. In Yasuda's method, it is claimed that the effects of porosity and tortuosity of the porous membranes on the flow of gas through the porous media are considered; it was believed, therefore, to be more applicable in the estimation of the pore radius for porous media.

It was interesting that the mean pore radius calculated from Hwang's method is also different depending on which gas was used in the experiment, as shown in Table 4.9. What is quite remarkable is that the values are almost exactly twice those obtained by Yasuda's method, as shown as in Table 4.10. Table 4.11 also shows the results calculated from the data which were obtained by other workers[101, 102]. It is difficult to avoid the conclusion that one of these equations is being used with an error of a factor of 2 in the basic equations.

Table 4.10 Comparison of mean pore radius values obtained by two methods

Testing Gases	Mean pore radius (nm)	
	Yasuda's method[134]	Hwang's method[138]
H_2	40.85	81.71
CH_4	21.33	42.66
CO_2	27.25	54.52
N_2	25.64	51.28

Table 4.11 Comparison of the mean pore radius values from data obtained by other workers[101, 102]

Testing Gases	Mean pore radius (nm)			
	Ref.[101]		Ref.[102]	
	Yasuda's method	Hwang's method	Yasuda's method	Hwang's method
H_2	8.95	17.91	2.02	4.04
CH_4	6.37	12.75	3.22	6.44
CO_2	3.80	7.61	6.33	12.66

Above all, the calculations show that the mean pore radius depends on the method used and the testing gases. This means that the mean pore radius calculated from gas permeation rates is only useful if different membranes are compared under similar conditions since the values cannot be said to be absolute. The method is therefore best used only for comparative purposes.

At this stage, Yasuda's method was adopted for determining the mean pore radius and effective porosity of the polyacrylonitrile hollow fibre membrane from the nitrogen permeation rates, because it has been accepted by many other workers [101, 102, 137, 142] to estimate the mean pore radius in hollow fibre membranes.

Table 4.12 shows the effect of varying spinning conditions and hollow fibre drying method on the pore radius and effective porosity of the membranes. From the results in Table 4.12, the calculated mean pore radius of PAN hollow fibre membranes varies from 4 nm to 26 nm, which depending on the conditions used. The concentration of polymer in the spinning solution and the jet stretch ratio during the spinning process play an important role in controlling the mean pore radius. When the polymer concentration in the spinning solution was slightly changed from 23.5 wt% to 25 wt% (from Batch No: 23.5/35/25 to Batch No: 25/35/21), the mean pore radius was changed from 25 nm to 14 nm and effective porosity from 0.65×10^{-2} to 1.32×10^{-2}. It seems that the higher concentration of polymer produces a smaller mean pore radius and more pores per unit area in the surface layer of the membrane. The jet stretch ratio during the spinning process also affects the mean pore radius. Increasing the jet stretch ratio decreases the pore radius, but the effective porosity of the fibre dried in air at a stretch ratio 0.67 is slightly increased, compared to Batch No: 25/35/21 fibre dried in air.

The controlled removal of water (using the solvent exchange method) during the membrane drying process results in an increased mean pore size, a greater effective porosity (except at stretch ratio 0.67) and a higher gas flux, as shown in Table 4.12. These results agree with the results using similar procedures to dry polyethersulphone (PES) hollow fibre membranes[94]. It indicates that a solvent exchange drying procedure can reduce the collapse of the pores and the densification of the top layer of the membranes. The explanation would be the replacement of water and residual solvent in the fibres by immersion in several solvents (nonsolvents for the polymer);

Table 4.12 Mean pore radius and effective porosity of PAN hollow fibre membranes[a]

Hollow Fibre Designation	Stretch Ratio	Drying method	Calculated Mean Pore Radius r (nm)	Effective Porosity $(\varepsilon/q^2)\times10^2$	N_2 flow rate $Q/\Delta p$ at 5×10^5 Pa (m^3/s Pa)$\times10^{-11}$
Batch No: 23.5/35/25	0.44	Air dried	25.64	0.65	0.160
Batch No: 25/05/00	0.44	Air dried S.E[b] dried	10.44 12.28	0.96 1.13	0.086 0.125
Batch No: 25/35/21	0.44	Air dried S.E dried	11.00 14.21	0.88 1.32	0.076 0.155
Batch No: 25/35/22	0.67	Air dried S.E dried	4.25 8.28	1.06 0.82	0.029 0.049

a: Based on N_2 permeation rates;
b: S.E means solvent exchange drying method.

water and residual solvent in the fibres will be replaced gradually by lower surface tension solvent, reduced the collapsing force.

The properties of porous polymer membranes prepared by dry-jet wet spinning processes are governed by the precipitation rate. On increasing the coagulation bath temperature, the precipitation rate will increase, as observed in the PAN film casting study. Therefore, the temperature of the coagulation bath should have an important effect on the pore radius of the porous membranes. As shown in Table 4.13, the mean pore radius of the membranes increases when the temperature is increased. The effective porosity ε/q^2 decreases with increasing coagulation bath temperature despite the increase in pore radius. This could be taken to indicate that the coagulation bath at higher temperatures tends to produce larger sized pores but fewer in number.

Table 4.13 Effect of coagulation bath temperature on the mean pore radius of PAN hollow fibre membranes

Hollow Fibre Designation	Drying method	Coagulation Bath Temperature (°C)	Mean pore radius (nm)	Effective porosity $(\varepsilon/q^2)\times10^2$
Batch No: 25/35/00	Solvent Ex.	30	12.94	5.26
		40	14.34	6.60
		50	21.21	2.72
		60	31.89	2.74

Table 4.14 Comparison of pore radius of flat film and hollow fibre membranes

Membrane description	Mean pore radius (nm)	References
PAN flat film	6 ~ 10	[105]
PAN flat film	38 ~ 40	[106]
PAN flat film	5 ~ 21	[111]
PAN hollow fibre	5 ~ 15	[143]
PAN hollow fibre	4 ~ 32	in this study
PSF hollow fibre	4 ~ 9	[101]
PSF hollow fibre	1 ~ 7	[102]

The calculated mean pore radius of polyacrylonitrile hollow fibre membranes depends on the spinning conditions and composition of the spinning solution. The average pore radius was larger than the mean pore radius of polysulphone hollow fibre membranes[101, 102]. However, it is of the order of magnitude of pore radius values obtained by other workers as shown in Table 4.14. The effective porosity (ε/q^2) of PAN hollow fibres calculated from nitrogen gas permeation data was in the range of

0.65×10^{-2} to 1.13×10^{-2} depended on the spinning conditions. The porosity of the whole hollow fibre was measured. The calculated porosity for a typical hollow fibre is 44%. The porosity of a porous membrane is defined as the fraction of the membrane volume which is not occupied by the polymer. Thus, if all the pores are interconnected (no dead ends), the entire pore volume participates in transport. The tortuosity can be calculated from the ratio between the porosity and the effective porosity:

$$q^2 = \frac{\varepsilon}{(\varepsilon/q^2)} \qquad (4\text{-}18)$$

Using the effective porosity 1.13×10^{-2} previously calculated from Batch No: 25/05/00, the value of q^2 was determined to be 38.93. If no dead-end pores existed in this fibre, the tortuosity factor q^2 would have been 38.93, an extremely high value considering that the tortuosity factor for a consolidated material is 2 from statistical considerations[135]. Therefore, it is most probable that very few of the pores that make up the void volume contribute to the gas transport. It seems that the majority of the pore structure is only for support. If, however, we assume the value of q^2 to be 2 for this asymmetric hollow fibre membrane, then the porosity in the top surface layer of the fibres can be calculated from equation (4-18):

$$\varepsilon = \left(\varepsilon/q^2\right)\cdot q^2 = 1.13\times10^{-2}\times2 = 2.26\times10^{-2}$$

This implies that out of the original 44% porosity only 2.26% porosity is active in gas transport through the hollow fibre wall. This is a typical situation for an asymmetric membrane which has a dense skin layer.

4. 3. 3 Resistance model approach to the permeation

Henis and Tripody[22] introduced a "resistance model" (RM) to describe the permeation of the composite membrane. In this composite membrane, a polymeric coating material can be used to coat a thin film on to the outside skin layer of the hollow fibre membranes. The thin film itself exhibits both low selectivity and low resistance, and serves as a sealant to plug any defects on the surface of an asymmetric integrally skinned membrane. The selectivity and the resistance of the composite membrane are determined by the skin layer of the membrane. The principal requirement for the sealant is low resistance coupled with the capability to effectively fill any defects in the skin layer of the support membrane.

The Henis and Tripody's RM approach is based on the analogies between the membrane permeation rate and electrical resistance. The permeation rate, or flux Q_i is given by equation (4-19):

$$Q_i = \frac{P_i A \Delta p_i}{l} \qquad (4\text{-}19)$$

where: Q_i is the permeation rate of component i; P_i is the intrinsic permeability of the membrane to component i; A is the cross-sectional surface area of membrane available for permeation; l is the thickness of membrane through which the component permeates; Δp_i is the partial pressure difference across the membrane.

In the electrical analogue, the permeation through a polymer membrane is mathematically equivalent to Ohm's law for current flow through a resistor:

$$I = \frac{E}{R} \tag{4-20}$$

The current I is conceptually equated with the permeation rate. The electrical potential E is analogous to the partial pressure difference and the electrical resistance R is then equivalent to the resistance to permeate flow. The resistance to permeate flow can then be defined to be R_i:

$$R_i = \frac{l}{P_i A} \tag{4-21}$$

Combining equations (4-19) and (4-21), gives:

$$Q_i = \frac{\Delta p_i}{R_i} \tag{4-22}$$

The permeation behaviour of a porous, asymmetric hollow fibre membrane with a coating material which is applied to one surface of the membrane is analogous to the flow of electricity through a series-paralleled array of resistors. These membranes thus are referred to as RM composite membranes. A schematic representation of the cross section of such a membrane and the electrical circuit analogue are shown in Fig. 4.5. Four regions are defined in this substrate membrane: a separating skin layer of

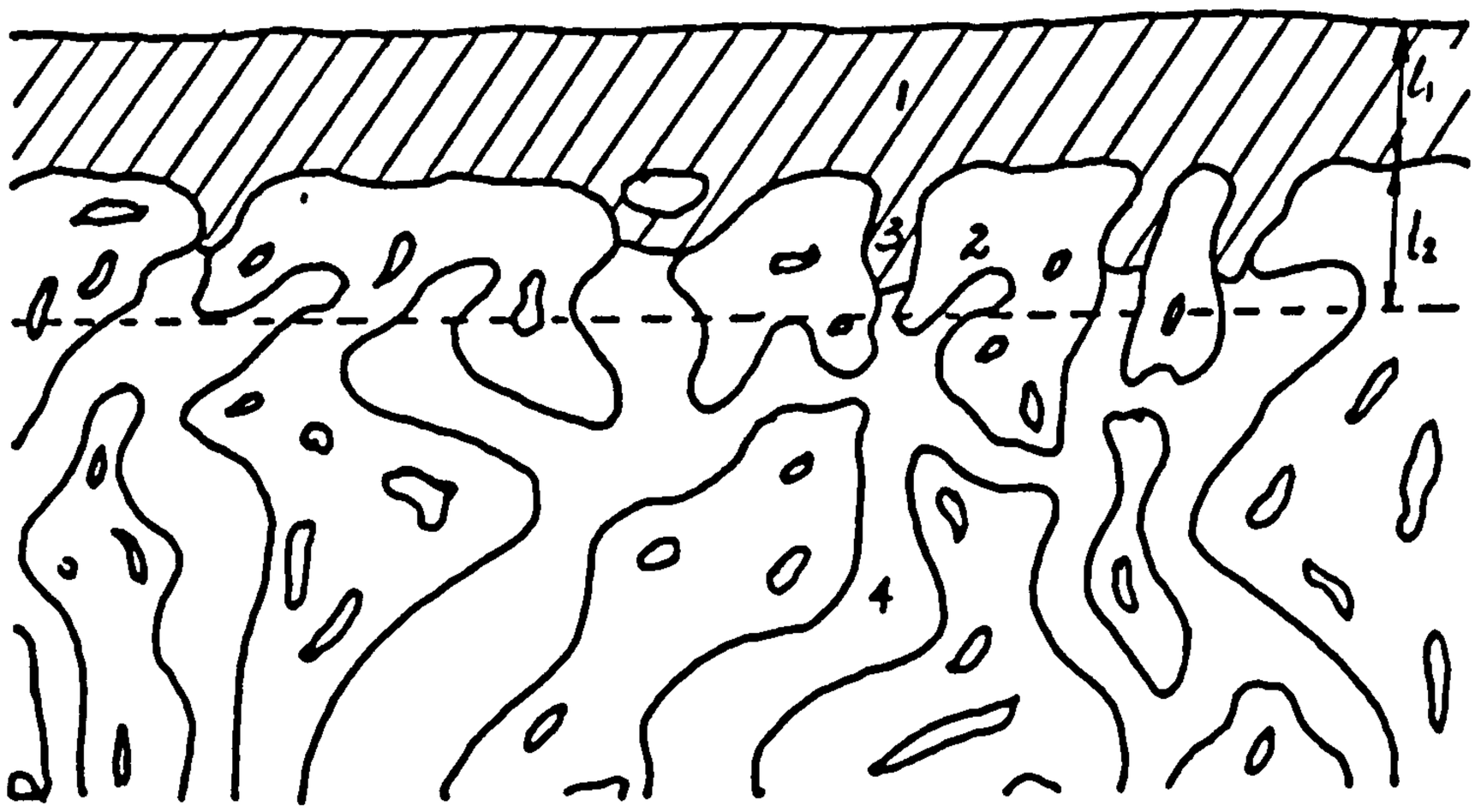

Schematic diagram of a porous RM composite

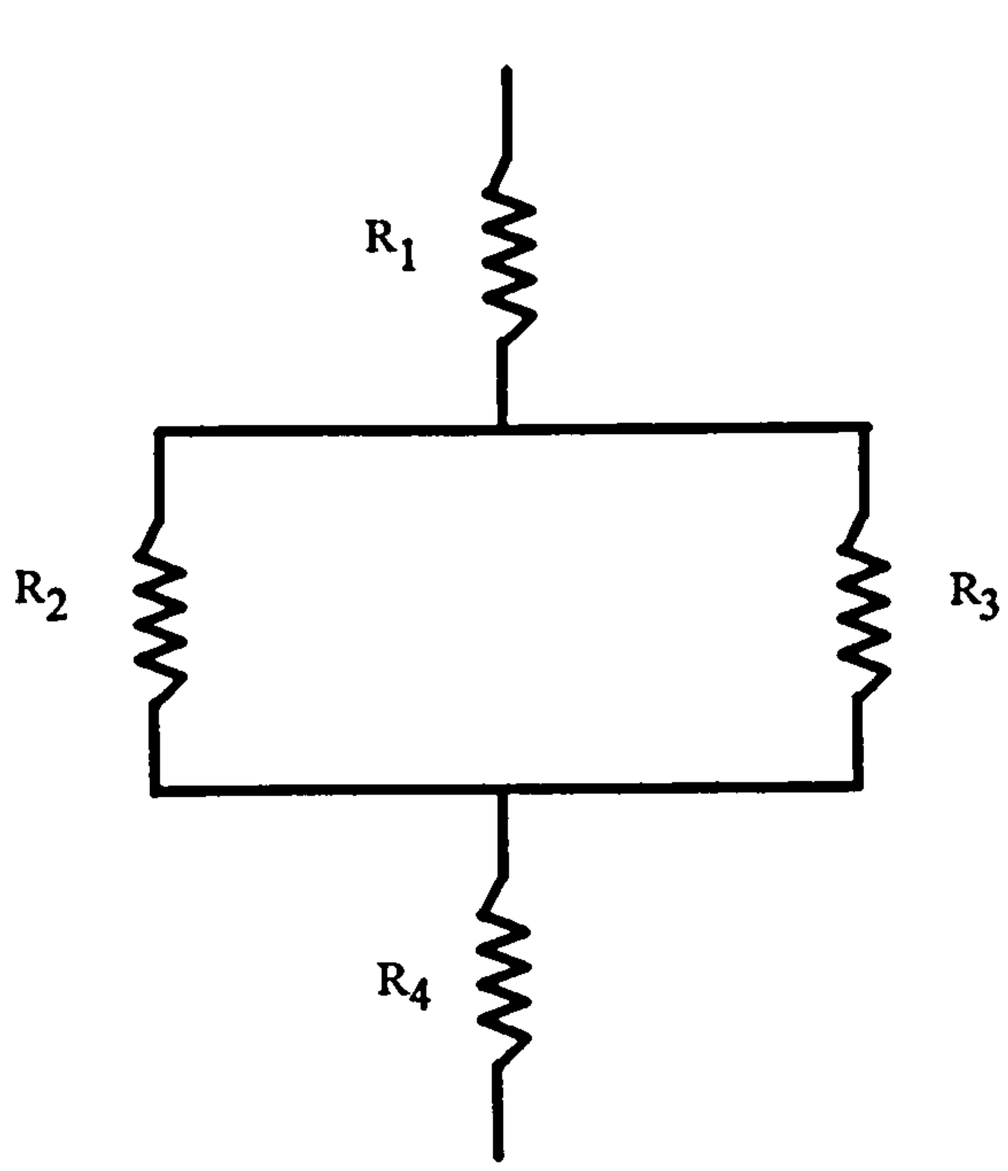

Electrical circuit analogue of an RM composite

Fig. 4.5 Representation of a porous asymmetric membrane and its electrical analogue

thickness l_2 (analogue R_2); defects or pores in the skin layer (analogue R_3); a highly porous substrate (analogue R_4) and the coating thickness l_1 (analogue R_1).

The total resistance to permeate flow R_t is a function of the resistance to flow in each of the regions defined within the membrane, which can be expressed as follows:

$$R_t = R_1 + \frac{R_2 R_3}{R_2 + R_3} + R_4 \qquad (4\text{-}23)$$

A very important factor in determining the permeation properties of such composite membranes is the surface porosity defined by A_3/A_2 where A_3 is the area covered by the pores and A_2 is the total separating skin surface area of the membrane to contribute to gas permeation. Unless A_3 is very much less than A_2, most of the gas will flow through the pores because the resistance to flow of the pores, R_3, is so much less than the resistance to flow of the skin portion of the surface, R_2. In this case, only Knudsen diffusion flow would be observed. When a coating is applied to the membrane, then the resistance of the coating R_1 can be added to the total resistance. From the standpoint of high flux, good separating properties and desirable substrate, the resistance R_4 should be negligible compared to R_1, R_2 and R_3. When the coating material fills the pores in the skin layer, the resistance of the pores, R_3, has been substantially increased by as much as 10^5 to 10^6[22] more than an open pore of equivalent area and depth even for the most permeable polymer.

Assuming that the coating material has penetrated and filled the pores to a depth equal to the thickness of the skin layer, then $l_3=l_2$ and the resistance in the pores is given by equation (4-24):

$$R_{3,i} = \frac{l_2}{P_{1,i} A_3} \tag{4-24}$$

where $R_{3,i}$ is the resistance to flow of gas *i* for the pores filled with coating material and $P_{1,i}$ is the intrinsic permeability of the coating material to gas *i*. It follows then that the resistance of the coating material and the skin layer are given by equations (4-25) and (4-26):

$$R_{1,i} = \frac{l_1}{P_{1,i} A_1} \tag{4-25}$$

$$R_{2,i} = \frac{l_2}{P_{2,i} A_2} \tag{4-26}$$

The total flux for the RM composite membrane is then given by equation (4-27):

$$Q_{t,i} = \Delta p_{t,i} \left(\frac{l_1}{P_{1,i} A_1} + \frac{l_2}{P_{2,i} A_2 + P_{3,i} A_3} \right)^{-1} \tag{4-27}$$

A uniform coating area A_1 on the RM composite membrane will always be equal to A_2+A_3. However, A_3 is much less than A_2. For simplicity, it can be assumed that $A_1=A_2$. Then equation (4-23) can be rearranged to obtain the flux per unit pressure drop and unit surface area, which is equivalent to the thickness-corrected permeability or permeation rate (P/l):

$$\frac{Q_{t,i}}{A_2\,\Delta p_{t,i}} = \left(\frac{P}{l}\right) = P' = \left\{\frac{l_1}{P_{1,i}} + \frac{l_2}{P_{2,i} + P_{1,i}\left(A_3/A_2\right)}\right\}^{-1} \qquad (4\text{-}28)$$

The separation factor for two gases *i* and *j* is the ratio of the (P') values:

$$\alpha_{i/j} = \frac{P'_i}{P'_j} \qquad (4\text{-}29)$$

Using equation (4-28), the permeation rate of PAN hollow fibre membranes can then be calculated for a particular gas if the morphological parameters of the membranes are known. The permeability coefficients for polyacrylonitrile and other polymers with the gases H_2, CO_2 and CH_4 were found from the literature[125, 144 ~ 147], as shown in Table 4. 15.

Table 4.15 Intrinsic gas permeation properties of polymers[a]

Polymer	$P_i(H_2)$	$P_i(CO_2)$	$P_i(CH_4)$	$\alpha_{H2/CH4}$	$\alpha_{CO2/CH4}$
PAN	1.0×10^{-11}[144]	2.8×10^{-13}[145]	1.0×10^{-15}[125]	10000	280
PSF[148]	10.8×10^{-10}	5.7×10^{-10}	2.1×10^{-11}	51.43	27.14
PDMS[b][146]	6.5×10^{-8}	3.23×10^{-7}	9.4×10^{-8}	0.69	3.44
CA[c] [147]	12.0×10^{-10}	4.75×10^{-10}	1.5×10^{-11}	79.99	31.66

a: P_i is the permeability coefficient, cm^3(STP) cm/cm^2 s cmHg;
b: PDMS is polydimethylsiloxane;
c: CA is cellulose acetate (D=2.45).

In order to demonstrate how this resistance model can be used to describe the performance of PAN hollow fibre membranes, let us suppose that the hollow fibre membranes have a similar composition to the resistance model composite membrane, which consist of a porous, asymmetric substrate membrane with a coating material. The morphological parameters, such as the effective separating layer thickness l_2, surface porosity A_3/A_2 and coating thickness l_1 were assumed values as show in Table 4. 16 (a) and (b). Tables 4. 16 and 4. 17 show the effect of these parameters on the permeation rates P'_{H2} and separation factors $\alpha_{H2/CH4}$ and $\alpha_{CO2/CH4}$.

According to the calculations in the Tables, the resistance model predicts that the coating thickness has little effect on the permeation rate P'_{H2} and the separation factors $\alpha_{H2/CH4}$ and $\alpha_{CO2/CH4}$ for a fibre with a relatively thick separating layer ($l_2 \geq$ 0.05 μm). Increasing the separating thickness decreases the permeation rates, but has little effect on the separation factors. The separation factors are much more sensitive to variations in the surface porosity. These results show that a lower surface porosity would be necessary for a PAN composite hollow fibre membrane to approach its intrinsic separation factors when silicone rubber is used as the coating material. However, it also reveals that the permeation rates of this kind of PAN composite membrane would be quite a lot lower than for the comparable PSF composite membrane as shown in Table 4. 18. Indeed, it can be predicted from the RM model that higher permeation rates and separation factors could be obtained from a PAN membrane only if it could be produced with a much lower surface porosity, i.e. 1×10^{-7} and an effective separating layer of less than 0.05μm. Such parameters are achievable from the permeation rates obtained with an RM composite membrane based on PSF. But such a thin separating layer and low surface porosity may be difficult to achieve in practice.

Table 4. 19 shows the expected permeation rates and separation factors for CA coated PAN hollow fibre membranes with the same parameters used as in the PAN

Table 4. 16(a) Calculated effect of coating thickness, separating layer and surface porosity on permeation rates P'_{H_2} and separation factors α_{H_2/CH_4} and α_{CO_2/CH_4} for an RM composite membrane consisting of PDMS coated PAN hollow fibres

$P_1(H_2)=6.5\times10^{-8}$ cm^3(STP) cm/cm^2 s cmHg

$P_1(CO_2)=3.23\times10^{-7}$ cm^3(STP) cm/cm^2 s cmHg

$P_1(CH_4)=9.4\times10^{-8}$ cm^3(STP) cm/cm^2 s cmHg

Fixed parameters:

$P_2(H_2)=1.0\times10^{-11}$ cm^3(STP) cm/cm^2 s cmHg

$P_2(CO_2)=2.8\times10^{-13}$ cm^3(STP) cm/cm^2 s cmHg

$P_2(CH_4)=1.0\times10^{-15}$ cm^3(STP) cm/cm^2 s cmHg

Surface porosity:	Coating thickness:	Separating layer thickness: l_2=0.001(μm)			Separating layer thickness: l_2=0.05(μm)		
A_3/A_2	l_1(μm)	P'_{H_2} (GPU)[a]	α_{H_2/CH_4}	α_{CO_2/CH_4}	P'_{H_2} (GPU)	α_{H_2/CH_4}	α_{CO_2/CH_4}
1×10^{-6}	0.5	93.4	98.4	6.34	2.01	106	6.37
	1.0	87.2	91.9	6.34	2.01	106	6.37
	1.5	81.7	86.1	6.34	2.00	106	6.37
	2.0	76.9	81.1	6.34	2.00	106	6.37
1×10^{-4}	0.5	146	1.64	3.46	3.29	1.75	3.46
	1.0	132.	1.54	3.46	3.28	1.75	3.46
	1.5	119	1.46	3.46	3.28	1.75	3.48
	2.0	109	1.40	3.46	3.27	1.75	3.47

a: GPU=1.0×10^{-6} cm^3(STP) cm/cm^2 s cmHg

Table 4. 16(b) Calculated effect of coating thickness, separating layer and surface porosity on permeation rates P'_{H_2} and separation factors α_{H_2/CH_4} and α_{CO_2/CH_4} for an RM composite membrane consisting of PDMS coated PAN hollow fibres

Surface porosity: A_3/A_2	Coating thickness: l_1(μm)	Separating layer thickness: l_2=0.2(μm)			Separating layer thickness: l_2=0.25(μm)		
		P'_{H_2} (GPU)[a]	α_{H_2/CH_4}	α_{CO_2/CH_4}	P'_{H_2} (GPU)	α_{H_2/CH_4}	α_{CO_2/CH_4}
1×10^{-6}	0.5	0.50	106	6.35	0.40	106	6.34
	1.0	0.50	106	6.35	0.40	106	6.34
	1.5	0.50	106	6.35	0.40	106	6.34
	2.0	0.52	106	6.35	0.40	106	6.34
1×10^{-4}	0.5	0.82	1.75	3.46	0.66	1.76	3.46
	1.0	0.82	1.75	3.46	0.59	1.76	3.46
	1.5	0.82	1.75	3.46	0.59	1.76	3.46
	2.0	0.82	1.75	3.46	0.59	1.76	3.46

Table 4.17 Calculated effect of surface porosity on permeation rates P'_{H_2} and separation factors α_{H_2/CH_4} and α_{CO_2/CH_4} for an RM composite membrane consisting of PDMS coated PAN hollow fibres

Surface porosity A_3/A_2	Coating thickness: l_1=0.5(μm) Separating layer thickness: l_2=0.05(μm)		
	P'_{H_2} (GPU)	α_{H_2/CH_4}	α_{CO_2/CH_4}
1×10^{-7}	2.00	965.6	30.03
1×10^{-6}	2.01	105.8	6.37
2×10^{-6}	2.02	53.51	4.90
5×10^{-6}	2.06	21.90	4.02
1×10^{-5}	2.13	11.31	3.73
1×10^{-4}	3.29	1.75	3.46

Table 4.18 Calculated effect of coating thickness, separating layer and surface porosity on permeation rates P'_{H_2} and separation factors α_{H_2/CH_4} and α_{CO_2/CH_4} for an RM composite membrane consisting of PDMS coated PSF hollow fibres

				$P_1(H_2)=6.5\times10^{-8}$ cm^3(STP) cm/cm^2 s cmHg $P_1(CO_2)=3.23\times10^{-7}$ cm^3(STP) cm/cm^2 s cmHg $P_1(CH_4)=9.4\times10^{-8}$ cm^3(STP) cm/cm^2 s cmHg		
Fixed parameters:				$P_2(H_2)=10.8\times10^{-10}$ cm^3(STP) cm/cm^2 s cmHg $P_2(CO_2)=5.7\times10^{-10}$ cm^3(STP) cm/cm^2 s cmHg $P_2(CH_4)=2.1\times10^{-11}$ cm^3(STP) cm/cm^2 s cmHg		
Surface porosity:	Coating thickness:	Separating layer thickness: l_2=0.05(μm)			Separating layer thickness: l_2=0.25(μm)		
A_3/A_2	l_1(μm)	P'_{H_2} (GPU)	α_{H_2/CH_4}	α_{CO_2/CH_4}	P'_{H_2} (GPU)	α_{H_2/CH_4}	α_{CO_2/CH_4}
1×10^{-6}	0.5	185	44.00	26.63	42	49.58	26.95
	1.0	162	38.60	26.23	41	48.05	26.87
1×10^{-4}	0.5	186	30.72	18.49	42	34.61	18.71
	1.0	163	26.95	18.24	41	33.54	18.65

Table 4.19 Calculated effect of coating thickness, separating layer and surface porosity on permeation rates P'_{H_2} and separation factors α_{H_2/CH_4} and α_{CO_2/CH_4} for an RM composite membrane consisting of CA coated PAN hollow fibres

				$P_1(H_2)=12.0\times10^{-10}$ cm^3(STP) cm/cm^2 s cmHg $P_1(CO_2)=4.75\times10^{-10}$ cm^3(STP) cm/cm^2 s cmHg $P_1(CH_4)=1.5\times10^{-11}$ cm^3(STP) cm/cm^2 s cmHg		
Fixed parameters:				$P_2(H_2)=1.0\times10^{-11}$ cm^3(STP) cm/cm^2 s cmHg $P_2(CO_2)=2.8\times10^{-13}$ cm^3(STP) cm/cm^2 s cmHg $P_2(CH_4)=1.0\times10^{-15}$ cm^3(STP) cm/cm^2 s cmHg		
Surface porosity:	Coating thickness:	Separating layer thickness: l_2=0.05(μm)			Separating layer thickness: l_2=0.25(μm)		
A_3/A_2	l_1(μm)	P'_{H_2} (GPU)	α_{H_2/CH_4}	α_{CO_2/CH_4}	P'_{H_2} (GPU)	α_{H_2/CH_4}	α_{CO_2/CH_4}
1×10^{-6}	0.5	1.85	9102	275	0.39	9681	131
	1.0	1.71	8455	274	0.39	9535	131
1×10^{-4}	0.5	1.87	3739	130	0.40	3982	3.46
	1.0	1.73	3471	130	0.39	3919	3.46

RM composite membranes in Table 4. 16. As the results show in Table 4. 19, higher separation factors can be expected when CA is coated on the PAN hollow fibres, and the separation factors of this RM composite membranes are not so sensitive to variations in surface porosity. It is interesting to note that a polymer which has a lower permeability than PDMS, as a coating material, makes a better coating for PAN than silicone rubber. And, it seems to be possible to approach the intrinsic separation factors of PAN hollow fibre membranes if the coating thickness is less than 1 μm and the surface porosity less than 1×10^{-6}. But the calculated gas permeation rates are still quite low, because of the higher resistance of PAN to gas permeation. These calculated separation factors will be compared with experimental values in the next section.

4. 3. 4 Effect of surface modifications on gas permeation performance of PAN as-spun hollow fibre membranes

PAN as-spun hollow fibre membranes in module form were tested for gas transport properties as described in section 2.5. The calculated average of the mean pore size and the effective surface porosity for various PAN as-spun hollow fibre membranes are 4 ~ 32 nm and 0.65×10^{-2} ~ 1.13×10^{-2}, respectively. The permeation rates of hydrogen, carbon dioxide and methane gases were found to be higher than those of PSF hollow fibre membranes measured under the same circumstances, too high in fact to be measured satisfactorily in the testing rig. This higher permeation rate was believed to be caused by the higher mean surface porosity of the PAN membranes.

For an integrally skinned structure, the membrane consists of a porous support layer with one surface covered with a very thin, low porosity separating layer. The separation of the gases occurs in the separating layer, while the microporous substrate provides the membrane with mechanical strength. The basic requirement in

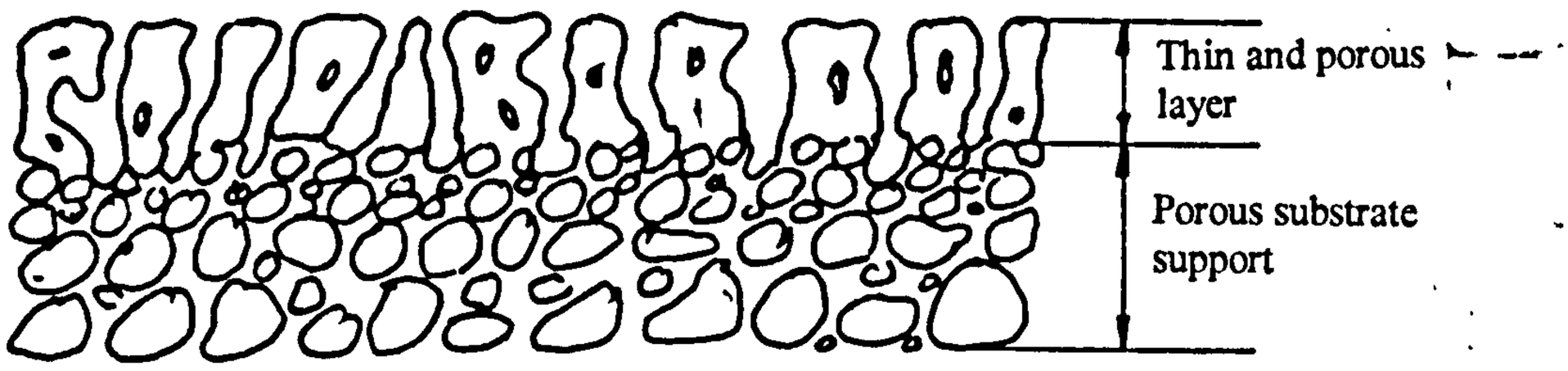

Fig. 4.6 A schematic diagram of an integrally porous skinned membrane

the fabrication of practical membranes is obtaining a minimum resistance to flow through the membrane coupled with maximum selectivity. According to the characteristics of mean pore radius and effective porosity, and the micrographs obtained by SEM, a schematic diagram of the membrane is as shown in Fig. 4.6. The diagram illustrates an integrally porous fibre with a very thin but porous skin layer.

For this kind of structure, surface modifications would be necessary before the membranes were used for gas separations. If the effective surface porosity is not reduced, then the optimum gas permeation rates and separation factors cannot approach the values of PSF hollow fibre membranes.

In order to improve the gas separation performance of the PAN hollow fibre membranes, techniques such as annealing and other surface modifications were used in attempts to reduce the pore radius and the surface porosity of the fibres. These were then examined both before and after dip coating procedures.

4. 3. 4. 1 Dip coating

A dip coating technique was the effective method used by Monsanto[148] to seal surface micropores. This gives a composite membrane in which the permeation properties are governed by the hollow fibre structure and not the coating material. After the dip coating, the previous Knudsen diffusion through the micropores is eliminated and thus solution-diffusion type transport becomes predominant in the skin layer of the hollow fibres. The polymers used in the dip coating method are essentially highly permeable and intrinsically play very little part in the selectivity of the membrane. In other words, this highly permeable polymer presents far less resistance to flow than the defect free separating layer of the membrane, but much more resistance to the flow than the pores. The coating essentially blocked flow through the pores and defects in the surface without changing the flow appreciably through the underlying effective separating layer of the membranes. Major advantages of the method are cheapness and ease of application of coating. The constraints of the method are that the coating polymer must be soluble in a solvent which a) does not swell or dissolve the membrane polymer, and b) has a low enough surface energy to ensure adhesion to the fibre surface. The silicone rubber (Sylgard 184) was chosen for its high permeability, and low selectivity.

PAN as-spun hollow fibre membranes were subjected to coating with Sylgard 184 using the dip coating technique, as described in section 2. 4. 2. 1. Before Sylgard coating, the gas permeation rates of PAN as-spun hollow fibre membranes were too

Table 4.20 Effect of coating procedure on gas permeation properties

Module	Permeation rate constant (GPU)[a]			Separation factor	
	P'_{H_2}	P'_{CO_2}	P'_{CH_4}	α_{H_2/CH_4}	α_{CO_2/CH_4}
No.1: AS [b]	too high to measure				
CAS [c]	4.24	9.63	3.79	1.12	2.54
No.2: AS	too high to measure				
CAS	3.99	8.13	3.02	1.32	2.69
PSF[101] CAS	57.39	28.88	1.37	41.89	21.08

a: GPU=1×10^{-6} cm^3/cm^2 s cmHg;
b; AS is As-spun hollow fibre membranes;
c: CAS is the as-spun hollow fibre membranes coated with Sylgard 184.

high to be measured in the usual way on the testing rig. After coating with Sylgard 184, the gas permeation rate was dramatically reduced to a value more than 20 to 40 times lower than before coating. By comparison, in the case of polysulphone (PSF) hollow fibre membranes, the gas permeation rate was reduced only by about 50% after coating with Sylgard 184.

The measured individual gas permeation rates and the calculated separation factors α_{H_2/CH_4} and α_{CO_2/CH_4} of PAN hollow fibre membranes are shown in Table 4.20. The low permeation rates indicated that the micropores on the surface of the membranes must have been blocked by the coating material. If the coating material blocked all the pores on the surface of the membrane, so that a defect-free skin layer was formed, solution-diffusion type transport of the test gas should take place in the coated hollow fibre. From the results in Table 4.20, the separation factors for the membranes were not as high as expected. On the contrary, they gave very low separation factors.

According to the RM composite membrane model, if the surface porosity of the PAN hollow fibre membranes is equal to 1×10^{-4}, the separation factors $\alpha_{H2/CH4}$ and $\alpha_{CO2/CH4}$ will be 1.75 and 3.46, respectively. This indicates that the surface porosity of the PAN hollow fibre is quite large. The separation factors are lower than the values predicted by RM, which implies that the coating procedure may not be sufficient to seal all the pores in the fibres. As a result, the final separation factors of the coated membranes reflect a combination of Knudsen flow with the solution-diffusion flow.

Fig. 4.7 and Fig. 4.8 show the effect of increasing the immersion time in the coating procedure on the gas permeation rates and separation factors of PAN hollow fibre membranes. From these figures, it can be seen that the permeation rates decreased with increasing immersion time in the coating solution. The gas permeation rates for the membrane dropped dramatically in the first 4 minutes of immersion. For longer periods of immersion, the gas permeation rates of the membrane tended to limiting values. This means that most of the micropores in the surface of the membranes had been blocked by the coating material within 4 minutes coating time, increasing the resistance to gas flow. While the separation factor $\alpha_{CO2/CH4}$ increased slightly with increasing immersion time, the separation factor $\alpha_{H2/CH4}$ seemed less affected by changes in the immersion period. This is caused by the gas flow changing from Knudsen flow to solution-diffusion flow after coating. The separation factor $\alpha_{CO2/CH4}$ is lower than $\alpha_{H2/CH4}$ in Knudsen flow. When the micropores have been blocked by the coating material, the separation factors of the membranes will combine the separation factor of the polymeric membrane material (PAN) and the coating material. If the surface porosity of the hollow fibre is larger than 1×10^{-4}, the separation factor $\alpha_{CO2/CH4}$ will become greater than $\alpha_{H2/CH4}$ after coating with silicone rubber.

These results are probably due to the large pore radius and surface porosity in the surface of the membranes, and especially the lower intrinsic gas permeation properties

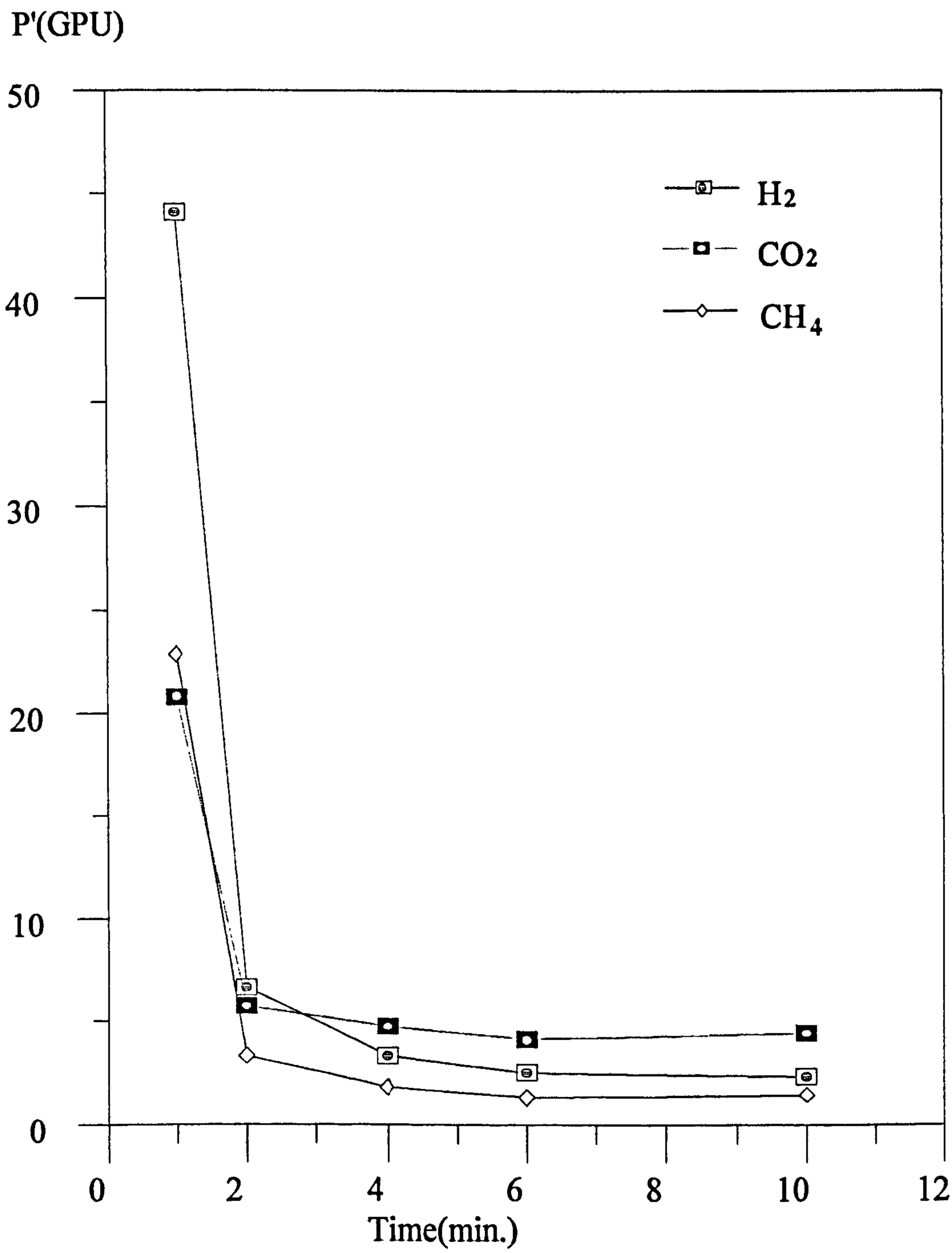

Fig. 4.7 Effect of coating time on the gas permeability

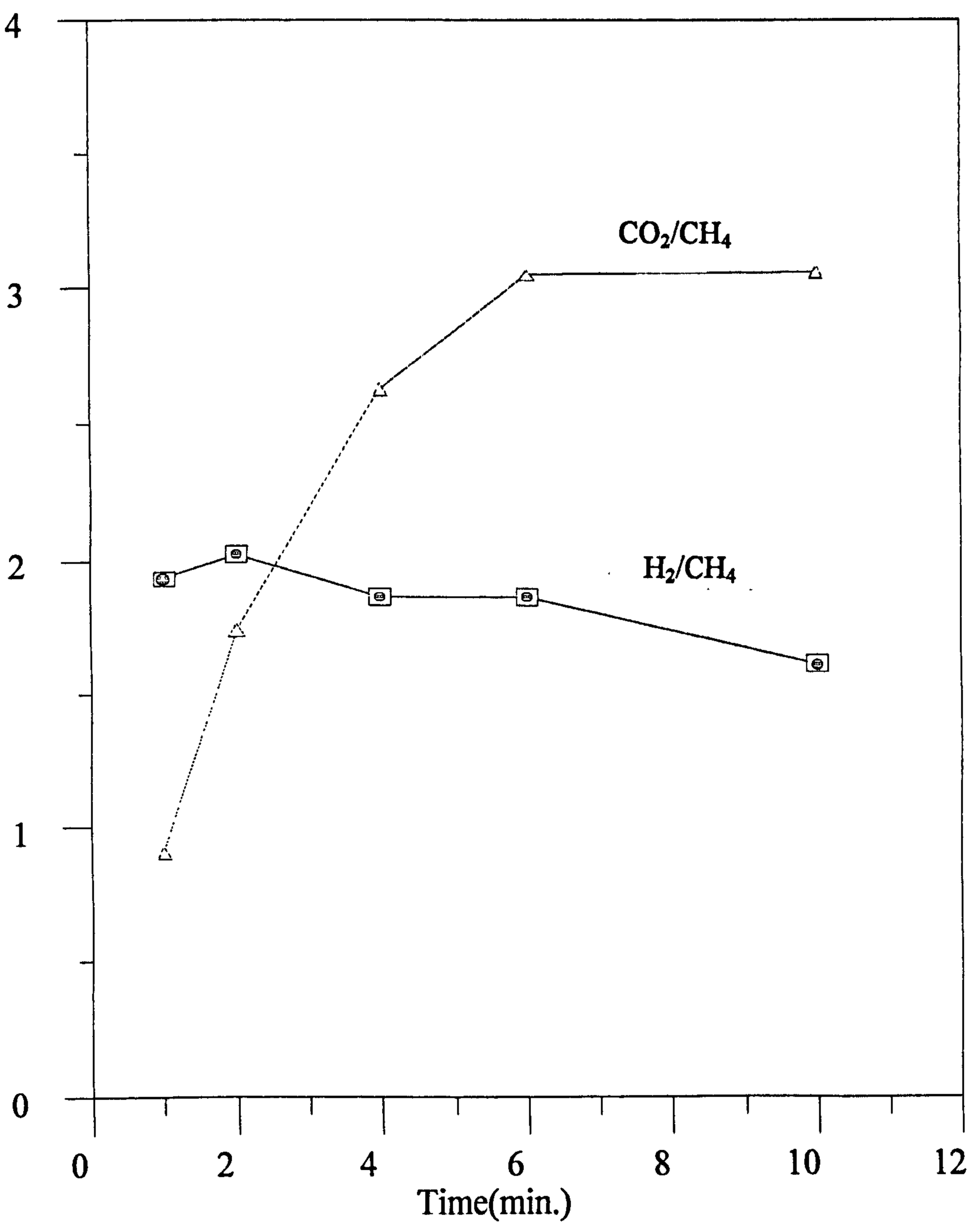

Fig. 4.8 Effect of coating time on the gas separation factors

of PAN polymer. For PAN as-spun hollow fibre membranes, the gas permeation rate is mainly dominated by the mean pore radius (surface porosity) on the surface of the membranes. Once the pores are blocked by the coating material, the gas permeation rate of the membrane is dominated by the solution-diffusion flow if the pores are completed sealed by the coating material. The permeation rate of the membrane will decrease because of the increased resistance to gas passing through the membrane. If the resistance to gas flow in the pores blocked by the coating material is lower than that in the skin layer of the PAN hollow fibre, then, the separation factor of the membrane will be mainly determined by the properties of the lower resistance material. If the membrane polymer has a very low permeability, the gas flows predominantly through the plugged pores, when the hollow fibre membranes are coated. The membranes will exhibit separation factors which are a combination of factors for the coating material and the PAN polymer. Fig. 4.8 shows that the separation factor α_{H_2/CH_4} of the PAN hollow fibre membrane is higher than the coating material value, and α_{CO_2/CH_4} is still less than the coating material value. If the coating material can seal all the pores properly, then the separation factors of the membranes should be the same as or higher than both of the separation factors (α_{H_2/CH_4}=0.69 and α_{CO_2/CH_4}=3.44) of the coating material. These results indicated that the coating material may not have blocked all the pores completely, even after 10 minutes immersion in the coating solution.

In order to confirm whether it is possible to improve the separation factors by choosing a polymer with a relatively lower permeability as a coating material, another coating polymer was required. Cellulose acetate (CA) was chosen as the second coating material in this experiment. A 0.8% cellulose acetate solution in acetone was prepared and then the hollow fibre module was subjected to coating using the same procedure as with Sylgard. The results are shown in Table 4.21.

Table 4.21 Effect of CA as coating material on the gas permeation rate of PAN hollow fibre membrane

Module	Permeation rate constant (GPU)			Separation factor	
	P'_{H_2}	P'_{CH_4}	P'_{CO_2}	α_{H_2/CH_4}	α_{CO_2/CH_4}
No. 32:					
AS	too high to measure				
CAS	2.42	0.26	0.44	9.31	1.69

After coating, the permeation rates of the membranes decreased. The separation factors α_{H_2/CH_4} and α_{CO_2/CH_4} were 9.3 and 1.69, respectively, which are far lower than the intrinsic separation factors of PAN polymer (α_{H_2/CH_4}=10000 and α_{CO_2/CH_4}=280) and the coating materials (α_{H_2/CH_4}=80 and α_{CO_2/CH_4}=31.17)[147], and also lower than the values of the membranes predicted by RM. The separation factor α_{CO_2/CH_4} is lower than that of the CA coating material, which indicates that the pores are not all blocked by the coating material completely. Thus, Kundsen flow (α_{H_2/CH_4}=2.82 and α_{CO_2/CH_4}=0.60) still contributed to the separation factor of the PAN hollow fibre membranes.

From the results obtained, it seems likely that the PAN hollow fibre has too high a surface porosity (large mean pore radius) which makes it very difficult for coating materials to seal the pores to form a defect-free thin film on the surface of the fibre. A reduced surface porosity will be necessary before PAN hollow fibre membranes show improved separation factors.

4. 3. 4. 2 Annealing

a) Hot water treatments

As-spun hollow fibres, which were in module form, were subjected to hot water treatments in an attempt to close some of the pores on the surface of the hollow fibre. It was observed that the fibres were shrunk and twisted when immersed in the hot water. It indicated that the water had exerted a significant plasticizing effect on the PAN hollow fibres. Because PAN has a relatively low glass transition temperature [131], it was hoped that some pores would collapse on the surface of the membrane after treatment with hot water.

The effect of hot water treatments on the permeation properties of the membranes was quite marked. This treatment dramatically reduced the permeation rate for all the gases, but the separation factors were still in the range of Knudsen diffusion, as shown in Table 4.22. It appears that the treatment did produce a reduced surface porosity in the skin layer, i.e., some pore closure occurred. When these hot water treated samples were coated with Sylgard 184, the membrane had improved separation factors α_{H_2/CH_4} and α_{CO_2/CH_4}, which are 10.26 and 3.52, respectively. Both of them are higher than that of the silicone coating material. These results also showed that the coating material blocked the pores effectively, because the separation factors of the coated membranes were higher than that of the coating material, even though, the separation factors of the membrane were still lower than expected.

The lower separation factors indicate that most of the gases pass through the coating material rather than PAN polymer. The final separation factor of the membranes are a combination of separation factors of the coating and PAN polymer materials. The P'_{H_2} gas permeation rate shows only 0.85 (GPU). This means that hot water

Table 4.22 Hot water treatment effect on the hollow fibre permeability and separation factors

Module	State/Treatment	Permeability(GPU) P'_{H_2}	Separation factor α_{H_2/CH_4}	α_{CO_2/CH_4}
No. 3	AS	too high to measure		
	2 minutes at 90 °C H_2O	29.63	2.37	0.64
	CWTAS [a]	0.85	10.26	3.52

a: CWTAS is Sylgard coated fibres after the fibres were treated in hot water.

treatments do accelerate pore closure, probably reducing the surface porosity at the sacrifice of increasing the separating layer thickness. It has been noticed that in this case, the fibres exhibit a very low permeability, especially for P'_{CH_4}. The very low permeability is because of the impermeable nature of the polymer and the thick skin layer of the hollow fibres.

b) Annealing treatments in vacuum oven

In order to investigate the effect of heat treatment on the PAN hollow fibres, fibres in module form were subjected to heating in a vacuum oven at temperatures between 40 °C and 190 °C for half an hour each time. Fig. 4.9 and Fig. 4.10 show that as the temperature increased, the gas permeability of the fibres decreased. At the same time, the fibre dimensions also changed. At temperatures below 80 °C, the gas permeability of the fibres decreased only slightly with temperature, and the shrinkage of the fibre in diameter and length were of the order of only 0.4%. If the fibre was treated at temperatures above 80 °C , the gas permeability decreased very rapidly, and the shrinkage in diameter and length were of the order of 4.4% and 3.3%,

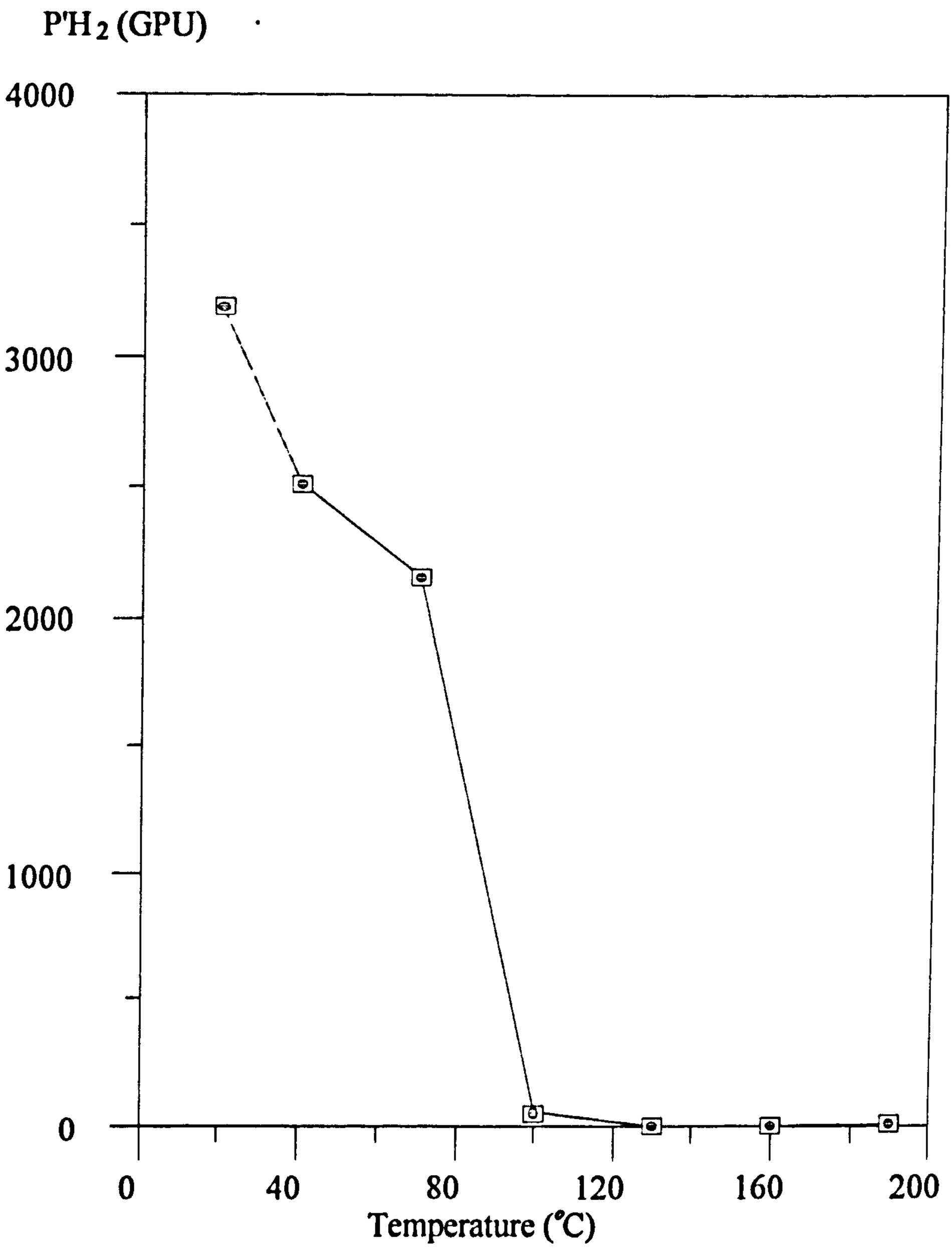

Fig. 4.9 Effect of heat treatments on the gas permeability

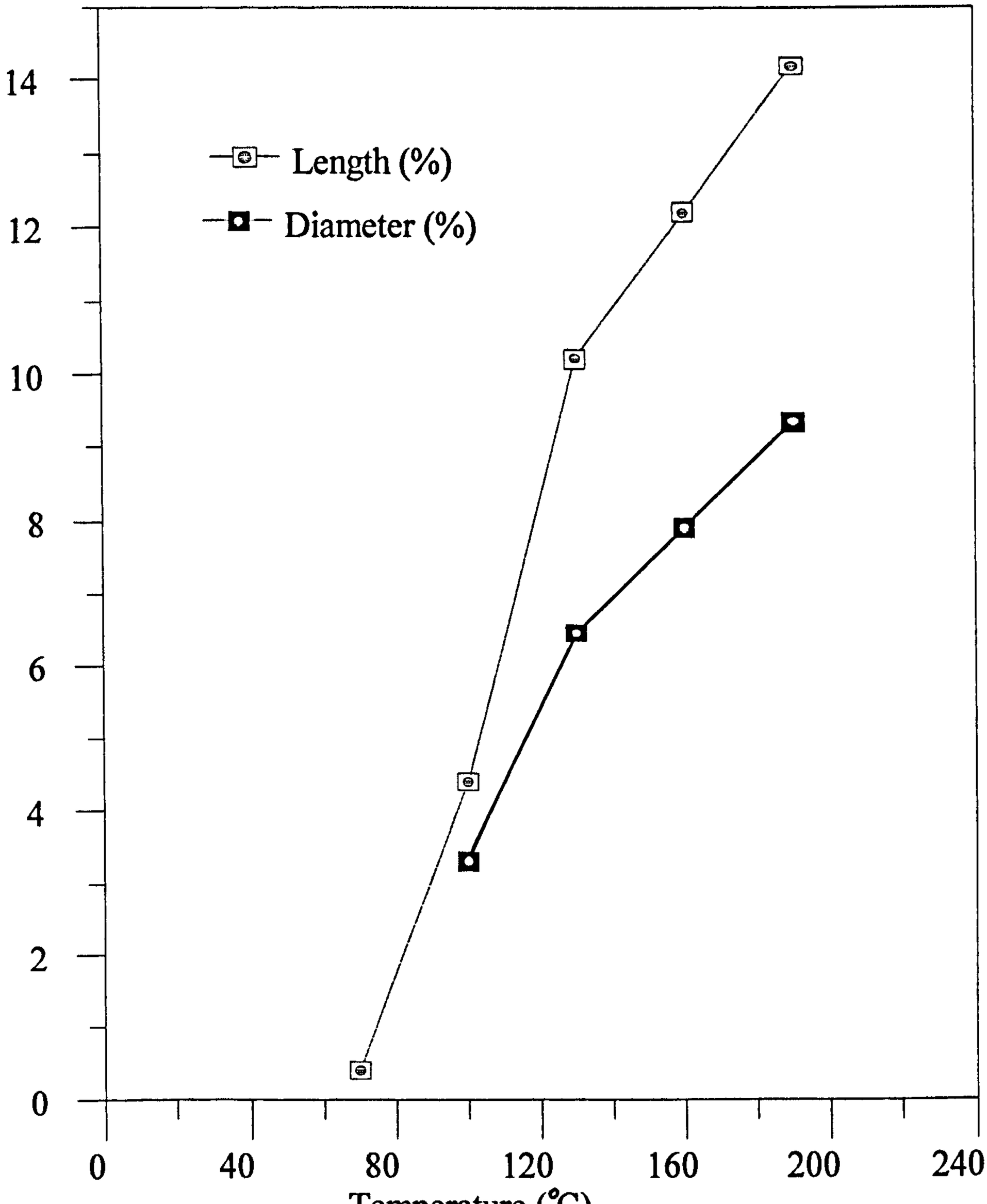

Fig. 4.10 Effect of heat treatments on the shrinkage of PAN hollow fibre

Table 4.23 Effect of vacuum annealing treatment on gas permeation rate of PAN hollow fibre membranes

Module	State/Treatment	Permeability (GPU)	Separation factor	
		P'_{H_2}	α_{H_2/CH_4}	α_{CO_2/CH_4}
No. 13	AS	too high to measure		
	30 min. 100 °C in vacuo	52.45	3.19	0.55
	CVTAS [a]	0.51	6.15	2.47

a:CVTAS is Sylgard coated fibres after the fibres were treated in the oven.

respectively at 90 °C. At this temperature, close to the Tg of the polymer, the pores on the surface of the fibres may be able to close although the porous structure underneath the skin of the hollow fibre will also collapse during the treatment. A less porous surface and a denser skin layer will form, reducing the gas permeability. Simultaneously, the dimensions of the hollow fibres will change. When the fibres were treated at 130 °C, the gas permeability continued to fall. If the temperature was increased further, the fibre began to change in colour from white to brown as the polymer underwent the reactions associated with the cyclization process. Table 4.23 showed that for fibres treated at 100 °C for 30 minutes, the gas permeability was very low and the separation factors were still in the range of Knudsen flow. After the sample was coated with Sylgard, the membrane not only showed very low permeation rates, but also low separation factors.

Unfortunately, only limited modifications of the PAN hollow fibre membrane were obtained by annealing treatments in hot water and by heating in a vacuum oven. Under these treatment conditions, the PAN hollow fibre membranes will be close to

or above the Tg value for Courtelle. While surface pores will tend to close, at the same time, the porous substructure underneath the selective skin layer will also tend to collapse. This will increase the effective thickness of the separating layer, so that the permeation rate through the membrane decreases. That a large surface porosity existed in the PAN hollow fibre was shown by the results of measuring gas permeation rates and separation factors of the membranes. Without the hot water treatment, the coating fails to block all the pores properly because of the large surface porosity. The separation factor α_{CO_2/CH_4} of this kind of membrane is less than that of the coating material. When the fibres were subjected to a hot water treatment, the separation factor α_{CO_2/CH_4} of the coated fibres was higher than the coating material. It indicates that the coating material can block the pores after the treatment. But the separation factors are far less than the intrinsic separation factors of PAN, and the membranes show very low permeation rates.

Other attempts to modify the permeation rate of the membranes were made. What was necessary was to modify the separating layer of the polymer without losing the underlying porous substructure.

4. 3. 4. 3 Other surface modifications

PAN as-spun hollow fibre membranes were treated with hydroxylamine in an attempt to form a separating layer containing the amidoxime group[149] (see section 2. 5. 2. 2). The chemical reaction was carried out when a module was immersed in the hydroxylamine solution at a temperature of 75 °C for 25 minutes to 30 minutes. After 25 to 30 minutes treatment, the hollow fibres became yellow brown in colour, and the fibre no longer dissolved in DMF (but it did split and swell in the solvent). This suggested that some reaction had occurred. The hollow fibre became very brittle if it was treated for more than 25 minutes in the hydroxylamine solution at 75 °C.

Table 4.24 Effect of hydroxylamine treatment on gas transport of PAN hollow fibre membrane

Module:	State/treatment	Permeability P'_{H2}(GPU)	Separation factor $\alpha_{H2/CH4}$	$\alpha_{CO2/CH4}$	$\alpha_{H2/CO2}$
No.5	AS 30 min. 75 °C NH_2OH	too high to measure too brittle to handle			
No.6	25 min. 75 °C NH_2OH	0.768	2.28	0.44	
	CHTAS [a]	0.272	- [b]	-	10.98
No. 7	1 min. 90 °C NH_2OH	8.52	2.15	0.60	
	CHTAS	0.77	6.27	1.43	4.38

a: CHTAS is Sylgard coated fibres after the fibres were treated in a hydroxylamine solution;
b: - means the permeation rates for CH_4 is too low to be measured satisfactorily.

After treatment in the solution, the gas permeation rates of the membrane decreased, as compared to the original membrane, probably because the treatment causes pore closure at 75 °C; the results are shown in Table 4. 24. After coating with Sylgard 184, the membrane showed still lower permeation rates, especially for CH_4. When the membrane was treated in the solution at 90 °C for one minute, the P'_{H2} permeation rate of the membrane was higher than that of the membrane treated at 70 °C for 25 minutes. But the separation factor was lower than the separation factor of the coating material, which means that the coating material was still not able to seal all the pores completely.

In order to try to modify the separating layer without simultaneous plasticization, a modification of the selective skin layer of the membrane at room temperature was required. After several trials, a module was immersed in cuprammonium hydroxide

Table 4.25 Effect of cuprammonium hydroxide solution treatment on the gas transport of PAN hollow fibre membranes

Module No:	State/treatment	Permeability P'_{H_2}(GPU)	Separation factor α_{H_2/CH_4}	α_{CO_2/CH_4}
No: 15	AS	too high to measure		
	Treated overnight	753.18	2.63	0.61
	CCTAS [a]	10.00	1.78	1.99
No: 17	AS	too high to measure		
	Treated overnight	2155.84	2.47	0.58
	CCTAS	3.86	1.86	1.99

a: CCTAS is Sylgard coated fibres after the fibre treated in cuprammonium hydroxide solution.

solution at room temperature overnight. The membranes became yellow brown in colour, and the fibre no longer dissolved in DMF. This result suggested that some kind of interaction took place between the polymer and the reagent. The results of measuring the gas permeation properties of this kind of membrane are shown in Table 4.25. The detailed study of the treatment of the PAN hollow fibre with cuprammonium hydroxide is discussed in Chapter 5.

The results in Table 4.25 show that the uncoated membrane, after treatment, showed very higher permeation rates. It means that the treatment at room temperature had only a small effect on closing the pores on the surface of the membrane. The gas transport is still in the range of Knudsen flow. After coating, the separation factor α_{CO_2/CH_4} shown in Table 4.25 is less than the coating material, which indicates large pores on the surface causing the coating material to fail to seal all the pores properly, so that some Knudsen flow contributed to the separation factors α_{H_2/CH_4} and α_{CO_2/CH_4}

of the coated membranes. The gas permeation rates of the coated membrane are still lower than that of equivalent PSF hollow fibre membranes. The membranes after treatment with cuprammonium hydroxide solution do not shown any interesting results for gas separation performance despite some kind of interaction that took place between the polymer and the reagent, which may be useful for applications in some other field.

4. 3. 5 Dual-bath coagulation spinning system

In the light of the disappointing results obtained when trying to modify PAN hollow fibre membranes by annealing and other surface modifications, it was believed that the high porosity on the separating surface layer and the low intrinsic permeation properties of PAN were responsible for the low separation factors and low gas permeation rates observed. In order to improve the surface porosity of the fibre, a dual-bath coagulation spinning system was next tried. In this spinning process, the polymer solution contacts with two successive nonsolvent baths, whereby the first bath initiates the formation of a dense top layer and the second bath cause the actual polymer precipitation. It has been reported that hollow fibre membranes produced by this method have higher gas separation factors and do not need any additional coating procedure[94].

The dual-bath coagulation method used for spinning PAN hollow fibres is illustrated in Fig. 4.11. The degassed dope was fed from the pot under 25 psi nitrogen pressure into a metering pump, and then passed through a filter pack into a heated tube before passing through the spinneret. After the spinneret, the formed hollow fibre was passed through an air gap of 60 mm before entering the first nonsolvent coagulation bath. After immersing in the first bath, the first bath outlet guide roller was used to deliver the fibre through the bath and into the second coagulation bath. The second

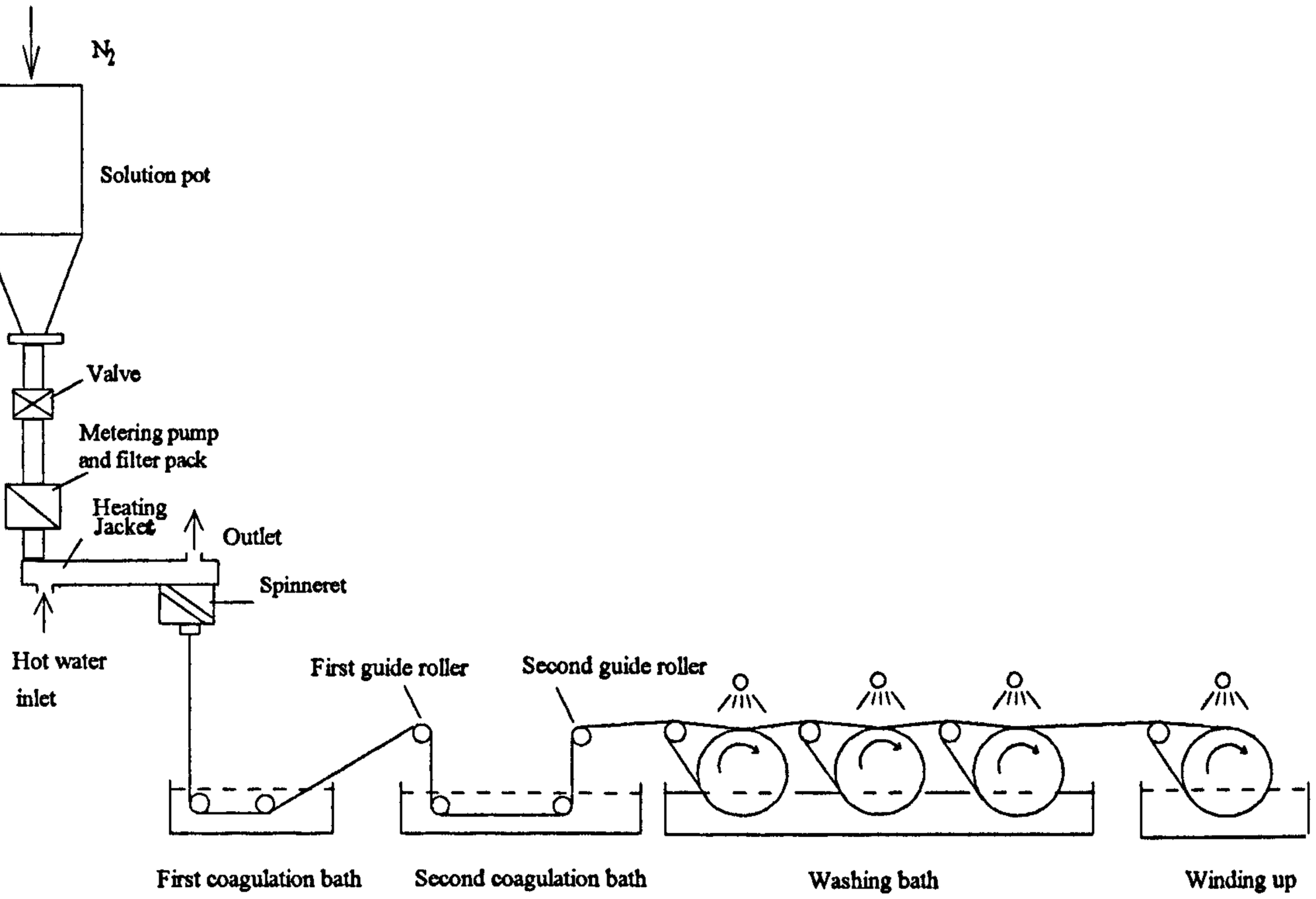

Fig. 4.11 Schematic diagram of a dual-bath coagulation spinning process

bath outlet guide roller was used to deliver the fibre out of the second bath and onto a series of washing rollers and a collecting drum.

In the single coagulation bath spinning system, PAN hollow fibres made from the spinning solution containing 25 wt% PAN and 5 wt% $CuSO_4$ $5H_2O$ in DMF showed high surface porosity according to the experimental results and RM prediction. In this dual-bath coagulation spinning system, the hollow fibres take a longer time than in the single coagulation bath spinning system before becoming fully coagulated in the second coagulation bath. Butyl ether was used as one additive in the spinning solution in order to reduce the loss of porosity of the hollow fibres during the drying procedures.

The spinning conditions of batch No. 25/30/20D are given in Table 4.26. In the first coagulation bath, three different coagulants were used. The results of the gas permeation performance of these PAN hollow fibre membranes are shown in Table 4. 27. For the air dried samples, the gas permeation rates of the as-spun hollow fibre membranes were too high to be measured when water acted as a coagulant in the first bath. When water/$ZnCl_2$(9:1) and 1-pentanol were used as coagulants in the first bath, respectively, the results show that quite low gas permeation rates P'_{H_2} were obtained only when 1-pentanol was the coagulant in the first bath. The gas separation factors α_{H_2/CH_4} and α_{CO_2/CH_4} of these as-spun hollow fibre membranes show the gases following Knudsen behaviour. After coating, the separation factors of these hollow fibre membranes were both higher than that of the coating material, which indicated that the coating material had successfully sealed the pores, so that the separation factors of the membranes lay between the coating material and PAN itself. The low separation factors α_{H_2/CH_4} and α_{CO_2/CH_4} of the membranes showed again that most of gas still passed through the coating material rather than the PAN. In the case of 1-pentanol as a nonsolvent in the first coagulation bath, the separation factors α_{H_2/CH_4} and α_{CO_2/CH_4} were 22.31 and 9.92 respectively which is much higher than that of the other two modules when water and water/$ZnCl_2$ were used in the first coagulation bath. According to the RM prediction (see Table 4.17), these high separation factors can only be obtained when silicone rubber coated PAN hollow fibre membranes have less surface porosity. These results imply that lower surface porosity PAN hollow fibres could be produced by the dual-bath spinning system, but low gas permeation rates P'_{H_2} would be obtained because this system would lead to increase the skin layer thickness.

For the samples dried by solvent exchange methods, the gas permeation rates of the as-spun hollow fibre membranes were very high, so that they were not satisfactorily measured by the soap film flow meter used in this study. After coating, the gas

Table 4.26 Spinning conditions of the dual-bath coagulation spinning system

Spinning batch No.	25/30/20/00D
Spinning solution composition:	PAN//$CuSO_4$/Butyl ether =25/3/2 (wt%)
Spinneret dimension	580/330/150 μm
Polymer extrusion temperature:	60 °C.
N_2 pressure:	25 psi
Internal coagulant injection rate:	1.06 ml/min.
Internal coagulant temperature:	40 °C.
Linear extrusion rate:	16.35 m/min.
Water injection temperature:	40 °C.
First coagulation bath length:	30 cm.
First jet gap:	0.6 cm.
Coagulant in the first bath:	A: Water; B: Water/$ZnCl_2$=90/10; C: Pentanol.
First coagulation bath temperature:	Room Temperature.
Coagulant in the second bath	Water
Second coagulation bath temperature:	60 °C.
Second coagulation bath length:	100 cm.
Second jet gap:	0.6 cm.
Wind-up speed:	11.40 m/min.

Table 4.27. First coagulation bath composition effect on the gas permeability and selectivity

Module	Drying method	P'_{H2}(GPU)	$\alpha_{H2/CH4}$	$\alpha_{CO2/CH4}$
A: 1st bath is water				
AS		-----[a]		
CAS		27.47	1.50	3.50
B: 1st bath is water/$ZnCl_2$				
AS	Dried in air:	827.33	2.71	0.62
CAS		11.98	2.58	4.45
C: 1st bath is 1-pentanol				
AS		42.88	2.51	0.60
CAS		1.86	22.31	9.92
A: 1st bath is water				
AS		-----		
CAS		30.05	1.47	3.92
B: 1st bath is water/$ZnCl_2$				
AS	S.E. dried:	-----		
CAS		22.28	1.54	3.76
C: 1st bath is 1-pentanol		-----		
AS				
CAS		3.77	6.08	4.01

a: gas permeation rate is too high to be measured satisfactorily.

permeation rates of these coated membranes were higher than the equivalent samples dried in air, but there was no positive improvement in gas separation factors.

A further two spinning runs were carried out under the dual-bath coagulation spinning conditions, with 1-pentanol as nonsolvent in the first coagulation bath and water as nonsolvent in the second coagulation bath. The compositions of the polymer spinning solutions are shown in Table 4.28. The gas permeation rates and

separation factors of the membranes are shown in Table 4.29. For the as-spun hollow fibre membranes, the gas permeation rates are very low in comparison to the results of sample C in Table 4.27 for the air dried module; these low gas permeation rates in modules DB2 and DB3 are related to the low porosity of the separating layer or a more dense skin layer. The separation factors α_{H_2/CH_4} and α_{CO_2/CH_4} are close to the separation factors of Knudsen flow. After coating, the membranes exhibit very low gas permeation rates, especially for CH_4 and CO_2; for the latter, the gas permeability could not be detected even after 30 minutes under 100 psi. This means that there is a possibility that higher separation factors could be obtained. Unfortunately, there was no sign of improvement in gas permeation rates.

Table 4.28 The composition of spinning solutions and nonsolvent used in the dual-bath coagulation system

Batch No:	Polymer concentration wt%	Solvent/Additive wt%	Nonsolvent in first Bath	Nonsolvent in second bath
25/30/20/02D DB2	25	DMF/$CuSO_4$/Butyl ether =70/3/2	pentanol	water
25/35/00D DB3	25	DMF/$CuSO_4$ =71.5/3.5	pentanol	water

Above all, PAN hollow fibre membranes produced by the dual-bath coagulation system show very low gas permeability in coated as well as as-spun fibre form. This result implies that the hollow fibres produced by the system may have a more dense skin layer and fewer defects on the surface of the fibres. The low gas permeability of the membranes is believed to be associated with the low intrinsic gas permeability of PAN polymer. In order to improve the gas permeability of PAN hollow

Table 4.29 Gas permeability and selectivity of PAN hollow fibre membranes (Module DB2 and DB3)

Module	P'_{H_2}(GPU)	α_{H_2/CH_4}	α_{CO_2/CH_4}
DB2: 66(1)			
AS	1.88	3.21	0.64
CAS	0.50	N/A	N/A
DB2:96(1)			
AS	1.83	3.39	0.60
CAS	0.63	N/A	N/A
DB3:36(1):			
AS	1.18	3.18	0.52
CAS	0.24	N/A	N/A
DB3:66(1):			
AS	2.07	4.60	0.63
CAS	0.37	N/A	N/A

fibre membranes, it is necessary to reduce the skin layer thickness, or look for other feasible methods to modify the surface structure to increase the gas permeability. The results obtained by the dual-bath coagulation system demonstrated that the low intrinsic gas permeability of PAN polymer and the skin layer thickness of the fibres must limit the usage of PAN hollow fibre membranes for gas separations.

CHAPTER 5

REVERSIBLY CROSSLINKED PAN HOLLOW FIBRES

5. 1 Introduction

In order to prevent the porous structure in PAN hollow fibres from collapsing during attempts at post spinning modification, a modification of the fibres was carried out at room temperature by treatment with cuprammonium hydroxide solution. Cuprammonium hydroxide was chosen after initial experiments with aqueous copper salt solutions and ammonia. Treatment with aqueous copper sulphate alone or ammonia solution alone produced no fibre crosslinking. However, combinations of cuprous chloride and ammonia solution did produce fibre insoluble in DMF, and hence presumed crosslinked, though the results were irreproducible.

After the treatment with cuprammonium hydroxide solution (see section 2. 5. 2. 3), it was found that the PAN hollow fibres were coloured and also no longer soluble in the usual organic solvents such as DMF, DMAC, DMSO and NMP. This surprising result indicated the possibility of a new structure with a more rigid configuration, whether from a crosslinked structure from a PAN-copper ion complex or via reaction between nitrile groups and base giving a conjugated structure.

A literature search did not reveal any paper or patent dealing with the modification of PAN hollow fibre with copper or ammonia. However, the modification of PAN fibres with reagents containing copper ions for a variety of applications have been reported in the literature[121 ~ 124, 150]. For example, the treatment of stretched PAN fibres with aqueous copper salts such as cuprous chloride showed an improved moduls of 16 GPa[123]. Similarly, it had been reported that the mechanical properties, such as strength and modulus, of carbon fibres converted from precursor PAN fibre pre-treated with cuprous chloride are much higher than those obtained from untreated precursor fibres[154].

In this chapter, further experiments are described which were carried out in order to investigate the coloration and insolubility of the PAN fibres.

5. 2 Characterisation of the crosslinked fibres

Standard acrylic fibres, such as "Courtelle"(copolymer), "Dralon"(homopolymer) (see section 2. 1. 1), and the PAN hollow fibres, were immersed in a 150 ml measuring cylinder containing cuprammonium hydroxide solution (see section 2. 5. 2. 3).

The weight increase of hollow fibre after treatment with cuprammonium hydroxide solution, and the weight-loss of the crosslinked hollow fibres after treatment in DMF were determined (see section 2. 5. 2. 3); the latter indicates the extent of the crosslinking in the PAN hollow fibres. The ratio of the diameter of the crosslinked PAN hollow fibre in DMF to the diameter of the original fibre was also measured to determine the extent of fibre swelling and hence estimate the degree of crosslinking.

5. 3. Results and discussion

5. 3. 1 Coloration and insolubility of the PAN fibres

Table 5. 1 shows the coloration and insolubility of the PAN fibres after being treated with cuprammonium hydroxide solution at room temperature. All the fibres were no longer completely soluble in the usual organic solvents. It was also noticed that the colour of the fibres changed from white to yellow, through to yellow brown, and to dark brown depending on whether they were porous or solid fibres, and the treatment time. For the porous PAN hollow fibre, the colour change was more intense than for

Table 5.1 The coloration and solubility of various fibres after treatment with cuprammonium hydroxide solution

Sample	Treatment time (Days)	Colour of the fibre	Solubility in the solvents*
PAN hollow fibre	5	brown	no
	10	↓	no
	15	dark brown	no
Courtelle (Copolymer)	5	yellow brown	no
	10	↓	no
	15	brown	no
Dralon (homopolymer)	5	yellow brown	no
	10	↓	no
	15	brown	no

*: the solvents are the usual solvents for PAN fibres, such as DMF, DMAC, DMSO, and NMP; solubility test carried out at room temperature overnight, and 80°C for 30 min., respectively.

Table 5.2 Results of elemental analysis

Sample	Elemental Content(%)			
	N	C	H	Cu [c]
PAN hollow fibre	23.8	65.3	5.65	≤0.2
Crosslinked PAN hollow fibre [a]	23.3	63.3	5.05	0.6
Residual PAN hollow fibre [b]	23.3	63.05	5.15	0.5

a: the fibre treated in the reagent for 18 h;
b: the treated fibre, extracted with DMF for one week, then removed from solvent, washed in fresh DMF, then rinsed in water for 24 h, dried by solvent exchange method;
c: determined by atomic absorption.

the solid fibres such as "Courtelle" and "Dralon" under the same treatment conditions. The coloration of the porous fibre developed from brown to dark brown after 5 days' treatment. At the same time, the coloration of the solid fibres developed from yellow brown to brown. Porous fibres achieved some insolubility within a few hours of treatment with cuprammonium hydroxide solution, whereas the solid, 'non-porous' fibres required several days treatment with the reagent. This is likely to be due to the increased surface area available in a porous structure which will enhance diffusion of the reagent and increase the reaction rate.

Table 5.2 shows the elemental analysis data of the PAN hollow fibre before and after treatment with cuprammonium hydroxide solution. The data showed that the elemental contents of N, C, H in the PAN hollow fibres were slightly changed, and that copper is present in the PAN hollow fibres after the treatment (the level of copper, based on the N/Cu ratio, corresponds to one copper per 167 nitrile units). The copper content in the residual PAN hollow fibre (i.e. after DMF extraction) is reduced by about 16%, while the other elements show no significant change. This result indicates that the PAN hollow fibre has absorbed copper ions from the reagent, and that the copper in the polymer, which makes the polymer insoluble in the usual solvents, cannot be extracted by DMF. It is also possible that reactions which occur producing the coloration in the fibre may also make it insoluble.

Table 5.3 shows the effect of the treatment time on the properties of the PAN hollow fibre. From the Table, it can be seen that the ratio of the diameter of the PAN hollow fibre in DMF to the original fibre decreased with increasing treatment time, indicating that the fibre was becoming more crosslinked and less swollen in DMF solvent. At the same time, the coloration developed from yellow to dark brown, and the PAN hollow fibre became more and more brittle. These changes in coloration, insolubility and the brittleness of the fibre were presumed to reflect a more rigid configuration in

Table 5.3 Effect of the treatment time on the properties of the PAN hollow fibres

Treatment time (hour)	Weight increase W_A(%)	Weight-loss W_L(%)	D/d*	Colour of the fibre
0	0	100	∞	white
18	3.84	50.86	1.17	yellow
42	4.34	20.81	1.15	yellow-brown
66	6.70	16.07	1.15	brown
110	7.16	9.51	1.13	dark brown

*: the ratio of the diameter of the fibre in DMF to the original fibre diameter.

the newly-formed structure caused by the reaction between the PAN polymer and cuprammonium hydroxide, which made the fibres insoluble in DMF.

More importantly, as shown in Table 5.3, the fibre becomes increasingly insoluble in DMF as shown by the decreasing value of W_L and the increasing value of W_A as the treatment time is increased. The increasing extent of reaction indicated by the values of W_L and W_A support the reduced swelling of the fibre as shown by the D/d values. Fig. 5.1 and Fig. 5.2 show the weight increase (%) of the fibres after treatment with cuprammonium hydroxide and the weight-loss (%), i.e., the percent of polymer still soluble in DMF decreases as a function of time, respectively.

Fig. 5.3 shows the states of the crosslinked PAN hollow fibres in DMF solvent. It can be seen that the colour of the swollen fibres changes from yellow, through yellow brown, to dark brown, as the swelling of the fibre in the solvent decreases. It also shows that no matter how swollen the fibre is, the fibre still maintains its form in the solvent.

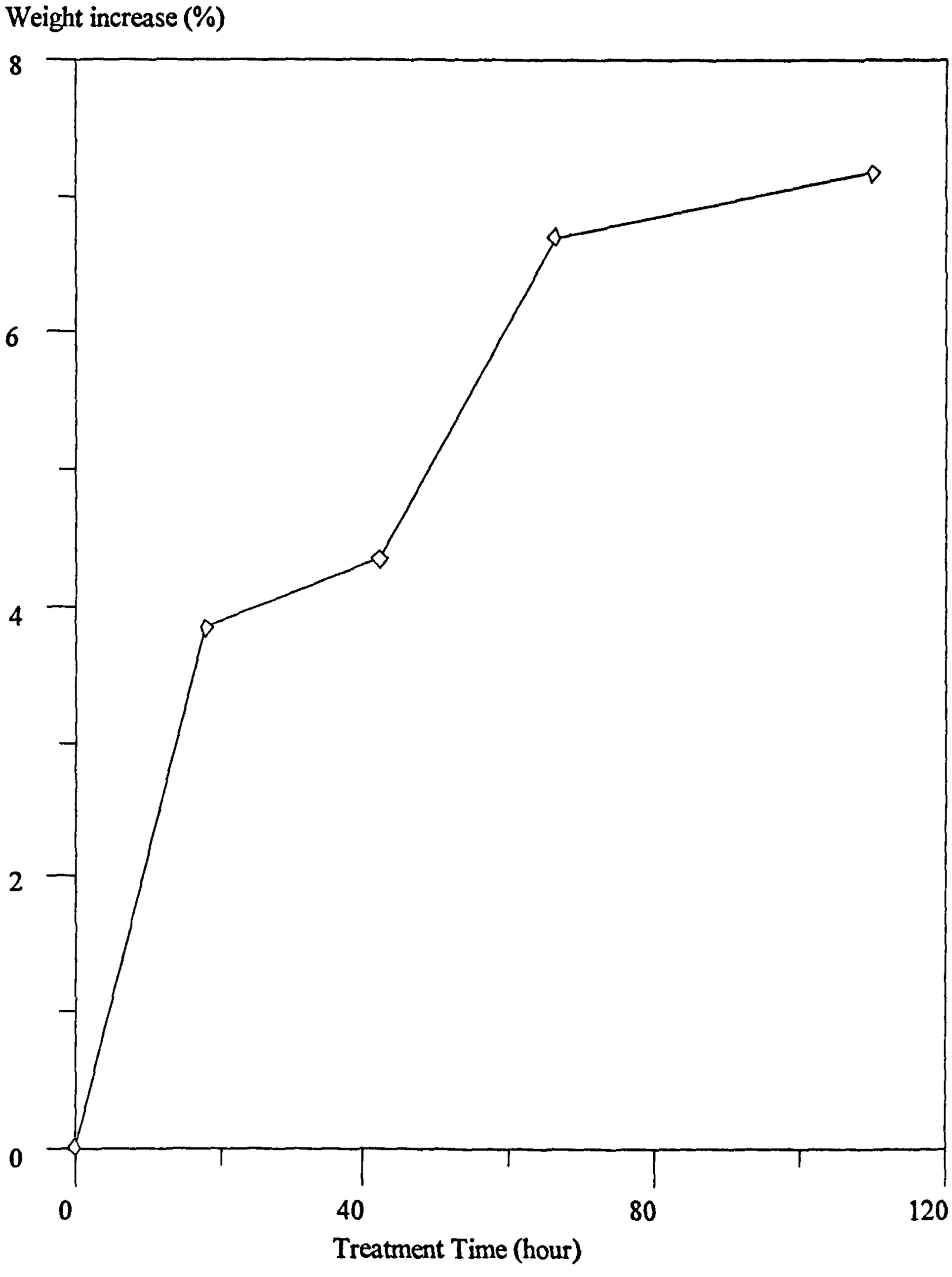

Fig. 5.1. The weight increase (%) versus the treatment time with the reagent

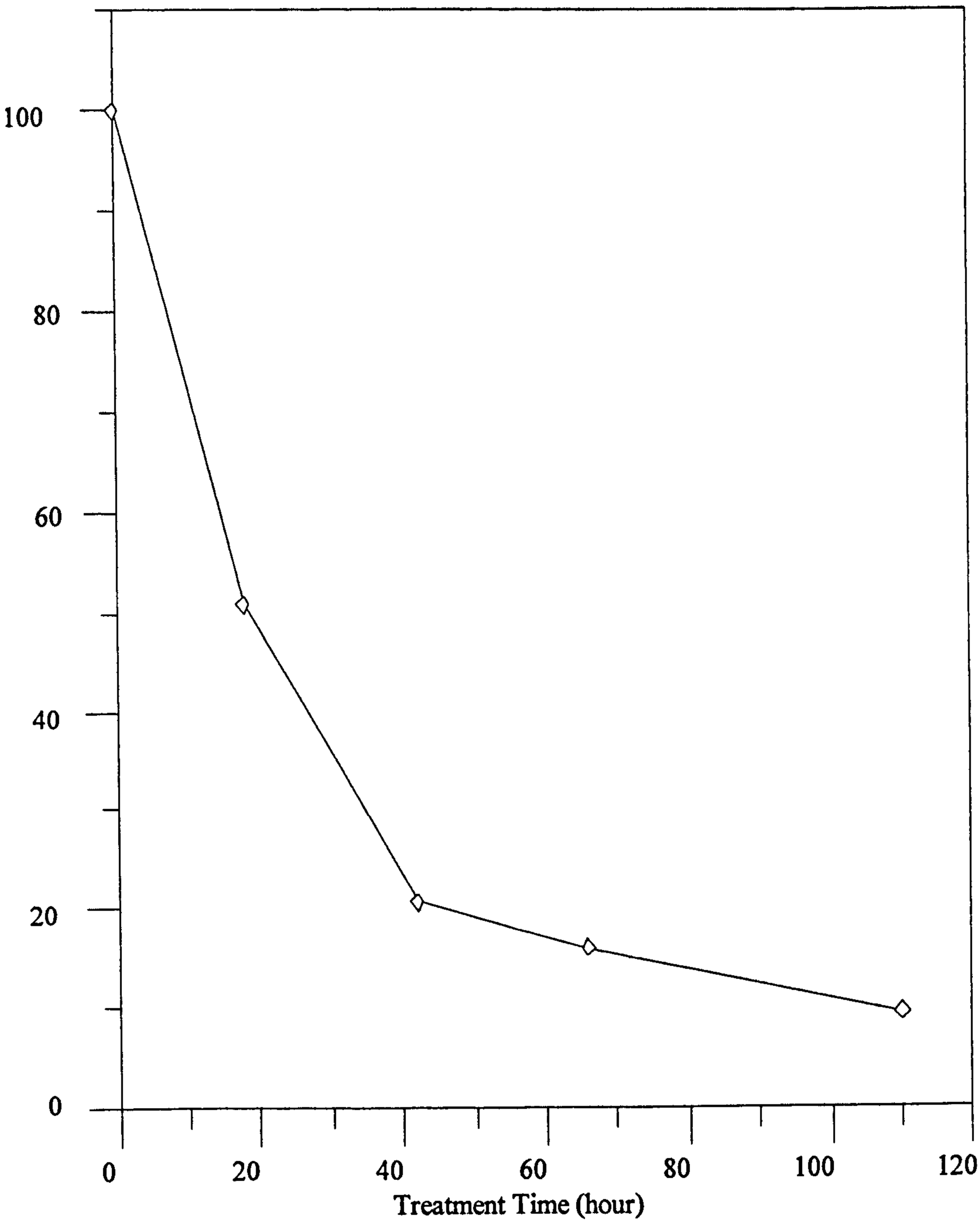

Fig. 5.2 The weight-loss (%) versus the treatment time with the reagent

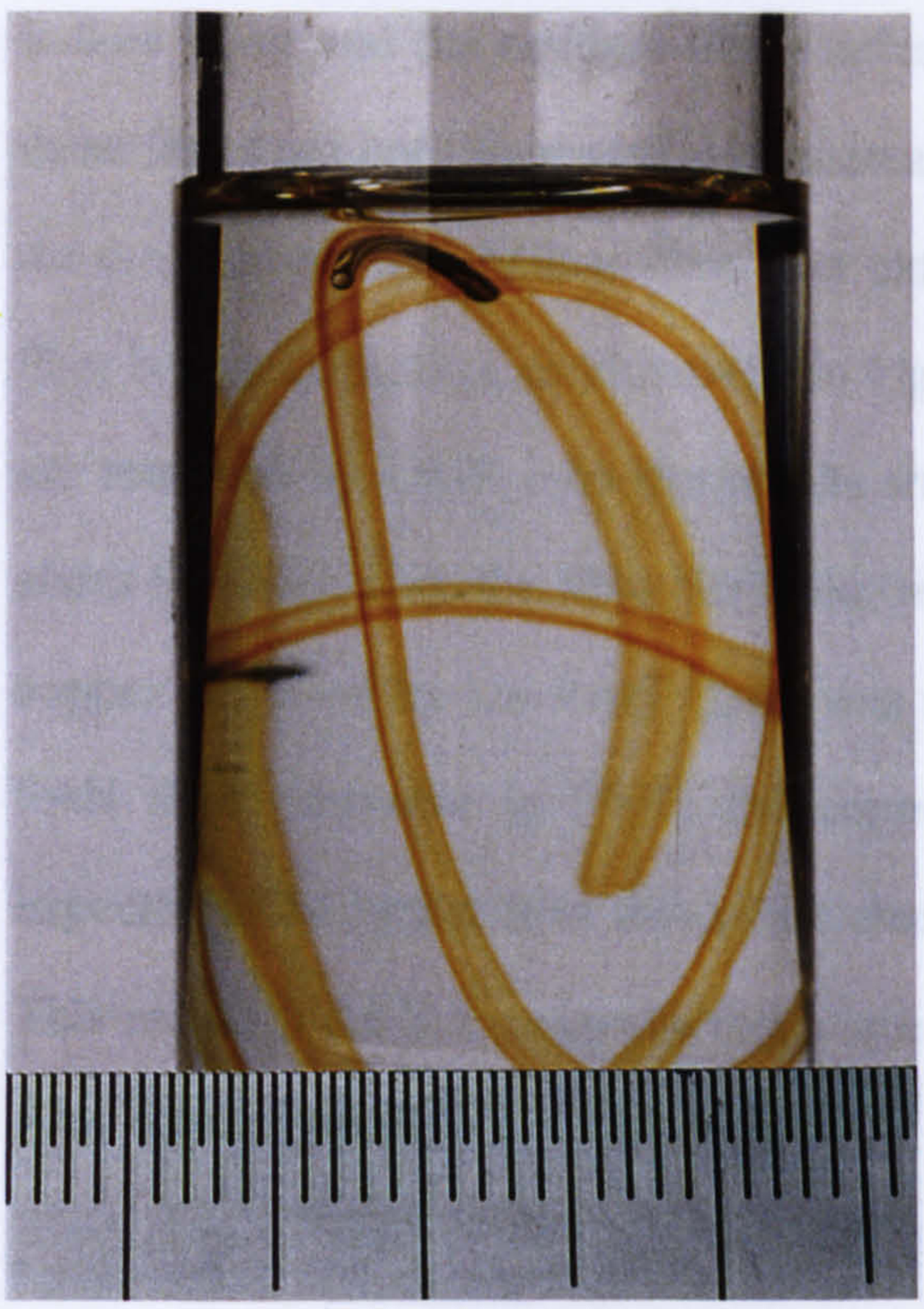

(a): 18 h

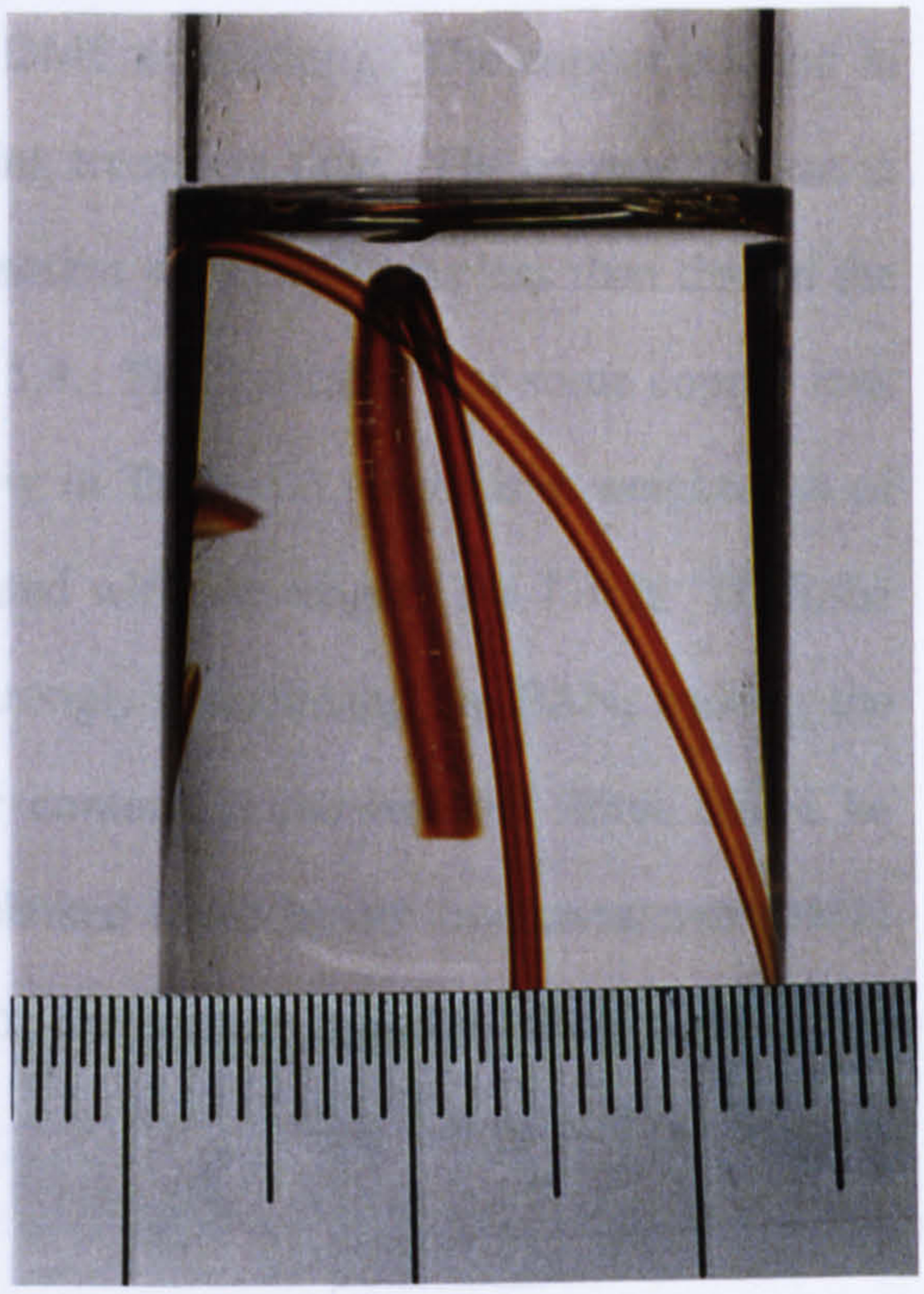

(b): 42 h

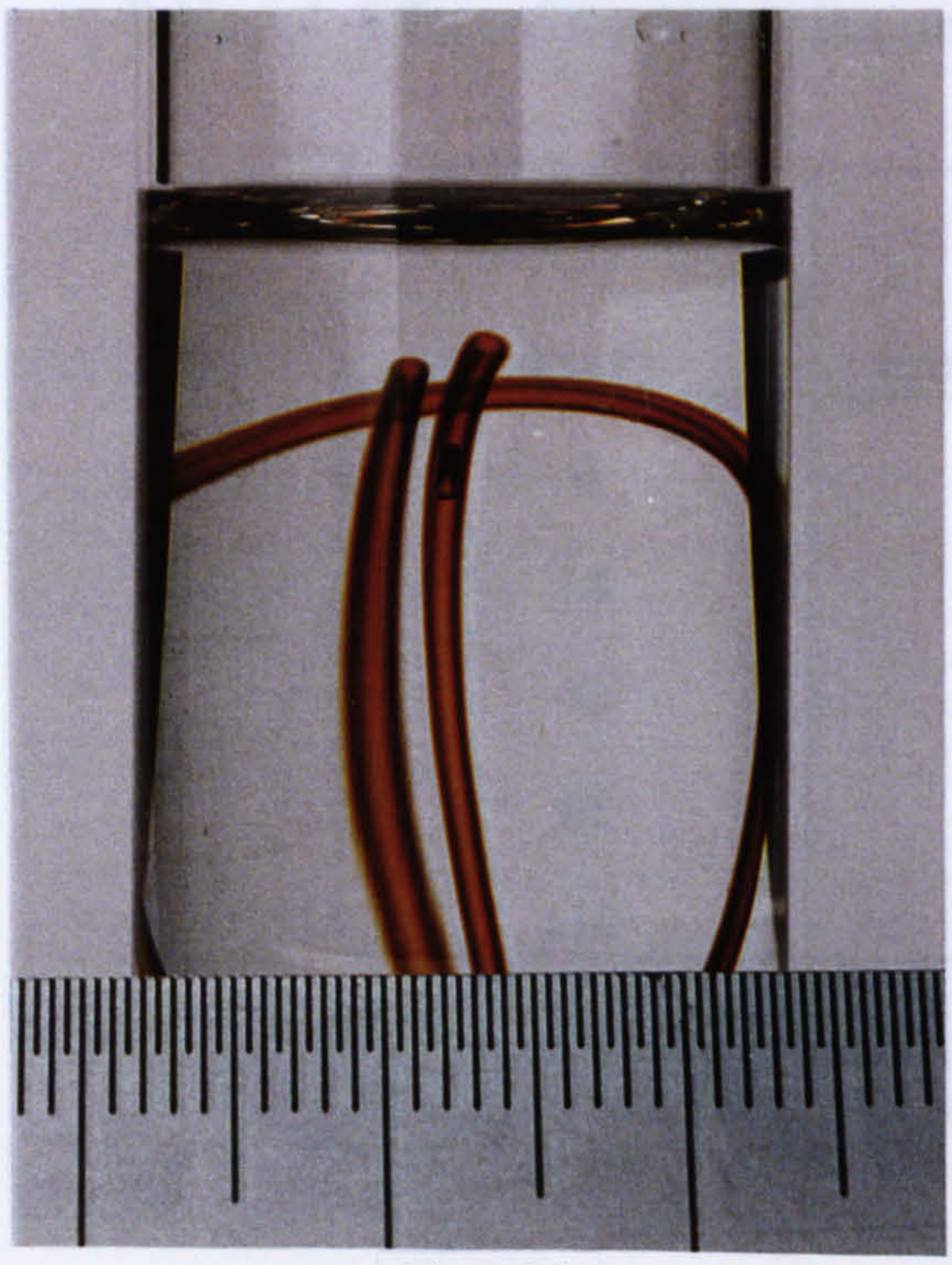

(c): 66 h

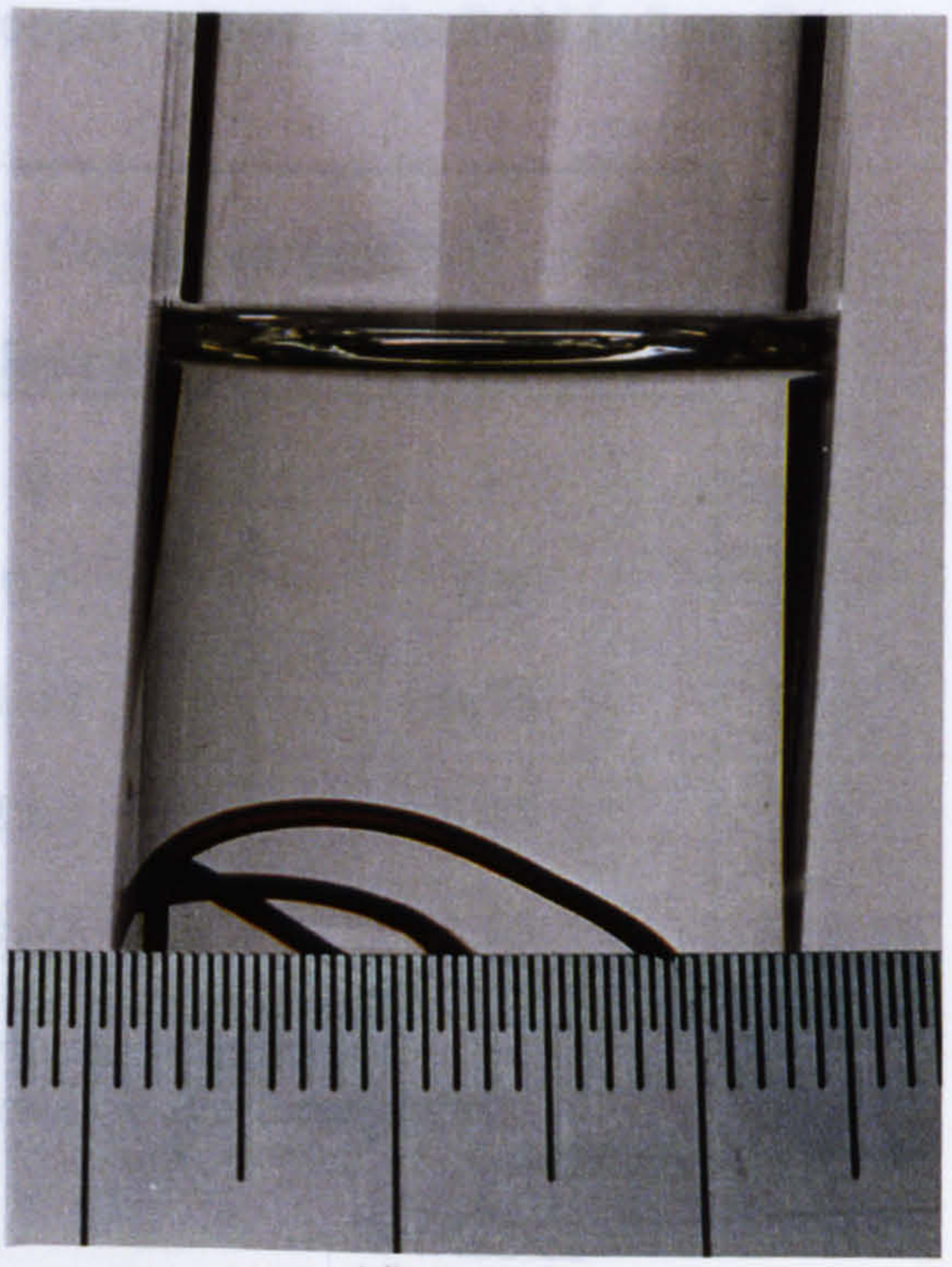

(d): 110 h

Fig. 5.3 The PAN hollow fibres after treated with the reagent for different time and then stored in DMF solvent for two days: (a): 18 h; (b): 42 h; (c): 66 h; (d): 110 h.

Table 5.4 shows the effect of the treatment time on the copper content in the PAN hollow fibres and the residual fibres (after DMF extraction). The copper content in these fibres are both increased with increasing treatment time. The copper content in the crosslinked PAN hollow fibre after extraction with DMF was less than that of the fibre before extraction, as illustrated in Fig. 5.4. This indicates that some copper ions are removed by DMF. As the results show in Table 5.3, there is a weight-loss of about 9% even after the fibre has been treated with the reagent for 110 h. If all the copper absorbed by the PAN fibres was strongly crosslinking the PAN, making the PAN fibres insoluble in DMF, the copper content in the residual fibres might be expected to be higher than that in the crosslinked fibres before treatment with DMF. This result, therefore, suggests that some of the copper is quite loosely held in the PAN structure, i.e., is not complexed.

Table 5.4 Effect of treatment time on copper content in the PAN hollow fibre

Treatment time (hour)	Copper content(%)[a]	
	Crosslinked fibre	Residual fibre[b]
0	0	-
18	0.6	0.5
42	1.35	0.75
66	1.60	0.95
110	1.95	1.55

a: Copper content was obtained by atomic absorption.
b: Insoluble crosslinked PAN hollow fibre after treatment in DMF for one week.

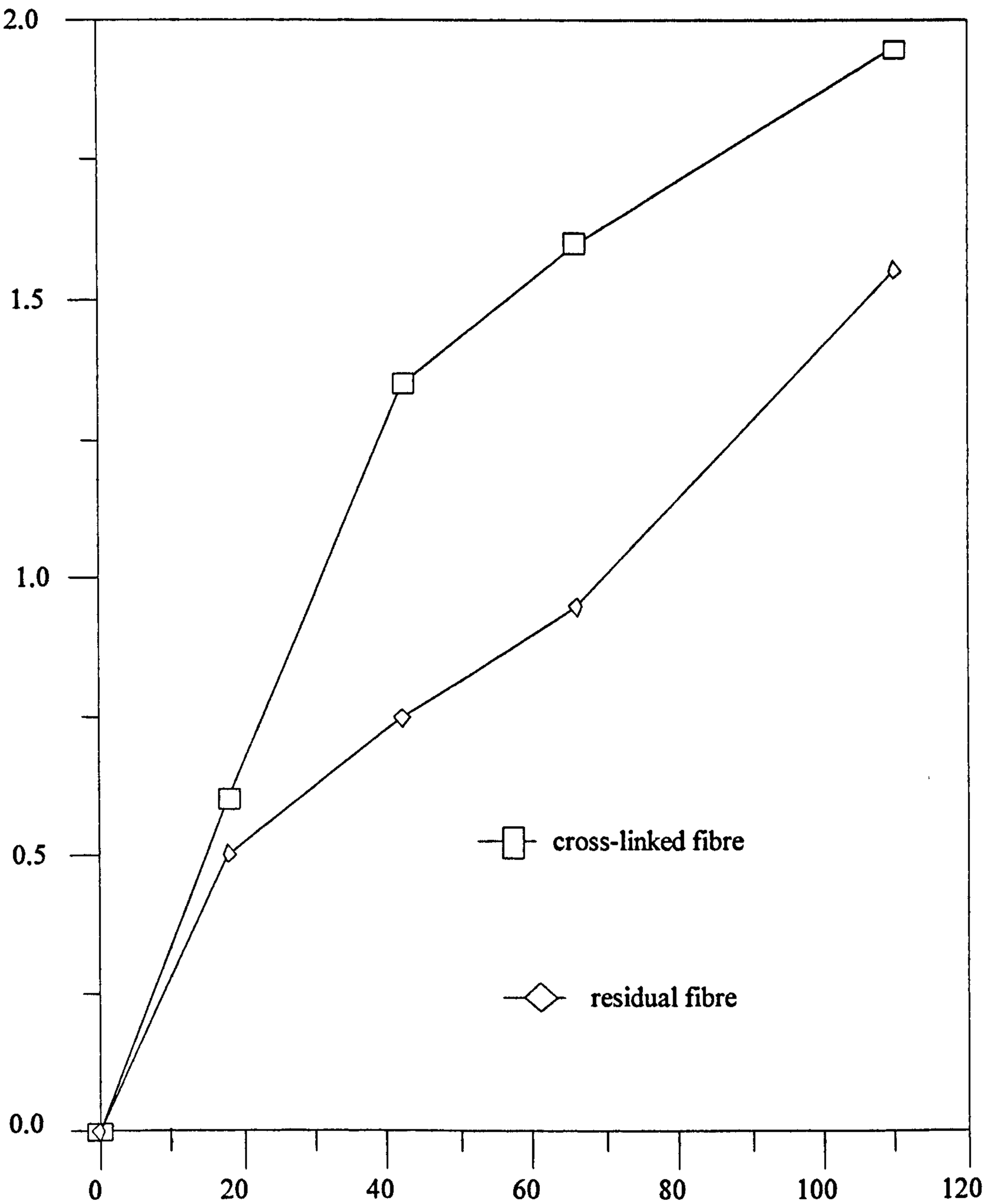

Fig. 5.4 Copper content (%) in the fibre and its residual fibre versus the treatment time with the reagent

The decoloration of the crosslinked PAN hollow fibre was observed when the fibres were treated with 0.1M EDTA solution (see section 2. 5. 2. 4). Table 5.5 shows that the properties of the crosslinked fibre progressively changed during extraction of the copper with EDTA solution at room temperature.

During EDTA extraction, the colour of the fibre changed progressively from yellow brown to light yellow colour. The swelling of the fibre in DMF increased with extraction time, as shown by the ratio of D/d in Table 5.5. After extraction for two weeks, the fibre was again soluble in the usual solvents. This reversible behaviour of the crosslinked PAN fibre after extraction with EDTA indicates that the insolubility of the fibre is not caused by the formation of a conjugated carbon-nitrogen structure. Some kind of structure, formed by the copper ions, existed in the PAN fibre, because there is no evidence to show that EDTA solution would destroy a conjugated carbon-nitrogen structure.

It also can be seen that the copper ions in the crosslinked fibre can be removed by conc. HCl. After 6 h immersion in the HCl, the copper content in the treated fibre had fallen to zero, indicating that the copper in the fibre had been fully extracted by the acid. After this extraction, the fibre was soluble in the usual common solvents for PAN fibres, as shown in Table 5.5.

The crosslinked PAN hollow fibre is not soluble in the usual organic solvents, but it was found that the crosslinked fibre will dissolve in nitric acid. Table 5.6 shows the solubility of the crosslinked fibre extracted by inorganic acids. After the fibre had been immersed in dilute hydrochloric (HCl) solution for 24 h, it was still insoluble in DMF solvent. Some decoloration of the fibre was noted, changing from yellow brown to yellow. The swelling of the fibre in DMF increased after the treatment in dilute HCl for 24 h. However, the crosslinked fibre did dissolve in DMF when a few

Table 5.5 The properties of the crosslinked PAN hollow fibre after extraction by EDTA solution and conc. HCl

Sample	Extraction time (hour)	Copper content (%)	Colour	D/d	Soluble in Solvent*
A	0	1.3	yellow brown	1.19	No
B	EDTA: 6	0.3	yellow	2.25	No
C	24	0.25	yellow	2.75	No
D	168	0.15	yellow	3.02	No
E	336	0.15	yellow	∞	yes
F	conc. HCl 6	Nil	-	-	yes

* Solubility test was carried out in DMF, DMAC, DMSO and NMP solvents.

Table 5.6 Solubility of the crosslinked PAN hollow fibre after treatment with inorganic acids

Sample	Solvent/Temperature	Solubility
Crosslinked PAN hollow fibre	Nitric acid/25°C	Yes
	DMF/25°C+ a drop of HCl	Yes
	DMF/80°C+ a drop of HCl	Yes
Crosslinked PAN hollow fibre extracted with dilute HCl for 24 h	DMF/25°C	No
	DMF/80°C	No

drops of conc. HCl were added to the solvent in which the fibres were immersed. This could be explained by the HCl extracting the copper ions from the crosslinked structure, producing the uncrosslinked structure which then dissolves in DMF.

Fig. 5.5 shows the copper content in the fibre after the EDTA extraction. In the first 6 h treatment, the desorption of copper from the treated hollow fibre by EDTA is fast, though the later process becomes very slow. Even after two weeks treatment, copper ions can still be detected. The whole process of desorption of copper ions from the crosslinked PAN fibre is a fairly slow process in comparison to the desorption of copper ions from chitosan fibres by EDTA[151].

According to the above results, it is believed that the insolubility of the fibre is caused by a crosslinking structure, in which the copper ions complex with the -CN functional groups of the polymer. It is also believed that the coloration of the PAN fibres during the cuprammonium hydroxide treatment might involve a reaction initiated by the inorganic base $\{Cu(NH_3)_4\}(OH)_2$. Overall, therefore there may be two different reactions occurring.

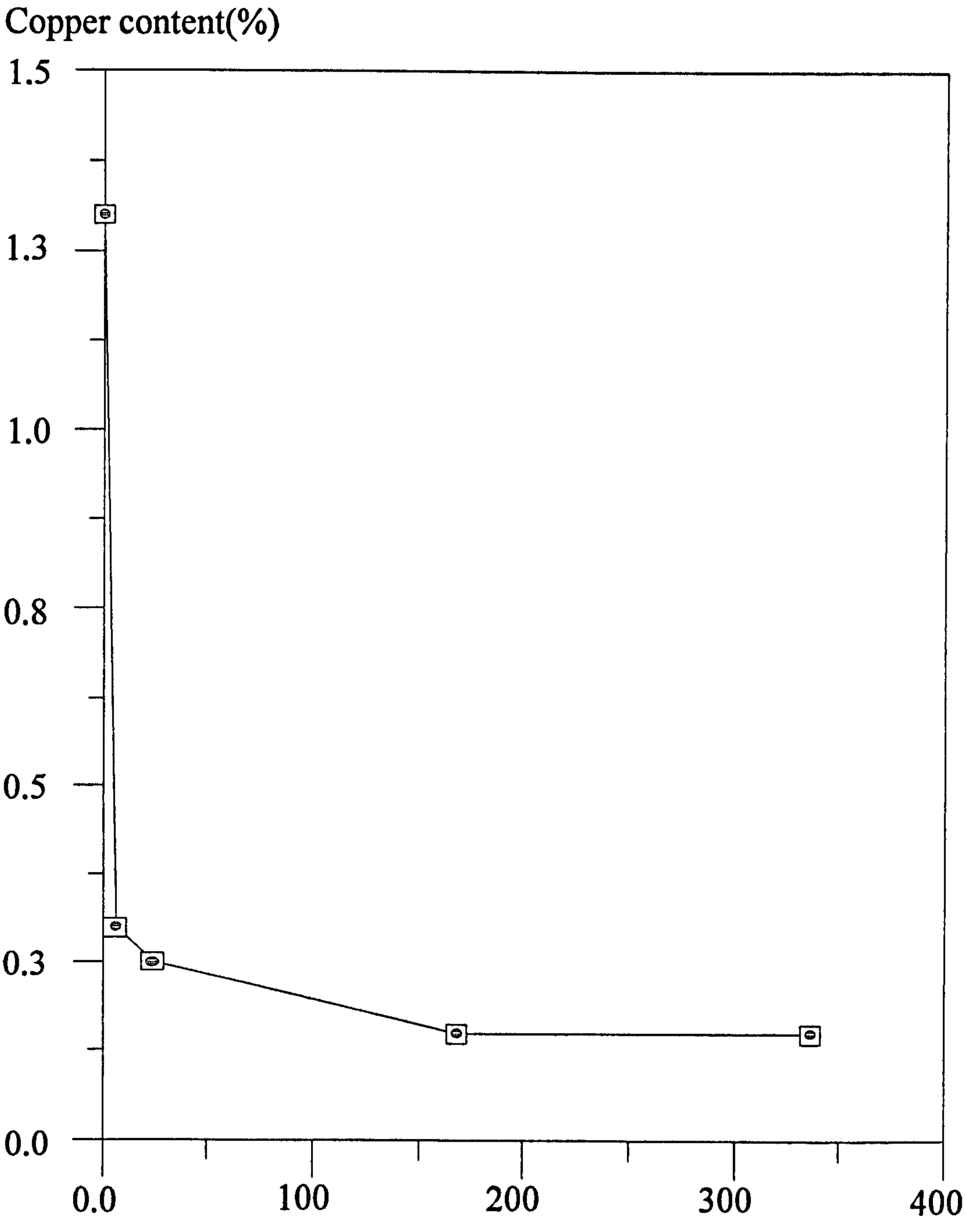

Fig. 5.5 Copper content (%) in the crosslinked fibre after extraction with EDTA solution

5. 3. 2 Thermogravimetric and mechanical properties of the crosslinked fibres

Fig. 5.6 shows the TGA traces of the crosslinked and the original PAN hollow fibres, together with that of Courtelle fibre. From the TGA traces, there are two main stages of degradation. In the crosslinked PAN hollow fibres, the first stage begins earlier than in the original fibre at about 290 °C, 20 °C earlier than with the original fibres. The crosslinked fibre loses less weight in the first stage (as shown by the derivative TGA trace) and also in the second step. Overall, the crosslinked copper containing fibre loses about 10% less weight on pyrolysis to 700 °C compared to the original hollow fibre. Such an effect is to be expected if the cuprammonium hydroxide caused crosslinking between the -CN groups on adjacent PAN chains. The TGA trace for Courtelle fibre is given for comparison and shows some small difference from the hollow fibre, spun from redissolved Courtelle. It must be noted that the hollow fibre might well have contained a small amount of copper (<0.2%) left over from the spinning and this might account for the difference in the TGA.

The changes in the characteristics of the thermal degradation of the PAN hollow fibre confirm that there must be some difference in structure in the fibres after treatment with the cuprammonium hydroxide solution. This structure is proposed as a crosslinked structure so that the lower weight-loss of this crosslinked PAN fibre occurs because this structure is more thermally stable. However, it is interesting that the onset of weight-loss is a little earlier in the crosslinked fibre.

Table 5.7 shows that the maximum rate of weight-loss decreases with increasing copper content in the fibres for both steps of the thermal breakdown. This indicates again that the crosslinked structure resists the thermal degradation process. The residual weight of the fibre at 700°C also increases with the increase in copper

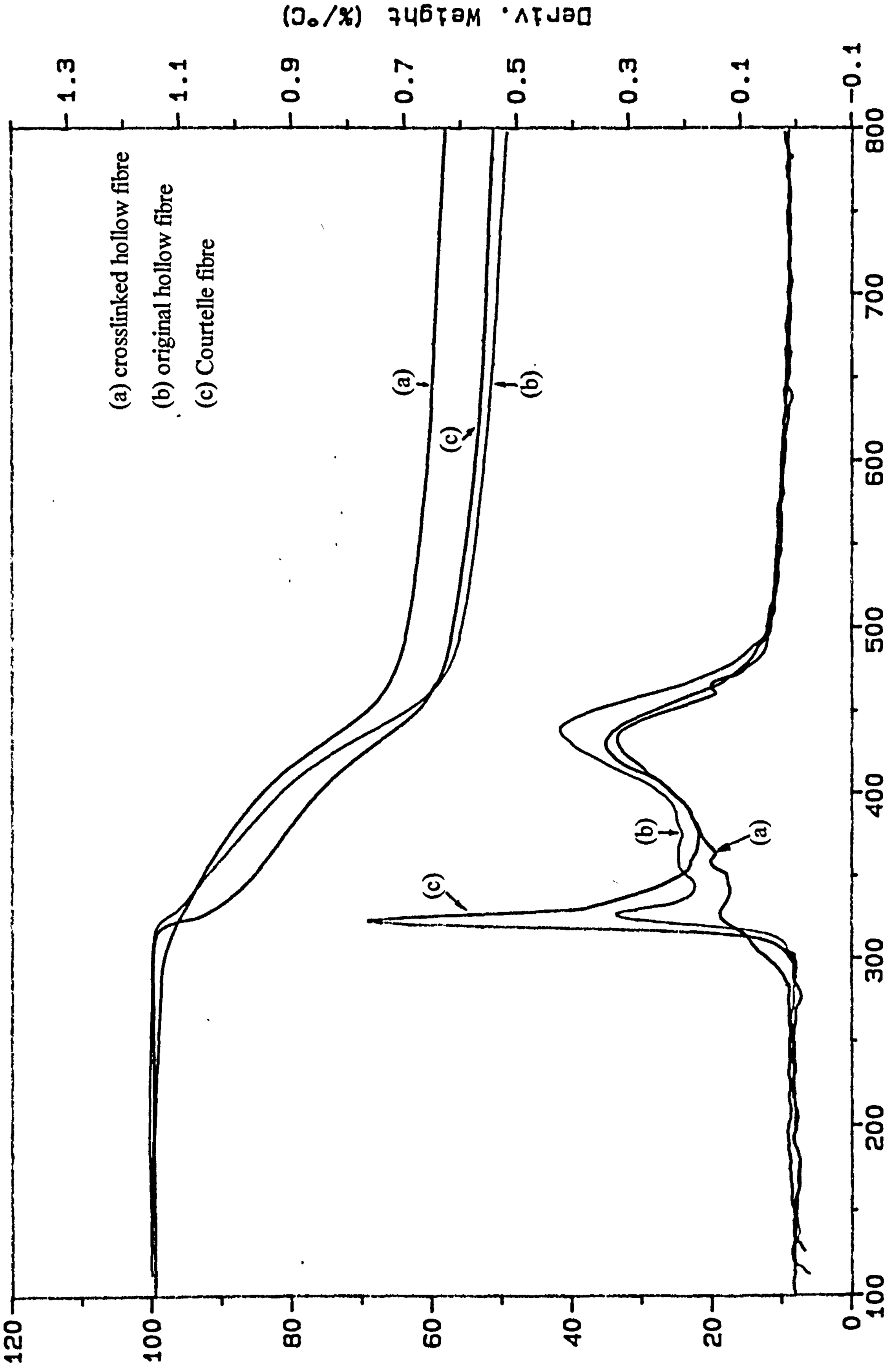

Fig. 5.6 TGA traces of the original and crosslinked hollow fibres

Table 5.7 Thermogravimetric analysis (TGA) of PAN hollow fibre

Sample	Copper content (%)	Onset temp. for weight-loss at first stage (°C)	Max. rate of weight-loss at the first stage (%/°C)	Max. rate of weight-loss at the second stage (%/°C)	Residual weight at 700°C (%)
A	0	314.7	0.314	0.423	50.7
B	0.6	292.0	0.167	0.391	55.1
C	1.35	289.2	0.135	0.341	59.4
D	1.60	286.3	0.143	0.361	55.7
E	1.95	285.3	0.131	0.344	57.6

content in the fibre. This result is expected. Fig. 5.7 and Fig. 5.8 illustrate the data. From these Figs., it seems that there is a "turning point" at the cross-linking treatment time of 42 h (sample C), or 1.35% Cu content. Above this point, the changes brought about by increasing the copper content from 1.35 to 1.6% now produce reverse effects to those observed below 1.35% Cu. However, a further increase from 1.6% to 1.95% Cu is followed by a decrease in the rates of degradation and an increase in the residual weight at 700 °C. It is not possible to decide if these later results reflect errors in the measurements or whether there is another phenomenon occurring; it is thought more likely to be error at this stage.

Table 5.7 also shows the effect of varying the copper content on the weight-loss onset temperature which decreases with increasing copper content in the fibres. This indicates that the more copper in the fibre, the earlier the onset of thermal degradation. The first stage of thermal degradation in the crosslinked PAN fibre might be catalysed by the copper ions in the fibres. Fig. 5.9 shows the DSC traces of

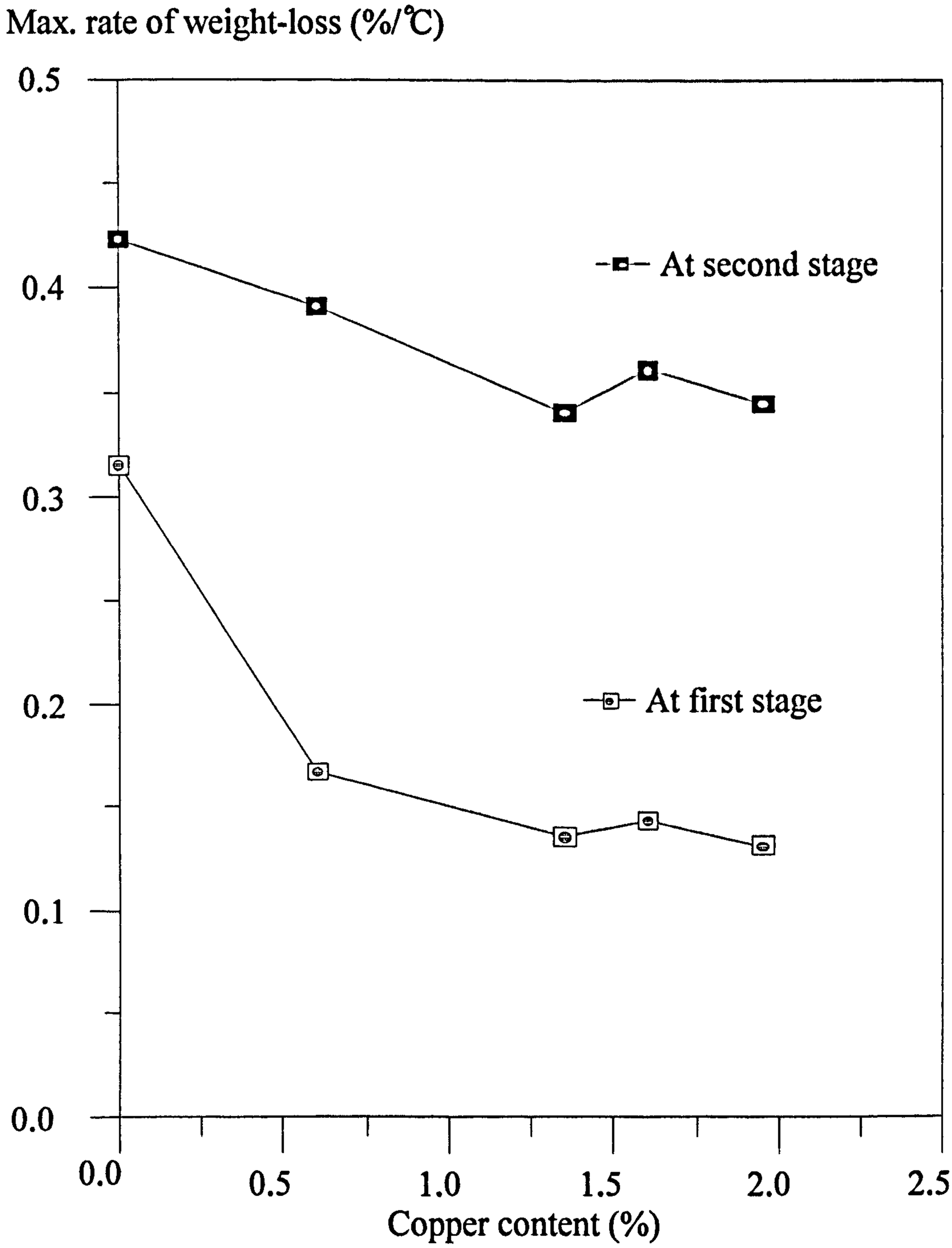

Fig. 5.7 The maxium rate of weight-loss versus the copper content in the hollow fibre

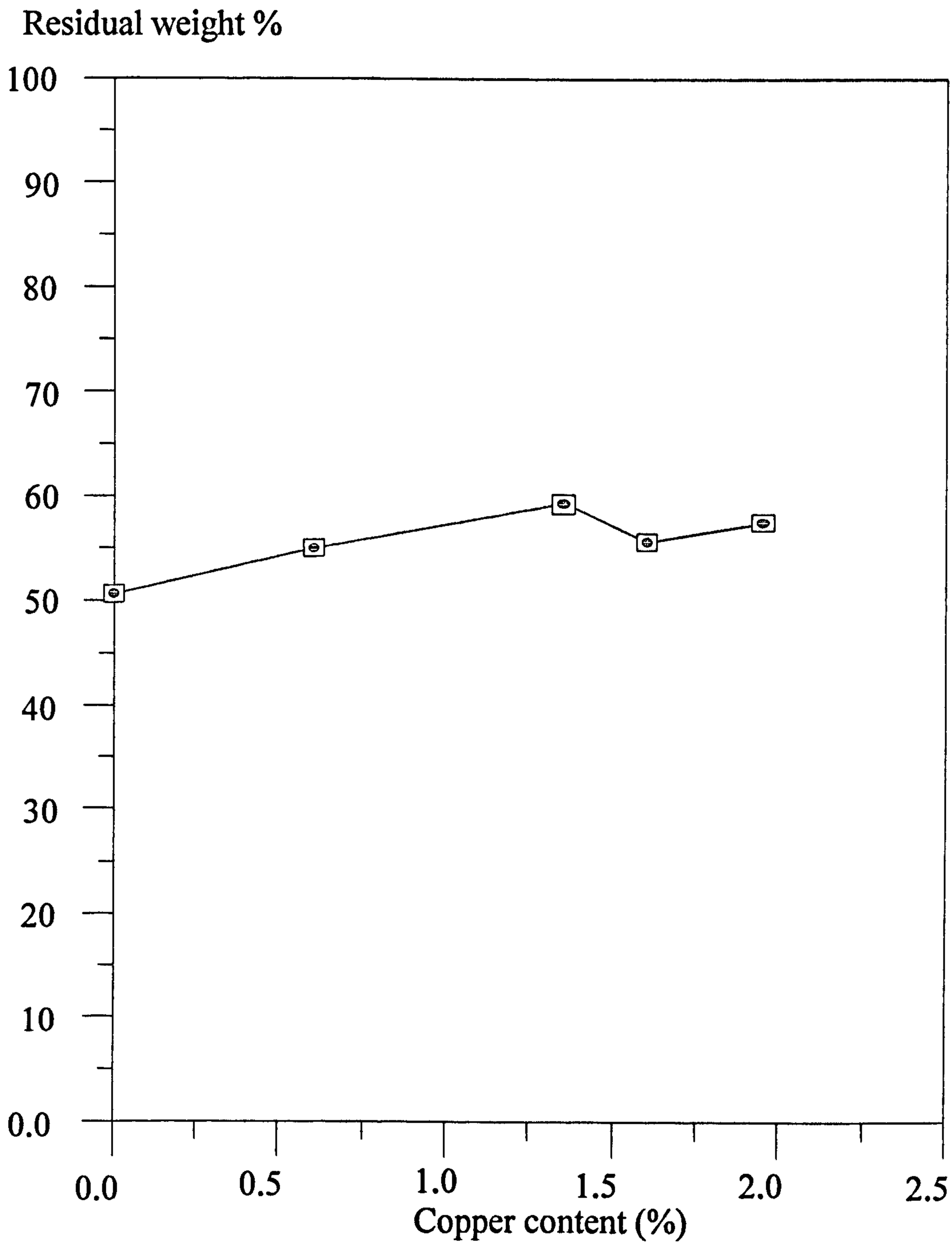

Fig. 5.8 The residual weight-loss (%) versus the copper content in the hollow fibre

the PAN hollow fibre and the crosslinked PAN hollow fibre. It shows very large changes in the characteristics of the exothermic peak. For the crosslinked PAN hollow fibre, the cyclization reaction of the fibre takes place at a lower temperature and its exothermic peak temperature is about 15 °C lower than that of the original PAN hollow fibre. The exothermic peak is reduced and broadened for the crosslinked PAN fibre. Similar results were also obtained by Mathur et al[150], when CuCl was incorporated into the PAN structure; it enhanced the rate of cyclization by 20%. Therefore, it was claimed that CuCl acts as a strong initiator of the cyclization reaction of PAN fibres. From this view point, the results obtained in the present study indicate that the cupric ions present in the PAN hollow fibre may also initiate the cyclization reaction of PAN fibre.

Table 5.8 shows the results of measuring the crosslinked PAN hollow fibre tensile and elongation properties. Fig. 5.10 and Fig. 5.11 show the relationship between the copper content in the crosslinked fibre and the fibre tensile strength and elongation properties. It is clear that as the copper content in the crosslinked fibre is increased, the hollow fibre tensile strength is increased, and at the same time, the elongation at break is decreased. This result is in agreement with the results observed in studies of a similar crosslinked polymer[152]. In the crosslinked polymer, the chain displacement of the polymer is restricted by the crosslinking, so that the elongation is decreased with increasing copper content. At the same time, the crosslinking produces a 'net-like' structure in the polymer chains, so that the tensile strength of the hollow fibre is increased.

The flexibility of the crosslinked PAN hollow fibre decreases with increasing copper content in the fibre. After treatment with the reagent for 66 h (copper content 1.6%), the crosslinked PAN hollow fibre became brittle, so that it broke easily on handling.

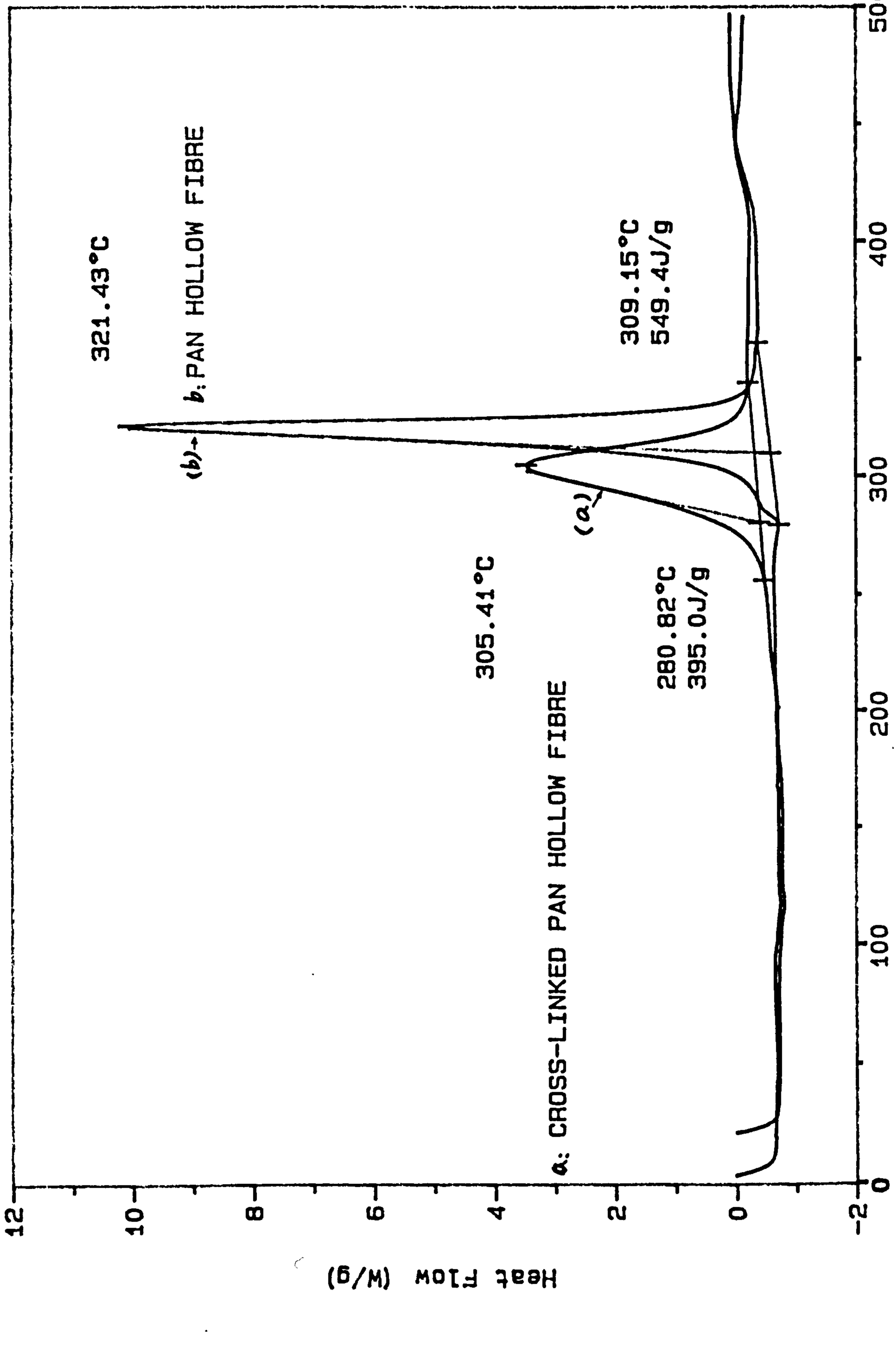

Fig. 5.9 DSC traces of the original and crosslinked hollow fibre treated for 18 h.

Table 5.8 Mechanical properties of crosslinked PAN hollow fibre

Sample	Copper content (%)	Tensile strength (g)(s. d)	Elongation (%)(s. d)
A	0	425.9(12.9)	9.98(1.94)
B	0.6	464.3(21.8)	8.88(1.30)
C	1.35	477.5(21.7)	7.74(1.43)
D	1.60	481.5(18.2)	7.19(1.37)
E	1.95	494.8(15.4)	5.95(0.41)

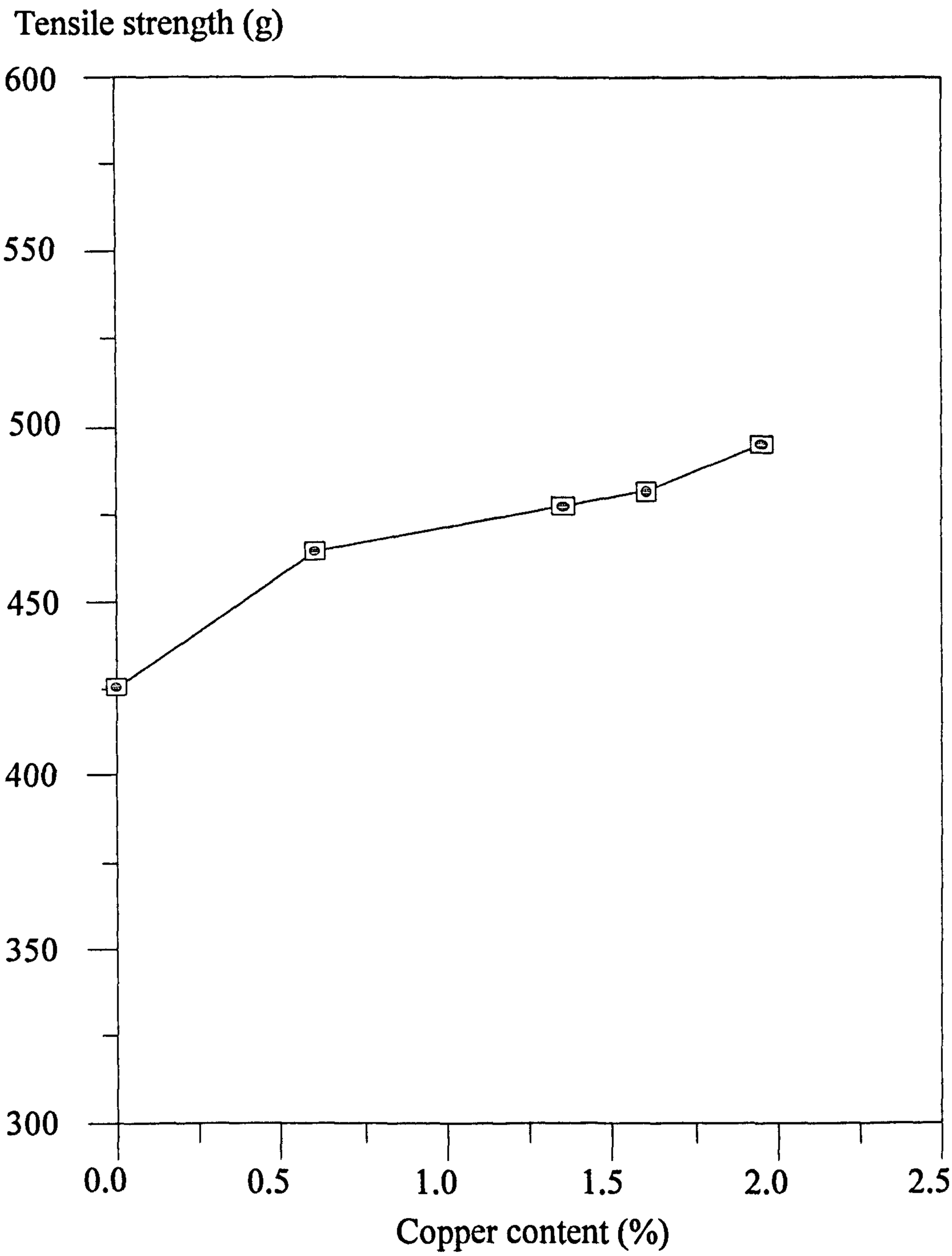

Fig. 5.10 Tensile strength of the hollow fibre versus the copper content in the fibre

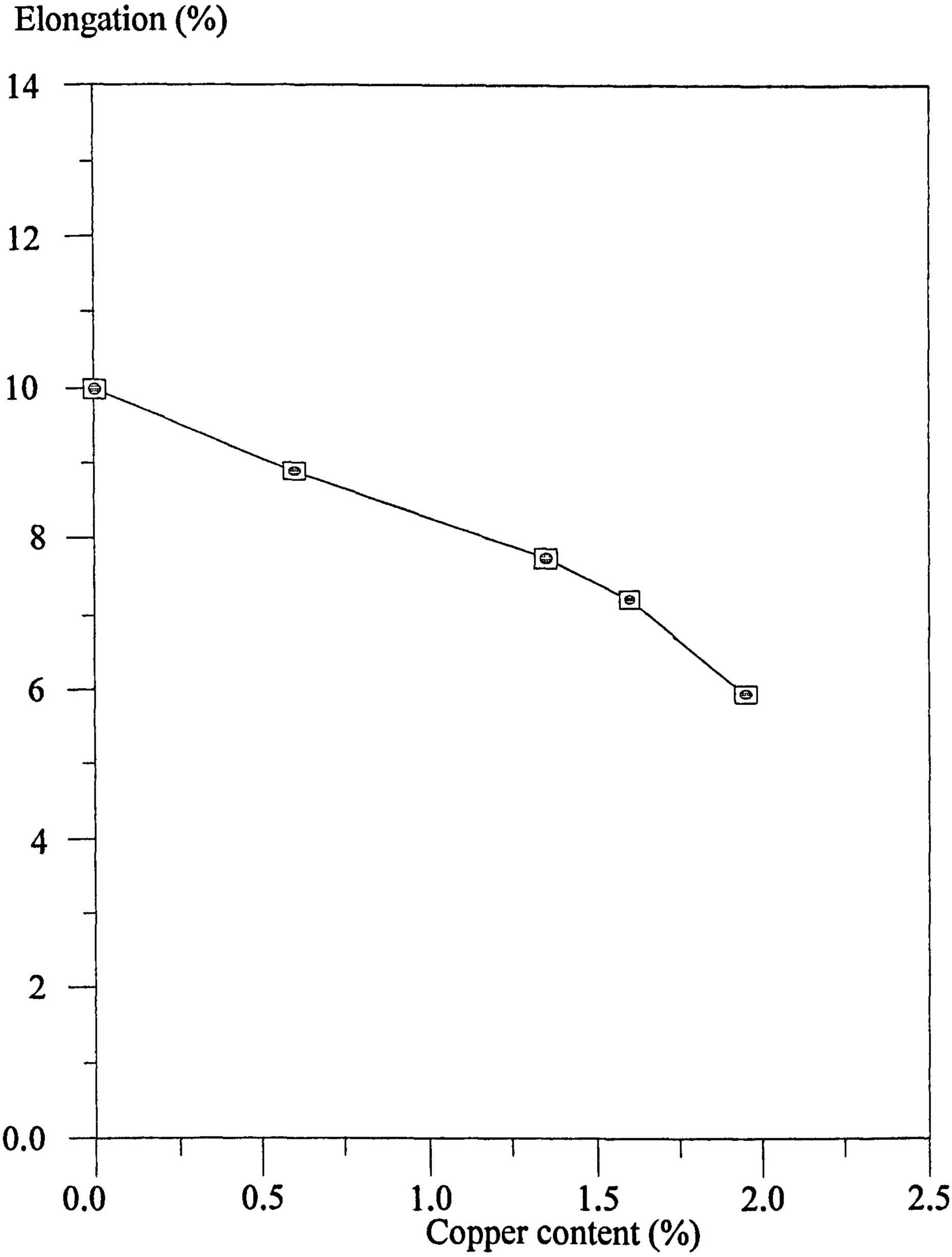

Fig. 5.11 Elongation of the hollow fibre versus the copper content in the fibre

5. 3. 3 Complexes involving PAN

PAN can be dissolved in concentrated aqueous solutions of $ZnCl_2$ (40 ~ 60%) and fibres can be spun from such solutions[153]. The interaction of the nitrile lone pair electrons with Zn^{2+} is associated with a shift of about 40 ~ 60 cm^{-1} in IR band[154]. Evidently, this interaction suffices to reduce the dipole-dipole interaction of the -CN groups of the polymer, thus permitting dissolution.

The complex formation of Cu(I) ions with nitrile groups had found an interesting application for dyeing acrylic fibres with anionic dyestuffs. The Cu(I) ion is readily absorbed by PAN and its copolymers, which then acquire almost unlimited affinity for many anionic dyes, permitting dyeing to very deep shades, including black[121, 155]. The mechanism is claimed to be due to the metal ions coordinatively bonding to the nitrile groups of the polymer. The original inorganic anion is electrostatically bound to the copper-nitrile complex, and is then gradually displaced by the slower diffusing, but more tightly bound dyestuff anion[154].

PAN fibre can be crosslinked with $[Cu(NH_3)_4](OH)_2$ as found in this study. For the complex cations of cupric copper, such as the amine type $[Cu(NH_3)_n]X_2$, the number of molecules of ammonia co-ordinated to the copper ions is normally 4, but it may be 6 as in $[Cu(NH_3)_6]Br_2$ and $[Cu(NH_3)_6]I_2$, or 2 as in pale blue $[Cu(NH_3)_2](NO_2)_2$, made by warming violet-blue $[Cu(NH_3)_4](NO_2)_2$. In these amines, the nitrogen atoms are strongly bonded to the copper. In the case of $[Cu(NH_3)_4](OH)_2$, which is a strong base, the ammonia in the complex is less firmly bonded to copper. The complex is less stable, and the number of molecules of ammonia co-ordinated to the copper is often reduced from 4 to 2[156].

When the PAN fibres were immersed in the $\{Cu(NH_3)_4\}(OH)_2$ solution, a significant coloration of the fibres was observed over a period of hours. By contrast, when the

PAN hollow fibres were immersed in 50% aqueous sodium hydroxide solution at room temperature, no significant coloration was observed within five hours, when it might have been expected. This indicates that the coloration of PAN fibre is more rapidly initiated by cuprammonium hydroxide than by sodium hydroxide solution at room temperature. This may be interpreted as being due to the fact that the coloration of the fibre is initiated by the copper ammine complex at room temperature. Cu(I) and Cu(II) ions are able to form complexes with a wide variety of ligands, and the formation and dissociation of their complexes can occur very rapidly[157].

It is well known that when bases are added to PAN solutions, coloration occurs similar to that observed during thermal stabilization of PAN fibres[158]. In 1953, McCartney postulated that the colour was due to cyclization of the nitrile groups and this theory has become popular[158]. The mechanism of cyclization by nucleophilic attack on the nitrile carbon is as follows, Scheme 5.1:

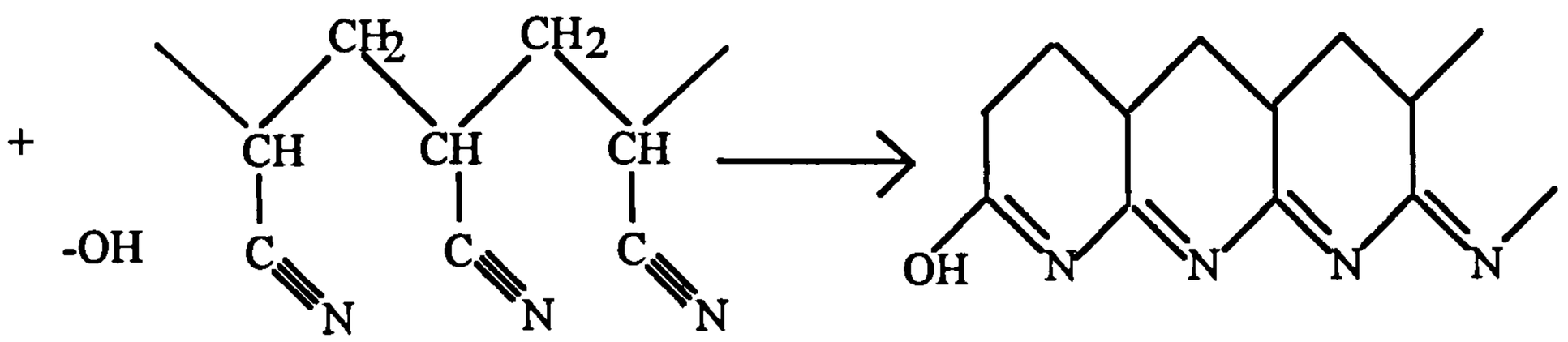

Scheme 5.1 The mechanism for initiation of cyclization by base[158]

La Combe[159] had observed that relatively small amounts of base bring about a relatively large development of colour in PAN fibres. He had proposed that a base-catalysed partial hydrolysis of PAN leads to a coloured product. The following reaction sequence has been proposed to explained the colour formation:

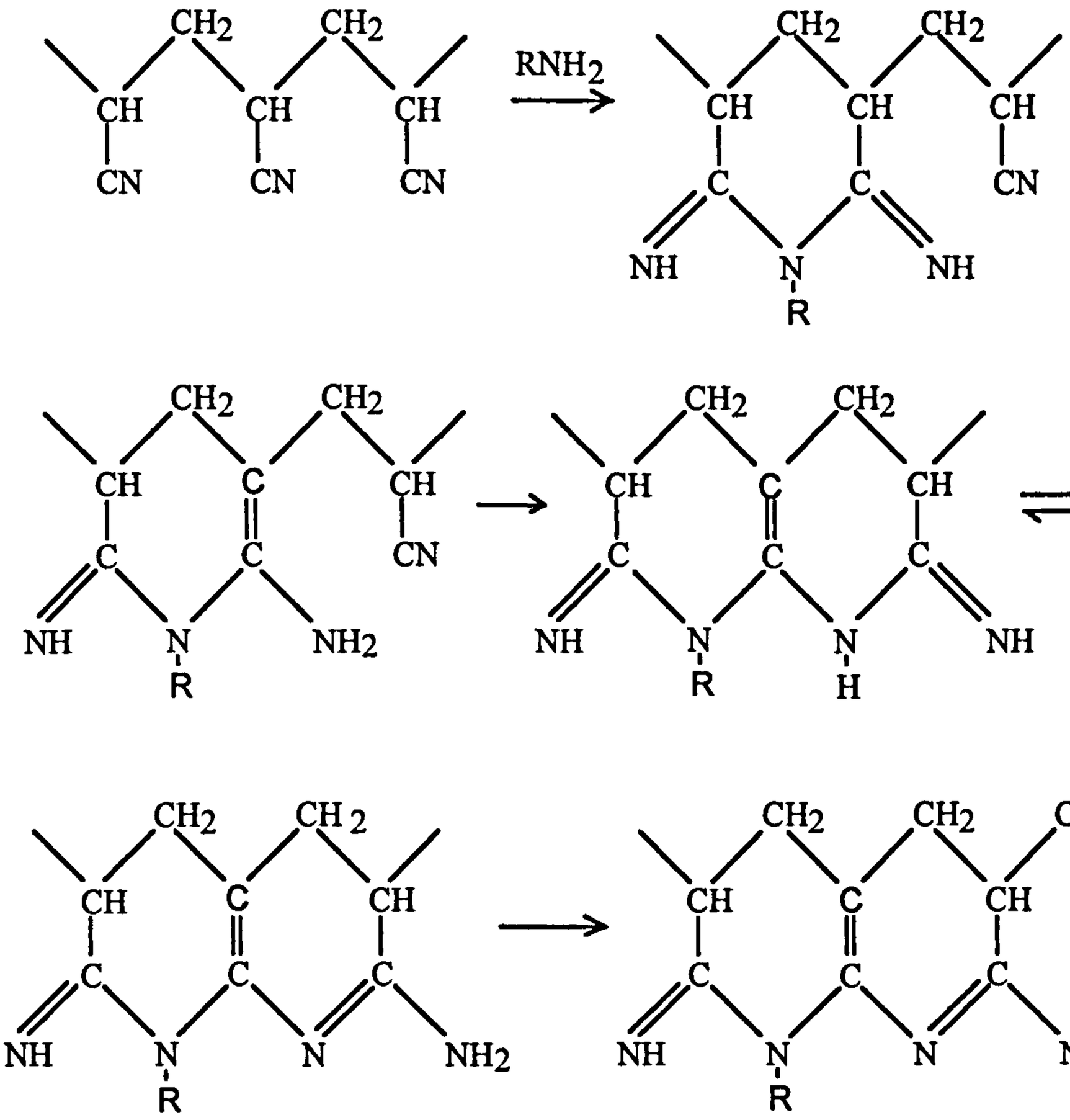

Scheme 5.2 The mechanism of dehydrogenation and cyclization by base and ammonia[159]

From the above considerations, it was claimed that small amounts of base lead to highly coloured structures, the conjugated carbon to nitrogen double bonds being responsible for the strong absorption at visible wavelengths.

Contrary to the above suggestions for the coloration of PAN fibres, Bashire et al[160] have found no evidence for the cyclization reaction which leads to conjugated structures even in red-black PAN polymer solutions after re-examining the effect of

base. They believed that some unidentified chromophore was present in very low concentrations but with a very intense absorption.

An examination of the crosslinked PAN fibres obtained in the present study was carried out using IR spectra. However, the IR results failed to show any significant changes of -CN absorption bands in the crosslinked PAN fibres. Figs 5.12 ~ 5.14 show the IR spectra of the original and the crosslinked PAN fibres, which had been treated with cuprammonium hydroxide for 15 days for Dralon and Courtelle, and 18 h for PAN hollow fibre. In these spectra, there are no significant differences between the crosslinked and the original fibres.

After more detailed analysis of the spectra, it was found that the absorbance ratio of A_{CN} at 2243 cm^{-1} to A_{CH2} at 1450 cm^{-1} increased after the crosslinking process. As shown in Table 5.9, the ratio A_{CN}/A_{CH2} increases with increasing time of crosslinking. When the crosslinked fibre was extracted with EDTA solution, the IR spectrum showed that the ratio A_{CN}/A_{CH2} decreased towards the original value. These processes imply that the -CN group absorbance increases or the $-CH_2$ absorbance at 1450 cm^{-1} decreases after the crosslinking treatment. This results seems to be unusual. If the crosslinking structure is formed by complexing of the $[Cu(NH_3)_4]^{2+}$ or $[Cu(NH_3)_2]^{2+}$ with the nitrile groups, it would be expected to affect the strength of the -C≡N bond because the strength of the -C≡N bond depends upon the electron distribution between C and N. Such a change in strength may be expected to give a shift to the -CN bond in the complexed form, but no such new peak was observed. The absorbance A_{CN} at 2243 cm^{-1} would be expected to decrease if the fibre were crosslinked via -CN groups and copper ions during the crosslinking treatment. The band from the -CN groups at 2243 cm^{-1} has not been found to shift, whilst, on the contrary, it is found that the absorbance ratio of A_{CN}/A_{CH2} is increased. This phenomenon must be related to the crosslinking process even though the mechanism is still not clear at this stage.

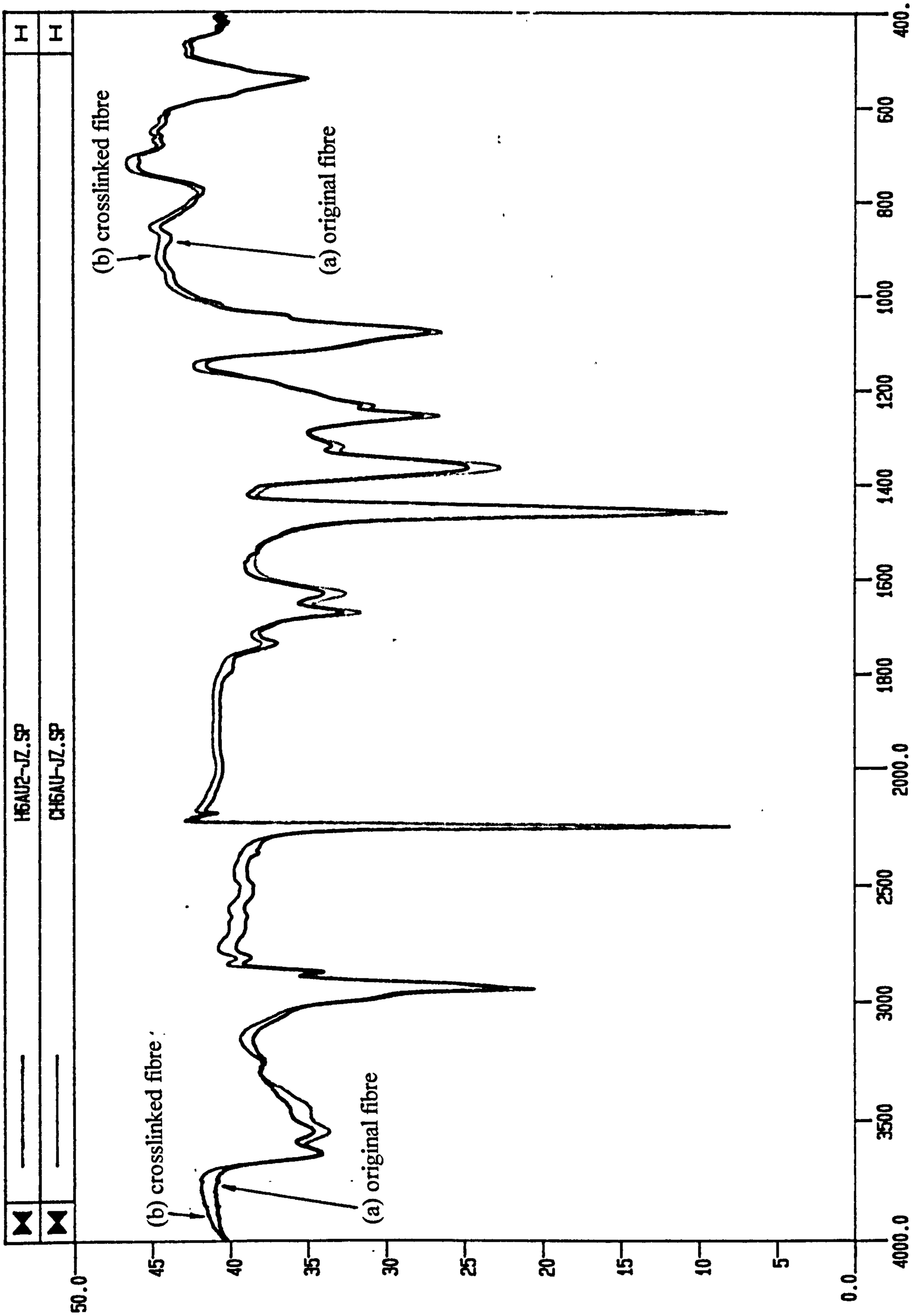

Fig. 5.12 FTIR spectra of Dralon (a) and its crosslinked fibre (b) treated for 15 days

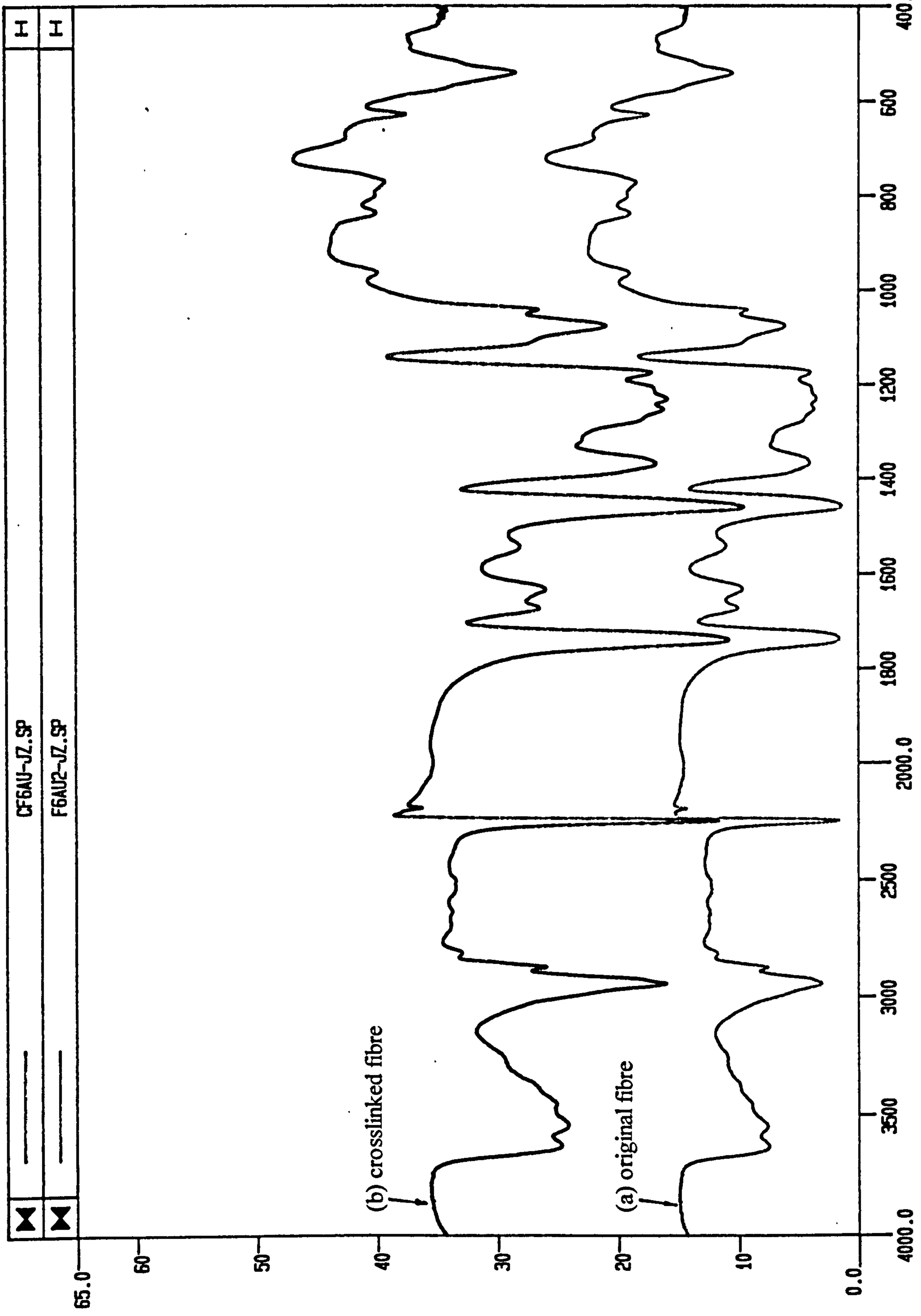

Fig. 5.13 FTIR spectra of Courtelle (a) and its crosslinked fibre (b) treated for 15

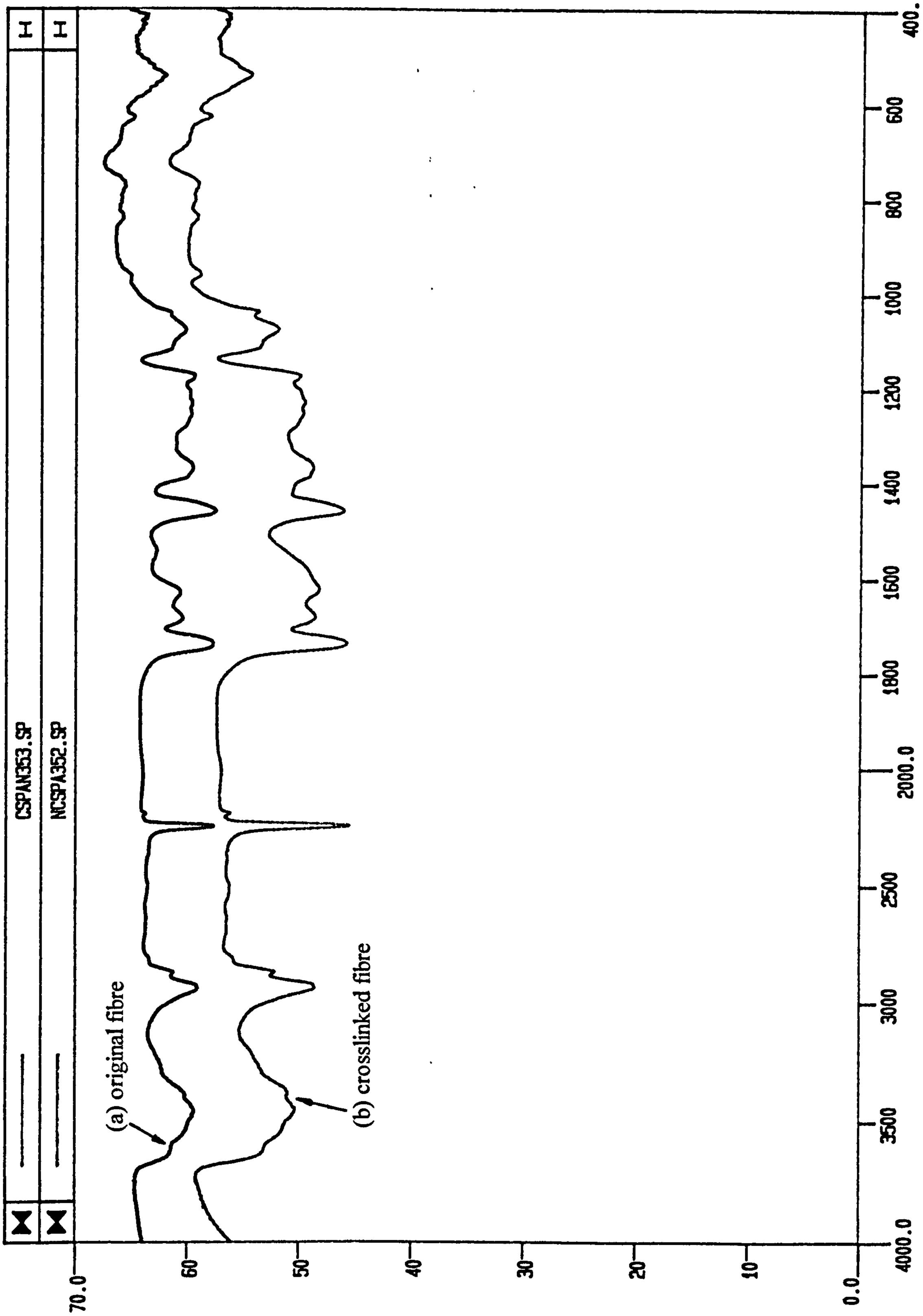

Fig. 5.14 FTIR spectra of PAN hollow fibre (a) and its crosslinked fibre (b) treated for 18 h.

Table 5.9 Effect of crosslinking on the absorbance ratio A_{CN}/A_{CH2} for various fibres

Sample	State/treatment	A_{CN}/A_{CH2} at 1450 cm^{-1}
Dralon(homopolymer)	Dralon	1.07
	Crosslinked Dralon treated for 15 days	1.08
Courtelle(co-polymer)	Courtelle	0.92
	Crosslinked Courtelle treated for 15 days	0.96
PAN hollow fibre-1#	Original HF	1.25
	Crosslinked HF treated for:	
	18 h	1.89
	42 h	1.96
	66 h	2.06
	110 h	2.58
PAN hollow fibre-2#	Crosslinked HF	1.56
	After 2 weeks EDTA extraction	1.34

Pyrolysis of the crosslinked and the original PAN hollow fibre samples at 200°C and 300°C were carried out under a nitrogen atmosphere in order to compare the results with those obtained by Wu et al[161]. According to their work, samples were prepared from solution-cast PAN films deposited on thin films of copper, and pyrolysis of these PAN/Cu samples at 200 °C for different times gave two new bands appearing at 2334 cm^{-1} and 2191 cm^{-1}. The 2334 cm^{-1} band was assigned to end-on co-ordinated nitriles in the pyrolyzed PAN films on copper; the 2191 cm^{-1} band indicated a side-on co-ordinated nitrile, according to their interpretation, as illustrated in Scheme 5.3:

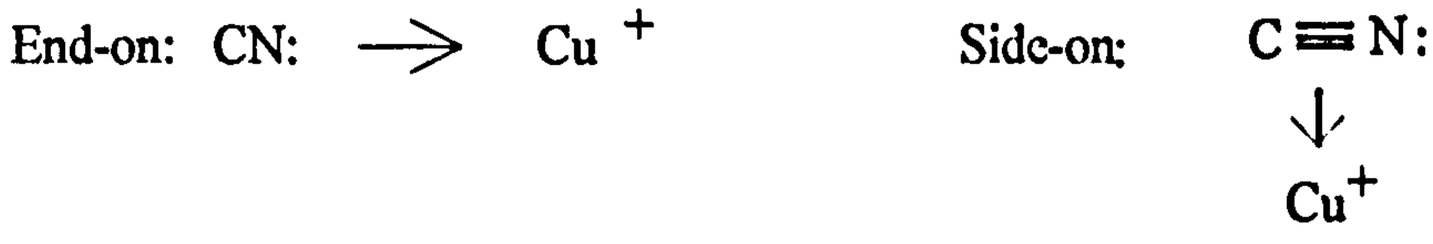

Scheme 5.3 The illustration of end-on and side-on co-ordinated nitrile[161]

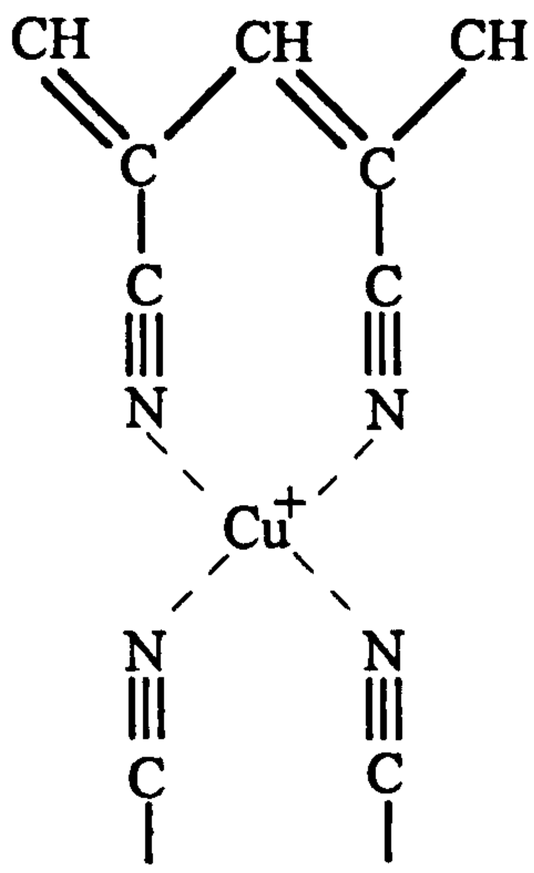

Scheme 5.4 Proposed chemical structure of PAN after pyrolysis at 200°C[161]

The chemical structure of this pyrolyzed PAN on copper, as proposed by Wu et al, is shown in Scheme 5.4, and is a simple model that does not take into account the possibilities of having both end-on and side-on co-ordinated nitrile groups in PAN simultaneously.

The results obtained in this study showed that there were no new bands in the IR spectra at 2334 cm^{-1} and 2191 cm^{-1} for the crosslinked fibre after pyrolysis at 200°C for 5 h and 300°C for 2 h, as shown in Fig. 5.15 and Fig. 5.16. So, there is no evidence for the structures proposed by Wu et al. However, there are some changes in the spectrum of pyrolysed crosslinked PAN fibre in comparison to the original

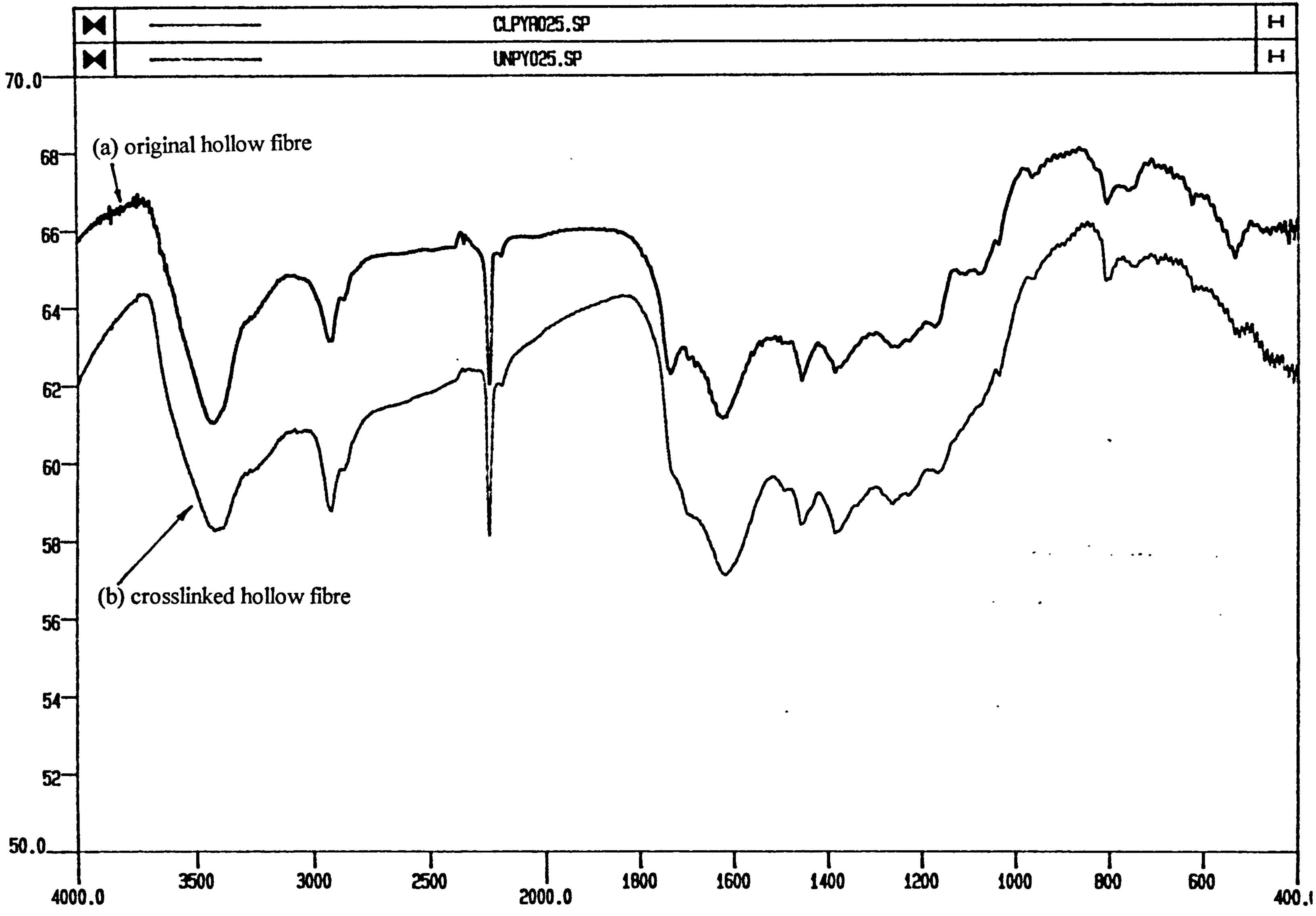

Fig. 5.15 FTIR spectra of the PAN hollow fibres pyrolysed at 200 °C for 5 h.
(a) original hollow fibre; (b) crosslinked hollow fibre treated for 18 h.

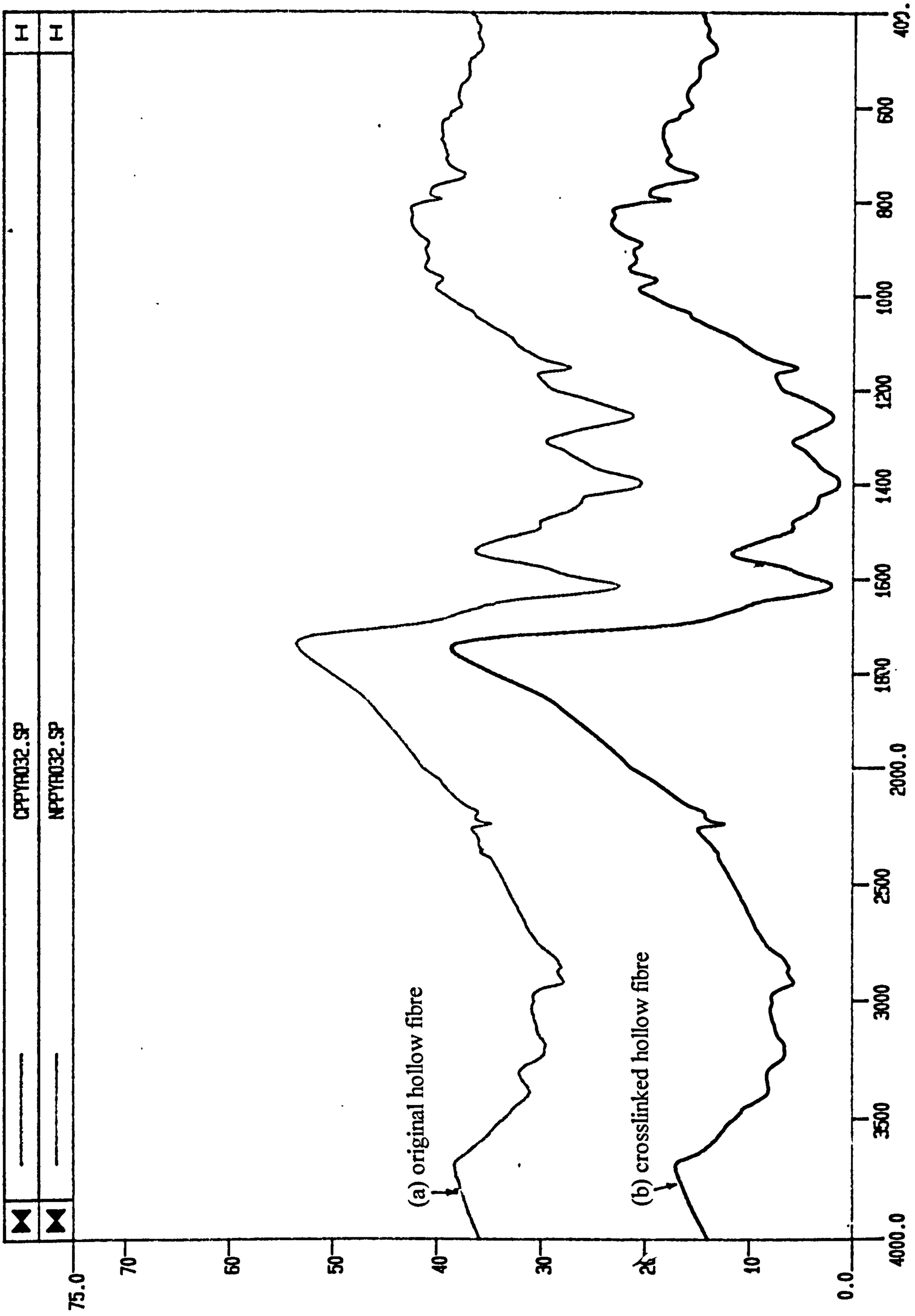

Fig. 5.16 FTIR spectra of the PAN hollow fibres pyrolysed at 300 °C for 2 h. (a) original hollow fibre; (b) crosslinked hollow fibre treated for 18 h.

PAN fibres after pyrolysis. The overall intensity of the absorption in the range of 1200 ~ 1800 cm^{-1} for the crosslinked fibre is slightly increased and the peaks become broadened. These results are believed to support the result that the copper present in the PAN fibre catalysed the cyclization reaction, similar to the results observed when CuCl was present in the PAN structure during pyrolysis[150].

El-Sonbati and Diab[162] reported that in the radical polymerisation of acrylonitrile in the presence of metal halides, the IR spectrum of the PAN-CuBr complex formed showed no change in the -CN absorption band. However, in the PAN-$CuBr_2$ complex, the -CN absorption band disappeared from its normal position (2243 cm^{-1}) and was replaced by two new bands which appeared at 3430 cm^{-1} and 3530 cm^{-1}. It seems that the PAN-$CuBr_2$ complex was reduced to form a PAN-CuBr complex during the radical polymerisation. The mechanism suggested by El-Sonbati and Diab[162] is shown in Scheme 5.5.

From the above results described in the literature[161, 162], it seems that the cuprous ion is quite likely to be complexed with -CN groups in PAN fibres. However, the results of the work done in the present study give no evidence to show that cupric ions were reduced to cuprous ions during the crosslinking procedure. The insolubility of PAN fibres after treatment with the reagent is interpreted as due to crosslinked structures existing in the fibres. The crosslinks seem to be formed by the $[Cu(NH_3)_4]^{2+}$ cations, but there is no infrared evidence to suggest the $[Cu(NH_3)_4]^{2+}$ cations complex with the -CN groups in the PAN fibre in this study, apart from the increase in A_{CN}/A_{CH2} described earlier. Of course, to produce a crosslinked structure may only require the complexing of a small fraction of the nitrile groups with $[Cu(NH_3)_4]^{2+}$; hence it may not be easy to detect such a small change in -CN groups by IR. Further investigation is necessary to find the exact mechanism of the coloration and insolubility. At this stage, it is supposed that the $[Cu(NH_3)_4]^{2+}$ cations

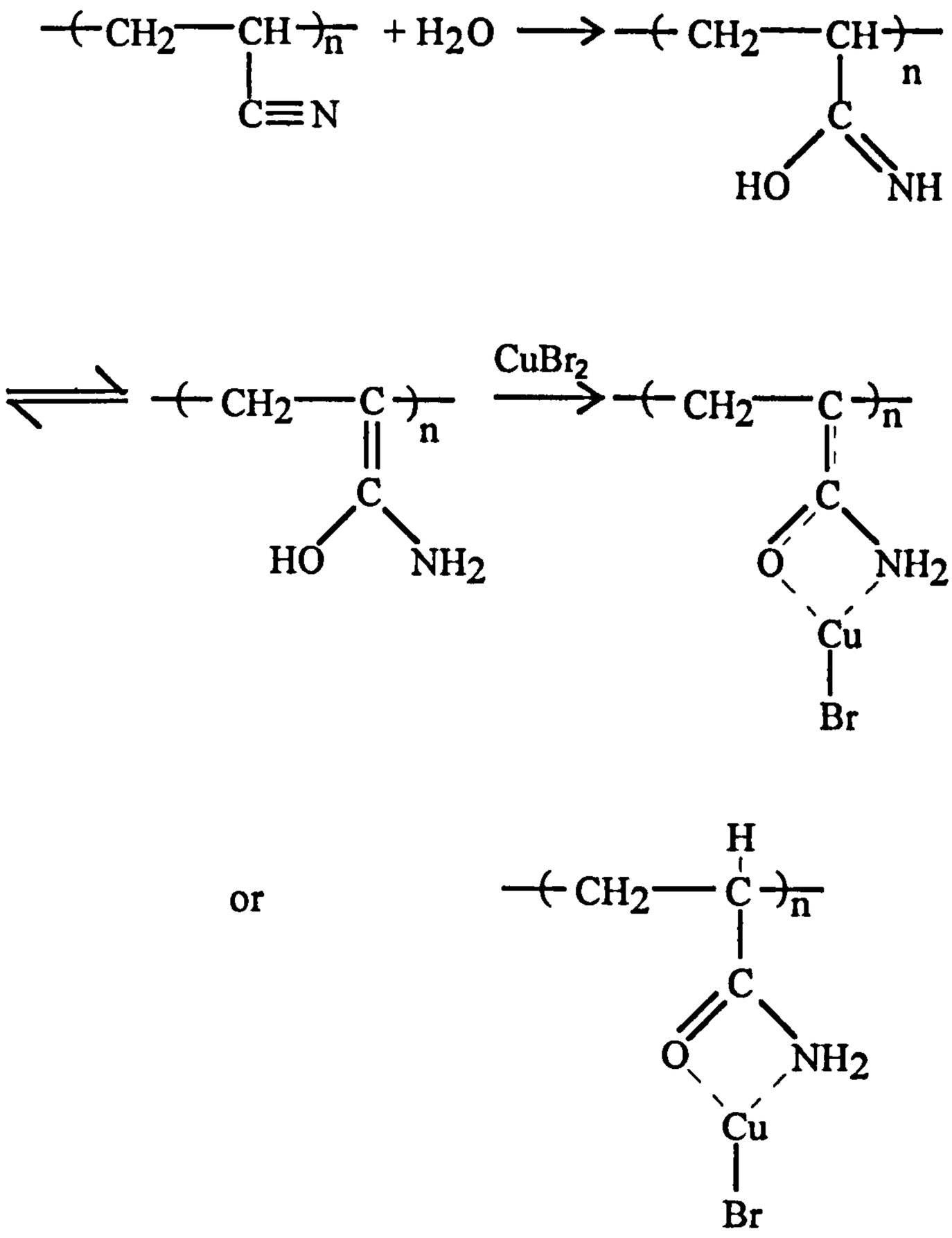

Scheme 5.5 The mechanism of PAN-CuBr complex formation during radical polymerisation[162]

interact with the -CN groups, forming crosslinked structures. Due to the highly polar nature of the nitrile groups, there is initially a partial negative charge on the nitrogen atom and this leads to the co-ordination with the Cu^{2+} ion. It is also possible that the $\{Cu(NH_3)_4\}(OH)_2$ might form $\{Cu(NH_3)_2\}(OH)_2$ to allow complex formation with the -CN groups of the PAN fibres. Two proposed crosslinking structures caused by the cuprammonium hydroxide solution are shown in Scheme 5.6.

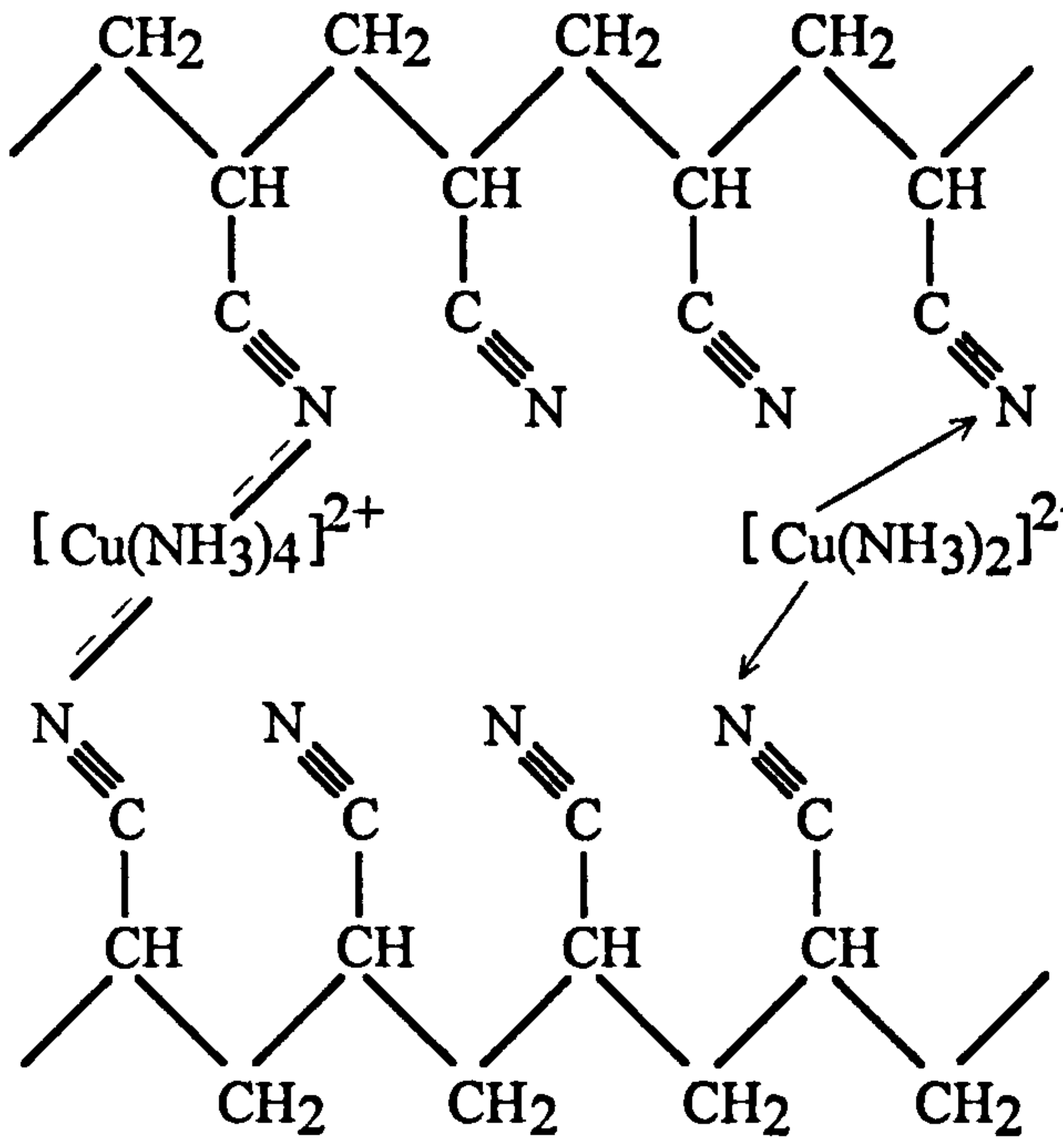

Scheme 5.6 Proposed crosslinking structures involving cuprammonium hydroxide

At this moment, it is not possible to rule out other structures which may form in the fibre after treatment with the reagent. These structures could also make a contribution to the coloration of the fibres. Experimental evidence has shown that partial decoloration of the crosslinked fibres takes place and the fibres recover their solubility in the usual organic solvents after the fibres are extracted with EDTA solution. This indicates that the crosslinking structure affects the coloration of the fibres, and that the $[Cu(NH_3)_2]^{2+}$ and $[Cu(NH_3)_4]^{2+}$ cations complex with EDTA more strongly than they do with -CN groups.

CHAPTER 6

CONCLUSIONS

6.1 General conclusions

Porous cast film

The porous substructure of PAN cast films can be changed by the appropriate choice of additives in the casting solution and the temperature of the coagulation bath. Of the additives used, inorganic compounds are more powerful than organic additives in altering the polyacrylonitrile cast film morphology. The addition of $CuSO_4$ to the PAN/DMF solution can produce a better film (i.e. with both a thin skin layer and a porous substructure, and with greater flexibility) than that produced by other additives used in this study. The copper ion (Cu^{2+}) in the casting solution is believed to form a complex with the DMF and also possibly with the -CN groups in PAN. These complexes accelerate the removal of the solvent from the cast film during the phase inversion process as shown by the decreased precipitation time. The presence of $CuSO_4$ in the casting solution acts as a "transient template" to promote pore formation in the final film.

Porous PAN hollow fibres

When 25 wt% polyacrylonitrile is dissolved in DMF in the presence of $CuSO_4 5H_2O$, porous hollow fibres can be obtained by a dry-jet wet spinning process. The as-spun hollow fibre membranes were successfully characterised by using gas permeability measurements. The calculated mean pore radius of the membranes is in the range of 4 nm to 32 nm. The calculated effective porosity of the membranes is in the range of 0.65×10^{-2} to 1.13×10^{-2}.

The gas permeation rate of these coated PAN hollow fibre membranes is quite a good deal lower than that of PSF hollow fibre membranes produced in the Department, and the separation factors of PAN hollow fibre membranes should show a combination of the separation factors of polymer and coating materials if the coating material can properly seal the pores on the surface. The larger pore size on

the surface of these membranes will make it more difficult to seal the pores with a coating material. If it is not possible to seal the pores properly, Knudsen flow will still occur and make a contribution to the separation factor of the membranes. As the properties of the polymer are very sensitive to temperature, it is difficult to modify the polymer at elevated temperatures. Modification at these temperatures causes pore closure and loss of the porosity of the fibres. According to the results predicted by RM, the separation factors of PAN hollow fibre membranes are very much more sensitive to the value of the surface porosity. The permeation rates of the PAN hollow fibre membranes after coating are quite low. For higher separation factors and permeation rates, lower surface porosity (less than 1×10^{-6}) and a thin separating layer (less than 0.05 μm) are required. For the PAN hollow fibres obtained here, the high surface porosity is a fatal disadvantage for fibre usage in gas separations.

The surface modification of the membranes by treatments with hydroxylamine and cuprammonium hydroxide solution did not give any improved results in gas separation performance.

Higher separation factors using PAN hollow fibre membranes were obtained when the fibres were spun by the dual-bath coagulation spinning system, but the gas permeation rates P'_{H2} were still very low (0.5 GPU). It has been demonstrated that PAN hollow fibres have a more porous surface layer, which seriously limits the separation factors of PAN hollow fibre membranes.

Crosslinking PAN fibres

Coloration and insolubility of PAN fibres are produced by treatment with cuprammonium hydroxide solution at room temperature. The interpretation of these results is that there is a newly formed crosslinked structure involving the copper complexed with the -CN groups of the polymer. Elemental analysis results show that the copper is present in the PAN after the treatment, which produces the coloration

and insolubility. The coloration (partially) and the insolubility are reversed when the copper is extracted by EDTA solution. TGA and DSC traces show that there are significant differences between the crosslinked and the original PAN hollow fibre. The changes in structure in the fibre result in changes in the fibre thermal stability, the tensile strength and the elongation at break.

There was no direct evidence from IR spectra for structures responsible for the coloration of the crosslinked fibre. The IR measurement may fail to detect any change in absorption bands, especially if the crosslinked groups concerned have only a low concentration. IR spectra do show some changes in the crosslinked fibre, in that the absorbency ratio of A_{CN}/A_{CH2} increases with increase of the copper content in the crosslinked PAN fibre. It is believed that the coloration is due partially to the complex formed between the copper and the -CN groups and partially to some other structure change, which is not easily detected.

The crosslinked structure is responsible for the insolubility of the PAN fibres. Possible structures have been proposed in this study, as shown in Scheme 5.6. At this stage, it is not possible to rule out other structures formed in the crosslinked fibre.

6.2 Future work

The aim of this work was to try to fabricate porous, asymmetric PAN hollow fibres and then to evaluate their gas separation performance. After failure to produce satisfactory porous PAN hollow fibre from PAN/DMF solution, a series of additives to the casting solution were examined in order to change the morphology of the PAN cast film produced by the phase inversion process. A porous, flexible PAN cast film and hollow fibre can be produced when $CuSO_4$ is present in the PAN/DMF solution. Further work is required to see if other salts are also able to modify the phase inversion and produce the required fibre structure which would allow PAN to be used in gas separations.

During the surface modification process, the coloration and the insolubility of the fibres were observed when the fibres were treated with cuprammonium hydroxide solution at room temperature. The insolubility of the fibre is presumed to be due to a newly formed crosslinked structure involving copper and the -CN groups of PAN polymer. It is necessary to understand the mechanism of this reaction, even though it is not directly related to membrane studies. There may be advantages in treating textile fibres with this reagent which can also be investigated. Additionally it may be possible to carry out heat treatments on PAN hollow fibres to produce more carbon-rich materials, which are useful for separations.

From the gas separation performance point of view, the PAN hollow fibre membranes showed very low gas permeabilities, which was related to its low intrinsic permeation coefficient and a thick separating skin layer on the fibres. It may be difficult to find the correct conditions to spin fibres with a thin, dense separating layer, or to modify the surface of the PAN fibre in order to alter the gas separation performance. The newer, and more permeable and selective polymers like the fluorinated polyimides have been developed recently. The problems is only how to

convert them into good asymmetric hollow fibre membranes. The PAN hollow fibre membranes obtained here with mean pore radius in the range of 4 nm to 32 nm are clearly not suitable for gas separations, but they may be useful in the field of ultrafiltration.

For the application of filtration in chemical industries at which higher temperatures may be required, carbon based porous hollow fibre membranes may have a potential usage in this field. Converting crosslinked porous PAN hollow fibres obtained in this study to carbon based fibres will be very interesting work to carry out.

APPENDIX

Works carried out for British Gas Plc

This section describes work carried out for British Gas Plc. In this work, hollow fibre membranes were produced from four different polymers, which were provided by the company. The spinning solutions and spinning conditions are shown in Table A.1 and Table A.2.

The precipitation times of solution-cast films and the zero shear rate viscosity of these five spinning solutions are shown in Table A.3.

From the results shown in Table A.3, Sample A (Udel PS-3500) gave the highest viscosity. Sample C (Radel R-5000NT) showed the lowest viscosity and the longest precipitation time. In the case of TMDP-PEES, a higher viscosity and a longer precipitation time was observed in 1-Fp (Sample E) than that in NMP (Sample D).

Figs. A.1 ~ A.5 and the data in Table A.4 show the characteristics of the hollow fibres. The two hollow fibres which were spun from samples B (Fig. A.2) and C (Fig. A.3) with long precipitation time(> 150 sec.), and low viscosity(<30 pa.s) exhibited lumens which were not central and also non-circular. Hollow fibres which were produced from samples A (see Fig. A.1), D and E (see Fig. A.2 & A.3) with short precipitation times and high viscosities resulted in circular lumens which were also centralised.

The concentrations of macrovoids in these fibres varied and are compared in Table A.4. Hollow fibres which were spun from samples D & E exhibited a high and intermediate concentration of macrovoids, respectively, whereas sample A showed a macrovoid free structure and samples B & C yielded a very low concentration of macrovoids.

Table A.1 Spinning Solutions (A~E)

Sample	Polymer	Solvent	Polym. Conc. (wt%)
A	Udel PS-3500	1-Fp:Fa/9:1[a]	30
B	Radel A-200NT	1-Fp:Fa/9:1	30
C	Radel R-5000NT	NMP[b]	30
D	TMDP-PEES	NMP	21.5
E	TMDP-PEES	1-Fp	21.5

a:1-Fp:Fa = 1-formyl-piperidine:formamide

b:N-methyl-2-pyrrolidinone

Table A.2 Spinning Conditions

Spinneret dimensions	580/330/150 μm
Polymer extrusion temperature	45 °C
Coagulation bath temperature	5 °C
N_2 pressure	25 psi
Jet gap	60 mm
Linear extrusion rate	16.35 m/min.
Wind up speed	7.1 m/min.
Jet stretch	0.43
Water injection rate	1.00 ml/min.

Table A.3 Spinning solution viscosity and precipitation time

Sample	Precipitation Time (sec.) in water bath at 22 °C	Viscosity η (pa.s) at 45 °C
A	81.7	98.93
B	158.5	27.89
C	307.6	24.34
D	32.2	40.01
E	49.0	81.48

Table A.4 Characteristics of the hollow fibres

Sample	Fibre Dimension [a] O.Dμm (s.d [c])	I.Dμm (s.d [c])	Macrovoids Status [b]	X-section of the Fibres
A	542 (25.65)	293 (18.89)	–	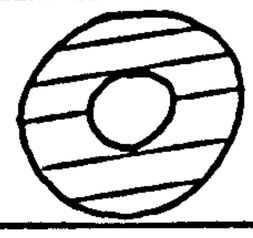
B	531 (15.84)	281 (27.51)	+	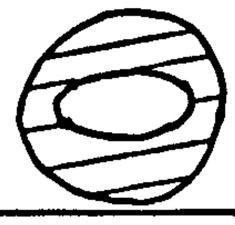
C	520 (12.70)	271 (19.23)	+	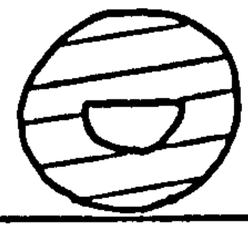
D	458 (18.29)	262 (14.66)	++	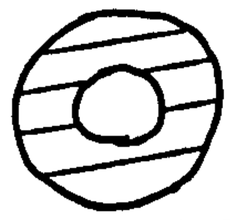
E	482 (15.07)	259 (16.93)	+	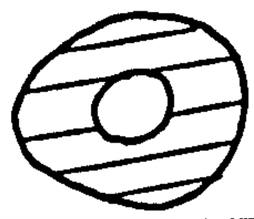

a: all data measured by optical microscopy;
b: – macrovoid-free; + intermediate to low concentration; ++ high concentration;
c: standard deviation.

When the concentration of TMDP-PEES polymer in 1-Fp solvent was increased from 21.5 wt% to 30 wt%, the concentration of macrovoids was significantly decreased as shown in Figs. A.6 and A.7 (samples F and G). When the concentration of the polymer was 21.5 wt%, the concentration of macrovoids also decreased if a solvent/non-solvent system was used (samples H and I), as shown in Figs. A.8 and A.9, in comparison to the structure obtained in 1-Fp and NMP solvents (Figs. A.4 & A.5).

The gas permeation rates and separation factors of these hollow fibre membranes are shown in Table A.5. The separation factor α_{CO_2/CH_4} of the as-spun hollow fibre membranes observed were higher than that of Knudsen flow ($\alpha_{CO_2/CH_4} = 0.62$). If the gas only passed through the defects on the surface of the skin layer of the fibres, the separation factor should be equal to that of Knudsen flow. The results obtained indicate that the gases not only pass through the defects (Knudsen flow), but also pass through the dense skin layer (diffusion-solution flow). (All measurements were made on samples which had been washed for 18 days).

The permeation rates and separation factor of coated hollow fibre membranes made from 21.5 wt% TMDP-PEES polymer in 1-Fp (Sample E) are 39.32 GPU for CO_2, 1.18 GPU for CH_4 and 33.35 for α_{CO_2/CH_4}, which are slightly higher than those of Udel PSF-3500 hollow fibre membrane. Comparison of samples D and E shows that the former has a lower selectivity α_{CO_2/CH_4} than the latter. This is believed to be due to the high concentration of macrovoids and defects on the surface of the fibre in sample D. As the SEM micrograph shows in Fig. A.4, the fibre structure has not only a higher concentration of macrovoids than that of sample E, but also there are crevices in the wall of the fibre, which are likely to affect the permeation rate P'_{CH_4} for Sylgard coated fibres. The hollow fibre membranes made from 30 wt% Radel A-2000NT(B) and Radel R-5000NT(C) show lower separation factors α_{CO_2/CH_4} than TMDP-PEES and Udel PSF-3500.

Table A.5 Gas permeation rates and selectivity of as-spun and coated hollow fibre membranes

Sample	Module Status	P'_{CO_2}(GPU) [a]	P'_{CH_4}(GPU)	α_{CO_2/CH_4}
A:	As-spun HF	236.1	254.8	0.93
	Sylgard coated HF[b]	36.69	1.11	32.94
B:	As-spun HF	336.77	484.85	0.69
	Sylgard coated HF	40.37	3.05	13.26
C:	As-spun HF	11.38	6.38	1.78
	Sylgard coated HF	8.47	0.54	15.68
D:	As-spun HF	70.71	36.70	1.93
	Sylgard coated HF	39.15	1.64	23.89
E:	As-spun HF	59.96	5.48	10.94
	Sylgard coated HF	39.32	1.18	33.35

a: GPU = $1\times10^{-6}\times cm^3\ cm^{-2}\ s^{-1}\ cmHg^{-1}$, all data measured at 100 psi;

b: Hollow fibres coated in isopentane solution of 5% Sylgard 184, 0.05% curing agent.

Table A.6 Spinning solutions (F~I)

Sample	Polym. Conc. (wt%)	Solvent
F	25 % TMDP-PEES: 30g	1-Fp
G	30 % TMDP-PEES 30g	1-Fp
H	21.5 % TMDP-PEES 30g	1-Fp:Fa = 95:5
I	21.5 % TMDP-PEES 30g	1-Fp:PA = 90:10

Table A.7 Diameter of the hollow fibres after drying by different methods

Sample	Fibre Diameter			
	S.E. Dried [a]		Air. Dried	
	O.D(μm) (s.d)	I.D(μm) (s.d)	O.D(μm) (s.d)	I.D(μm) (s.d)
F	624 (40.06)	349 (37.55)	587 (43.73)	312 (26.16)
G	686 (37.00)	421 (22.87)	630 (19.32)	386 (25.47)
H	638 (29.74)	371 (26.85)	591 (20.79)	314 (29.13)
I	624 (40.88)	342 (32.93)	608 (52.03)	333 (41.11)

a: dried by solvent exchange drying method.

The fibre diameter and residual solvent content in the as-spun hollow fibres from the spinning solutions listed in Table A.6 were examined by optical microscopy and thermal analysis (TGA). Table A.7 shows the values of fibre diameters (O.D and I.D) after using a solvent exchange drying method compared with drying in air. The measurements show that the diameters of the fibres, which were dried by the solvent exchange drying method, were larger than those which were allowed to dry in air. This indicates that the solvent exchange drying method can prevent compaction of the porous structure of the fibre to some extent during the drying procedure.

The residual solvent content in the as-spun hollow fibres was examined after the fibres were washed for different times and dried using the two different methods. The residual solvent content was only small in the fibre after a thorough washing treatment over a period of two and a half weeks, as shown in Table A.8. The TGA

Table A.8 Effect of drying method and washing time on the residual solvent content of hollow fibres

Sample	Washing time (Day)	Residual solvent content (%)	
		Air dried	S.E dried
F	2	5.65	1.05
	18	0.36	0.13
G	2	3.27	1.08
	18	0.41	0.12
H	2	8.59	1.97
	18	0.32	0.11
I	2	5.63	1.10
	18	0.35	0.11

traces in Fig. A.10 (sample F) show that the amount of the residual solvent content decreased with increasing washing time.

Table A.8 also shows that the drying method also affects the residual solvent in the fibres. When the fibre was subjected to drying by solvent exchange, the TGA traces in Fig. A.11 (sample F) showed that the amount of the residual solvent content in the fibre was reduced in comparison to that after drying in the open air. Fig. A.12 and Fig. A.13 show the residual solvent content in the fibres as a function of washing time by both drying methods. These results indicate that the residual solvent in the fibre can be further reduced if the fibre is dried by a solvent exchange drying method.

From the above results, hollow fibre membranes made from TMDP-PEES polymer showed better gas separation properties than that those of Radel A-200NT and Radel R-5000NT, and Udel PS-3500. It was shown that macrovoid-free structured hollow fibres are obtained when the polymer concentrations are 30 wt% TMDP-PEES polymer in 1-Fp pure solvent system and Udel PS-3500 polymer in 1-Fp:Fa = 9:1.

For a polymer concentration of 21.5 wt% TMDP-PEES in the spinning solution, macrovoids can be reduced when a solvent/non-solvent system is used. The residual solvent content was only a small amount in the fibre (0.3% for air dried, 0.1% for solvent exchange drying method) after thorough washing treatment over two and a half weeks. The diameter of the fibre dried by solvent exchange drying method was larger than that of samples dried in the open air.

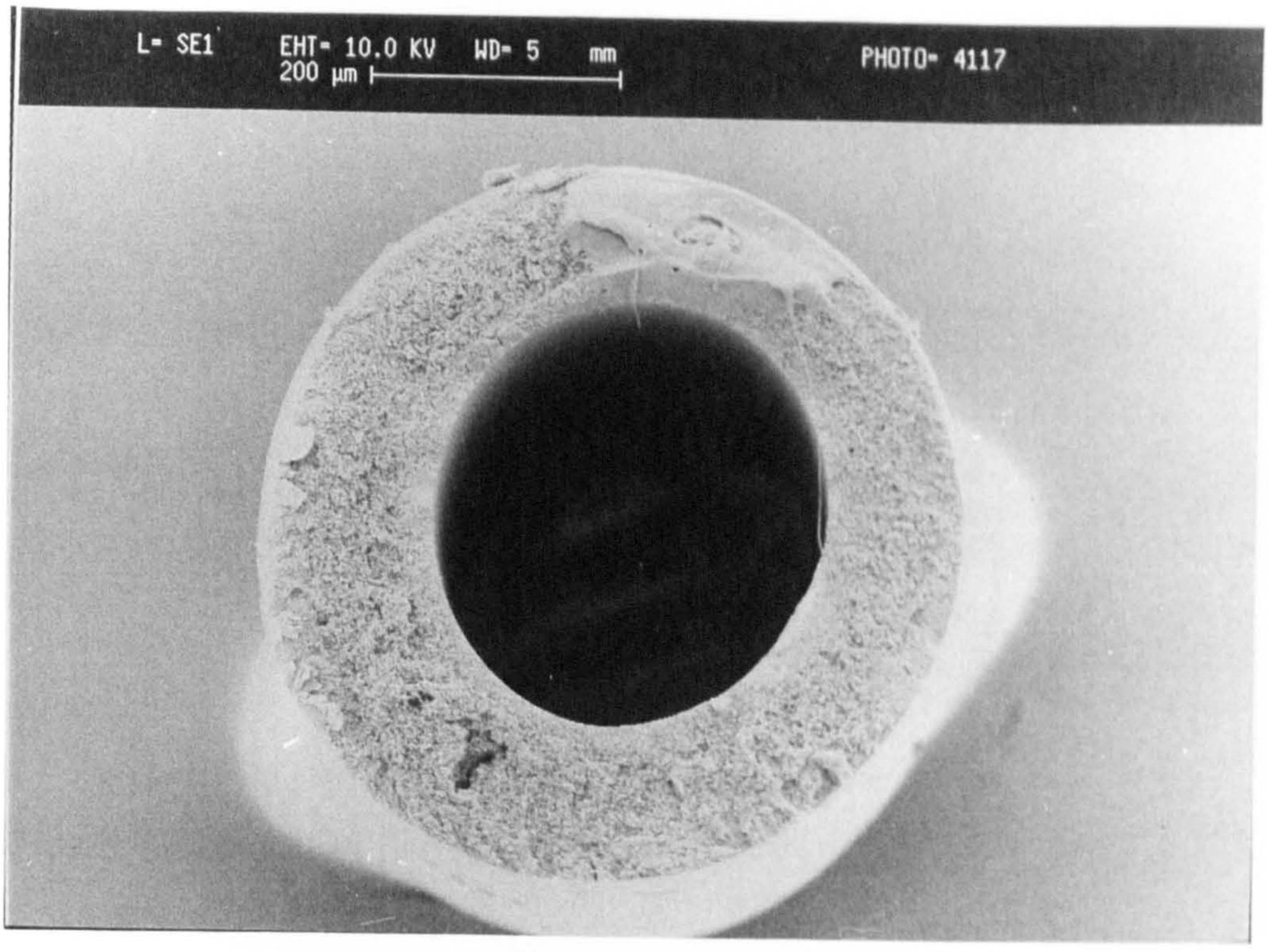

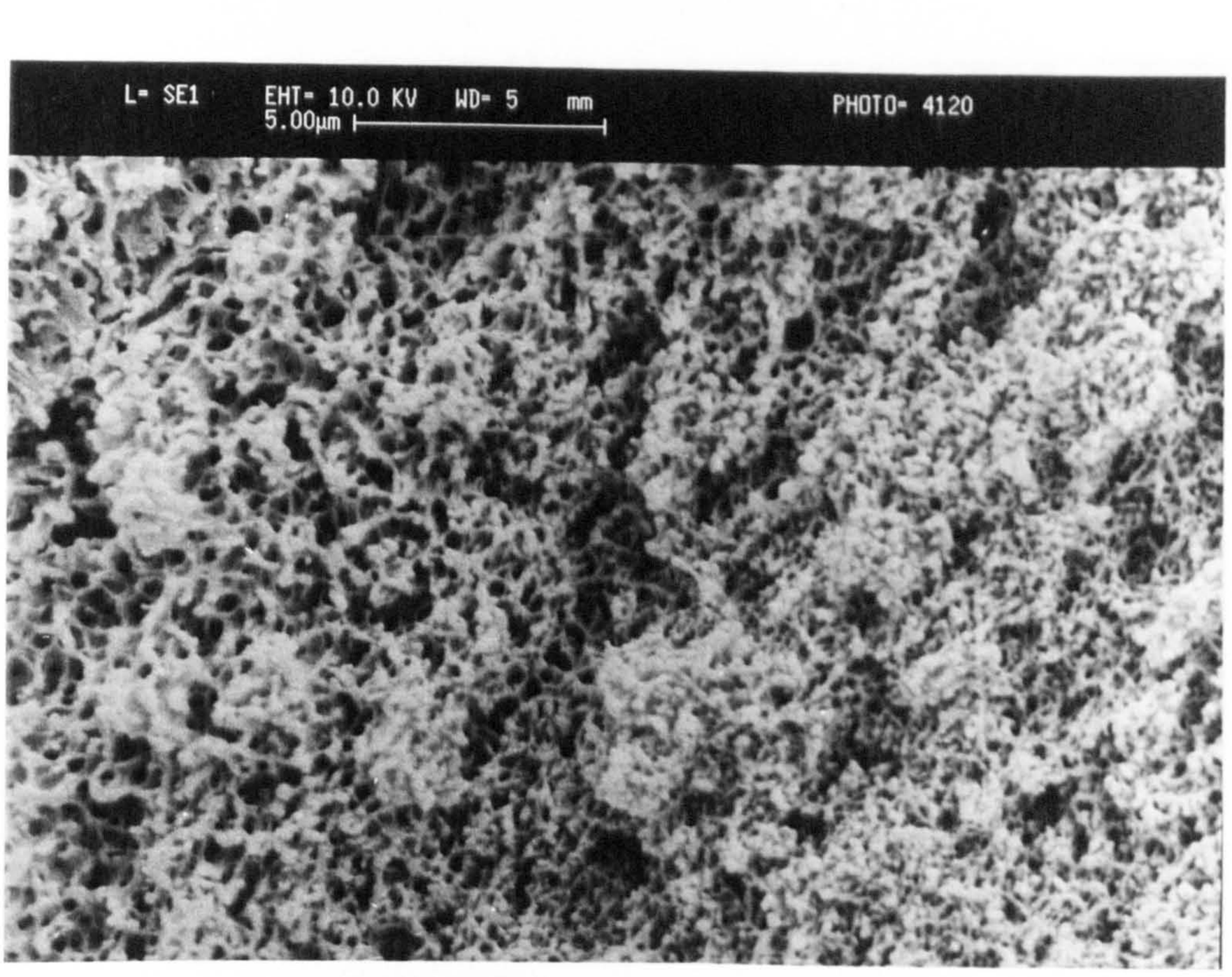

Fig. A.1 SEM micrographs of cross-section of fibre spun from 30 wt% Udel PS-3500 in 1-Fp:Fa = 9:1

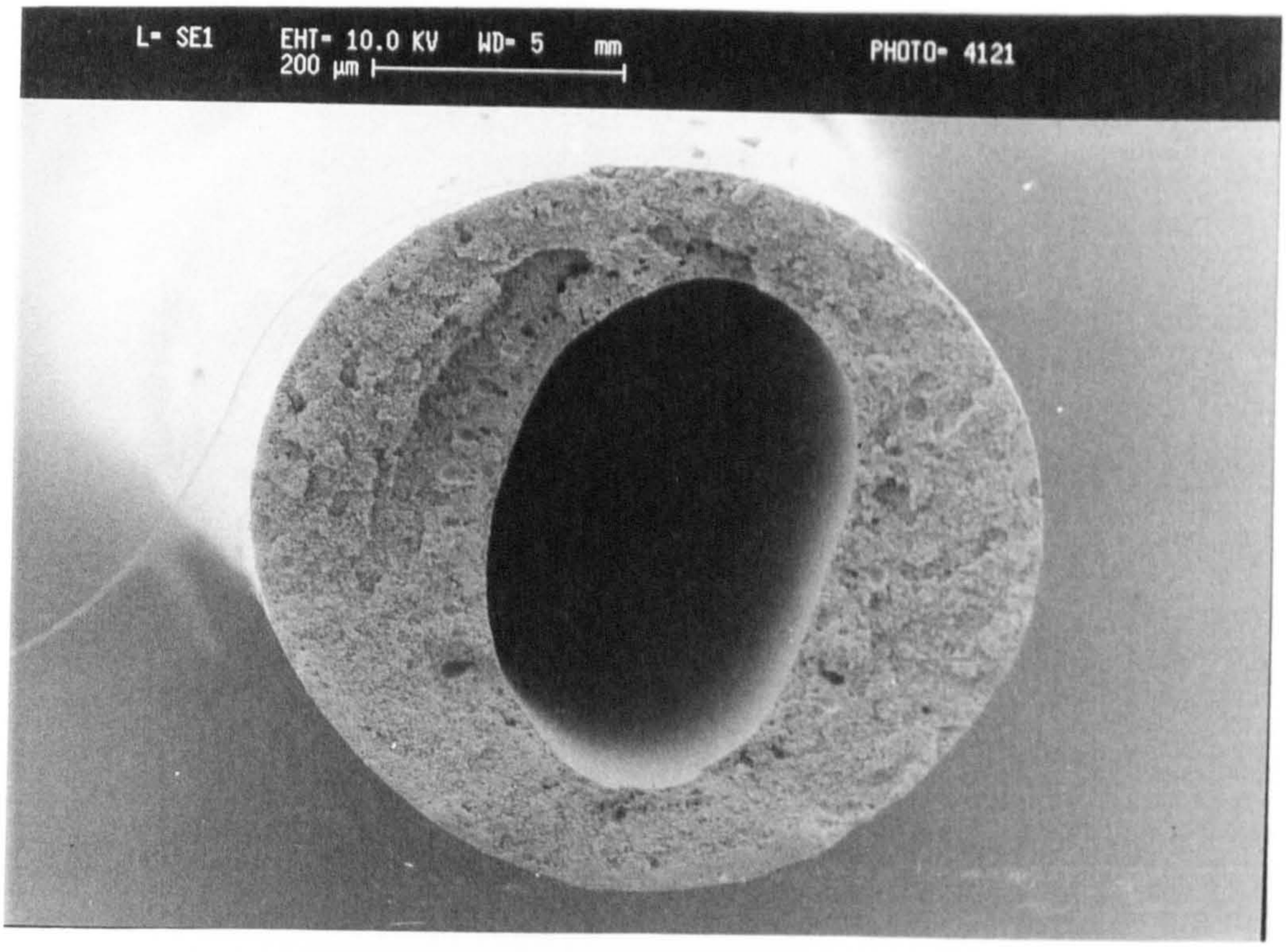

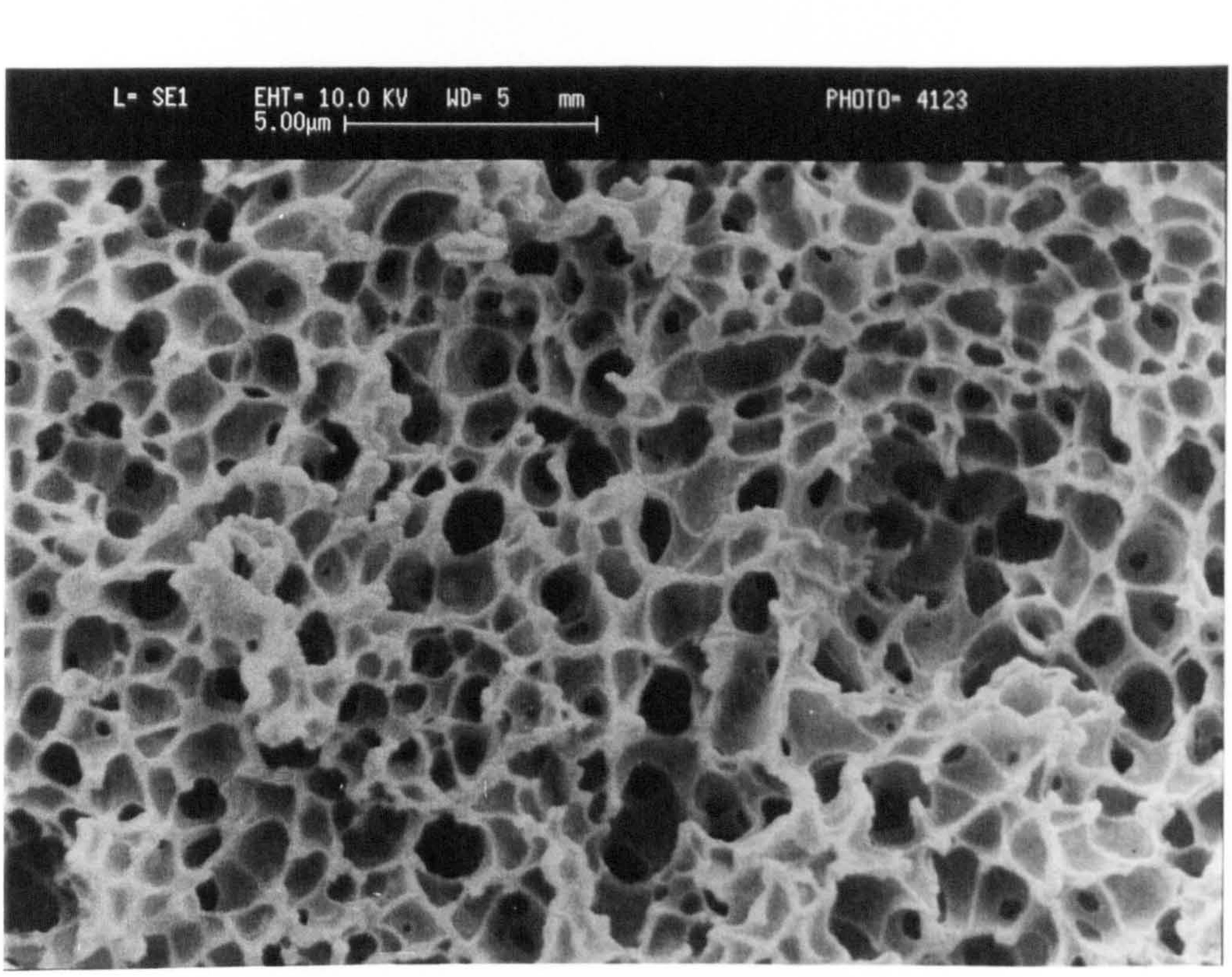

Fig. A.2 SEM micrographs of cross-section of fibre spun from 30 wt% Radel A-200NT in 1-Fp:Fa = 9:1

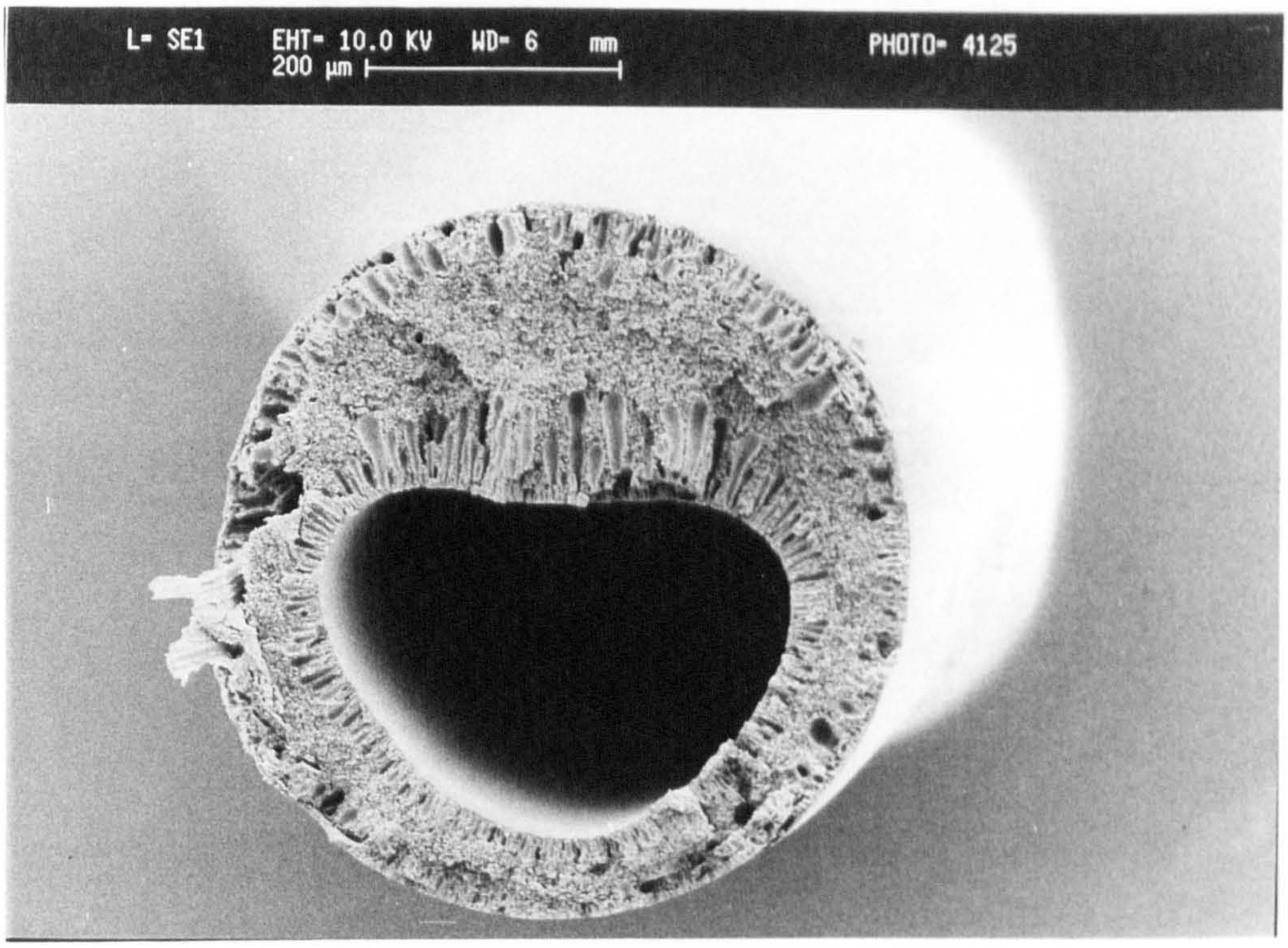

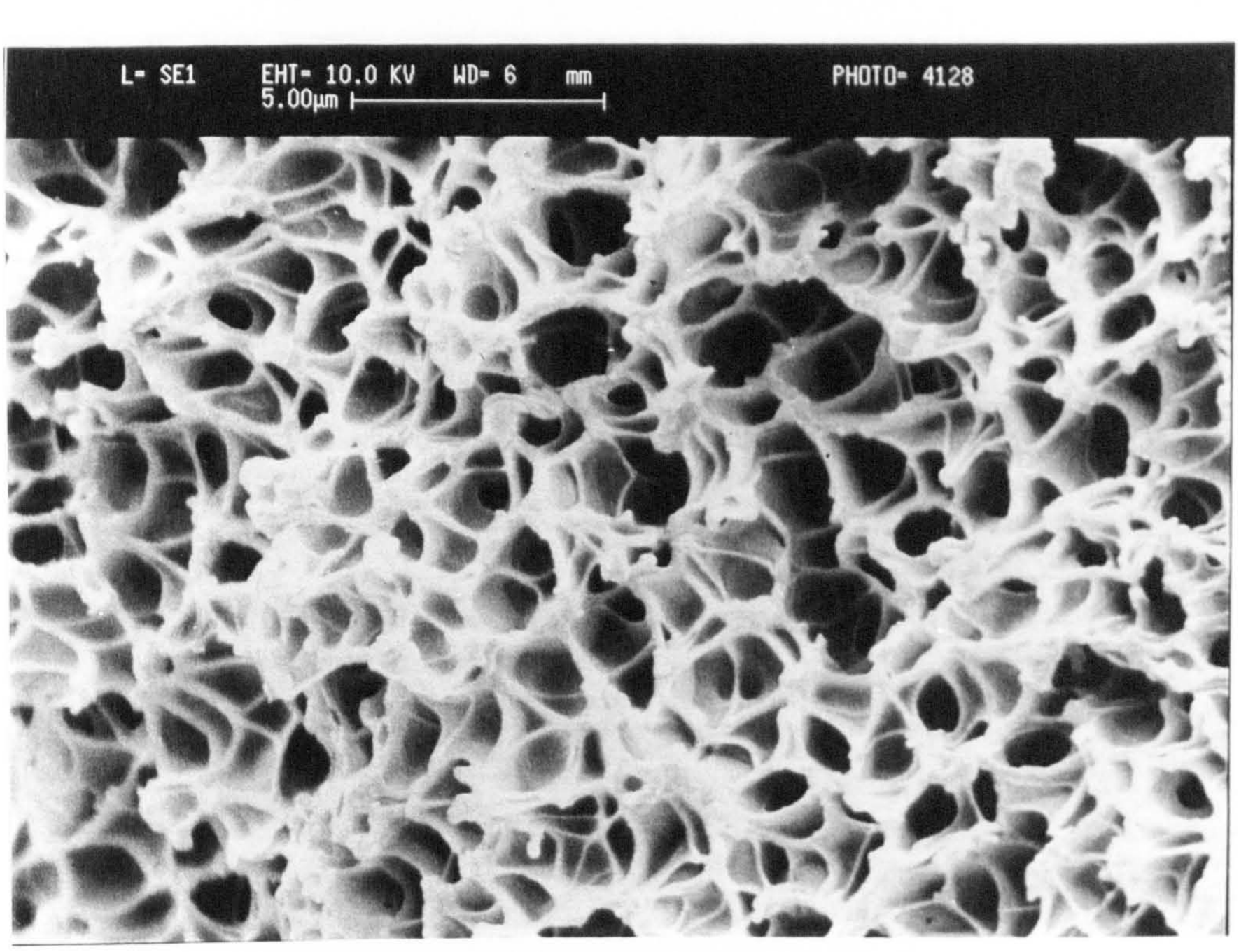

Fig. A.3 SEM micrographs of cross-section of fibre spun from 30 wt% Radel R-5000NT in NMP

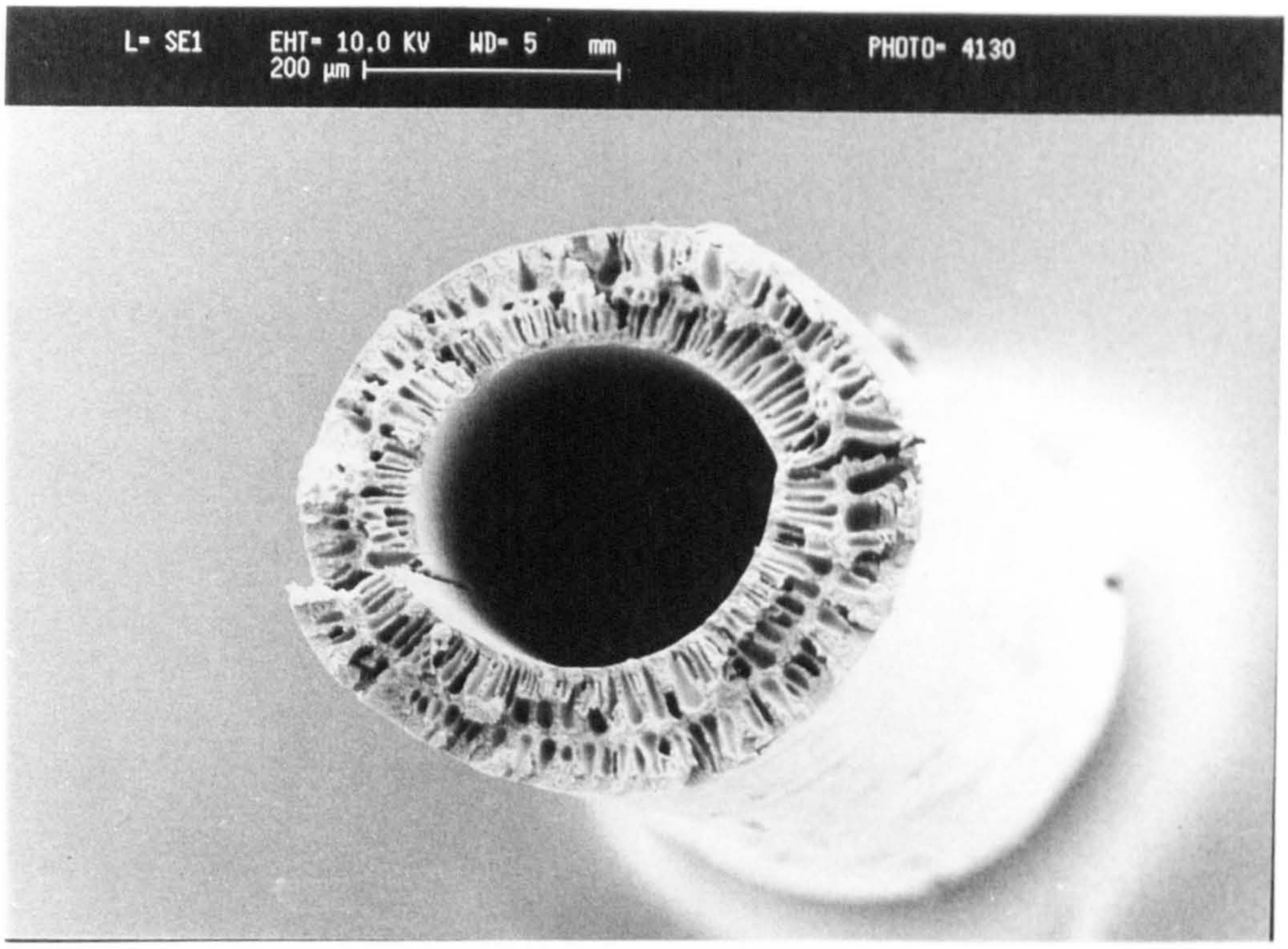

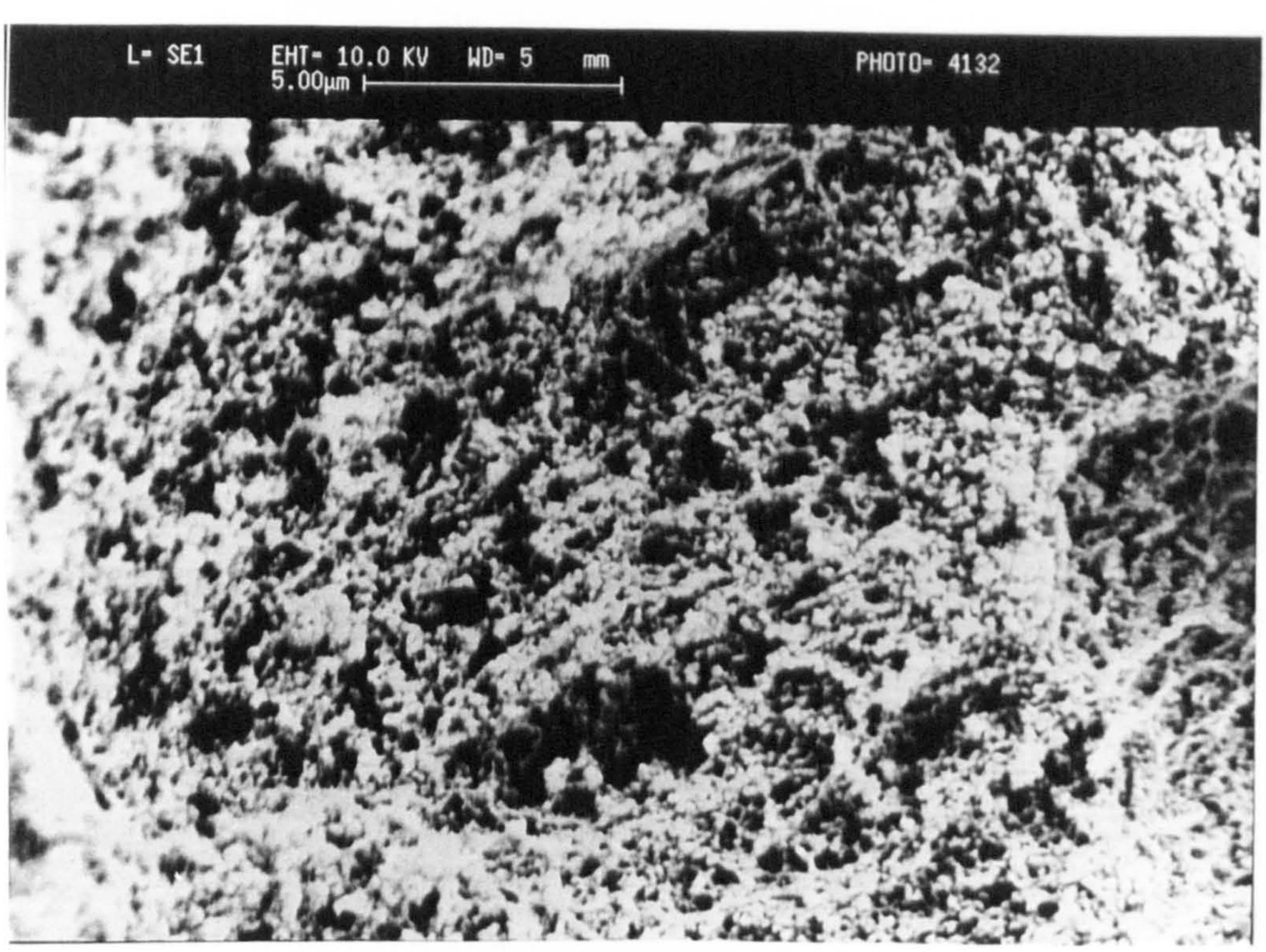

Fig. A.4 SEM micrographs of cross-section of fibre spun from 21.5 wt% TMDP-PEES in NMP

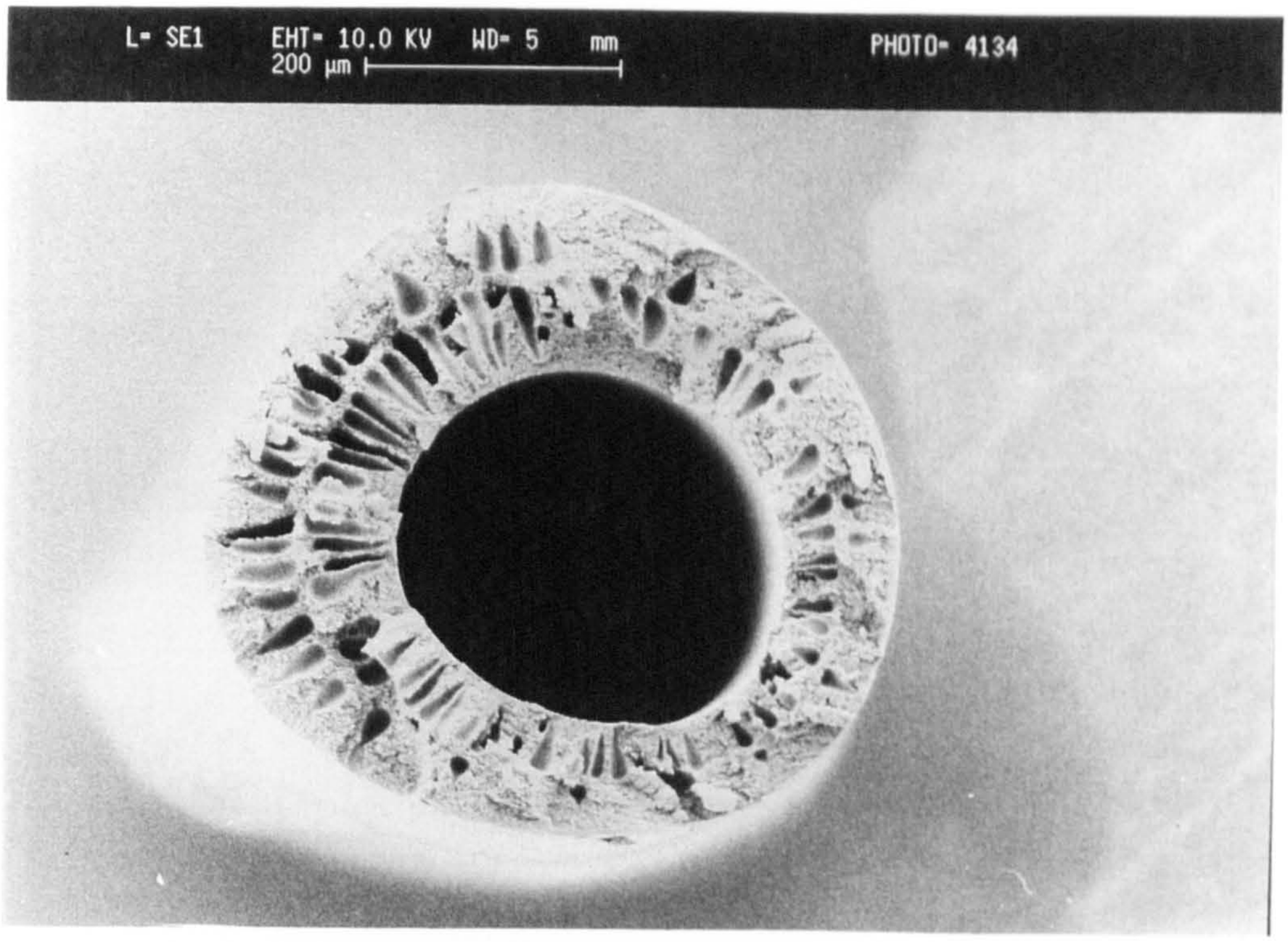

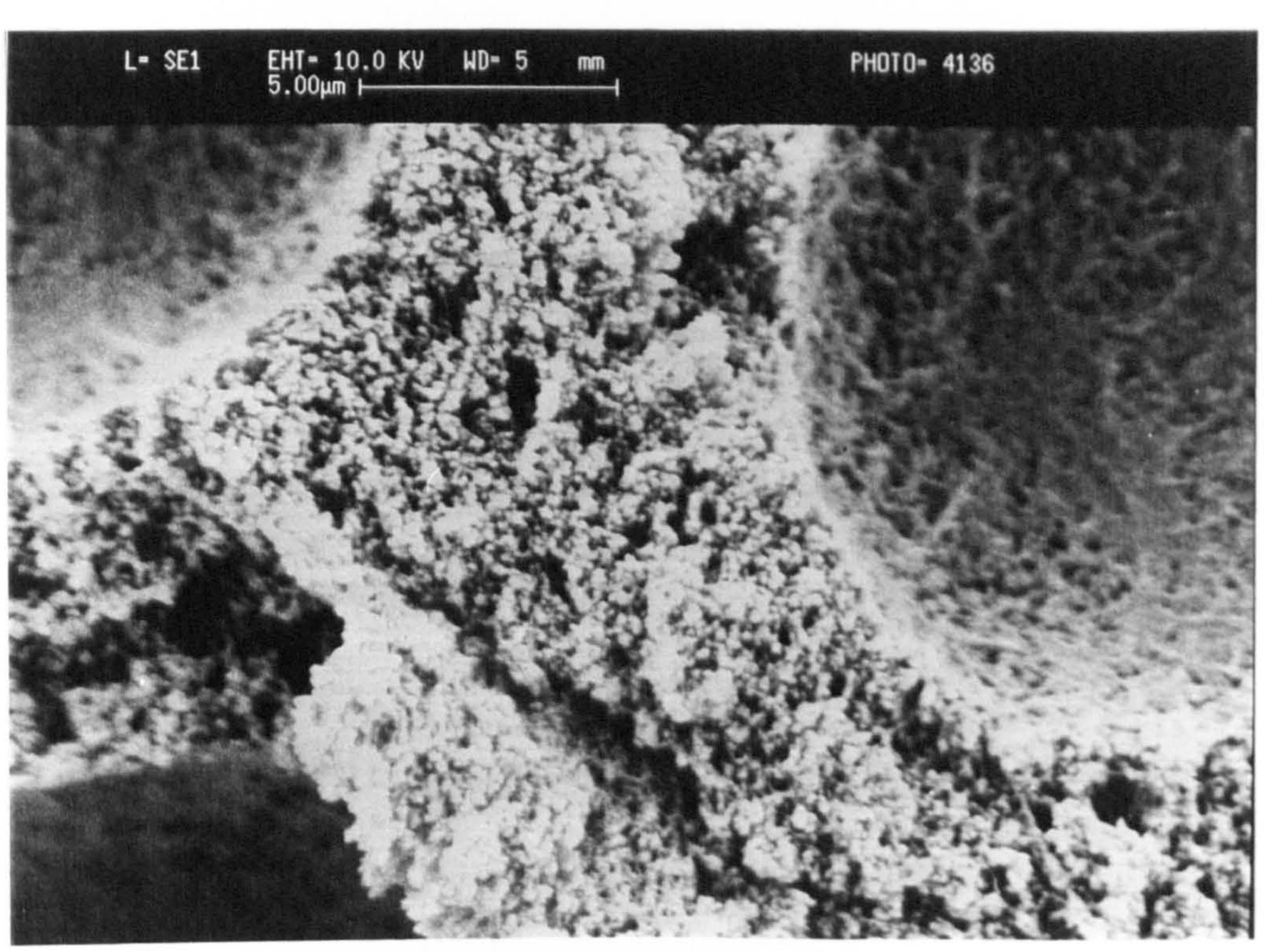

Fig. A.5 SEM micrographs of cross-section of fibre spun from 21.5 wt% TMDP-PEES in 1-Fp

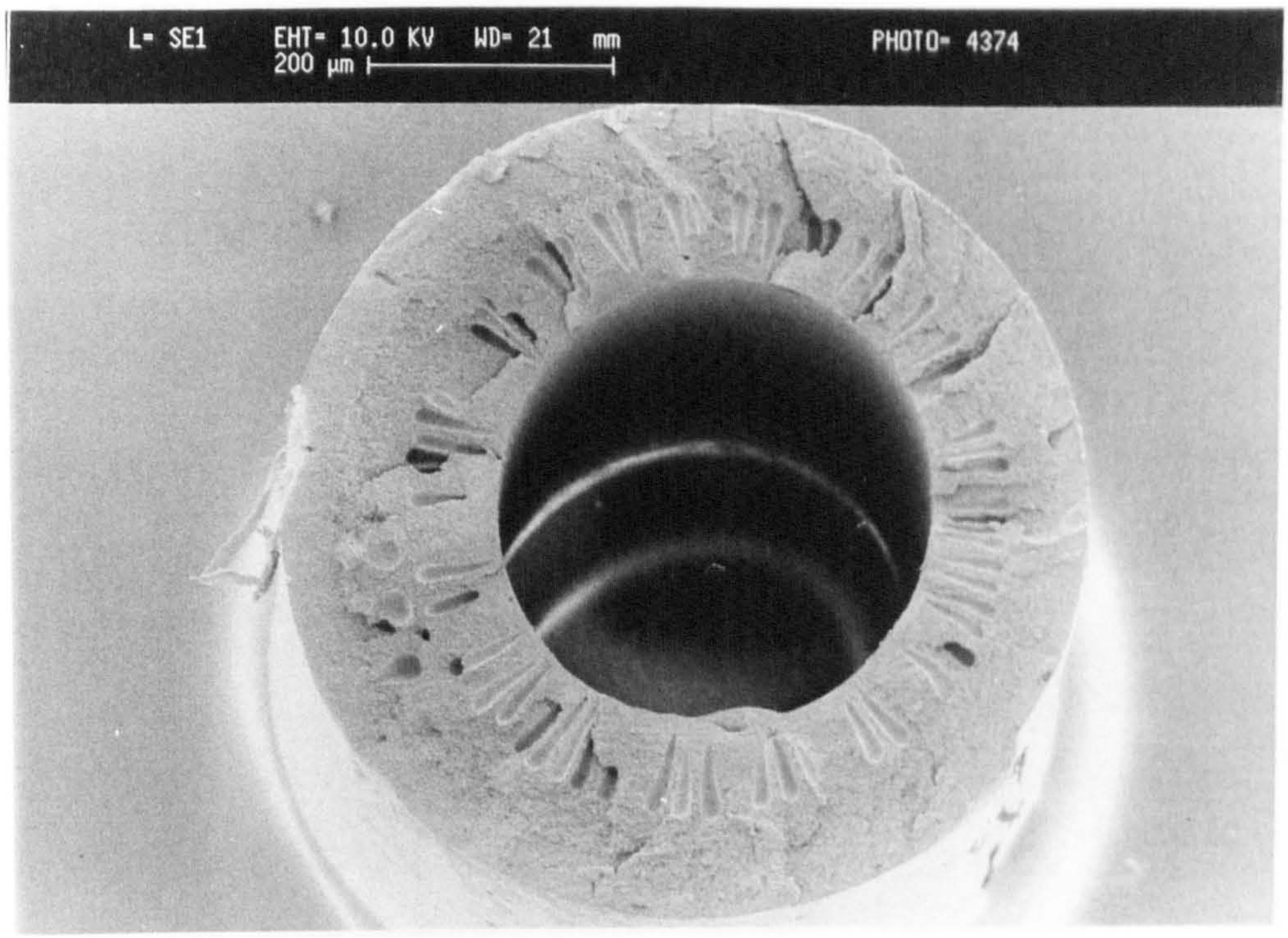

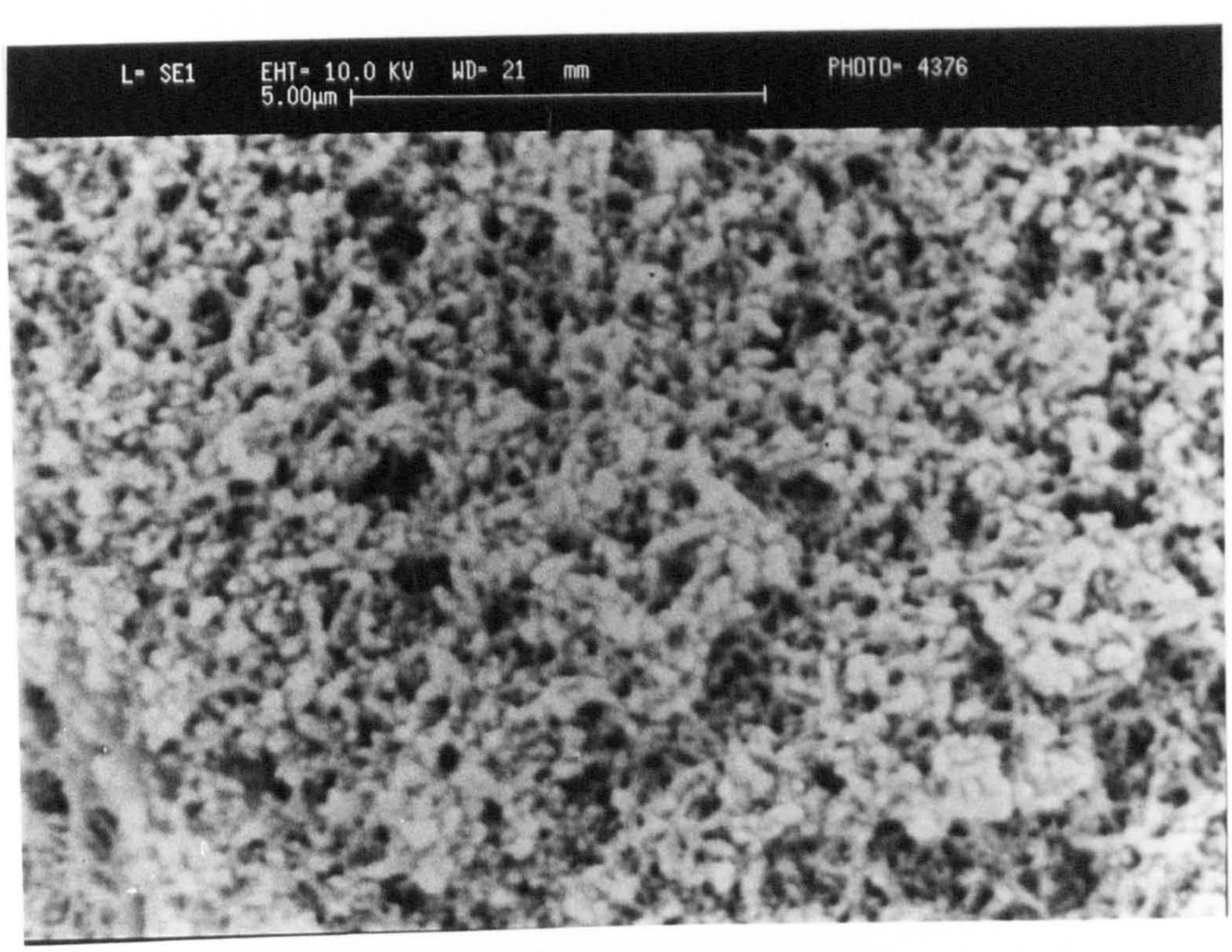

Fig. A.6 SEM micrographs of cross-section of fibre spun from
25 wt% TMDP-PEES in 1-Fp

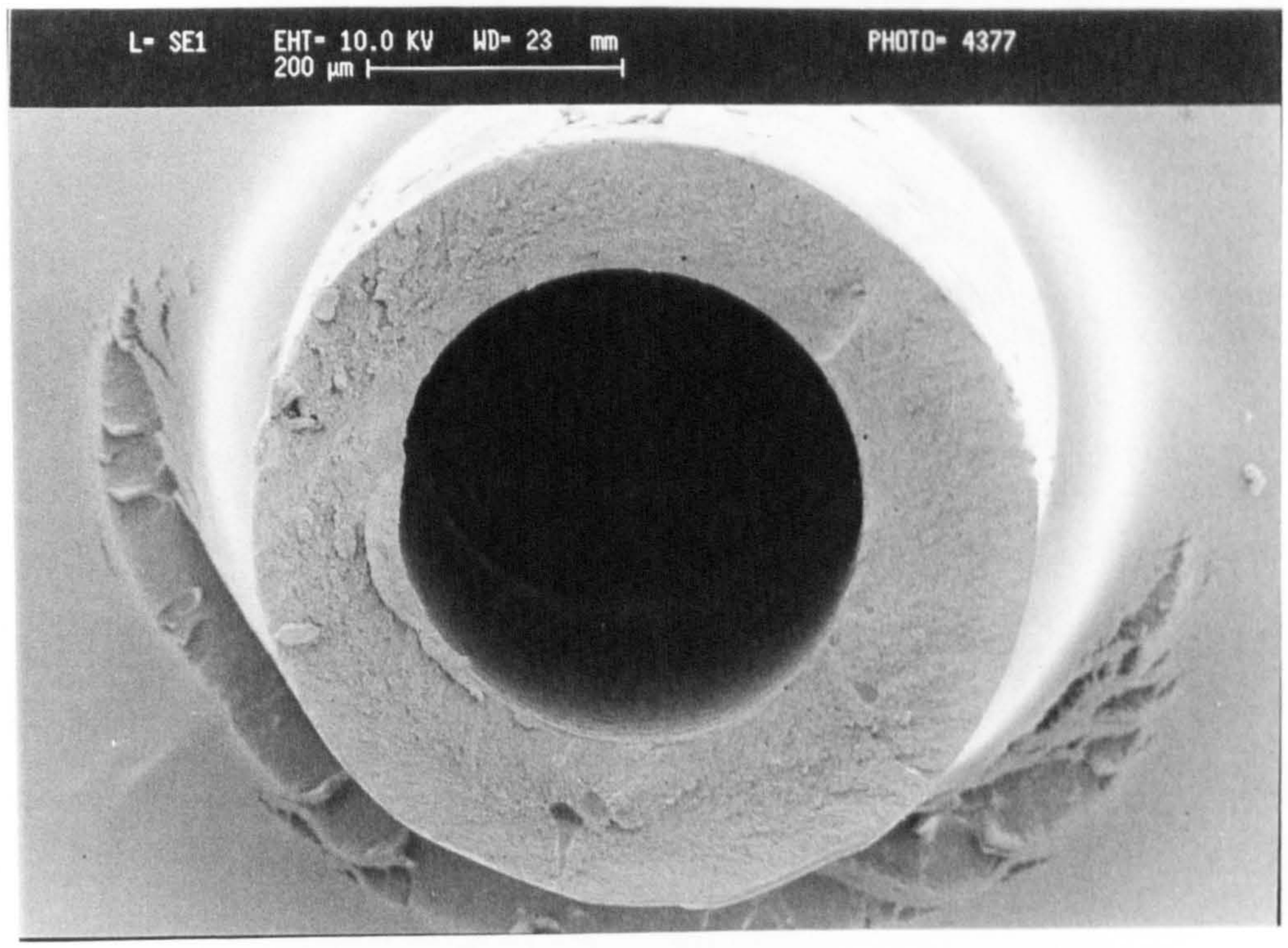

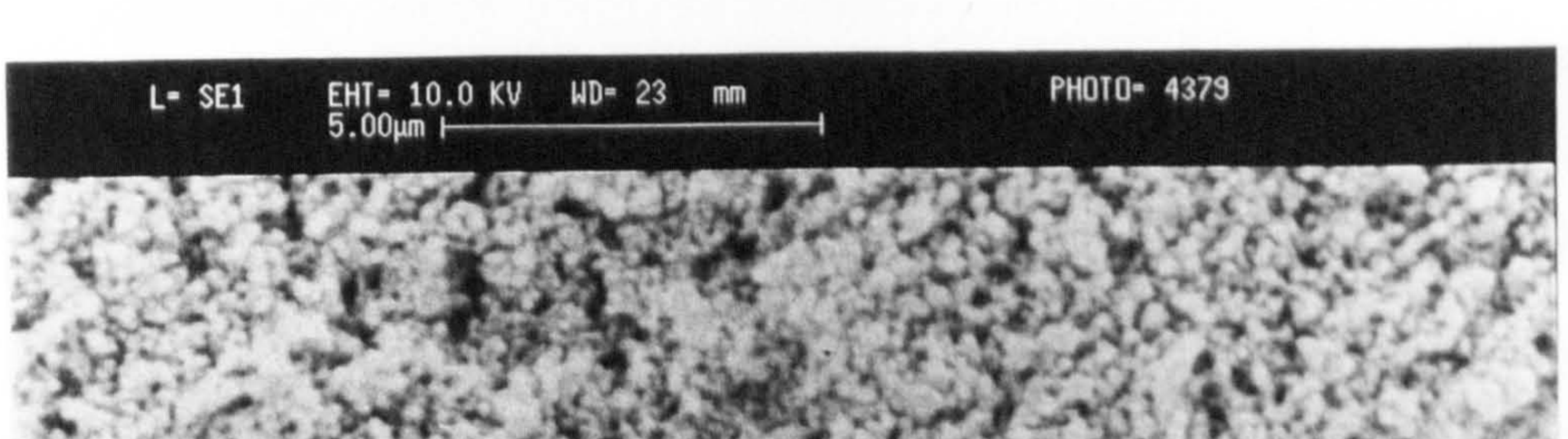

Fig. A.7 SEM micrographs of cross-section of fibre spun from 30 wt% TMDP-PEES in 1-Fp

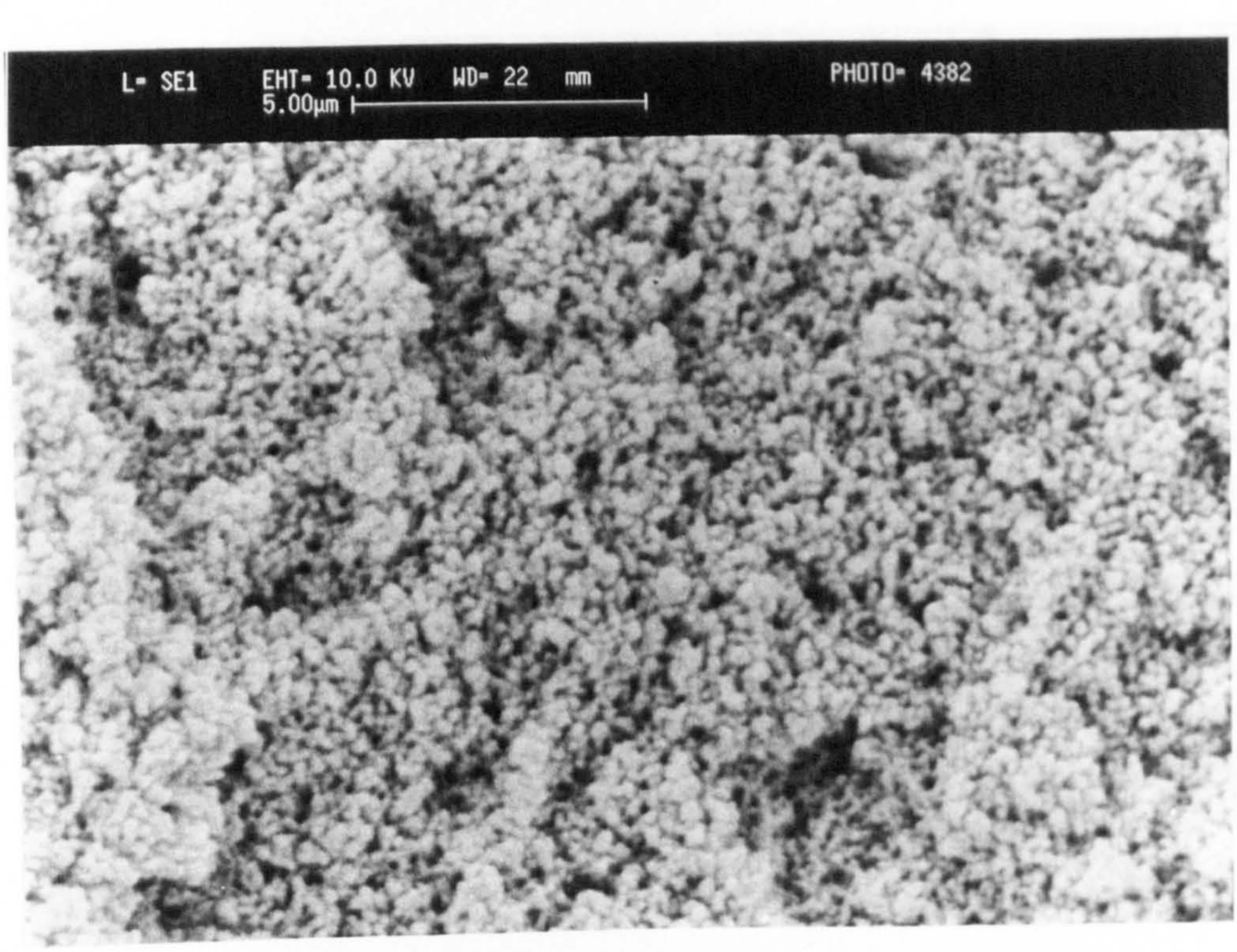

Fig. A.8 SEM micrographs of cross-section of fibre spun from 21.5 wt% TMDP-PEES in 1-Fp:Fa = 95:5

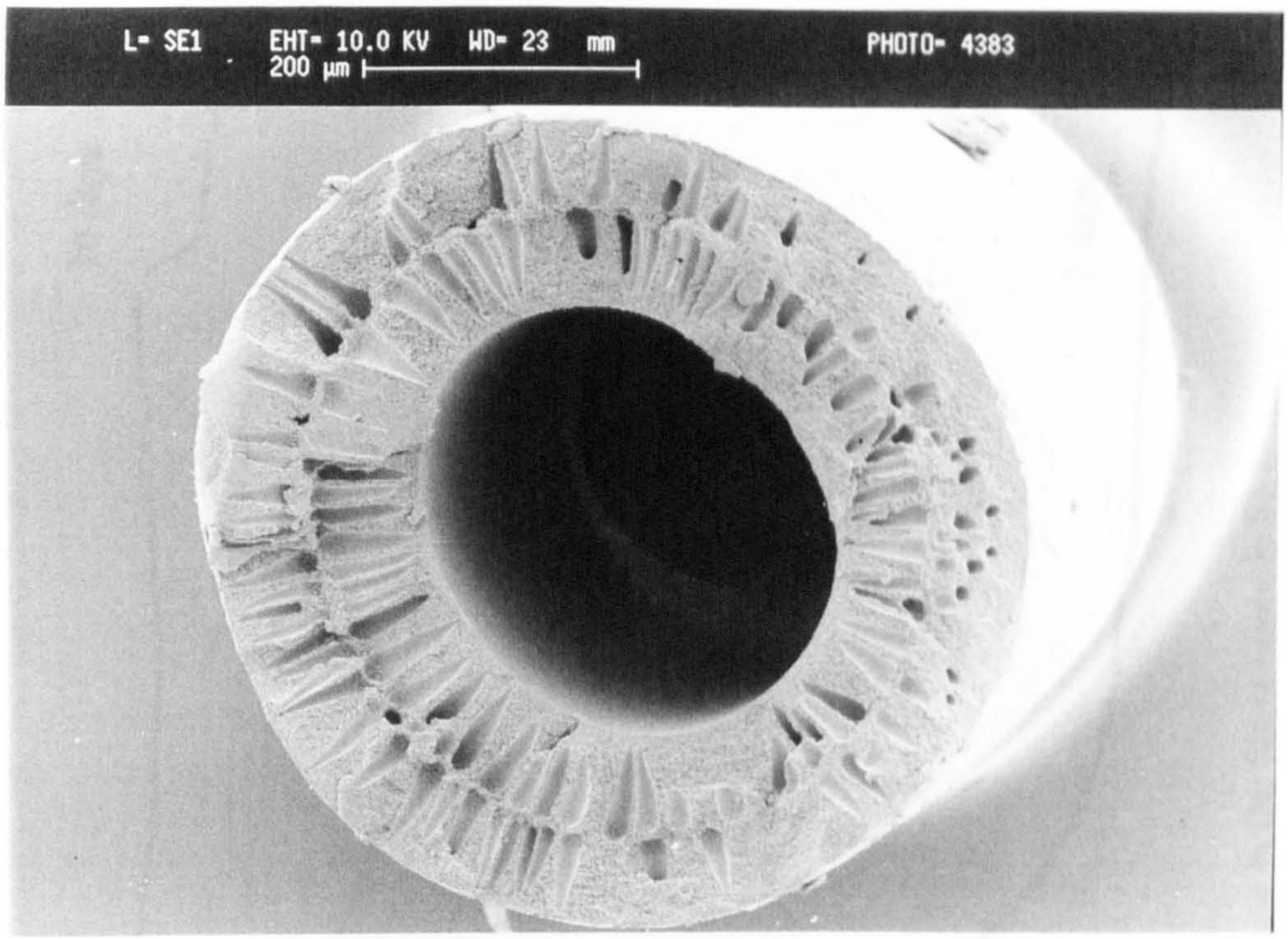

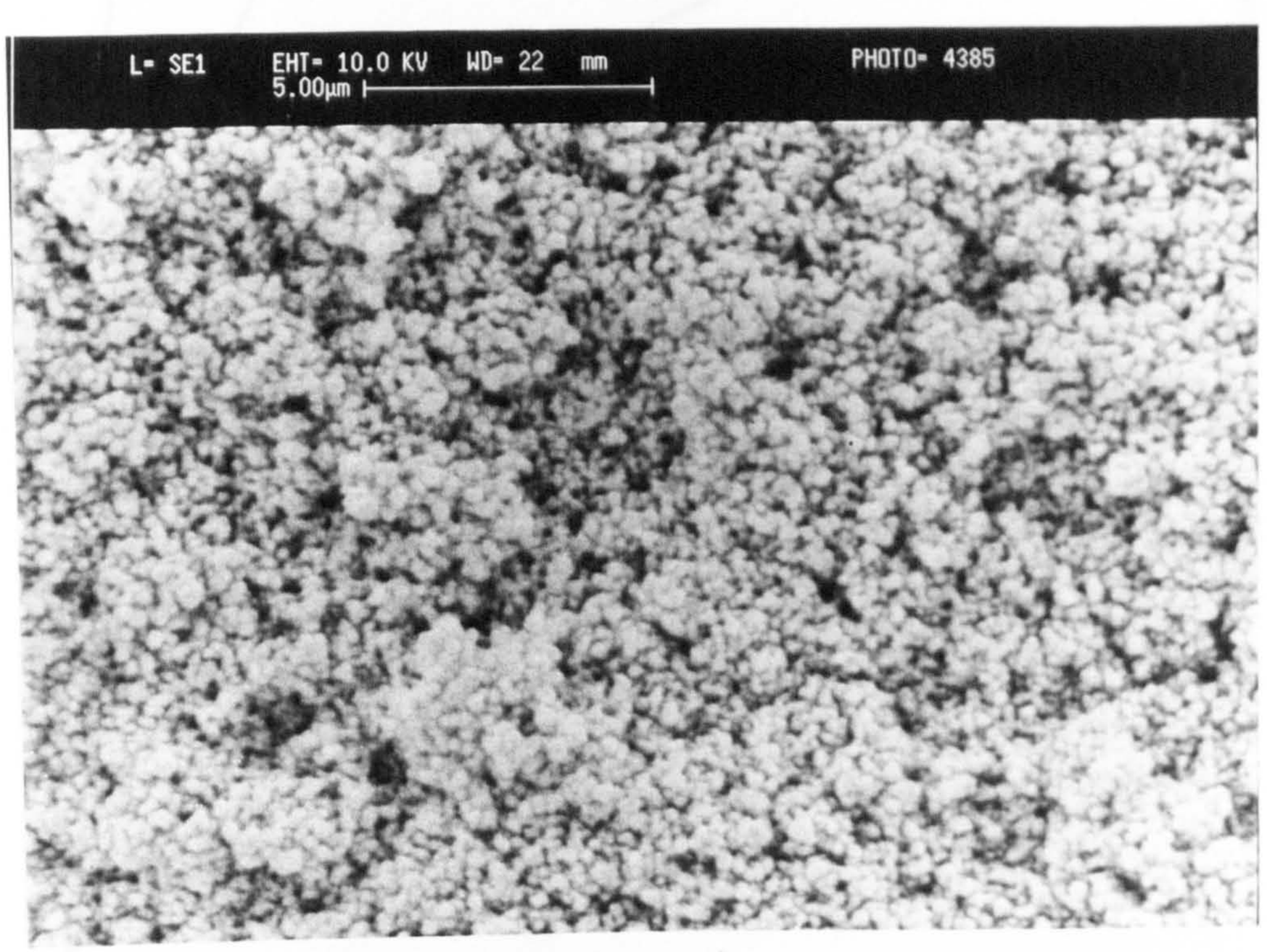

Fig. A.9 SEM micrographs of cross-section of fibre spun from 21.5 wt% TMDP-PEES in 1-Fp:PA = 9:1

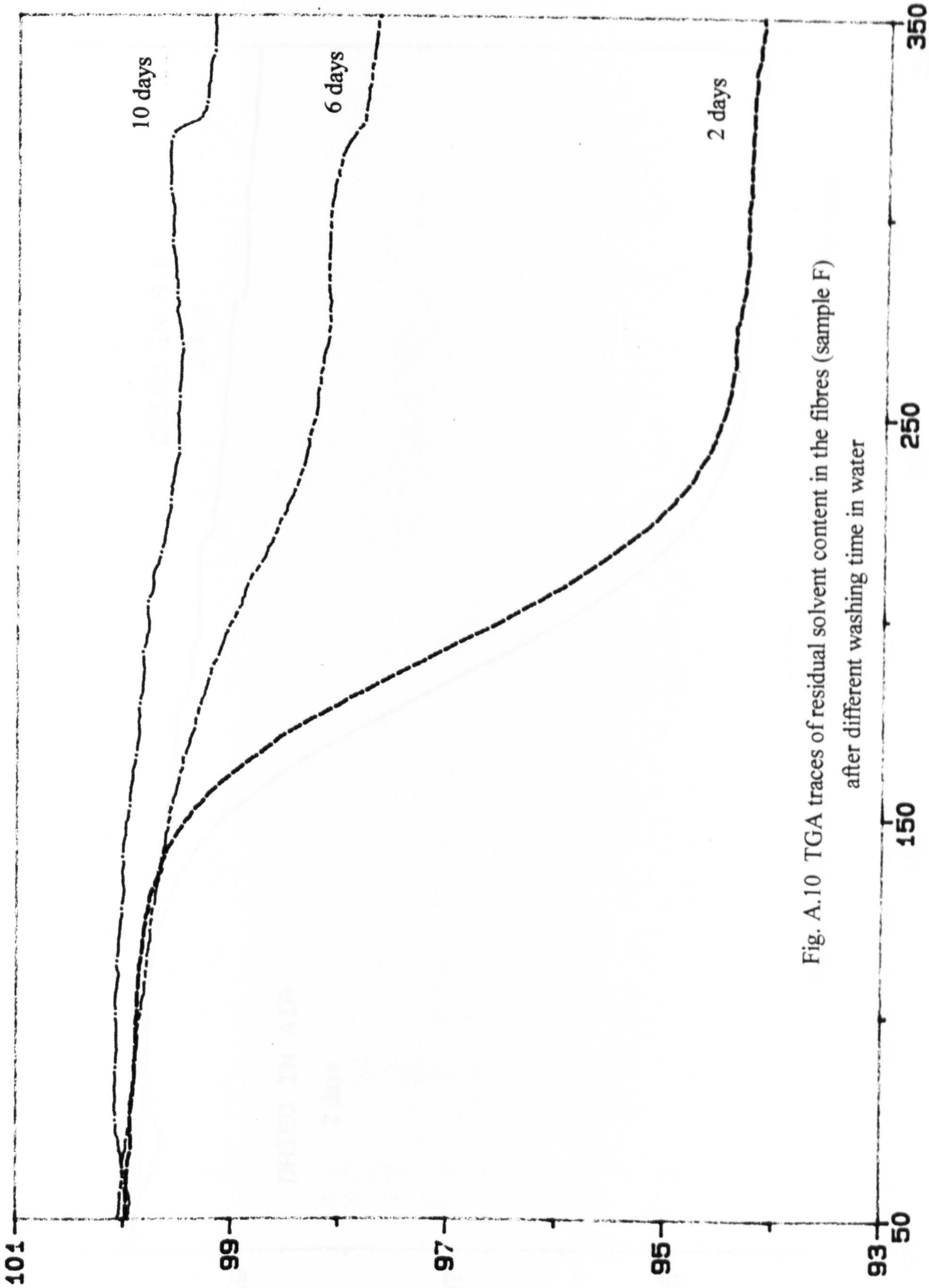

Fig. A.10 TGA traces of residual solvent content in the fibres (sample F) after different washing time in water

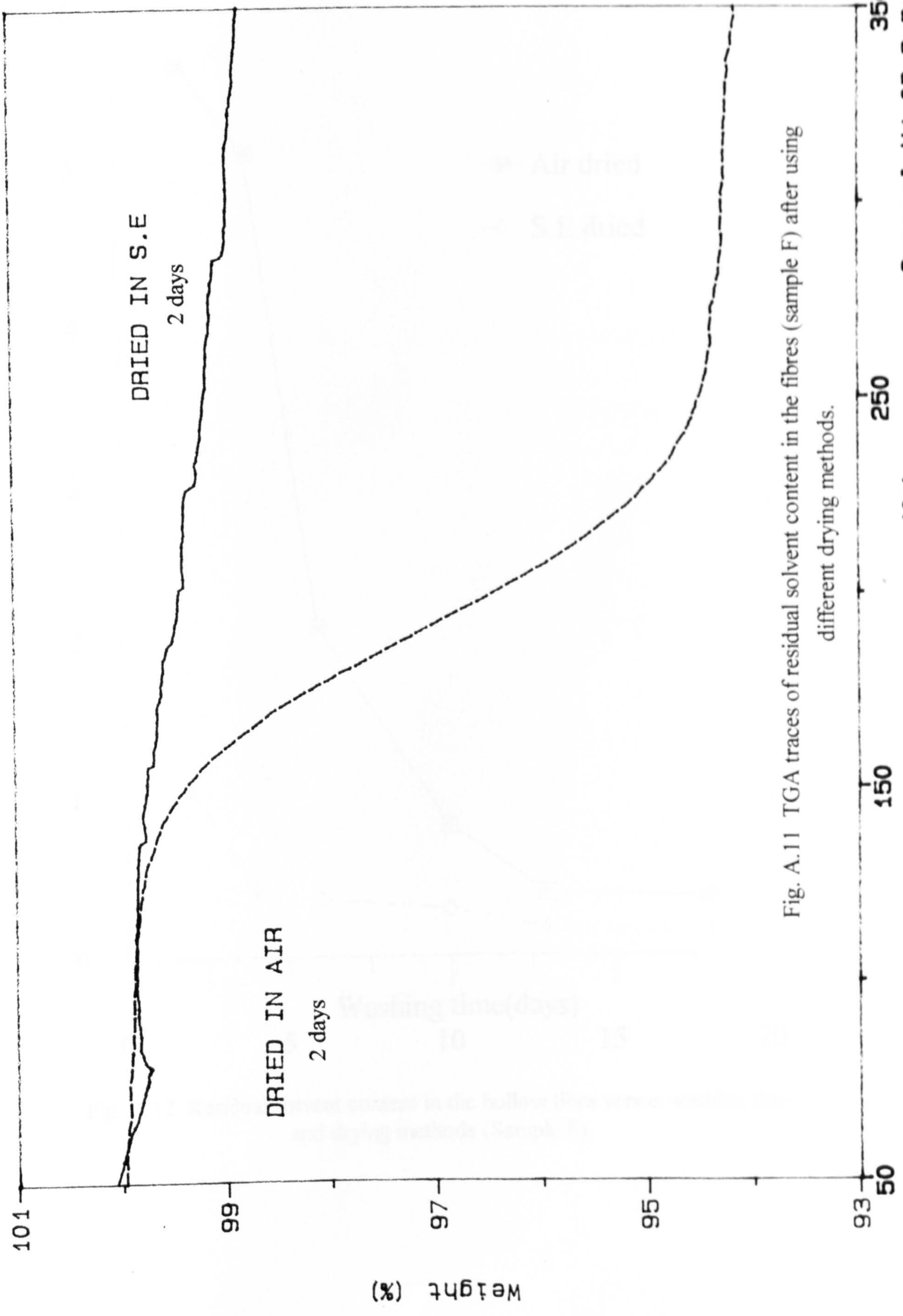

Fig. A.11 TGA traces of residual solvent content in the fibres (sample F) after using different drying methods.

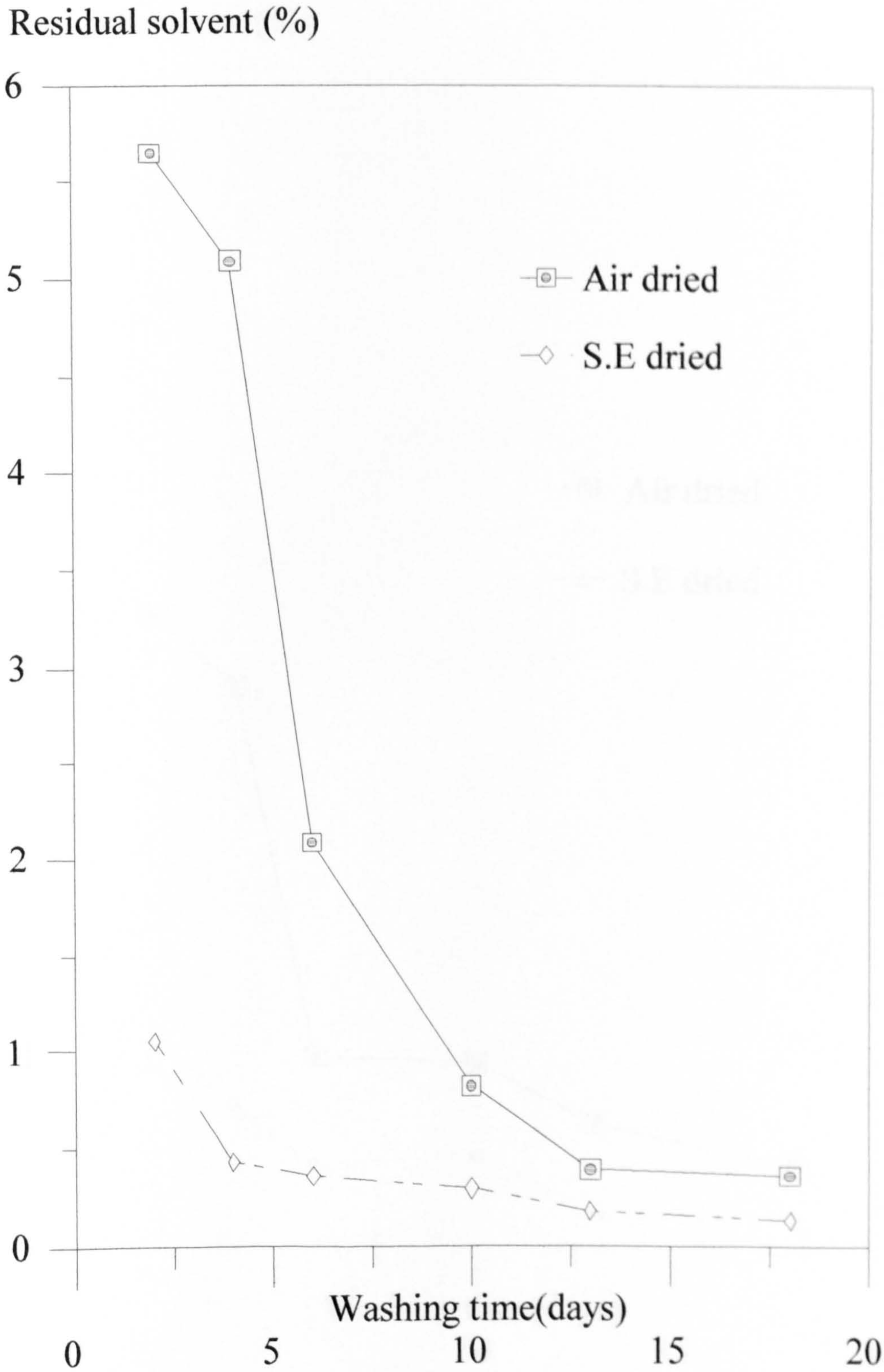

Fig. A.12 Residual solvent content in the hollow fibre versus washing time and drying methods (Sample F)

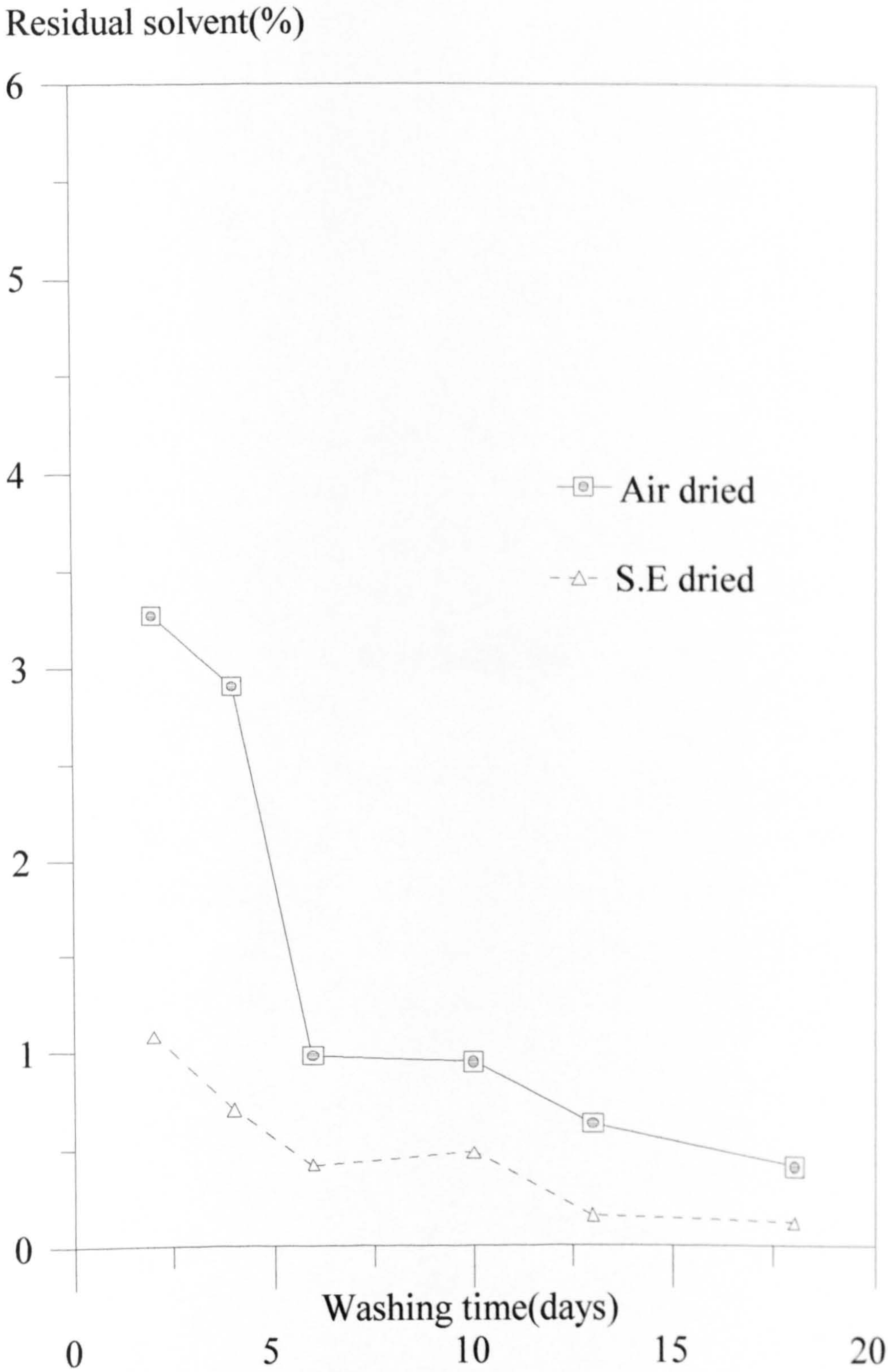

Fig. A.13 Residual solvent content in the hollow fibre versus washing time and drying methods (Sample G)

REFERENCES

1. Lonsdale, H. K., *J. Memb. Sci.*, **10**, 81 (1982).
2. Koros, W. J. and Fleming, G. K., *J. Memb. Sci.*, **83**, 1 (1993).
3. Ho, W. S. W. and Sirkar, K. K., *Membrane Handbook*, 1st ed., Van Nostrand Reinhold, New York, 20 (1992).
4. Hoehn, H. H., *Materials Science of Synthetic Membranes,* ACS Symp. Ser., 269, Amer. Chem. Soc., Washington, DC, Chapter 4, 81 (1985).
5. Mitchell, J. H., *Roy. Inst. J.,* **2**, 101, 307 (1831).
6. Schoenbein, C., British Patent 11,402 (1846).
7. Fick, A., *Ann. Phys. Chem.*, **94**, 59 (1855).
8. Lhermite, M., *Ann. Chem. Phys.*, 43(3), 420 (1855).
9. Graham, T., *Phil. Mag.*, **32**, 401 (1866).
10. Stannett, V., *J. Memb. Sci.*, **3**, 97 (1978).
11. Schumacher, W., *Ann. Phys. Chem.*, **110**, 337 (1860).
12. Baranetzky, J., *Pogg. Ann.*, **147**, 195 (1872).
13. Bechhold, H., *Biochem. Z.*, **6**, 379 (1907).
14. Karplus, H., Cited by F. Erbe, *Kolloid Z.*, **63**, 277(1933)
15. Loeb, S. and Sourirajan, S., *Advan. Chem. Ser.,* **38**, 117 (1962).
16. Vos, K. D, and Burris, F. O., *Ind. Eng. Chem., Proc. Res. Dev.*, **8**, 84 (1969).
17. Antonson, C. R., Gargner, R. J., King, C. F. and Ko, D. Y., *Ind. Eng. Chem., Proc. Des. Dev.*, **16**, 463 (1977).
18. U.S. Patent 3, 822, 202 (1974).
19. Pye, D. G. and Hoehn, H. H., *J. Appl. Polym. Sci.*, **22**, 287 (1976).
20. Panar, M., Hoehn, H. H. and Hebert, R. R., *Macromolecules*, **6**, 777 (1973).
21. (a) U.S. Patent 4, 068, 387 (1978).
    (b) U.S. Patent 4, 080, 743 (1978).
    (c) U.S. Patent 4, 080, 744 (1978).
    (d) U.S. Patent 4, 120, 098 (1978).
22. Henis, J. M. S., and Tripodi, M. K., *J. Memb. Sci.*, **8**, 233 (1981).

23. Kesting, R., *Synthetic Polymeric Membranes: A structural Perspective*, 2nd ed., John Wiley & Sons, New York (1985).

24. Stern, S. A., *Industrial Processing with Membranes*, Lacey, R. E. and Loeb, S. (eds.), Wiley-interscience, New York, Chapter 13, 279 (1972).

25. Grand, J., *The Mathematics of Diffusion*, 2nd ed., Clarendon, Oxford (1975).

26. Stannett, V. T., Koros, W. J., Paul, D. R., Lonsdale, H. K. and Baker, R. W., *Adv. Polym. Sci.*, **32**, 69 (1979).

27. Chern, R. T., Koros, W. T., Hopfenberg, H. B. and Stannett, V. T., *Materials Science of Synthetic Membranes*, ACS Symp. Ser., 269, Amer. Chem. Soc. Washington, DC. Chapter 2, 25 (1985).

28. Michaels, A. S., Vieth, W. R. and Barrie, J. A., *J. Appl. Phys.*, **34**, 1 (1963).

29. Naylor, T. De-V., *Comprehensive Polymer Science*, Booth, C. and Price, C. (eds), 1st ed., Pergamon, Press, Oxford. Chapter 20, 643 (1989).

30. Kesting, R. E. and Fritzsche, A. K., *Polymeric Gas Separation Membranes*, 2nd ed., John Wiley & Sons, New York, 31 (1993).

31. Ho, W. S. W. and Sirkar, K. K., *Membrane Handbook*, 1st ed., Van Nostrand Reinhold, New York, 29 (1992).

32. Paul, D. R. and Koros, W. J., *J. Polym. Sci., Part B: Polym. Phys.*, **14**, 675 (1976).

33. Koros, W. J. and Paul, D. R. and Huvard, G. S., *Polymer*, **20**, 956 (1979).

34. Petropoulos, J. H. and Roussis, P. P., *J. Polym. Sci., Part A-2*, **8**, 1411 (1970).

35. Stern, S. A. and Saxena, V., *J. Memb. Sci.*, **7**, 47 (1980).

36. Saxena, V. and Stern, S. A., *J. Memb. Sci*, **12**, 65 (1982).

37. Stern, S. A. and Zhou., S., *J. Polym. Sci., Part B: Polym. Phys.*, **27**, 205 (1989).

38. Vieth, W. R. and Sladek, K. J., *J. Colloid. Sci.*, **20**, 1144 (1965).

39. Kesting, R. E. and Fritzsche, A. K., *Polymeric Gas Separation Membranes*, 2nd ed., John Wiley & Sons, New York, 35 (1993).

40. Koros, W. J., Chan, A. H. and Paul, D. R., *J. Memb. Sci.*, **2**, 165 (1977).

41. Koros, W. J. and Hellums, M. W., *Encyclopedia of Polymer Science and Engineering*, 2nd. ed., John Wiley & Sons, New York, (Supplement Volume) 724 (1989).

42. Fujita, H., *Diffusion in Polymers*, Crand, J. and Park, G. S.(eds.), Academic Press, New York, Chapter 3, 75 (1968).

43. Vrentas, J. S. and Duda, J. L., *J. Appl. Polym. Sci.*, **21**, 1715 (1977).

44. Stern, S. A., Kulkarni, S. S. and Frisch, H. L., *J. Polym. Sci., Part B: Polym. Phys.*, **21**, 467 (1983).

45. Vrentas, J. S. and Duda, J. L., *Encyclopedia of Polymer Science and Engineering*, 2nd. ed., John Wiley & Sons, New York, **5**, 36 (1986).

46. Park, G. S., *Diffusion in Polymer*, Crand, J. and Patk, G. S. (eds.), Academic Press, New York, Chapter 5, 141 (1968).

47. Kapur, S. and Rogers, C. E., *J. Polym. Sci., Part B: Polym. Phys.*, **10**, 2107 (1972).

48. Vrentas, J. S. and Hou, A. C., *J. Appl. Polym. Sci.*, **36**, 1933 (1988).

49. Ho, W. S. W. and Sirkar, K. K., *Membrane Handbook*, 1st ed., Van Nostrand Reinhold, New York, 35 (1992).

50. Kesting, R. E. and Fritzsche, A. K., *Polymeric Gas Separation Membranes*, 2nd ed., John Wiley & Sons, New York, 42 (1993).

51. Maeda, Y. and Paul., D. R., *J. Memb. Sci.*, **30**, 1 (1987).

52. Chiou, J. S. and Paul, D. R., *J. Appl. Polym. Sci.*, **34**, 1037 (1987).

53. Teplykov, V. and Meares, P., *Gas Sep. Purif.*, **4**, 2, 66 (1990).

54. Paul, D. R. and Yampol'SkII, Y., *Polymeric Gas Separation Membranes*, CRC Press, Baca Raton, 100 (1994).

55. McHattie, J. S., Koros, W. J. and Paul, D. R., *Polymer*, **32**, 2618 (1991).

56. Hellums, M. W., Koros, W. J., Schmidhauser, J. C., *J. Memb. Sci.*, **67**, 75 (1992).

57. Aitken, C. L., Koros, W. J. and Paul, D. R., *Macromolecules*, **25**, 3424 (1992).

58. Aitken, C. L., Koros, W. J. and Paul, D. R., *Macromolecules*, **25**, 3651 (1992).

59. Aguilar-Vega, M. and Paul, D. R., *J. Polym. Sci., Part B: Polym. Phys.*, **31**, 1599 (1993).

60. Aitken, C. L. and Paul, D. R., *J. Polym. Sci., Part B: Polym. Phys.*, **31**, 1061 (1993).

61. Stern, S. A. *J. Memb. Sci.*, **94**, 1 (1994).

62. Kim, T. H., Koros, W. J., Husk, G. R. and O'Brien, K. C., *J. Memb. Sci.*, **37**, 45 (1988).

63. Coleman, M. R. and Koros, W. J., *J. Memb. Sci.*, **50**, 285 (1990).

64. Tanaka, K., Kita, H., Okano, M. and Okamoto, K., *Polymer*, **33**, 585 (1992).

65. Matsumoto, K. and Xu, P. *J. Memb. Sci.*, **81**, 23 (1993).

66. Stern, S. A., Liu, Y. and Field, W. A., *J. Appl. Polym. Sci., Part B: Polym. Phys.*, **31**, 939 (1993).

67. Skyes, G. F. and St. Clair, A. K., *J. Appl. Polym. Sci.*, **32**, 3725 (1986).

68. Walker, D. R. B. and Koros, W. J., *J. Memb. Sci.*, **55**, 99 (1991).

69. Anderson, M. K., Maters, B. R., Reiss, H., and Kaner, R. B., *Science*, **252**, 1414 (1991).

70. US Patent, 4, 364, 759 (1982).

71. US Patent, 5, 011, 637 (1991).

72. US Patent, 5, 085, 774 (1992).

73. Scott, J., *Hollow Fibre Manufacture and Application, Chem. Techn. Rev.*, 194, Noyes Data Cor., New Jersey (1981)

74. Paul, D. R. and Yampol'SkII, Y., *Polymeric Gas Separation Membranes*, CRC Press, Baca Raton, 217 (1994).

75. Koehnen, D. M., Mulder, M. H. V. and Smolders, C. A., *J. Appl. Polym. Sci.*, **21**, 199 (1977).

76. Smolders, C. A., *Polymer Science and Technology,* Cooper, A. R. (ed.), Plenum Press, New York, 13 (1980).

77. Burghardt, W. R., Yilmaz, L. and McHugh, A. J., *Polymer*, **28**, 2085 (1987).

78. Cohen, C., Tanny, G. B. and Prager, S., *J. Polym. Sci., Part B: Polym. Phys.*, **17**, 449 (1979).

79. Strathmann, H., Kock, K., Amar, P. and Baker, R. W., *Desalination*, **16**, 179 (1975).

80. US Patent, 4, 902, 422 (1990).

81. US Patent, 4, 493, 629 (1985).

82. Chung, T. S., Kafchinski, E. R. and Foley, P., *J. Memb. Sci.*, **75**, 181 (1992).

83. Smolders, C. A., Reuvers, A. J., Boom, R. M. and Weink, I. M., *J. Memb. Sci.*, **73**, 257 (1992).

84. Anderson, J. E. and Ullman, R., *J. Appl. Phys.*, **44**, 4303 (1973).

85. Fromer, M. A. and Messalam, R. M., *Ind. Eng. Chem., Prod. Res. Dev.*, **12**, 328 (1973).

86. Matz, R., *Desalination*, **10**, 1 (1972).

87. Craig, J. P., Knudsen, J. P. and Holland, V. F., *Textile Res. J.*, **32**, 435 (1962).

88. Grobe, V., Mann, G. and Duwe, G., *Fasenforsch Textiltechn.*, **17**, 142 (1966).

89. Kesting, R. E. and Fritzsche, A. K., *Polymer Gas Separation Membranes*, 2nd ed., John Wiley & Sons, New York, 205 (1993).

90. Cabasso, I., Klein, E. and Smith, J. K., *J. Appl. Polym. Sci.*, **21**, 165 (1977).

91. Kesting, R. E. and Fritzsche, A. K., *Polymer Gas Separation Membranes*, 2nd ed., John Wiley & Sons, New York, 203 (1993).

92. US, Patent, 4, 855, 048 (1989).

93. Kesting, R. E., Fritzsche, A. K., Murphy, M. K., Cruse, C. A., Handermann, A. C., Malon, R. F. and Moore, M. D., *J. Appl. Polym. Sci.*, **40**, 1557 (1990).

94. van't Hof, J. A., Reuvers, A. J., Boom, R. M., Rolevink, H. H. M. and Smolders, C. A., *J. Memb. Sci.*, **70**, 17 (1992).

95. Kesting, R. E. and Fritzsche, A. K., *Polymer Gas Separation Membranes*, 2nd ed., John Wiley & Sons, New York, 77 (1993)

96. Weller, S. and Steiner, W. A., *Chem. Eng. Prog.*, **46**, 585 (1950).

97. Spillman, R. W., *Chem. Eng. Prog.*, **85**, 41 (1990).

98. Maclean, D. L., *Membranes in Gas Separation and Enrichment*, 4th BOC Priestley Conference, 382 (1986).

99. Ho, W. S. W. and Sirkar, K. K., *Membrane Handbook*, 1st ed., Van Nostrand Reinhold, New York, 80 (1992).

100. Senn, S., *Ph.D. Thesis*, The University of Leeds, Leeds, UK (1988).

101. Brown, P. J., *Ph.D. Thesis*, The University of Leeds, Leeds, UK (1992).

102. Deshmukh, S., *Ph.D. Thesis*, The University of Leeds, Leeds, UK (1994).

103. Shilton, S. J., *Ph.D. thesis*, University of Strathclyde, UK (1992).

104. Chung, Tai-sung, Kafchinski, E. R., Kohn, R. S., Poly, P. and Starff, S. R., *J. Appl. Polym. Sci.*, **53**, 701 (1994).

105. Fritzsche, A. K., Arevalo, A. R., Moore, M. D. and O'Hara, C., *J. Memb. Sci.*, **81**, 109 (1993).

106. Gao, C. Lu, X and Sun, X., *Desalination*, **62**, 89 (1987).

107. Petrov, S., Dimov, A., Petkova, S. and Petkova, P., *J. Memb. Sci.*, **64**, 183 (1991).

108. Wang, Q., Chen, X., Shen, X. and Hou, Z., *J. of China Textile University*, 16(1), 19 (1990).

109. Henmi, M. and Yoshioka, T., *J. Memb. Sci.*, **85**, 129 (1993).

110. Scott, J., *Hollow Fibre Manufacture and Applications, Chem. Techn. Rev.*, 194, Noyes Data Cor. New Jersey, 118 (1981).

111. Koop, G. H., Nolten, J. A. M., Mulder, M. H. V. and Smolders, C. A., *J. Memb. Sci.*, **81**, 57 (1993).

112. Ziabicki, A., *Fundamentals of Fibre Formation*, John Wiley & Sons, 302 (1976).

113. Ziabicki, A., *Fundamentals of Fibre Formation*, John Wiley & Sons, 342 (1976).

114. Knudsen, J. P., *Text. Res. J.*, **33**(1), 13 (1963).

115. Formmer, M. A. and Lancet D., *Reverse Osmosis Membrane Research*, Plenum Press, New York, 85 (1972).

116. Bottino, A., Capannelli, G. and Muncort, S., *Membranes Processes*, Drioli E. and Nakagaki M. ed., (1986).

117. Padhye, M. R. and Karandikar, A. V., *J. Appl. Polym. Sci.*, **30**, 667 (1985).

118. Madauler, Audy F., *Bull. Soc. Chem. France*, 1456 (1966).

119. Cotton, F. A. and Francis, R., *J. Amer. Chem. Soc.*, **82**, 2986 (1960).

120. Ann, Juple Jungbauer M., *Nature*, **202**, 209 (1964).

121. Feild, T. A. and Fremon, G. H., *Text. Res. J.*, **21**(8), 531 (1951).

122. JP 56, 128 311 (1980).

123. Mathur, R. B. Gupta, D., Bahl, O. P. and Dhami, T. L., *Fibre Science and Technology*, **20**, 227 (1984).

124. Li, J., *J. China Textile University*, (Eng. ed.), 9(2), 32 (1992).

125. Li, N. N., *Recently Developments in Separation Science*, CRC Press, 2, 107 (1975).

126. U.S. Patent 3, 172, 741 (1965).

127. Pinnau, I. and Koros, W. J., *J. Memb. Sci.*, **71**, 81 (1992).

128. Ekiner, O. M. and Vassilators., *J. Memb. Sci.*, **53**, 259 (1990).

129. Strathman, H.; *Material Science of Synthetic Membrane*, ACS symp. Ser. 269, Amer. Chem. Soc., Washington, DC., Chapter 8, 165 (1985).

130. Kesting, R. E., *J. Appl. Polym. Sci.*, **41** 2739 (1990).

131. Hearle, J. W. S. and Miles, L. W. C., *The Setting of Fibre and Fabrics*, John William Stanly, Wattford, 109 (1971)

132. Uchytil, P., Nguyen, X. Q. and Broze, Z., *J. Memb. Sci.*,. **73**, 47 (1992).

133. Fouda, A., Chen, Y., Bai, J. and Matsuura, T., *J. Memb. Sci.*, **64**, 263 (1991).

134. Yasuda, H. and Tasi, J. T., *J. Appl. Polym. Sci.*, **18**, 805 (1974).

135. Carman, P. C., *Flow of Gases Through Porous Media*, Butterworth, London (1956).

136. Weast, R. C., *Handbook of Chemistry and Physics*, 60th Edition, CRC Press (1980).

137. Cabasso, I., Robert, K. Q., Klein, E. and Smith, J. K., *J. Appl. Polym. Sci.*, **21**, 1883 (1977).

138. Hwang Sun-Tak, Kammermeyer Karl., *Membranes in Separations* Techniques of Chemistry, John Wiley and Sons, New York, **12**, 500 (1975).

139. Kesting, R. E. and Fritzsche, A. K., *Polymeric Gas Separation Membranes*, 2nd ed., John Willey & Sons, New York, **21** (1993).

140. Present, R. D. and Pollard, W. G., *Phys. Rev.*, **73**, 762 (1948).

141. Shindo, Y., Hakuta, T., Yoshitome, H. and Inoue, H., *Sep. Sci. and Tech.*, **20**, 73 (1985).

142. Nago, S. and Mizutani, Y., *J. Appl. Polym. Sci.*, **56**, 253 (1995).

143. Musahiro, H. and Toshio, Y., *J. Memb. Sci.*, **85**, 129(1993)

144. Henis, J. M. S. and Tripody, M, K., *Sep. Sci. and Tech.*, **15**(4), 1059 (1980).

145. Chiou, J. S. and Paul, D. R., *J. Polym. Sci. Part B. Polym. Phys.* **25**, 1699 (1987).

146. Sweeting, O. J. and Bixler, H. J., *Science and Technology of polymer film*, Willey-Interscience, New York. **2**, 85 (1971).

147. Kesting, R. E. and Fritzsche, A. K.; *Polymeric Gas Separation Membranes*, 2nd ed., John Willey & Sons, New York, 155 (1993).

148. US Patent 4, 230, 460 (1980).

149. Sorenson, W. R. and Campbell, T. W., *Preparative Methods of Polymer Chemistry*, 2nd ed., John Wiley & Sons, New York, 237 (1968).

150. Mathur, R. B., Gupta, D., Bahl, O. P. and Dhami, T. L., *Fiber Science and Technology*, **20**, 227 (1984).

151. Qin, Y., *J. Appl. Polym. Sci.*, **49**, 727 (1993).

152. Li, J., Pan,. D., Pan, W. L. and Wu, Z. Q., *J. China Textile University*, (Eng. ed.), 7(4), 13 (1990).

153. U.S Patent 3, 346, 685 (1967).

154. Henric-Olive, G. and Olive. S., *Advanccs in Polymer Science*, **32**, 148 (1979)

155. Rath, H., Rehm, H., Rummler, H. and Specht, E., *Melliand Textilber*, **38**, 431 (1957).

156. Durrant, P. J., *Introduction to Advanced Inorganic Chemistry*, Longman, 2nd ed., 1115 (1970).

157. Bacon, R. G. R. and Hill, H. A. O., *Quartely Review*, **19**, 100 (1965).

158. McCartney, J. R., *US Natl. Bur. Stand. Circ.*, **525**, 123 (1953).

159. La Comber, E. M., *J. Polymer Sci.*, **24**, 152 (1957).

160. Bashire, Z., Manns, G., Service, D. M., Bott, D. C., Herbert, I. R., Ibbett, R. N. and Church, S. P., *Polymer*, **32**(10), 1826 (1991).

161. Wu, C. R. and Liedberg, B., *J. Polymer Sci., Part B: Polym. Phys.* **26**, 1127 (1988).

162. El-Sonbati, A. Z. and Diab, M. A., *Acta Polymerica*, **39**, 124 (1988).